INVESTIGATING THE ROLE OF NITRITE IN THE CARDIOVASCULAR SYSTEM

by

Sophie Worrall

A thesis submitted to the University of Birmingham for the degree of Master of Science by Research

Supervisor: Dr Melanie Madhani
School of Clinical and Experimental Medicine
College of Medical and Dental Sciences
University of Birmingham, UK
June 2018

Abstract

Introduction and aims: Nitric oxide (NO) bioavailability and responsiveness decrease with age, leading to a rise in platelet activation and aggregation, however very little evidence exists on the changes to platelet function in the elderly. Platelet and vascular responses to NO are also impaired in patients with heart failure with reduced ejection fraction (HFrEF) when compared to healthy volunteers, due to scavenging of NO with subsequent reduction to soluble guanylate cyclase (sGC), thus limiting the therapeutic potential of NO donors. "Platelet NO resistance" is widely recognised in HFrEF, but the existence of the phenomenon in heart failure with preserved ejection fraction (HFpEF) remains to be elucidated. Many pharmacotherapeutic agents utilised in HFrEF are ineffective in HFpEF, thus the discovery of a novel agent that circumvents "platelet NO resistance" is desirable. Previous studies have shown nitrite to inhibit platelet aggregation in healthy volunteers, however the underlying mechanism(s) of the anti-aggregatory effects of nitrite remain unclear. We aimed to investigate platelet function in the elderly, the potential for nitrite to be used as an anti-platelet agent in patients with HFpEF, and the role of NO/sGC/ALDH2 in nitrite-mediated platelet inhibition.

Methods and results: Platelet responses to nitrite and the NO donor sodium nitroprusside (SNP) were compared in: **1)** young *vs* old healthy volunteers, **2)** age-matched old healthy volunteers, heart failure with preserved ejection fraction with chronic atrial fibrillation (HFpEF-AF) patients and chronic atrial fibrillation (CAF) patients, and **3)** ALDH2 WT *vs* KO mice. Nitrite-mediated platelet inhibition was assessed in the presence of NO scavengers/an sGC inhibitor, whilst vasodilator-stimulated phosphoprotein (VASP) phosphorylation was measured using Western blotting. Platelet responses to the sGC stimulator BAY 41-2272 were also assessed in the presence of nitrite/SNP. Nitrite and SNP

triggered concentration-dependent attenuation of platelet aggregation in healthy volunteers and CAF pateints. A diminished response to SNP was observed in washed platelets from HFpEF-AF patients, whilst the anti-aggregatory effects of nitrite were not impaired. Nitrite also activated sGC independently of NO, phosphorylated VASP and exhibited synergistic activity with BAY-41-2272 in human platelets, whilst required ALDH2 to inhibit platelet aggregation in mice.

Conclusion: We demonstrate for the first time that the phenomenon of "platelet NO resistance" exists in HFpEF-AF, whilst also revealing that high concentration nitrite is able to circumvent "platelet NO resistance" in washed platelets independently of NO. We also show that platelet function is maintained in the elderly population, whilst revealing the involvement of ALDH2 in nitrite-mediated platelet inhibition in mice.

Acknowledgments

I am very grateful for all the help received during my graduate studies at the University of Birmingham and this research project would not have been possible without guidance from several people.

Firstly, I would like to express my gratitude to my primary supervisor, Dr Melanie Madhani, for giving me the opportunity to complete this project, and for her unwavering support, patience and understanding throughout. I am indebted to Dr Melanie Madhani, as without her continued encouragement, the completion of this thesis seemed impossible. I would also like to thank my lab peers, Dr Alessandra Borgognone, Dr Hannah Noordali, Dr Fiona Ashford and Dr Eakkapote Prompunt, for their invaluable guidance and for making my time in the lab an enjoyable experience. The completion of certain studies would also have not been possible without Dr Alessandra Borgognone's and Dr Eakkapote Prompunt's kind assistance.

I would also like to thank the Medical Research Council, who kindly provided financial support for this project, and my secondary supervisor, Professor Ed Rainger.

Finally, I would like to acknowledge my family and friends, for continually supporting and believing in me when I did not. Without their encouragement, the preparation of this thesis would also have not been possible.

Statement of contribution to research

The studies were designed with assistance from my primary supervisor, Dr Melanie Madhani.

Execution

Dr Melanie Madhani acquired the relevant ethical approvals for the studies. I recruited a large proportion of the human subjects and helped to manage the ALDH2 mouse colony. The aggregation experiments detailed in Chapter 3 were conducted by myself, however Dr Alessandra Borgognone assisted with the Western blotting analysis. Dr Alessandra Borgognone and Dr Eakkapote Prompunt also assisted with a small number of the aggregation experiments described in Chapter 4. All aspects of the ALDH2 study detailed in Chapter 5 were undertaken by myself.

Data analysis

The data was organised and analysed by myself, with guidance from Dr Melanie Madhani.

Published papers

1. Borgognone, A., Shantsila, E., **Worrall, S.M**., Prompunt, E., Loka, T., Loudon, B.L., Chimen, M., Rainger, G.E., Lord, J.M., Turner, A., Nightingale, P., Feelisch, M., Kirchhof, P., Lip, G.Y.H., Watson, S.P., Frenneaux, M.P. and Madhani, M. (2018) Nitrite circumvents platelet resistance to nitric oxide in patients with heart failure preserved ejection fraction and chronic atrial fibrillation. **Cardiovasc Res**, 114 (10): 1313-1323.

Table of Contents

Chapter 1: General introduction 1

1.1 Overview 2

1.2 Heart failure 3

1.3 Platelets and their functions in health 6

1.4 Primary haemostasis 10

1.4.1 Platelet adhesion 10

1.4.2 Platelet activation 11

1.4.2.1 ADP and 5HT 15

1.4.2.2 TXA_2 15

1.4.2.3 Thrombin 16

1.4.2.4 Polymorphonuclear leukocytes 16

1.4.3 Platelet aggregation 17

1.5 Secondary haemostasis 18

1.6 Negative regulators of haemostasis 20

1.7 Nitric oxide 20

1.7.1 Nitric oxide synthase 20

1.7.1.1 Endothelial nitric oxide synthase 21

1.7.2 The nitric oxide (NO)-soluble guanylate cyclase (sGC)-cyclic guanosine monophosphate (cGMP)-protein kinase G (PKG) signalling cascade in platelets 23

1.7.3 Nitrosation and nitration in platelets 25

1.7.4 The biphasic role of nitric oxide in platelets 27

1.8 Platelet dysfunction in cardiovascular disease 28

1.8.1 Nitric oxide bioavailability and oxidative stress in heart failure 28

1.8.2 Chronic atrial fibrillation in heart failure 30

1.9 Treatment for heart failure 30

1.9.1 Nitric oxide donors and ‘NO resistance’ 30

1.9.2 Nitrite as a potential substitute for nitric oxide donors 31

1.9.2.1 Nitrite during hypoxic and acidic conditions 31

1.9.2.2 Dietary sources of nitrate/nitrite 32

1.9.2.3 Nitrite during normoxic conditions 32

1.9.3 The role of nitrite in HF 34

1.9.4 The role of nitrite on platelet aggregation 34

1.10 Summary 37

1.11 Objectives 38
Chapter 2: Research methods 40
2.1 Human experiments 41
2.1.1 Human ethics 41
2.1.2 Human subjects 41
2.1.3 Human washed platelet aggregation study 42
2.1.3.1 Collection of human blood 42
2.1.3.2 Preparation of washed human platelets 44
2.1.3.3 Human platelet count 47
2.1.3.4 Human platelet aggregation 48
2.1.3.4.1 Oxyhaemoglobin preparation 49
2.1.3.4.2 $NaNO_2$, SNP, PTIO, ODQ, BAYER 41-2272 and collagen preparation 53
2.1.3.4.3 Human LTA experiments 56
2.1.3.5 Data analysis (human platelet aggregation) 62
2.1.4 Western blotting (human platelet samples) 64
2.1.4.1 Platelet homogenate preparation (human platelet samples) 64
2.1.4.2 Sodium dodecyl sulfate–polyacrylamide gel electrophoresis (SDS-PAGE) 70
2.1.4.3 Wet transfer 72
2.1.4.4 Antibody incubation and film development (human platelet samples) 74
2.1.4.5 Data analysis (Western blotting) 76
2.2 Animal experiments 77
2.2.1 Animal ethics 77
2.2.2 Genotyping 77
2.2.2.1 Sample digestion, DNA isolation and extraction 77
2.2.2.2 Polymerase chain reaction 80
2.2.2.3 Agarose gel electrophoresis 83
2.2.3 ALDH2 blood and tissue harvest 85
2.2.3.1 Collection of mouse blood 85
2.2.3.2 Collection of mouse tissue 87
2.2.4 Mouse washed platelet aggregation study 88
2.2.4.1 Preparation of washed mouse platelets 88
2.2.4.2 Mouse platelet count 89
2.2.4.3 Mouse platelet aggregation 90
2.2.4.4 Data analysis (mouse platelet aggregation) 90

2.2.5 Western blotting (mouse platelet and tissue samples) 91
2.2.5.1 Platelet homogenate preparation (mouse platelet samples) 91
2.2.5.2 Tissue homogenate sample preparation (mouse liver, skeletal muscle and cardiac tissue samples) 92
2.2.5.3 Protein assay 94
2.2.5.4 SDS-PAGE 96
2.2.5.5 Wet transfer 96
2.2.5.6 Antibody incubation and film development 96
2.2.5.7 Data analysis (Western blotting) 98
2.2.6 Oil red O staining 99
2.2.6.1 Tissue sectioning 99
2.2.6.2 Oil red O staining 100
2.2.6.3 Data analysis (ORO staining in ALDH2 WT and KO tissue samples) 103
2.3 Statistical analysis 103
Chapter 3: Exploration of platelet function and nitrite in young vs old healthy volunteers 104
3.1 Introduction 105
3.2 Hypothesis and specific aims 108
3.2.1 Hypothesis 108
3.2.2 Specific aims 108
3.3 Research methods 109
3.4 Results 109
3.4.1 Subject characteristics 109
3.4.2 Determining the concentration response to collagen on platelet aggregation in young and old healthy volunteers 110
3.4.3 $NaNO_2$ inhibits platelet aggregation in young and old healthy volunteers 112
3.4.4 SNP inhibits platelet aggregation in young and old healthy volunteers 114
3.4.5 $NaNO_2$ inhibits platelet aggregation via NO-independent pathway in young and old healthy volunteers 116
3.4.6 $NaNO_2$ inhibits platelet aggregation via the sGC pathway in young and old healthy volunteers 120
3.4.7 BAY 41-2272 (sGC stimulator) has a synergistic effect on $NaNO_2$ platelet aggregation responses in young and old healthy volunteers 122
3.4.8 $NaNO_2$ phosphorylates $VASPser^{239}$ in platelets from young healthy volunteers 128
3.4.9 $NaNO_2$ activates the sGC-cGMP-PKG-VASP signalling cascade via NO-independent pathway in platelets from young healthy volunteers 130

3.5 Discussion 132
3.5.1 Study limitations and future considerations 136
3.5.2 Conclusions 139
Chapter 4: Evaluation of the phenomenon of "platelet NO resistance" and nitrite in patients with HFpEF-AF and CAF only. 140
4.1 Introduction 141
4.2 Hypothesis and specific aims 142
4.2.1 Hypothesis 142
4.2.2 Specific aims 142
4.3 Research methods 142
4.4 Results 143
4.4.1 Subject characteristics 143
4.4.2 $NaNO_2$ circumvents the phenomenon of "platelet NO resistance" in HFpEF-AF patients 144
4.5 Discussion 148
4.5.1 Study limitations and future considerations 150
4.5.2 Conclusions 151
Chapter 5: Exploration of nitrite, lipid content and tissue morphology in ALDH2 WT and KO mice. 152
5.1 Introduction 153
5.2 Hypothesis and specific aims 158
5.2.1 Hypothesis 158
5.2.2 Specific aims 158
5.3 Research methods 159
5.4 Results 160
5.4.1 ALDH2 expression in ALDH2 WT and KO mice 160
5.4.2 Does $NaNO_2$ inhibit platelet aggregation via ALDH2? 162
5.4.3 ALDH2 WT and KO tissue staining 164
5.4.3.1 ORO staining in liver tissue 164
5.4.3.2 ORO staining in skeletal muscle tissue 166
5.4.3.3 Mayer's haematoxylin counterstaining in liver and skeletal muscle tissue 168
5.5 Discussion 170
5.5.1 Study limitations and future considerations 173
5.5.2 Conclusions 175
Chapter 6: General discussion 176

6.1 Introduction summary 177
6.2 Discussion 178
6.3 Study limitations and future directions 180
6.4 Conclusion 181
Chapter 7: References 182

List of tables

Table 1.1	Primary adhesions	11
Table 2.1:	Masses (g) of reagents required to make ACD solution (1L)	45
Table 2.2:	Volumes (mL) and masses (g) of reagents required to make 1mg/mL PGI_2 (2mL)	45
Table 2.3:	Masses (g) of reagents required to make MTB (1L/50mL)	45
Table 2.4:	OxyHb preparation (human LTA experiments)	51
Table 2.5:	$NaNO_2$, SNP, PTIO, ODQ and BAYER 41-2272 preparation (human LTA experiments)	54
Table 2.6:	Collagen preparations (human LTA experiments)	55
Table 2.7:	Volumes (mL) and masses (g) of reagents used to make 5x reduced Laemmli sample buffer (10 mL)	69
Table 2.8:	Volumes (µL) of reagents used to make 8% acrylamide SDS-PAGE gels (x2)	71
Table 2.9:	Volumes (µL) of reagents used to make SDS-PAGE reservoir buffer (1L)	71
Table 2.10:	Volumes (µL) and masses (g) of reagents used to make wet transfer buffer (2L)	72
Table 2.11	Western blotting antibodies (human platelet samples)	76
Table 2.12:	Optimum exposure time of the Amersham Hyperfilm™ to each membrane	76
Table 2.13:	Volumes of reagents (µL) used to produce the PCR master mix	81
Table 2.14:	ALDH2 primers used at a final concentration of 10µM during PCR	81
Table 2.15:	Concentration (mM) of reagents in the Krebs-Henseleit Buffer	87
Table 2.16:	Volumes (µL) of reagents used to make HB (50mL)	93
Table 2.17:	Volumes (µL) of reagents used to make BSA standards (300µL)	95
Table 2.18:	Western blotting antibodies (ALDH2 WT and KO platelet and tissue samples)	98
Table 2.19:	Optimum exposure time of the Amersham Hyperfilm™ to each membrane	98
Table 3.1:	Subject characteristics	109
Table 4.1:	Subject characteristics	143

List of figures

Figure 1.1	Signalling in haemostasis	8
Figure 1.2	Receptor-mediated platelet activation	14
Figure 1.3	Coagulation cascade	19
Figure 1.4	'Nitrate-nitrite-NO pathway' in normoxia and hypoxia	33
Figure 2.1	Blood collection kit	43
Figure 2.2:	Blood fractionation	46
Figure 2.3:	PD-10 desalting column setup for OxyHb preparation	51
Figure 2.4:	Aggregation protocols (human platelet samples)	60
Figure 2.5:	Trace analysis	62
Figure 2.6:	Preparation of platelet homogenates 1 (human samples)	67
Figure 2.7:	Preparation of platelet homogenates 2 (human samples)	68
Figure 2.8:	Gel sandwich	73
Figure 2.9:	ALDH2 PCR programme (thermal cycling)	82
Figure 2.10:	Identification of ALDH2 mouse genotype	84
Figure 2.11:	Blood collection via the IVC in ALDH2 WT and KO mice	86
Figure 2.12:	ORO and Mayer's haematoxylin staining protocol	102
Figure 3.1:	Platelet aggregation responses to 1, 3 and 10μg/mL collagen in young and old healthy volunteers	111
Figure 3.2:	Platelet aggregation responses in young and old healthy volunteers following $NaNO_2$ incubation	113
Figure 3.3:	Platelet aggregation responses in young and old healthy volunteers following SNP incubation	115
Figure 3.4:	Platelet aggregation responses in young and old healthy volunteers following: a) SNP, b) $NaNO_2$, c) OxyHb, d) OxyHb + SNP or e) OxyHb + $NaNO_2$ incubations	117
Figure 3.5:	Platelet aggregation responses in young and old healthy volunteers following: a) SNP, b) $NaNO_2$, c) PTIO, d) PTIO + SNP or e) PTIO + $NaNO_2$ incubations	119
Figure 3.6:	Platelet aggregation responses in young and old healthy volunteers following: a) SNP, b) $NaNO_2$, c) ODQ, d) ODQ + SNP or e) ODQ + $NaNO_2$ incubations	121

Figure 3.7: Platelet aggregation responses in young and old healthy volunteers following incubations with BAY 41-2272 123
Figure 3.8: Platelet aggregation responses in young and old healthy volunteers following: a) BAY 41-2272, b) $NaNO_2$ or c) $NaNO_2$ + BAY 41-2272 incubations 125
Figure 3.9: Platelet aggregation responses in young and old healthy volunteers following: a) BAY 41-2272, b) SNP or c) SNP + BAY 41-2272 incubations 127
Figure 3.10: Time profile of $VASP^{ser239}$ phosphorylation in platelets from young healthy volunteers following $NaNO_2$ or SNP incubations 129
Figure 3.11: $VASPser^{239}$ phosphorylation in platelets from young healthy volunteers following: a) $NaNO_2$ b) ODQ, c) ODQ + $NaNO_2$, d) PTIO, e) PTIO + $NaNO_2$, f) OxyHb or g) OxyHb + $NaNO_2$ incubations 131
Figure 4.1: Platelet aggregation responses in old healthy volunteers, HFpEF-AF patients and CAF patients following $NaNO_2$ incubation 145
Figure 4.2: Platelet aggregation responses in old healthy volunteers, HFpEF-AF patients and CAF patients following SNP incubation 147
Figure 5.1: ALDH2 expression in platelets and tissues obtained from ALDH2 WT and KO mice 161
Figure 5.2: Platelet aggregation responses in ALDH2 WT and KO mice following SNP or $NaNO_2$ incubation 163
Figure 5.3: ORO staining in ALDH2 WT and KO liver tissue sections 165
Figure 5.4: ORO staining in ALDH2 WT and KO skeletal muscle tissue sections 167
Figure 5.5: Mayer's haematoxylin counterstaining in ALDH2 WT and KO liver and skeletal muscle tissue 169

List of calculations

Calculation 2.1:	Example of washed platelet calculation (human platelet samples)	47
Calculation 2.2:	Example of OxyHb eluate concentration calculation (human LTA experiments)	52
Calculation 2.3:	Example of percentage aggregation calculation for human washed platelet samples	63
Calculation 2.4:	Example of washed platelet calculation (mouse platelet samples)	89
Calculation 2.5:	Reagent A/working reagent A requirement calculation	95

List of abbreviations

1-H-[1,2,4]oxadiazolo[4,3-a]quinoxalin-l-one	(ODQ)
2-Phenyl-4,4,5,5-tetramethylimidazoline-1-oxyl 3-oxide	(PTIO)
4-hydroxynonenal	(4-HNE)
Acid-Citrate-Dextrose	(ACD)
Adenosine diphosphate	(ADP)
Adenylyl cyclase	(AC)
Aldehyde dehydrogenase 2	(ALDH2)
Aldehyde dehydrogenase activators	(Aldas)
AMP-activated protein kinase	(AMPK)
Arachidonic acid	(AA)
Arterial blood pressure	(ABP)
Asymmetric dimethylarginine	(ADMA)
Atrial fibrillation	(AF)
Bovine serum albumin	(BSA)
Ca^{2+}-calmodulin	(CaM)
Calcium	(Ca^{2+})
Cardiac output	(CO)
Cardiovascular disease	(CVD)
Chronic atrial fibrillation	(CAF)
Cyclic adenosine monophosphate	(cAMP)
Cyclic guanosine monophosphate	(cGMP)
Cyclooxygenase-1	(COX-1)
Diacylglycerol	(DAG)
Ejection fraction	(EF)
End-diastolic volume	(EDV)
Endothelial nitric oxide synthase	(eNOS)
Enhanced chemiluminescence	(ECL)
Extracellular matrix	(ECM)
Flavin adenine dinucleotide	(FAD)
Flavin mononucleotide	(FMN)
G-protein coupled receptors	(GPCRs)
Gastrointestinal tract	(GIT)
Glyceryl trinitrate	(GTN)
Glycoprotein 1b-IX-V	(GP1b-IX-V)
Glycoprotein VI	(GPVI)
Guanosine diphosphate	(GDP)
Guanine nucleotide-binding protein	(G-protein)
Guanosine triphosphate	(GTP)
Heart failure	(HF)
Heart failure with preserved ejection fraction	(HFpEF)

Heart failure with preserved ejection fraction with chronic atrial fibrillation	(HFpEF-AF)
Heart failure with reduced ejection fraction	(HFrEF)
Heterozygous	(HET)
Homogenate buffer	(HB)
Horseradish peroxidase	(HRP)
Hydrogen peroxide	(H_2O_2)
Hydroxyl radical	(OH^-)
Inducible nitric oxide synthase	(iNOS)
Inferior vena cava	(IVC)
Inositol-1,4,5-trisphosphate	(IP_3)
Inter-cellular adhesion molecule-1	(ICAM-1)
Ischaemia reperfusion injury	(IRI)
Junctional adhesion molecules	(JAMs)
Knock-out	(KO)
Krebs-Henseleit buffer	(KHB)
Left ventricular heart failure	(LVHF)
Light transmission aggregation	(LTA)
Malondialdehyde	(MDA)
Mitogen-activated protein kinase	(MAPK)
Mn(III) tetrakis (4-benzoic acid) porphyrin	(MnTBAP)
Modified Tyrode's buffer	(MTB)
Myocardial infarction	(MI)
N-ethylmaleimide-sensitive factor	(NSF)
Neuronal nitric oxide synthase	(nNOS)
Nicotinamide adenine dinucleotide phosphate	(NADPH)
Nitric oxide	(NO)
Nitric oxide synthase	(NOS)
Nitrogen dioxide	(NO_2)
Oil Red O	(ORO)
Oxygen	(O_2)
Oxyhaemoglobin	(OxyHb)
p115-Rho guanine nucleotide exchange factor	(p115-RhoGEF)
Peroxynitrite	($ONOO^-$)
Phosphatidylinositol-3-kinase	(PI3K)
Phosphatidylinositol-4,5-bisphosphate	(PIP_2)
Phosphodiesterase	(PDE)
Phospholipase A2	(PLA_2)
Phospholipase C β	(PLCβ)
Phospholipase C γ2	(PLCγ2)
Platelet rich plasma	(PRP)
Polymorphonuclear leukocytes	(PMN)
Polyvinylidene fluoride	(PVDF)

Prostacyclin	(PGI_2)
Protease activated receptors	(PARs)
Protein kinase A	(PKA)
Protein kinase B	(Akt)
Protein kinase C	(PKC)
Protein kinase C type ϵ	(PKCϵ)
Protein kinase G	(PKG)
P-selectin glycoprotein ligand 1	(PSGL1)
Receptor tyrosine kinases	(RTKs)
S-nitrosoglutathione	(GSNO)
S-nitrosothiols	(SNOs)
Sarco/endoplasmic reticulum Ca^{2+} ATPase	(SERCA)
Serotonin	(5HT)
Sodium dithionite	($Na_2S_2O_4$)
Sodium dodecyl sulfate–polyacrylamide gel electrophoresis	(SDS-PAGE)
Sodium nitrite	($NaNO_2$)
Sodium nitroprusside	(SNP)
Soluble guanylate cyclase	(sGC)
Stroke volume	(SV)
Superoxide	(O_2^-)
Superoxide dismutase	(SOD)
Tetrahydrobiopterin	(BH_4)
Thromboxane A_2	(TXA_2)
Thromboxane prostanoid	(TP)
Tissue factor	(TF)
Tris acetate-EDTA	(TAE)
Vascular endothelial growth factor	(VEGF)
Vascular endothelial-cadherin	(VEC)
Vasodilator stimulated phosphoprotein	(VASP)
von Willebrand factor	(VWF)
Wild-type	(WT)
Xanthine oxidoreductase	(XOR)

Chapter 1: General introduction

1.1 Overview

Cardiovascular disease (CVD) is currently the number one cause of global deaths and affects approximately 17.5 million people worldwide (Bhatnagar et al., 2015). With an aging and growing population, and improved survival rates from cardiovascular events, it is estimated that these numbers may rise further (Chung and Lip, 2006). The vascular endothelium and platelets are involved in many aspects of cardiovascular health, including regulating vascular tone, haemostasis, thrombosis, and cell adhesion (Marti et al., 2012). In particular, altered platelet physiology associated with impaired nitric oxide (NO) bioavailability and increased oxidative stress has recently been implicated in the pathophysiology of a number of CVDs, including myocardial infarction (MI), atrial fibrillation (AF) and heart failure (HF) (Chung and Lip, 2006, Elahi et al., 2009; Marti et al., 2012; Procter et al., 2016; Stamboul et al., 2015). Abundant research is currently underway to understand the impairment of NO and platelet dysfunction in HF, and in particular to identify novel therapeutic interventions to inhibit platelet aggregation during this disease state. Herein, we will address these knowledge gaps whilst investigating nitrite in: **1)** young and old healthy volunteers, **2)** patients with heart failure with preserved ejection fraction (HFpEF) with chronic atrial fibrillation (CAF) (HFpEF-AF patients), and **3)** aldehyde dehydrogenase 2 (ALDH2) wild-type (WT) and knock-out (KO) mice.

1.2 Heart failure

HF is a persistent and progressive condition, whereby the heart is unable to pump blood effectively throughout the body. Unfortunately, HF is a huge public health issue that contributes significantly to the global burden of CVD and has an overall economic cost of approximately $108 billion per year (Borlaug, 2013; Bui et al., 2011; Cook et al., 2014; Roger, 2013). It has been estimated that approximately 23 million individuals are currently living with HF worldwide, and this prevalence is set to rise due to a number of factors, including: the increasing age of the general population, rising awareness and diagnosis of HF, advancements in HF medication and mechanical devices, improved survival of patients following MI and the shift from acute illness to chronic disease in developing countries (Bui et al., 2011**;** Chung and Lip, 2006; Roger, 2013).

There are various factors which have been shown to increase the risk of HF development, these include: **1)** clinical risk factors (e.g. hypertension, MI, diabetes, obesity, and smoking), **2)** immune-mediated risk factors (e.g. peripartum cardiomyopathy), **3)** infectious risk factors (e.g. viral, parasitic and bacterial infections), **4)** toxic risk factors (e.g. chemotherapy, cocaine and alcohol), **5)** genetic risk factors (e.g. congenital heart disease and family history), and **6)** morphological risk factors (e.g. left ventricular dysfunction and increased LV mass/internal dimension) (Bui et al., 2011). Moreover, early diagnosis of HF is also very challenging. Many features of the disease lack organ-specificity and obvious signs/symptoms are generally masked in the early stages by accompanying compensatory mechanisms (e.g. ventricular dilation/hypertrophy, vasoconstriction/venoconstriction and tachycardia) (Bui et al., 2011; Jackson et al., 2000). These compensatory mechanisms function to maintain cardiac output (CO) and arterial blood pressure (ABP) (thus preserve nutrient delivery) in the

short-term. However, long-term compensatory changes often lead to significant deteriorations in cardiac function (Jackson et al., 2000).

HF can be divided into groups based on left ventricular ejection fraction (EF). The most prevalent forms of HF include: **1)** left ventricular heart failure (LVHF) with reduced ejection fraction (HFrEF) (EF<40%) and **2)** LVHF with preserved ejection fraction (HFpEF) (EF≥50%) (ElGuindy and Yacoub, 2012; van Riet et al., 2016). Briefly, HFrEF (or systolic failure; ~49% of HF cases) generally results from a direct cardiac insult such as ischaemic damage or cardiomyopathy (e.g. genetics or deposition disease) (Loudon et al., 2016). A reduction in EF is due to loss of cardiac inotropy/decrease in ventricular contractility and is often caused by alterations in the signal transduction mechanisms regulating excitation-contraction coupling (ElGuindy and Yacoub, 2012; van Riet et al., 2016) In contrast, HFpEF tends to occur in patients with hypertension, metabolic syndrome, diabetes and obesity (Noordali et al., 2017). HFpEF (or diastolic failure; >50% of HF cases) is caused by adverse effects on ventricular filling and stroke volume (SV) (e.g. ventricular hypertrophy and reductions in ventricular lusitropy). EF is maintained during HFpEF as reductions in end-diastolic volume (EDV) and SV are generally proportional (ElGuindy and Yacoub, 2012; LeWinter and Meyer, 2013; van Riet et al., 2016).

Whilst current morbidity and mortality rates for HFrEF and HFpEF are relatively similar (e.g. 3-year mortality rates for HFrEF and HFpEF is approximately 32% and 26%, respectively), it has been estimated that HFpEF will become the most dominant HF phenotype within the next few decades (Burkhoff, 2012; Chung and Lip, 2006; Hall et al., 2014; van Heerebeek and Paulus, 2016). This prediction is based on the alarming rate at which HFpEF prevalence is

currently rising (~1% per year, relative to HFrEF prevalence), as well as the present shortage of effective HFpEF therapies (Borlaug, 2013; ElGuindy and Yacoub, 2012; van Heerebeek and Paulus, 2016). In recent clinical trials, therapies that have been shown to benefit HFrEF patients (e.g. neurohormonal antagonist treatments) had very little impact on the HFpEF outcome (Borlaug, 2013; ElGuindy and Yacoub, 2012). A number of theories have been proposed for the varied responses observed in HFrEF *vs* HFpEF patients, including: **1)** unique pathophysiologies in the two phenotypes, **2)** pathophysiological heterogeneity in the HFpEF patient population, **3)** higher mortality associated with other causes in HFpEF, since approximately 30% of HFpEF deaths have been shown to have a non-cardiovascular nature, and **4)** limited reverse remodelling in HFpEF due to the plasticity of the heart/vasculature in HFrEF potentially exceeding that in seen in HFpEF (Borlaug, 2013; Burkhoff, 2012). Further research into the underlying mechanism(s) of HFpEF and HFpEF therapies is warranted to address the predicted increases in HFpEF morbidity and mortality.

Since HFpEF is a heterogenous disease with numerous etiologies/comorbidities, current treatments are mostly directed at associated conditions and symptoms, such as hypertension and oedema (Oktay and Shah, 2015). The array of accompanying disorders provides potential for numerous treatment avenues, however for this study we have chosen to focus on the issue of platelet hyperaggregability and thrombosis in HFpEF (Chirkov and Horowitz, 2007; Chung and Lip, 2006; Oktay and Shah, 2015). Platelet function in health and HF will now be discussed, before addressing nitrite as a potential therapeutic intervention for the impairment of NO and platelet dysfunction in HFpEF.

1.3 Platelets and their functions in health

Platelets are derived from the cytoplasm of megakaryocytes and circulate in the blood for approximately 7-10 days at a concentration of ~150-400x10^9/L. These cell fragments are anuclear, however do contain other cellular features, including a cytoskeleton, canalicular and dense tubular systems, mitochondria, peroxisomes and granules (glycogen granules, α-granules and δ granules) (Daly, 2011; Michelson, 2010). Receptors on their surface interact with a large selection of agonists, antagonists and adhesive proteins, predominantly synthesised and secreted by the vascular endothelium and other platelets (Daly, 2011; Jin et al., 2005; Michelson, 2010; Sangkuhl et al., 2011). The downstream effects of these receptor interactions, along with the regulation provided by other signalling molecules (e.g. NO), determine platelet reactivity in a wide range of situations (Jin et al., 2005; Michelson, 2010; Sangkuhl et al., 2011).

Although platelets can be seen to participate in many processes, their primary physiological function is to assist in the formation of haemostatic thrombi during vascular injury (Li et al., 2010; Michelson, 2010). Platelets are often found in close association with the apical surface of the vascular endothelium and during normal physiological conditions, this positioning is desirable as it enables rapid detection of vascular damage (Michelson, 2010). Interactions between platelets and their activating factors (surface-bound and/or soluble) stimulate the subcellular fragments, causing them to bind, secrete and spread in the area of vascular damage. This process leads to the formation of a platelet plug and is known as primary haemostasis (Gale et al., 2011; Michelson, 2010; Palta et al., 2014). Insoluble fibrin generated through the proteolytic coagulation cascade, is then incorporated into the platelet plug for additional strength and stability, during a process recognised as secondary

haemostasis (Gale et al., 2011). Both arms of haemostasis occur simultaneously and are mechanically linked to ensure all effects are localised to the site of injury (Gale et al., 2011; Palta et al., 2014). Figure 1.1 provides an overview of the signalling pathways involved in haemostasis, whilst Sections 1.4 and 1.5 explore the primary and secondary processes in further detail.

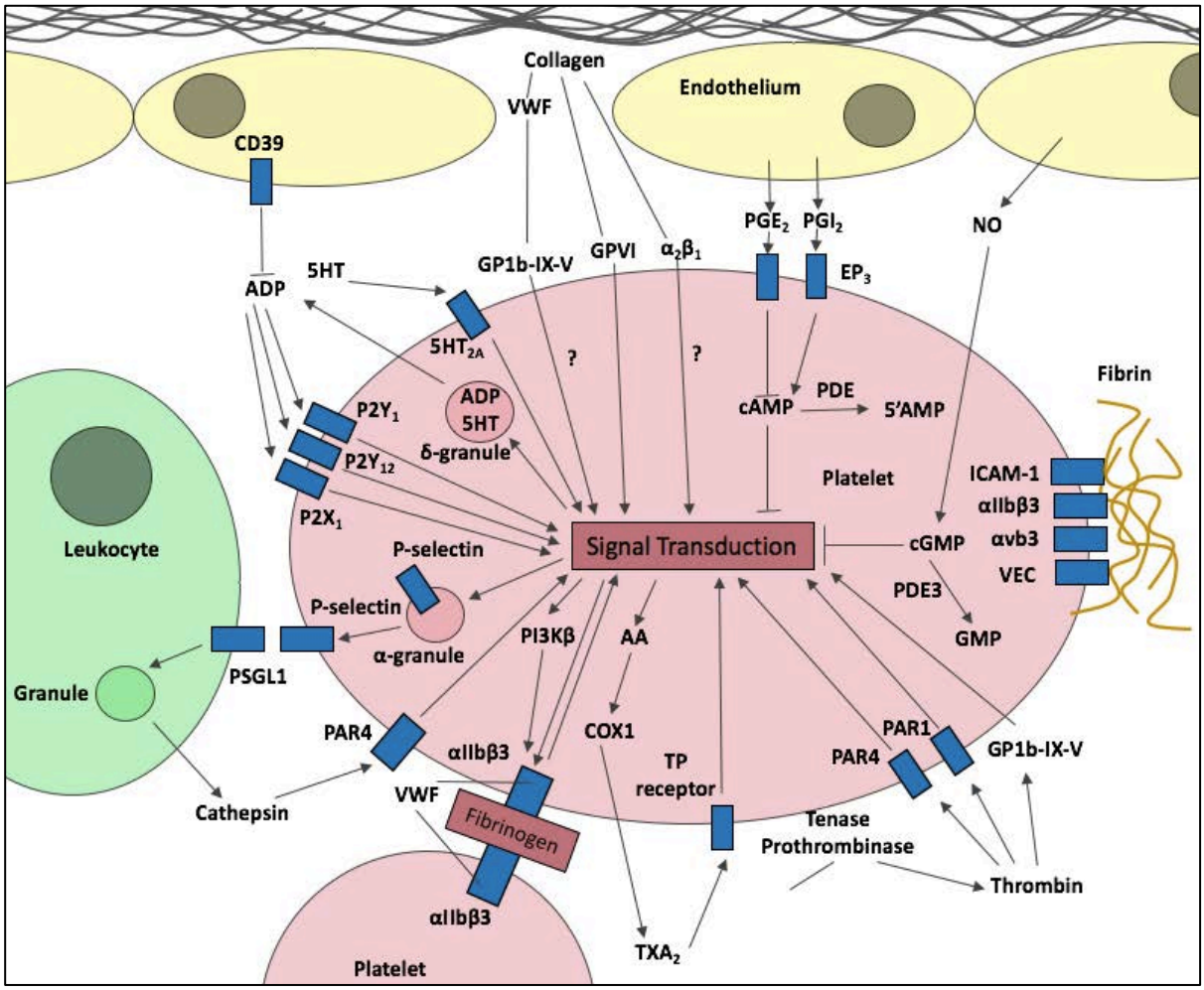

Figure 1.1: <u>Signalling in haemostasis</u>
Figure legend overleaf.
(Adapted from Michelson, 2010)

Figure 1.1 Signalling in haemostasis

At sites of vascular injury, platelet adhesion primarily results from interactions between: **i)** collagen-bound von Willebrand factor (VWF) and the platelet surface glycoprotein 1b (GP1b)-IX-V complex, **ii)** collagen and the platelet surface glycoprotein VI (GPVI), and **iii)** collagen and the platelet surface integrin α2β1. Collagen-GPVI binding initiates a second messenger cascade to cause platelet activation. A number of soluble agonists, including adenosine diphosphate (ADP), serotonin (5HT), thromboxane A2 (TXA_2) and thrombin, also act on platelet surface receptors to bring about platelet activation. ADP and 5HT (secreted from δ-granules following platelet activation) stimulate purinergic ($P2Y_1$, $P2Y_{12}$ and $P2X_1$) and serotonin ($5HT_{2A}$) platelet receptors, respectively. TXA_2 (produced by the platelet cyclooxygenase 1 (COX1)-dependent signalling pathway) interacts with thromboxane prostanoid (TP) receptors on the platelet surface. The terminal serine protease thrombin (produced on the procoagulant surface of activated platelets) stimulates protease activated receptors (PAR-1 and PAR-4)/the GP1b-IX-V complex on the platelet surface. Polymorphonuclear leukocytes (PMN) are also able to activate platelets. The binding of the platelet surface protein, P-selectin (secreted from α-granules following platelet activation), to P-selectin glycoprotein ligand 1 (PSGL1) on the surface of PMNs, activates PMNs. This activation leads to granular release of cathepsin G, which then acts on PAR-4 receptors to cause platelet activation. Platelet-platelet adhesion is primarily mediated by the binding of activated integrin αIIbβ3 to fibrinogen (at high flow rates VWF-integrin αIIbβ3 binding is also required). The close contact between aggregated platelets enables signalling through platelet integrins, junctional adhesion molecules (JAMs) and receptor tyrosine kinases (RTKs). This signalling, and the binding of insoluble fibrin to vascular endothelial-cadherin (VEC), inter-cellular adhesion molecule-1 (ICAM-1) and integrins αIIbβ3/αvb3 on the platelet surface, helps to stabilise the developing thrombus. Thrombus growth and stability is also regulated by a number of inhibitory signals. The action of prostacyclin (PGI_2) on PGI_2 receptors (IP) on the platelet surface, inhibits aggregation through the stimulation of adenylyl cyclase (AC)-cyclic adenosine monophosphate (cAMP)-protein kinase A (PKA) pathway. Nitric oxide (NO) also activates soluble guanylate cyclase (sGC) in platelets, which subsequently synthesises cyclic guanosine monophosphate (cGMP) from guanosine triphosphate (GTP). cGMP inhibits platelets aggregation through protein kinase G (PKG). cAMP and cGMP are rapidly degraded by phosphodiesterase enzymes (PDE).

(Adapted from Michelson, 2010)

1.4 Primary haemostasis

1.4.1 Platelet adhesion

Adhesive interactions between exposed extracellular matrix (ECM) components, such as collagen-bound von Willebrand factor (VWF), collagen, fibronectin, laminin and thrombospondin, and receptors on the surface of platelets, including the glycoprotein 1b-IX-V (GP1b-IX-V) complex, glycoprotein VI (GPVI) and integrins $\alpha_2\beta_1$, $\alpha_2\beta_3$ and $\alpha_6\beta_1$, are generally responsible for initiating thrombus formation at sites of endothelial injury (Figure and Table 1.1) (Gale et al., 2011; Rivera et al., 2009). These primary adhesions can be seen to vary with the rheological conditions (Jackson et al., 2003; Rivera et al., 2009; Savage et al., 1998). At low shear rates, such as in larger arteries and veins, platelet interactions with denuded subendothelial collagen, fibronectin and laminin are primarily responsible for platelet tethering (Jackson et al., 2003; Savage et al., 1998). However, at high shear rates, for example in stenotic arteries and the microvasculature, platelet adhesion becomes more or less reliant on collagen-bound VWF. Under these hemodynamic conditions, transient VWF interactions help to decelerate the platelets, enabling firm bonds with slower binding kinetics to form (e.g. collagen with GPVI or integrin $\alpha_2\beta_1$) (Jackson et al., 2003; Savage et al., 1998). High affinity interactions between VWF and the GP1bα domain of the GP1b-IX-V complex only occur when VWF is immobilized on the ECM (Gale et al., 2011; Schneider et al., 2007; Rivera et al., 2009; Wohner et al., 2012). This is because high levels of shear stress, generated by blood flow over tethered VWF, are required to extend the multimeric glycoprotein and thus reveal it's platelet-binding A1 domain (Gale et al., 2011; Schneider et al., 2007; Rivera et al., 2009; Wohner et al., 2012). The inability of soluble/unbound VWF to make high affinity interactions with platelets helps to prevent unnecessary

adhesions/aggregations under normal circulatory conditions (Gale et al., 2011; Rivera et al., 2009).

ECM components	Receptors on the platelet surface
Collagen-bound VWF	GP1b-IX-V complex
Collagen	GP1b-IX-V complex, GPVI or integrin $\alpha_2\beta_1$
Fibronectin	Integrin $\alpha_2\beta_3$
Laminin	Integrin $\alpha_6\beta_1$
Thrombospondin	GP1b-IX-V complex

Table 1.1: Primary adhesions

1.4.2 Platelet activation

The importance of the interaction between VWF and the GP1b-IX-V complex in platelet adhesion has been clearly defined, but its involvement in platelet activation still remains a controversial topic. Some research groups have detected weak activating signals downstream of VWF-GP1b-IX-V binding, whilst other groups have demonstrated that the GP1b-IX-V complex lacks signalling ability under the above conditions (Jackson et al., 2003). Nonetheless, the interaction between collagen and the constitutively active platelet collagen receptor, GPVI, has been shown to play an important role in early platelet activation (Gale et al., 2011; Mazzucato et al., 2009). As depicted in Figure 1.2, scaffold molecules and protein tyrosine kinases associated with GPVI activate phospholipase C γ2 (PLCγ2), following collagen binding (Stalker et al., 2012). The activated enzyme subsequently hydrolyses membrane phosphatidylinositol-4,5-bisphosphate (PIP_2) to produce second messenger's inositol-1,4,5-trisphosphate (IP_3) and diacylglycerol (DAG) (Jin et al., 2005; Stalker et al., 2012). Next, IP_3 bind receptors on the calcium (Ca^{2+}) storage site. This interaction initiates Ca^{2+} efflux from the dense tubular system and thus causes platelet cytosolic Ca^{2+}

concentration to increase from ~0.1μM in resting platelets to >1μM in activated platelets (Jin et al., 2005; Stalker et al., 2012). An increase in intracellular Ca^{2+} is essential for platelet activation and aggregation due to its association with: **1)** the activation of kinases required for platelet morphological change, such as spreading, **2)** the secretion of platelet granular content, including adenosine diphosphate (ADP) and serotonin (5HT) (Section 1.4.2.1), **3)** the activation of phospholipase A2 (PLA_2; Section 1.4.2.2), **4)** the activation of glycoproteins, such as integrins αIIbβ3 and $\alpha_2\beta_1$ (Section 1.4.3), and **5)** the presentation of a procoagulant surface (Section 1.5) (Jin et al., 2005; Rivera et al., 2009; Sangkuhl et al., 2011; Shin et al., 2017).

Once a monolayer of activated cells has been deposited over the exposed collagen, additional platelets from the flowing blood are recruited to the injury site (Rivera et al., 2009). Recruited platelets are predominantly activated by soluble agonists, such as ADP (Section 1.4.2.1), Thromboxane A_2 (TXA_2; Section 1.4.2.2), thrombin (Section 1.4.2.3) and cathepsin G (Section 1.4.2.4), which readily bind to and stimulate G-protein coupled receptors (GPCRs) on their surface (Figure 1.1 and 1.2) (Jackson et al., 2003; Rivera et al., 2009). Activation of GPCRs then promotes the exchange of guanosine diphosphate (GDP) for guanosine triphosphate (GTP) (the rate-limiting step in guanine nucleotide-binding protein (G-protein) activation), which then causes the associated G proteins (Giα, Gqα or G12α/G13α) to dissociate from the receptor and thus act on a wide range of effectors (Offermanns, 2006). In platelets, the co-ordinated action of soluble agonists on GPCRs brings about a number of effects, including: **1)** phospholipase C β (PLCβ) stimulation (via Gqα) leading to increases in cytosolic Ca^{2+} concentration and protein kinase C (PKC) activation, **2)** p115-Rho guanine nucleotide exchange factor (p115-RhoGEF) stimulation (via G12α/G13α) resulting in actin

skeleton reorganisation and platelet shape change, and **3)** inhibition of adenylyl cyclase (AC) (via Giα) leading to reductions in second messenger cyclic adenosine monophosphate (cAMP) production (Section 1.6.2) (Figure 1.2) (Offermanns, 2006; Rivera et al., 2009; Woulfe et al., 2004). Activated PKC also stimulates granule secretion, whilst morphological platelet changes facilitate the recruitment of additional platelets and neutrophils to the wound site (Offermanns, 2006; Rivera et al., 2009).

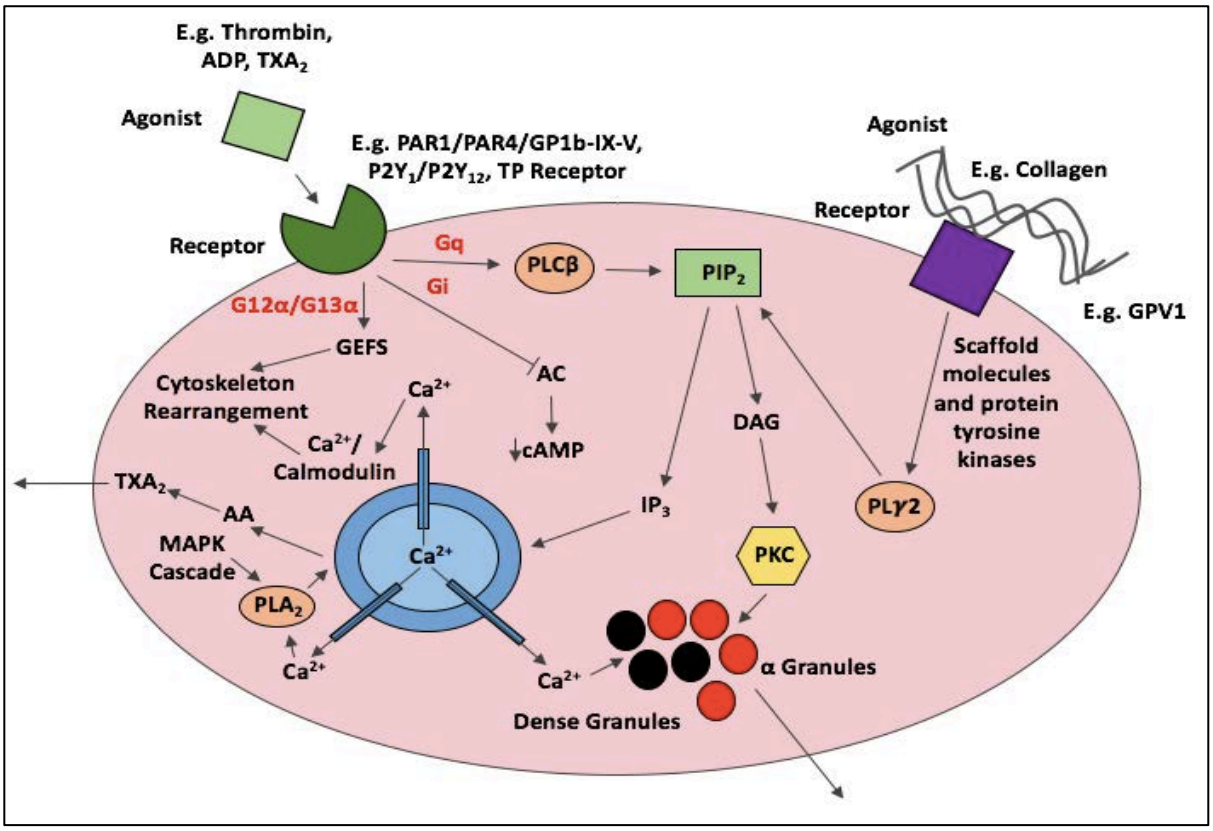

Figure 1.2: <u>Receptor-mediated platelet activation</u>
Platelet activation primarily results from the stimulation of second messenger cascades by receptor-agonist binding. Upon collagen binding, the platelet surface glycoprotein VI (GPVI) receptor activates phospholipase C γ2 (PLCγ2) though associated scaffold molecules/protein tyrosine kinases. Activated PLCγ2 hydrolyses membrane phosphatidylinositol-4,5-bisphosphate (PIP_2) to produce second messenger's inositol-1,4,5-trisphosphate (IP_3) and diacylglycerol (DAG), which then mediate separate activation pathways. IP_3 interacts with receptors on the calcium (Ca^{2+}) storage site to cause Ca^{2+} efflux and thus increase the cytosolic Ca^{2+} concentration. Free Ca^{2+} stimulates platelets by triggering the secretion of platelet granular content and by activating: **i)** kinases necessary for platelet morphological change, **ii)** phospholipase A2 (PLA_2) enzymes of the thromboxane (TXA_2) production pathway, and **iii)** glycoproteins essential for platelet aggregation. PLA_2 is also activated by mitogen-activated protein kinase (MAPK) pathway signalling, whilst DAG-stimulated protein kinase C (PKC) contributes to granule release. Soluble agonists primarily activate G-protein coupled receptors (GPCRs) on the platelet surface. ADP activates purinergic receptors ($P2Y_1$ and $P2Y_{12}$), whilst TXA_2 stimulates thromboxane prostanoid (TP) receptors, and thrombin triggers protease activated receptors (PAR-1 and PAR-4)/the glycoprotein 1b (GP1b)-IX-V complex. Gqα-coupled receptors (e.g. $P2Y_1$, TP, PAR-1 and PAR-4) stimulate phospholipase C β (PLCβ) to bring about increases in cytosolic Ca^{2+} concentration, whilst G12α/G13α-coupled receptors (e.g. TP, PAR-1 and PAR-4) activate guanine nucleotide exchange factors to cause cytoskeletal reorganisations. Adenylyl cyclase (AC) activity, and therefore cyclic adenosine monophosphate (cAMP) production, is inhibited by Giα-coupled receptors (e.g. $P2Y_{12}$, PAR-1). (Adapted from Jin et al., 2005)

1.4.2.1 ADP and 5HT

The soluble agonist ADP is secreted from δ-granules following platelet activation by collagen and/or soluble agonists (Michelson, 2010). Erythrocytes have also been shown to release ADP when in close association with vascular injury. ADP readily binds to purinergic GPCRs, $P2Y_1$ (coupled with Gqα) and $P2Y_{12}$ (coupled with Giα), on the surface of platelets (Gachet, 2008). These interactions lead to a full range of platelet activation events, such as increases in cytosolic Ca^{2+} concentration, protein phosphorylation, shape change, integrin αIIbβ3 activation, TXA_2 synthesis and granule secretion (Figure 2.2) (Gachet, 2008; Rivera et al., 2009). In addition, ADP also binds to $P2X_1$ receptors on the platelet surface. These ATP-gated non-selective ion channels, positively regulate collagen-induced platelet responses through their ability to facilitate Ca^{2+} influx and thus further increase the cytosolic Ca^{2+} concentration (Mahaut-Smith et al., 2011). Additionally, 5HT is also released from platelet δ-granules. 5HT contributes to platelet activation through its action on $5HT_{2A}$ receptors (Gale et al., 2011).

1.4.2.2 TXA_2

Platelet activation also triggers synthesis of the prostanoid TXA_2 in platelets. PLA_2 is an enzyme which liberates arachidonic acid (AA) from membrane phospholipids and is activated by increases in cytosolic Ca^{2+} concentration and/or mitogen-activated protein kinase (MAPK) pathway signalling (Figure 2.2) (Balsinde et al., 2002; Stalker et al., 2012). Released AA is metabolised by constitutively active cyclooxygenase-1 (COX-1) enzymes to form intermediate compounds, endoperoxides PGG_2 and PGH_2. Thromboxane sythetase is responsible for converting PGH_2 to the platelet agonist TXA_2 (Rivera et al., 2009; Stalker et al., 2012). Once produced, TXA_2 is released into the bloodstream, where it acts on

thromboxane prostanoid (TP) receptors (coupled to Gqα and G13α) on the platelet surface to bring about platelet activation events (Figure 2.2) (Rivera et al., 2009).

1.4.2.3 Thrombin

The serine protease thrombin is produced on the procoagulant surface of activated platelets. In addition to its essential role in the coagulation cascade (Section 1.5), thrombin also cleaves protease activated receptors (PARs) on the platelet surface, PAR-1 (coupled to Gqα, Giα and G12/13α) and PAR-4 (coupled to Gqα and G12/13α), to cause a full range of platelet activation events (Figure 2.2) (Gale et al., 2011; Rivera et al., 2009). Due to its high potency (thrombin concentrations as low as 0.1nM can be seen to activate platelets) and the efficient coupling observed between the PARs and PLCβ, thrombin is considered to be one of the most effective platelet activators (Rivera et al., 2009). Furthermore, the GP1bα domain of the GP1b-IX-V complex can also form high affinity bonds with thrombin. These thrombin-GP1b-IX-V complex interactions, which account for ~80-90% of the total protease that binds to platelets, can also provoke a full range of platelet activation events (Celikel et al., 2003; Dumas et al., 2003; Mazzucato et al., 1998).

1.4.2.4 Polymorphonuclear leukocytes

Recruited polymorphonuclear leukocytes (PMN) can also activate platelets (Sambrano et al., 2000; Zarbock et al., 2007). Platelet-PMN adhesions are generally initiated by adhesions between the platelet surface protein P-selectin, which is released from α-granules and subsequently expressed on the platelet surface following platelet activation, and P-selectin glycoprotein ligand 1 (PSGL1) on the surface of PMNs (Zarbock et al., 2007). This interaction subsequently facilitates the release of cathepsin G from PMNs, which in turn acts

on PAR-4 receptors to bring about platelet activation (Figure 2.2) (Sambrano et al., 2000; Zarbock et al., 2007).

1.4.3 Platelet aggregation

Following platelet activation, platelet-platelet adhesions can then form, and this process is known as "platelet aggregation". Platelet aggregation is primarily mediated by the binding of integrin αIIbβ3 to fibrinogen, however at high shear rates, interactions between VWF and integrin αIIbβ3 also contribute to this process (Figure 1.1) (Jackson et al., 2003; Rivera et al., 2009). Before facilitating platelet-platelet adhesions, integrin αIIbβ3 must undergo activation mediated by the cytoskeletal protein talin (Michelson, 2010; Rivera et al., 2009). Once stimulated by platelet activation events (e.g. increases in cytosolic Ca^{2+} concentration), talin interacts with the β3 cytoplasmic domain of integrin αIIbβ3, promoting the dissociation of the cytoplasmic tail/transmembrane domains of the αIIb and β3 subunits. This conformation change is required for αIIbβ3 activation and subsequent fibrinogen binding (Michelson, 2010; Rivera et al., 2009). Activated integrin αIIbβ3 also binds to other ligands which promote platelet aggregation, including collagen, VWF, fibronectin and vitronectin (Gale et al., 2011).

The developing thrombus is then stabilised by a late wave of signalling though integrins, junctional adhesion molecules (JAMs) and receptor tyrosine kinases (RTKs), and by the addition of insoluble fibrin to the aggregate (Section 1.5) (Rivera et al., 2009). This last-minute signalling leads to a host of events that are crucial for thrombus development, including cytoskeleton reorganisation, the formation/stabilisation of large aggregates, clot retraction, and the establishment of a procoagulant surface (Section 1.5) (Watson et al., 2005; Woulfe et al., 2004).

1.5 Secondary haemostasis

Secondary haemostasis is a process that occurs simultaneously to platelet aggregation and describes the involvement of the coagulation cascade in thrombus formation (Gale et al., 2011). Briefly, the coagulation cascade contains a number of serine proteases or factors, which interact to generate thrombin (Figure 1.3) **(**Walker and Royston, 2002). Once activated, thrombin readily cleaves fibrinogen to form insoluble fibrin strands **(**Walker and Royston, 2002; Mackman, 2009). These fibrin strands then bind to a number of receptors on the platelet surface, such as vascular endothelial-cadherin (VEC), inter-cellular adhesion molecule-1 (ICAM-1) and integrins αIIbβ3/αvb3 (Litvinov et al., 2016; Yokoyama et al., 1999). Deposition of a cross-linked fibrin mesh helps to support the developing platelet plug at sites of vascular injury, in addition to stabilising thrombi and preventing premature disaggregation in conditions of high shear **(**Walker and Royston, 2002).

The coagulation cascade is activated through two different pathways: **1)** the extrinsic/tissue factor pathway and **2)** the intrinsic/contact pathway (Figure 1.3) **(**Walker and Royston, 2002; Mackman, 2009). Both pathways converge to activate factor X and factor V, which subsequently combine to form prothrombinase complexes on the surface of platelets. These complexes function to catalyse the conversion of prothrombin to active thrombin, and together with thrombin comprise the common pathway (Figure 1.3) **(**Walker and Royston, 2002). The extrinsic pathway of activation is stimulated by the interactions between tissue factor (TF) (expressed in subendothelial tissue) and factor VII (Kirchhofer and Nemerson, 1996), which in turn leads to the activation of other factors that induce the production of small quantities of thrombin (Gale et al., 2011; Mackman, 2009). In contrast, the intrinsic pathway is activated by thrombin's actions on factor XII (Mackman, 2009). This pathway

utilises phospholipid surfaces, such as the exterior of activated platelets, to facilitate a cascade of zymogen conversions, which subsequently trigger the common pathway to significantly increase thrombin generation/positively regulate coagulation (Figure 1.3) (Gale et al., 2011; Mackman, 2009).

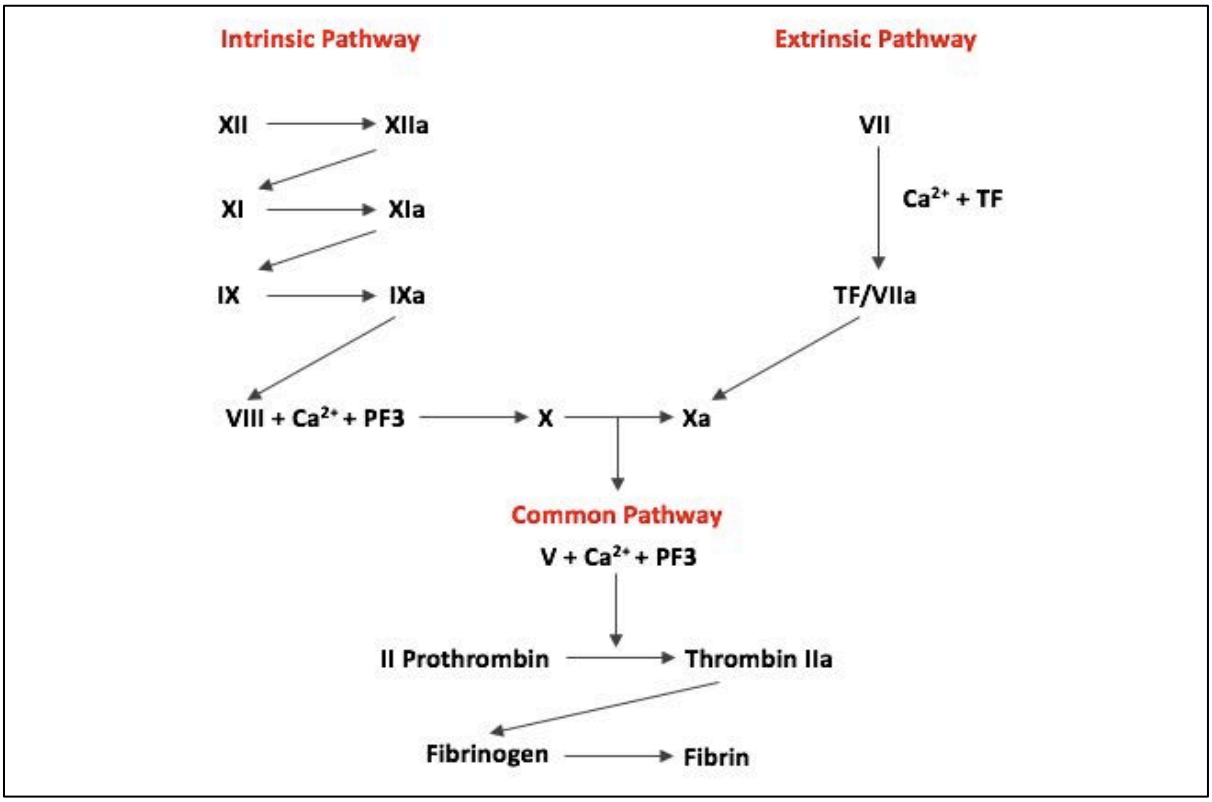

Figure 1.3: <u>Coagulation cascade</u>
The coagulation cascade is divided into three pathways: the extrinsic, intrinsic and common pathways. Firstly, the extrinsic pathway of activation is stimulated by the interactions between tissue factor (TF) and factor VII. Resultant TF/VIIa complexes activate factor X to Xa, hence triggering the common pathway and the production of small quantities of thrombin. The intrinsic pathway however, is stimulated by thrombin's actions on factor XII. The activation of factor XII to XIIa by thrombin leads to a cascade of factor stimulation (e.g. XI to XIa and IX to IXa). Once activated, factor IX then acts with its cofactor (factor VIII) to form tenase complexes, which activate factor X and hence stimulate the common pathway. Activation of the intrinsic pathway significantly increases thrombin production. Lastly, the common pathway consists of prothrombinase complexes, which form when factor Xa and Va combine on the surface of platelets, and thrombin. Prothrombinase complexes function to catalyse the conversion of prothrombin to active thrombin, which then cleaves fibrinogen to form insoluble fibrin strands. Deposition of a cross-linked fibrin mesh helps to support the developing platelet plug at sites of vascular injury. (Adapted from Gale et al., 2011)

1.6 Negative regulators of haemostasis

Under normal physiological conditions, thrombus growth and stability are also regulated by a number of inhibitory signals (Rivera et al., 2009; Stalker et al., 2012). Whilst restricting ECM-mediated platelet activation through its action as a physical barrier, the vascular endothelium also produces a number of these platelet inhibitors, including: **1)** NO, **2)** prostacyclin (PGI_2), **3)** ectonucleotidase CD39, **4)** tissue factor pathway inhibitor, and **5)** protein C (Jin et al., 2005; Stalker et al., 2012; Walker and Royston, 2002). Herein, only NO will be discussed in any further detail, due to the focus of this research project on NO impairment in HFpEF.

1.7 Nitric oxide

NO plays an important role in cardiovascular homeostasis (Förstermann and Sessa, 2012; Gkaliagkousi and Ferro, 2011). NO diffuses across membranes and interacts with a number of intracellular targets to induce various effects, such as regulating blood pressure, cardiac function and the inhibition of platelet aggregation (Gkaliagkousi and Ferro, 2011; Moncada et al., 1991). NO is highly unstable in the presence of oxygen (O_2), as it is rapidly converted to nitrogen dioxide (NO_2), and has an extremely short half-life (~5 seconds) in biological fluids (Gkaliagkousi and Ferro, 2011).

1.7.1 Nitric oxide synthase

Under normal physiological conditions, NO is produced by a family of nitric oxide synthase (NOS) enzymes (Förstermann and Sessa, 2012; Gkaliagkousi and Ferro, 2011). These enzymes produce NO via the ‘classical pathway’ by utilising the substrate L-arginine, oxygen

and a reduced co-substrate, nicotinamide adenine dinucleotide phosphate (NADPH) (Palmer et al., 1988). There are three different NOS enzyme isoforms: **1)** endothelial NOS (eNOS or NOS III), **2)** neuronal NOS (nNOS or NOS I) and **3)** inducible NOS (iNOS or NOS II) (Feng and Tollin, 2009; Förstermann and Sessa, 2012; Gkaliagkousi and Ferro, 2011). eNOS and iNOS are both expressed by endothelial cells and platelets, whilst nNOS is present in the central nervous system, spinal cord, sympathetic ganglia, adrenal glands and peripheral "nitroxidergic" (non-adrenergic and non-cholinergic) neurones (Förstermann and Sessa, 2012; Gkaliagkousi and Ferro, 2011; Randriamboavonjy and Fleming, 2005; Naseem and Riba, 2008). iNOS is produced by various other cell types, including macrophages, neutrophils, smooth muscle cells, cardiomyocytes, hepatocytes and chondrocytes (Soskić et al., 2011). Both eNOS and nNOS are constitutively expressed in cells and synthesise NO in response to increased intracellular Ca^{2+} concentrations, whereas cellular iNOS production is triggered by cytokines and other inflammatory mediators (e.g. lipopolysaccharides) (Palmer et al., 1988).

1.7.1.1 Endothelial nitric oxide synthase

eNOS-derived NO is considered to be the most important inhibitor of platelet aggregation. Endothelial cells and platelets express identical eNOS enzymes, however significantly more NO is produced by the vascular endothelium (Radomski et al., 1990). eNOS enzymes typically function as a dimer and are comprised of two identical monomers (Feng and Tollin, 2009; Förstermann and Sessa, 2012; Gkaliagkousi and Ferro, 2011). Each monomer contains a C-terminal reductase domain and a N-terminal oxygenase domain connected through a Ca^{2+}-calmodulin (CaM) binding domain, which reversibly binds CaM with increases in intracellular Ca^{2+} concentration (Feng and Tollin, 2009; Förstermann and Sessa, 2012;

Gkaliagkousi and Ferro, 2011). Binding sites for NADPH and the cofactors flavin adenine dinucleotide (FAD)/flavin mononucleotide (FMN) are located on the reductase domain, whilst haem, L-arginine and the cofactor tetrahydrobiopterin (BH_4) interact with the oxygenase domain (Feng and Tollin, 2009; Förstermann and Sessa, 2012). In functional eNOS enzymes, electrons are transferred from NADPH in one monomer to the haem site in the adjacent monomer, via cofactors FAD and FMN (Förstermann and Sessa, 2012; Gkaliagkousi and Ferro, 2011). The formation of eNOS dimers and subsequent interdomain electron transfer, only occurs in the presence of haem (Feng and Tollin, 2009; Förstermann and Sessa, 2012). Once sufficient L-arginine and BH_4 have bound to eNOS, the electrons at the haem site reduce/activate O_2 and oxidise L-arginine to form NO. L-arginine oxidation is a two-stage process, in which L-arginine is transformed into the intermediate, N^{ω}-hydroxy-L-arginine, before being converted into NO (Förstermann and Sessa, 2012). L-citrulline is also formed as a by-product of this process (Förstermann and Sessa, 2012; Gkaliagkousi and Ferro, 2011).

Stimuli that trigger increases in intracellular Ca^{2+} concentration, such as autacoids (e.g. histamine), hormones (e.g. vasopressin and catecholamines) and platelet-derived factors (e.g. ADP, 5HT and thrombin), activate eNOS constitutively expressed in endothelial cells and platelets (Busse and Mülsch, 1990; Gkaliagkousi and Ferro, 2011). eNOS stimulation can also be brought about by Ca^{2+}-insensitive manners (Gkaliagkousi and Ferro, 2011). For example, the activation of phosphatidylinositol-3-kinase (PI3K) and its downstream kinase protein kinase B (Akt), by shear stress, vascular endothelial growth factor (VEGF), oestrogen, bradykinin, insulin or hydrogen peroxide, also leads to the phosphorylation and stimulation of eNOS (Dimmeler et al., 1999; Fulton et al., 1999; Gkaliagkousi and Ferro,

2011). Akt-mediated eNOS activation occurs at basal intracellular Ca^{2+} concentrations due to the rise in the Ca^{2+} sensitivity of the CaM-dependent enzyme (eNOS) following phosphorylation (Gkaliagkousi and Ferro, 2011). Furthermore, eNOS is also phosphorylated by other kinases, such as cAMP-dependent protein kinase and protein kinase A (PKA), which following their activation by shear stress, VEGF, catecholamines, bradykinin or ATP, in turn increase NO production. In contrast, PKC and AMP-activated protein kinase (AMPK) reduce eNOS activity to attenuate NO synthesis (Fleming et al., 2001; Gkaliagkousi and Ferro, 2011; Loot et al., 2009).

1.7.2 The nitric oxide (NO)-soluble guanylate cyclase (sGC)-cyclic guanosine monophosphate (cGMP)-protein kinase G (PKG) signalling cascade in platelets

eNOS-derived NO activates the haem-containing cytosolic receptor, soluble guanylate cyclase (sGC) (Gkaliagkousi and Ferro, 2011; Naseem and Riba, 2008). Once activated, sGC then synthesises cyclic guanosine monophosphate (cGMP) from GTP (Gkaliagkousi and Ferro, 2011). In platelets, cGMP decreases cytosolic Ca^{2+} concentration, predominantly through its principle mediator cGMP-dependent protein kinase/protein kinase G (PKG), to inhibit platelet aggregation. Activation of the NO-sGC-cGMP-PKG signalling cascade brings about these reductions in platelet cytosolic Ca^{2+} concentration by activating the sarco/endoplasmic reticulum Ca^{2+} ATPase (SERCA) pumps, whilst inhibiting IP_3 receptors on the on the Ca^{2+} storage site (Gkaliagkousi and Ferro, 2011; Rao et al., 1990; Trepakova et al., 1999).

Furthermore, stimulation of the platelet NO-sGC-cGMP-PKG signalling cascade prevents platelet aggregation in a number of additional ways (Gkaliagkousi and Ferro, 2011). Firstly,

cGMP is known to inhibit the activation of PI3K in platelets (Gkaliagkousi and Ferro, 2011; Pigazzi et al., 1999). Since PI3K has recently been shown to stimulate integrin αIIbβ3 on the platelet surface, cGMP's actions on this kinase helps to inhibit platelet aggregation by preventing adhesions between integrin αIIbβ3 and fibrinogen (Gkaliagkousi and Ferro, 2011). Moreover, cGMP also indirectly upregulates platelet cytosolic cAMP levels by inhibiting the enzyme phosphodiesterase type 3 (PDE-3), which functions to catalyse cAMP hydrolysis (Gkaliagkousi and Ferro, 2011; Gresele et al., 2011; Naseem and Riba, 2008). The subsequent rise in cAMP, enables the second messenger to work synergistically with cGMP to prevent platelet aggregation (Gkaliagkousi and Ferro, 2011; Naseem and Riba, 2008). cAMP produced by activated AC readily stimulates PKA, which in turn acts on numerous target proteins to reduce cytosolic Ca^{2+} concentration (den Dekker et al., 2002; Schwarz et al., 2001). Activated PKA/PKG also phosphorylate numerous downstream targets, such as TP receptors and vasodilator stimulated phosphoprotein (VASP), to further blunt the platelet activation response (den Dekker et al., 2002; Gkaliagkousi and Ferro, 2011; Naseem and Riba, 2008; Schwarz et al., 2001). Following phosphorylation, TP receptors uncouple from their associated G proteins (Wang et al., 1998). This disruption to receptor function/TXA_2-mediated platelet activation contributes to the prevention of platelet aggregation (Gkaliagkousi and Ferro, 2011; Wang et al., 1998). Moreover, phosphorylation of VASP at Ser^{157} (PKA substrate) and Ser^{239} (PKG substrate), also dampens the platelet activation response (den Dekker et al., 2002; Naseem and Riba, 2008; Lohmann et al., 1997; Schwarz et al., 2001; Wentworth et al., 2006). Many research groups have demonstrated that phosphorylated VASP negatively regulates platelet activation, but the precise mechanism(s) remain unclear (Benz et al., 2016; Wentworth et al., 2006). Finally, phosphorylation of PDE-5 enzymes, which function to hydrolyse cGMP, and IP_3 receptors by PKA also helps to

inhibit platelet aggregation (den Dekker et al., 2002; Gresele et al., 2011; Schwarz et al., 2001).

1.7.3 Nitrosation and nitration in platelets

Recent evidence suggests that NO may also mediate platelet function through cGMP-dependent and -independent pathways, involving protein nitrosation (Gkaliagkousi and Ferro, 2011; Naseem and Riba, 2008). Firstly, protein cysteine thiol groups (-SH) readily react with NO derivatives (e.g. N_2O_3) to produce nitrosothiols (Naseem and Riba, 2008). This nitrosation process is both ubiquitous and reversible, and primarily functions to protect NO from inactivation whilst in the blood (Naseem and Riba, 2008; Stamler et al., 1992). Circulating NO is transported as either protein or non-protein S-nitrosothiols (SNOs) (e.g. S-nitroso-albumin, S-nitrosocysteine and S-nitroso-N-acetylpenicillamine), which release NO according to its availability and/or the oxidative status of the plasma (Rassaf et al., 2002). A number of enzymes and transporters, including membrane-bound protein disulfide isomerase, have been shown to deliver SNO-released NO into the platelet cytosol (Bell et al., 2007; Essex et al., 1995; Kleinbongard et al., 2006). These interactions facilitate intraplatelet NO accumulation and therefore the activation of the NO-sGC-cGMP-PKG pathway (Bell et al., 2007). The cGMP-dependent effects of these NO donors have been demonstrated in a number of experimental models and small clinical trials (Kaposzta et al., 2001; Scatena et al., 2005). For example, a reduction in markers of platelet activation (e.g. P-selectin and integrin αIIbβ3), neutrophil stimulation and asymptomatic embolisms have all been observed following S-nitrosoglutathione (GSNO) treatment (Kaposzta et al., 2001; Langford et al., 1994; Salas et al., 1998; Scatena et al., 2005; Ramsay et al., 1995). GSNO has also been identified as the most potent platelet inhibitor (Scatena et al., 2005).

Moreover, nitrosation of key thiol groups has also been shown to directly modulate the function of many proteins implicated in platelet activation and aggregation (Gkaliagkousi and Ferro, 2011; Naseem and Riba, 2008). For instance, *S*-nitrosation of *N*-ethylmaleimide-sensitive factor (NSF) and integrin αIIbβ3 in platelets, prevents platelet granule secretion and inhibits platelet-platelet adhesions, respectively (Naseem and Riba, 2008; Morrell et al., 2005; Walsh et al., 2007). *S*-nitrosation of NSF also indirectly inhibits platelet aggregation/thrombus formation by preventing the release of mediators that promote platelet, endothelial cell and leucocyte interactions (Gkaliagkousi and Ferro, 2011). Furthermore, S-nitrosation of the enzyme complex NADPH oxidase reduces superoxide (O_2^-) production (Gkaliagkousi and Ferro; Selemidis et al., 2007). Since BH_4 is rapidly oxidised by O_2^-, this nitrosation event helps to maintain cofactor availability, thereby preventing the uncoupling of eNOS and the production of O_2^- by the enzyme (Mueller et al., 2005; Selemidis et al., 2007).

Finally, irreversible protein nitration also mediates platelet function through cGMP-independent pathways (Gkaliagkousi and Ferro, 2011; Naseem and Riba, 2008). Nitration of amino acids containing phenolic rings (e.g. tyrosine) by the reactive oxidant peroxynitrite ($ONOO^-$) has been shown to inhibit platelet aggregation (Gkaliagkousi and Ferro, 2011). These modifications have been linked to the inhibition of COX-1 enzymes and a reduction in platelet surface receptors that interact with collagen and TXA_2 (Boulos et al., 2000; Olas and Wachowicz, 2007).

1.7.4 The biphasic role of nitric oxide in platelets

Although NO has been shown to inhibit platelet aggregation by numerous research groups, recent *in vivo* studies have demonstrated that platelet eNOS also activates platelets and promotes thrombosis in response to low-dose platelet agonists, such as ADP (Marjanovic et al., 2005). The NO-sGC-cGMP-PKG pathway plays an important role in eNOS-mediated platelet activation, whereby increases in cytosolic cGMP stimulates platelet granule secretion, leading to subsequent platelet activation (Li et al., 2003; Marjanovic et al., 2005; Stojanovic et al., 2006). It has therefore been suggested that NO plays a dual role in platelet function, with low concentrations of NO (e.g. NO produced by platelet eNOS) stimulating platelets and higher concentrations of NO (e.g. NO generated by the endothelial eNOS) inhibiting platelet activation and aggregation (Marjanovic et al., 2005). A few research groups however, disagree with this new hypothesis. These scientists question how NO derived from platelet eNOS can be activatory due to the fact that circulating platelets are continually exposed to the high concentrations of NO synthesised by endothelial eNOS (Naseem and Riba, 2008).

1.8 Platelet dysfunction in cardiovascular disease

Platelets play an essential role in cardiovascular thrombosis, and a rise in pro-aggregatory stimuli (e.g. fibrinogen, vWF, P-selectin and noradrenaline) and/or fall in anti-aggregatory substances, such as NO, is often observed during CVD (Chirkov and Horowitz, 2007; Chung and Lip, 2006; Michelson, 2010; Willoughby et al., 2002). As such, therapies that target key pathways of platelet activation and/or boost the levels of anti-aggregatory substances within the bloodstream are frequently used to prevent hyperaggregability and thrombosis in CVD (Michelson, 2010). NO impairment in HF will now be addressed, before moving onto current and potential treatment avenues for this disease state.

1.8.1 Nitric oxide bioavailability and oxidative stress in heart failure

It is estimated that the incidence of embolism and stroke is >9 times greater in HF patients when compared to the general population of the same age group, due to the association of HF with endothelial dysfunction and platelet abnormalities (Bauersachs and Widder, 2008; Chirkov and Horowitz, 2007; Chung and Lip, 2006). Diminished NO bioavailability has been reported in the coronary and peripheral vessels of both HFpEF and HFrEF patients (Fischer et al., 2005; López Farré and Casado, 2001; Yamamoto et al., 2015), whilst has also been shown to impair flow-mediated vasodilation in patients with both ischaemic and non-ischaemic etiologies of HF (Shantsila et al., 2012). This reduction in NO bioavailability results from a number of factors, including decreased eNOS expression, diminished arginine availability, up-regulation of asymmetric dimethylarginine (ADMA; an endogenous eNOS inhibitor) and/or the overproduction of reactive oxygen species (ROS) (Bauersachs and Widder, 2008; Comini et al., 1996; López Farré and Casado, 2001; Smith et al; 1996). Interestingly, numerous studies have also linked reductions in NO bioavailability to

impairments in myocardial perfusion, exercise intolerance, left ventricular remodelling, platelet activation and thrombogenesis in patients with HF (Chung and Lip, 2006; Fischer et al., 2005; López Farré and Casado, 2001).

Oxidative stress occurs when ROS production (e.g. O_2^-, hydrogen peroxide (H_2O_2) and hydroxyl radical (OH^-)) exceeds the capacity of the antioxidant defence systems (e.g. superoxide dismutase (SOD), catalase and glutathione), that function to scavenge and inactivate harmful ROS. For instance, SOD catalyses the breakdown O_2^- into H_2O_2 and O_2, whilst catalase and glutathione promote the decomposition of H_2O_2 into H_2O and O_2 (Förstermann, 2008). Numerous HFpEF and HFrEF studies have reported enhanced levels of O_2^- production (Hiebert et al., 2016). Under these conditions, O_2^- reacts rapidly with NO, causing substantial reductions in NO bioavailability and the formation of the $ONOO^-$ (Arimura et al., 2001; Bauersachs et al., 2001; Bauersachs and Widder, 2008). Several enzymes, such as NADPH oxidase, xanthine oxidase, uncoupled eNOS and enzymes of the mitochondrial respiratory chain are capable of producing O_2^- and have been linked with oxidative stress in HF (Bauersachs and Widder, 2008; Mueller et al., 2005).

As mentioned above, eNOS function is compromised in both HFpEF and HFrEF (Yamamoto et al., 2015). In conditions of oxidative stress, the flow of electrons between the eNOS domains uncouples from NO generation, thus leading to the production of O_2^- and $ONOO^-$ in place of NO (Bailey et al., 2014; Förstermann, 2008). $ONOO^-$ subsequently exacerbates oxidative stress in HF by oxidising/depleting BH_4 reserves, and thus promoting the uncoupling of eNOS dimers into single dysfunctional monomers (Abudukadier et al., 2013; Bailey et al., 2014; Bendall et al., 2005).

1.8.2 Chronic atrial fibrillation in heart failure

CAF, which also represents a major cause of morbidity/mortality in the ageing global population, often coexists with HFpEF (~40%) and HFrEF (~35%) (Lam et al., 2017; Linssen et al., 2011; Procter et al., 2015; Sartipy et al., 2017). As with HF, patients with CAF are associated with intra-arterial thrombosis and thromboembolism (Procter et al., 2015). Procter and colleagues have also recently reported platelet hyperaggregability, in part resulting from impaired NO signalling, in patients with early onset AF (Procter et al., 2015).

1.9 Treatment for heart failure

1.9.1 Nitric oxide donors and 'NO resistance'

Organic nitrates (e.g. glyceryl trinitrate (GTN)) are currently used to treat angina, MI and HF (Bailey et al., 2014; MacAllister, 2000). These NO donors rapidly improve reductions of NO bioavailability observed in patients with HF, but tolerance to these nitrates remains a persisting therapeutic problem (MacAllister, 2000). A number of studies have demonstrated that both the platelets and vasculature from HF patients exhibit reduced responsiveness to NO donors, such as GTN and sodium nitroprusside (SNP), a phenomenon referred to as 'NO resistance' (Anderson et al., 2004; Chirkov and Horowitz, 2007; Rajendran and Chirkov, 2008). ALDH2 is considered to be the principle enzyme responsible for vascular GTN bioactivation and NO release (Li et al., 2006; Mackenzie et al., 2005). However, following prolonged GTN exposure, depletion of ALDH2 reductant/s and subsequent oxidative inactivation of ALDH2 by O_2^- and $ONOO^-$, is thought to contribute to vascular GTN tolerance and thus 'vascular NO resistance' (Chen et al., 2005; Daiber and Münzel, 2015; D'Souza et al., 2011; Mayer and Beretta, 2008). The mechanism(s) behind "platelet NO resistance" remain less defined, but it has been postulated that reversible inactivation of sGC

and/or NO ‘scavenging’ by O_2^- are associated with this phenomenon (Anderson et al., 2004; Rajendran and Chirkov, 2008).

1.9.2 Nitrite as a potential substitute for nitric oxide donors

Nitrite is currently being investigated with the potential of becoming a novel therapeutic agent for many CVDs, including HF and ischaemic heart disease (Borlaug et al., 2015; Calvert and Lefer, 2009; Kevil and Patel, 2010). The physiological importance of nitrite and its precursor nitrate, which were previously considered to be biologically inert metabolic by-products of NO, was revealed following the recent discovery of the ‘nitrate-nitrite-NO pathway’ (Bailey et al., 2014; Borlaug et al., 2016; Lundberg et al., 2008). Nitrite therapy is not associated with the development of tolerance and has been shown to have cardioprotective, anti-aggregatory, anti-hypertensive and anti-apoptotic effects in various experimental models (Bailey et al., 2014; Borlaug et al., 2016**)**. These protective effects have been shown during hypoxic and acidic conditions, and very recently it has been proposed that nitrite may also mediate beneficial effects during normoxic conditions via an alternative mechanism (Borgognone et al., 2015; Omar et al., 2015).

1.9.2.1 Nitrite during hypoxic and acidic conditions

Under hypoxic and acidic conditions, nitrite produces NO via a NOS- and O_2-independent pathway known as the ‘nitrate-nitrite-NO pathway’ (Borlaug et al., 2016; Lundberg et al., 2008). Reduction of nitrite by various nitrite reductases, such as deoxyhaemoglobin, xanthine oxidoreductase (XOR) and ALDH2, helps to maintain NO production during hypoxia and acidosis when NOS function is compromised (Calvert and Lefer, 2009; Vitturi and Patel, 2011). *In vivo,* nitrite is oxidised to nitrate by cellular and acellular mechanisms, but nitrate

can also be reduced back to nitrite via the commensal bacteria within the oral cavity and in the gastrointestinal tract (GIT), and by XOR in host tissues (Bailey et al., 2014; Kleinbongard et al., 2003; Lundberg et al., 2008; Lundberg et al., 2009; Qin et al., 2012). Approximately 25% of circulating nitrate is taken up from the blood via the anion exchange channel sialin and secreted by the salivary glands into the saliva, before being reduced to nitrite by commensal bacteria on the surface of the tongue (Doel et al., 2005; Lundberg et al., 2008; Lundberg et al., 2009; Qin et al., 2012). Once swallowed into the stomach, nitrite is either protonated to form nitrous acid, which gives rise to NO through a series of reactions, or transits into the small intestine where it is reabsorbed into the circulatory pool of nitrite (Bailey et al., 2014; Butler and Feelisch, 2008).

1.9.2.2 Dietary sources of nitrate/nitrite

Green leafy vegetables (e.g. rocket, radish, spinach and beetroot), cured meats and drinking water are major sources of dietary nitrate that contribute to the circulating pool of nitrite (Bailey et al., 2014). For example, increased plasma nitrite levels have been observed within 30 minutes of beetroot juice ingestion, where nitrite levels peaked at 3 hours and remained high for approximately 24 hours (Kapil et al., 2014; McKnight et al., 1997). Once within the oral cavity, dietary nitrate is processed in the same way as described above and this cycle is known as the ‘enterosalivary recirculation pathway’ (Bailey et al., 2014).

1.9.2.3 Nitrite during normoxic conditions

Recent studies have revealed that nitrite can act as a normoxic signalling agent to mediate gene expression, cell proliferation, vasorelaxation, myocardial function and wound healing in a NO-independent fashion (Wang et al., 2012). It has been proposed that it may involve

intermediary $ONOO^-$ or NO_2 formation (Wang et al., 2012), but to our knowledge no further mechanistic information underpinning these effects is available.

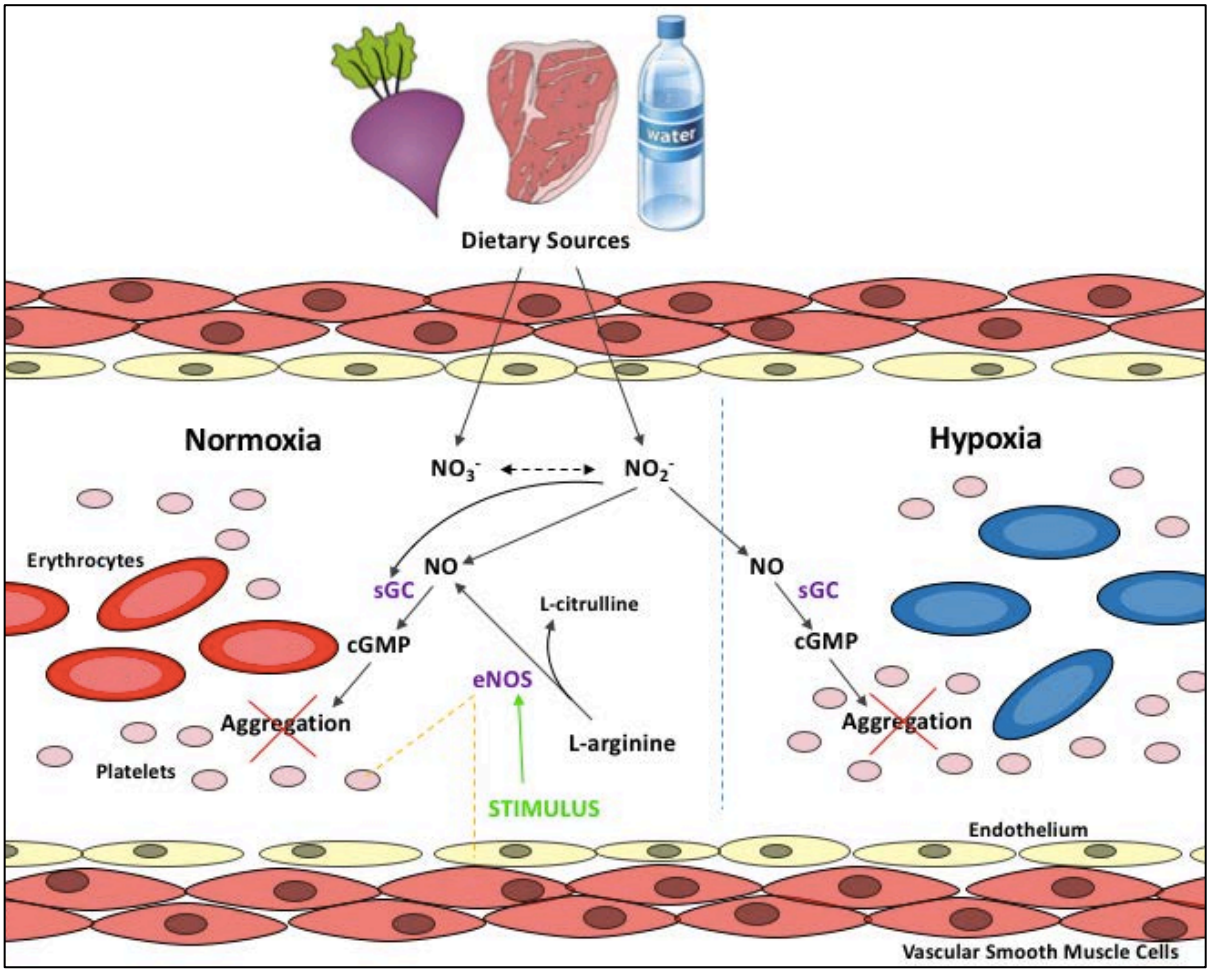

Figure 1.4: <u>'Nitrate-nitrite-NO pathway' in normoxia and hypoxia</u>
Typically, in normoxic conditions, stimuli activate endothelial nitric oxide synthase (eNOS) enzymes constitutively expressed in endothelial cells and platelets, to oxidise L-arginine to NO (L-citrulline is formed as a by-product). eNOS-derived NO activates soluble guanylate cyclase (sGC) in platelets, which then synthesises cyclic guanosine monophosphate (cGMP) from guanosine triphosphate (GTP). cGMP inhibits platelets aggregation through the cGMP-dependent protein kinase/protein kinase G (PKG). In hypoxic/acidic conditions, the 'nitrate-nitrite-NO pathway' produces NO independently of NOS and O_2. Nitrate obtained from dietary sources, such as green leafy vegetables, cured meat and drinking water, is reduced to nitrite and then NO, which can subsequently inhibit platelet aggregation via the sGC-cGMP-PKG pathway. Nitrite also inhibits platelet aggregation in normoxia through both NO-dependent and -independent mechanisms. The NO-independent actions of nitrite have been linked to a direct effect on sGC and are associated with cGMP production. (Adapted from Bailey et al., 2014)

1.9.3 The role of nitrite in HF

Numerous preclinical and clinical studies have demonstrated the beneficial effects of nitrite treatment in HF patients. Short-term infusions of sodium nitrite ($NaNO_2$) has been shown to improve cardiac and pulmonary hemodynamics in HFrEF patients (Ormerod et al., 2015). Whilst, $NaNO_2$ infusion or inhalation have also been shown to attenuate hemodynamic abnormalities (e.g. increased cardiac filling pressures, pulmonary hypertension and insufficient CO reserve) that are present at rest and/or develop during exercise (hypoxic/acidic conditions) in HFpEF patients (Borlaug et al., 2015; Borlaug et al., 2016). Moreover, recent studies in patients with HFpEF have revealed improvements in exercise capacity, vasodilation and CO reserve following dietary nitrate supplementation (beetroot juice) (Borlaug et al., 2016; Eggebeen et al., 2016; Zamani et al., 2015). These improvements have been observed with both single and repeated doses (daily treatments over a one-week period) of oral nitrate (Eggebeen et al., 2016; Zamani et al., 2015). These beneficial effects are postulated to be mediated via the nitrite-NO pathway, and it appears to be prominent during exercise when compared with steady state conditions (Borlaug et al., 2015)

1.9.4 The role of nitrite on platelet aggregation

Numerous whole-blood and platelet rich plasma (PRP) aggregation studies from healthy subjects have shown that nitrite inhibits platelet aggregation through an erythrocyte-dependent mechanism via deoxyhaemoglobin (Corti et al., 2013; Dautov et al., 2014; Parakaw et al., 2017). Velmurugan and colleagues have demonstrated in healthy human volunteers that oral administration of nitrate (beetroot juice or potassium nitrate capsules) increased circulating nitrate and nitrite, and attenuated platelet aggregation in response to ADP/collagen in whole-blood samples (Velmurugan et al., 2013). Furthermore, a reduction in

P-selectin expression and rise in platelet cGMP production were associated with the inhibitory effects of nitrate/nitrite in whole-blood, whilst nitrite had no effect on platelet aggregation in PRP (Corti et al., 2013; Srihirun et al., 2012; Velmurugan et al., 2013). Recent studies have also revealed that in the presence of erythrocytes, nitrite inhibits platelet aggregation via the conversion to NO by the reductase activity of partially deoxygenated haemoglobin, and increases VASP phosphorylation at the Ser^{239} site in platelets (Parakaw et al., 2017; Srihirun et al., 2012).

The involvement of deoxyhaemoglobin in nitrite-NO reduction has also been demonstrated in murine platelet studies (Corti et al., 2013; Park et al., 2013). Firstly, reductions in circulating nitrate and nitrite have been shown to cause increases in platelet activity and ATP release in C57BL/6 mice (Park et al., 2013). A variety of techniques were employed by the research group to manipulate mouse plasma nitrate/nitrite concentration, including antibiotics, NOS inhibitors, low nitrate/nitrite diets and the disruption of the eNOS gene. Interestingly, dietary restriction resulted in the lowest whole-blood values (Park et al., 2013). A prolonged bleeding time was also observed in the C57BL/6 mice following nitrate/nitrite supplementation (via drinking water), when compared to controls and mice on a low nitrate/nitrite diet (Park et al., 2013). Moreover, in eNOS WT and KO mice, nitrite administration resulted in a five-fold greater increase in plasma nitrite levels in KO mice when compared to WT mice (Apostoli et al., 2014). In addition, during an *in vivo* model of radiolabelled platelet aggregation, a rise in plasma nitrite was seen to inhibit platelet function in eNOS KO mice, when compared to WT mice (Apostoli et al., 2014). Nitrite therapy in rats has also been associated with increased plasma nitrate/nitrite concentration and reduced thrombi weight *in vivo*, in addition to the inhibition of whole-blood platelet aggregation in response to collagen *ex vivo* (Kramkowski

et al., 2016). The XOR inhibitor, febuxostat, was shown to partially reverse the anti-thrombotic effects of $NaNO_2$ in rats, whilst the anti-aggregatory effects of nitrite were completely reversed by febuxostat and another XOR inhibitor, allopurinol (Kramkowski et al., 2016).

To date, most studies have investigated the effects of nitrite in whole-blood aggregation and PRP. To determine whether nitrite inhibits platelet aggregation independently of haemoglobin and other plasma proteins, we have recently shown that nitrite inhibits platelet aggregation in washed platelets from young healthy subjects. We showed that high concentrations of nitrite (1mM) increased cGMP generation and phosphorylated VASP at ser^{239} from washed platelets (Borgognone et al., 2015). In addition, another study has demonstrated that isolated platelets can generate transient NO-cGMP signals independently of NOS. These signals were also recorded following $NaNO_2$ treatment and were enhanced with Sildenafil (a PDE5 inhibitor) in both the presence and absence of nitrite (Apostoli et al., 2014). These findings therefore suggest that nitrite can inhibit platelet aggregation independently from haemoglobin and extracellular proteins (Apostoli et al., 2014; Borgognone et al., 2015).

Furthermore, platelet studies have revealed that 1mM nitrite can also trigger cGMP production in isolated platelets, whilst under normoxic conditions (Borgognone et al., 2015). Nitrite was seen to stimulate cGMP generation in these platelets through both NO-dependent and -independent mechanisms (Borgognone et al., 2015). The NO-independent actions of nitrite have been linked to an uncharacterised direct effect on sGC (Borgognone et al., 2015).

1.10 Summary

Since both platelet and vascular responses to NO are impaired in HFpEF when compared to healthy volunteers, due to scavenging of NO with subsequent reduction to sGC, this limits the therapeutic potential of NO donors. Although NO resistance is well understood in the vasculature, the mechanism(s) behind "platelet NO resistance" are far less defined. The potential for the 'nitrate-nitrite-NO pathway' to act as a novel therapeutic strategy for numerous cardiovascular diseases is undoubtedly clear. Since protective effects of nitrite have been observed in numerous HF and platelet studies, this suggests that nitrite may have the potential to act as a novel therapeutic intervention for the impairment of NO and platelet dysfunction in HFpEF. As such, nitrite therapy would help to combat predicted increases in HFpEF morbidity and mortality. To date, the existence of platelet NO resistance in patients with HFpEF and the potential for nitrite to circumvent "platelet NO resistance" in this disease state remains to be elucidated. Considering that CAF often coexists with HFpEF, nitrite will be investigated in two patient cohorts: **1)** patients with HFpEF-AF and **2)** patients with CAF only. We therefore hypothesise that nitrite can circumvent the phenomenon of "platelet NO resistance" in HFpEF-AF patients, independently of NO.

1.11 Objectives

Despite promising scientific discoveries in both experimental and clinical studies on the role of NO and/or nitrite in CVDs, this research project aims to address knowledge gaps relating to the phenomenon of "platelet NO resistance" and the role of nitrite on platelet function in patients with HFpEF-AF.

To support the HFpEF-AF study and develop our understanding of nitrite biology, the effects of nitrite will also be investigated in: **1)** young *vs* old healthy volunteers and **2)** ALDH2 WT *vs* KO mice. These experiments aim to explore the effects of ageing on platelet function and nitrite-mediated inhibition, whilst the animal experiments will address the role of ALDH2 in the anti-aggregatory effects of nitrite and lipidosis.

Several small-scale studies were undertaken and are summarised in chapters as follows:

1) **Chapter 3: Exploration of platelet function and nitrite in young *vs* old healthy volunteers.**

Light transmission aggregation (LTA) experiments will be conducted in healthy volunteers to determine suitable parameters (e.g. collagen concentration) for HFpEF-AF/CAF experiments, whilst exploring the effect of ageing on platelet function and nitrite-mediated inhibition. The potential for nitrite to act synergistically with an sGC stimulator (BAY 41-2272) will also be studied during these LTA experiments. Additionally, to understand the normal physiological $NaNO_2$ mechanism in platelets, the effect of $NaNO_2$ on $VASPser^{239}$ phosphorylation will also be investigated in healthy volunteers using Western blotting.

2) **Chapter 4: Evaluation of the phenomenon of "platelet NO resistance" and nitrite in patients with HFpEF-AF and CAF only.**

Using LTA experiments, we will assess whether "platelet NO resistance" exists in patients with HFpEF-AF and the potential for nitrite to circumvent this phenomenon in HFpEF patients.

3) **Chapter 5: Exploration of the anti-aggregatory effects of nitrite, lipid content and tissue morphology in ALDH2 WT and KO mice.**

In this chapter, we will use ALDH2 WT and KO mice to assess the underlying mechanisms of ALDH2 cardioprotection. LTA experiments will be conducted in ALDH2 WT and KO mice to determine the importance of ALDH2 in the anti-aggregatory effects of nitrite, whilst the lipid content/morphology of ALDH2 WT and KO liver and skeletal muscle tissue will also be investigated using staining.

These additional topics and experiments will be discussed further in their chapters.

Chapter 2: Research methods

2.1 Human experiments

2.1.1 Human ethics

The human experiments adhered to the Declaration of Helsinki and were approved by multiple ethical review committees, including the University of Birmingham Ethical Review Committee and the West Midlands – Coventry and Warwickshire Research Ethics Committee.

2.1.2 Human subjects

Young healthy volunteers (n=13, 9 men and 4 women aged between 21 and 41; mean=28.0±5.8), old healthy volunteers (n=11, 8 men and 3 women aged between 65 and 79; mean=72.3±5.0), HFpEF-AF patients (n=29, 21 men and 8 women aged between 67 and 79; mean=74.3±6.2) and patients diagnosed with CAF in the absence of HF or any known coronary artery disease (n=8, 4 men and 4 women aged between 65 and 86; mean=73.9±7.9) were recruited for washed platelet aggregation experiments. The heathy volunteers and patients were assigned to the pharmacological experiments at random, with each treatment group containing 8-11 participants. Blood obtained from the young healthy volunteers was also used for Western blotting experiments. All healthy volunteers were Caucasian, free of any cardiovascular risk factors, non-smokers, not on any regular medications, and had not taken anti-platelet drugs (such as aspirin and ibuprofen) for 10 days prior to blood donation. Established criteria for HFpEF-AF diagnosis, which included participants who have an EF >55% and persistent AF, was met by all patients (Camm et al., 2010; Lang et al., 2006; McMurray et al., 2012; Shantsila et al., 2016). EF was determined by echocardiography. Patients with CAF demonstrated permanent AF without evidence of HF or coronary artery

disease. Written consent was provided by all the healthy volunteers and patients who participated in the study.

2.1.3 Human washed platelet aggregation study

2.1.3.1 Collection of human blood

Human blood samples were collected as previously described (Pearce et al., 2004; Senis et al., 2009). Firstly, a VACUETTE® Safety Blood Collection Set, containing a winged safety needle, flexible tubing, luer adapter and vacutainer tube holder (Greiner Bio-One; Figure 2.1), was carefully assembled under sterile conditions. First aid pre-injection swabs (70% IPA Alcohol; Robinson Healthcare) were then used to decontaminate the donor's skin at the venepuncture site (the antecubital fossa). A tourniquet, which functioned to distend the donor's veins by limiting blood flow back to the heart, was then applied to the donor's upper arm, roughly a hand width above the venepuncture site. The winged safety needle was then slowly inserted into a visible vein (either the basilic, cephalic or median cubital vein) within the antecubital fossa. Once venous blood began to flow into the flexible tubing, a 9mL vacutainer comprising 3.8% sodium citrate (VACUETTE®; sodium citrate prevented blood coagulation by chelating the calcium within the sample) was inserted into the vacutainer holder, where the vacutainer seal was pierced by the luer adapter (Figure 2.1). Venous blood was then slowly drawn into the vacutainer until the max fill line was reached. Each volunteer donated ~27mL of blood (3x 9mL vacutainers with a 1:9 ratio of sodium citrate to blood). Following the completion of blood donation, the tourniquet was removed and the needle was carefully extracted and discarded. Gauze was then pressed onto the needle entry site to minimise bleeding and prevent bruising. Blood-filled vacutainers were labelled, gently mixed by inversion and then stored at room temperature until further processing was possible.

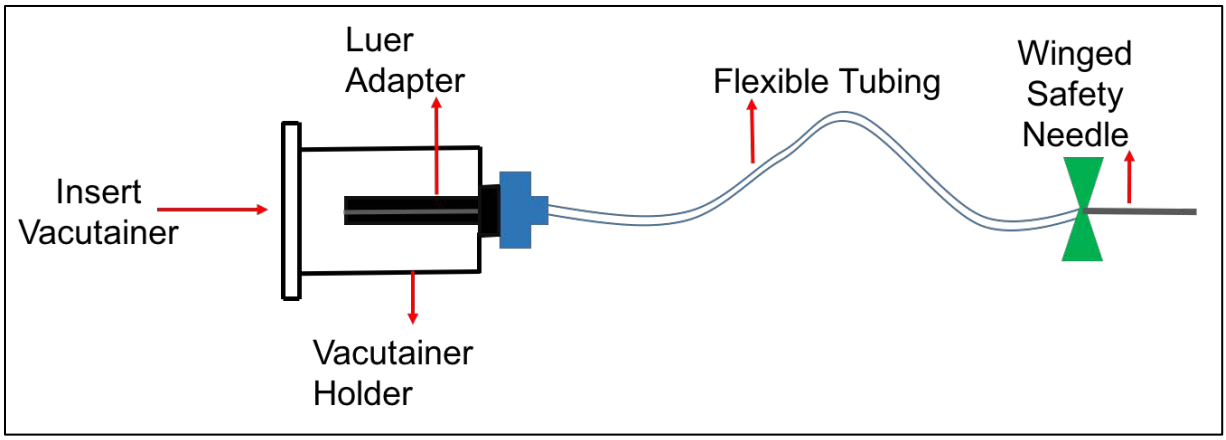

Figure 2.1: Blood collection kit
The blood collection kit was assembled under sterile conditions. To construct the kit, the luer adapter was first detached from the flexible tubing (the luer adapter, flexible tubing and winged safety needle arrived preassembled). The luer adapter was then inserted through the bottom of the vacutainer holder and secured in place by the flexible tubing, which reattached to the luer adapter at the top of the vacutainer holder.

2.1.3.2 Preparation of washed human platelets

A well-established washed platelet protocol from the Watson Research group was used to prepare the human platelets (Borgognone et al., 2014; Jarvis et al., 2002; Pearce et al., 2004; Senis et al., 2009). Briefly, warmed Acid-Citrate-Dextrose (ACD) solution (an anticoagulant and acidifying agent which chelated calcium and regulated pH; Table 2.1) was added to the blood-filled vacutainers at a 1:10 dilution (1mL of ACD was added to 9mL of the blood/sodium citrate mixture). The vacutainers were then gently mixed by inversion, before being centrifuged (Denley BS400 Centrifuge, Swinging Bucket) at 1000rpm (200g) for 20 minutes at room temperature, to fractionate the blood samples (Figure 2.2). The separated plasma was then aspirated (care was taken to avoid the buffy coat; Figure 2.2) and pipetted into sterile 15mL falcon tubes. Approximately 7-10mL of plasma was collected per volunteer. Next, 6µL of 1mg/mL PGI_2 (6µL PGI_2 aliquots were stored at -20°C; Table 2.2) was pipetted into the plasma to prevent premature platelet activation during high speed centrifugation. The plasma was then centrifuged (Denley BS400 Centrifuge, Swinging Bucket) at 3000rpm (1000g) for 10 minutes at room temperature, to pellet the platelets. The resultant supernatant was then aspirated, and the pelleted platelets were re-suspended in 1.5mL ACD (Table 2.1) and 12.5mL Modified Tyrode's Buffer (MTB; on the day of experimentation 45mg glucose had been added to 50mL MTB and the pH had been adjusted (using a H12210 pH meter; HANNA Instruments) to 7.3 at 37°C; Table 2.3).

Reagents *(Manufacturer)*	**Molecular Weight**	**Mass in 1L** (g)
Sodium Citrate.$2H_2O$ *(SIGMA-ALDRICH®)*	294.1	28.48
Glucose *(Fisher Scientific UK)*	180.2	20
Citric Acid.H_2O *(SIGMA-ALDRICH®)*	210.1	16.4

Table 2.1: Masses (g) of reagents required to make ACD solution (1L)

Reagents *(Manufacturer)*		**Mass** (mg)	**Volume** (mL)
Tris Buffer (pH 9.1)	Trizma Base *(SIGMA-ALDRICH®)*	240	
	Hypure™ Cell Culture Grade Water *(Hyclone™)*	-	40
PGI_2	Tris Buffer (pH 9.1)	-	1
	PGI_2 *(Cayman Chemical)*	1	-

Table 2.2: Volumes (mL) and masses (g) of reagents required to make 1mg/mL PGI_2 (2mL)

Reagents *(Manufacturer)*	**Molecular Weight**	**Final Concentration** (mM)	**Mass in 1L** (g)	**Mass in 50mL MTB** (g)
NaCl *(SIGMA-ALDRICH®)*	58.4	134	7.826	-
KCl *(VWR®)*	75.0	2.9	0.218	-
$Na_2HPO_4.12H_2O$ *(SIGMA-ALDRICH®)*	358.1	0.34	0.122	-
$NaHCO_3$ *(Fisher Scientific UK)*	84.0	12.0	1.008	-
HEPES *(SIGMA-ALDRICH®)*	238.1	20.0	4.762	-
$MgCl_2$ *(SIGMA-ALDRICH®)*	95.2	1.0	0.095	-
Glucose *(Fisher Scientific UK)* (*added on the day of the experiment)	180.2	5.0	-	0.045

Table 2.3: Masses (g) of reagents required to make MTB (1L/50mL)

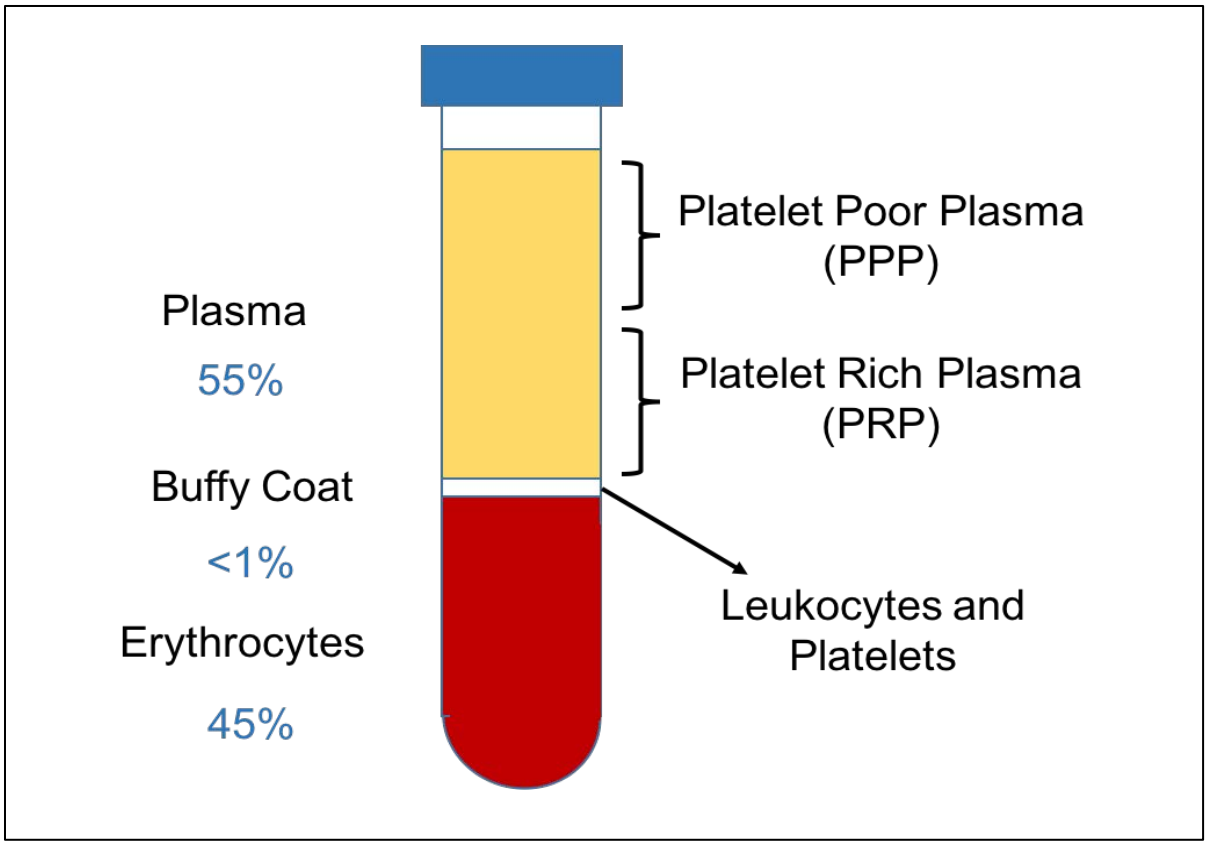

Figure 2.2: Blood fractionation
The unique structure of blood enabled it to be separated into its component parts through centrifugation. When centrifuged at the low speed of 1000rpm (200g), blood samples separated into three fractions: **1)** plasma (55%), **2)** the buffy coat (<1%) and **3)** erythrocytes (45%). The plasma comprised two phases, platelet poor plasma (PPP; plasma containing a low number of platelets, <10,000 platelets/mL) and platelet rich plasma (PRP; plasma containing a high number of platelets), whilst the buffy coat contained leukocytes and a small number of platelets.

2.1.3.3 Human platelet count

A Coulter counter (Z^{TM} Series COULTER COUNTER®; Beckman Coulter) was used to identify the number of platelets present per millilitre of sample (washed human platelets). Firstly, the Coulter system was flushed with isotonic buffered diluent (COULTER® ISOTON®) to ensure that platelet counts were not skewed by previously measured samples. Next, the human platelet samples were diluted (5µL of each sample was added to 10mL of ISOTON) and the platelets were then counted (platelets/mL). Three readings were taken per sample and averages were calculated (platelets/mL).

Next, 6µL of 1mg/mL PGI_2 was added to the washed human platelets. The washed platelets were then gently mixed by inversion and centrifuged (Denley BS400 Centrifuge, Swinging Bucket) at 3000rpm (1000g) for 10 minutes at room temperature, to pellet the platelets for the final time. The supernatant was then aspirated, and the washed platelets were re-suspended in MTB (Table 2.3) at a concentration of $2x10^8$ platelets/mL (Calculation 2.1) for LTA experiments. Before commencing the LTA experiments, the washed platelets were rested for one hour to allow time for PGI_2 degradation (Borgognone et al., 2014; Jarvis et al., 2002; Pearce et al., 2004; Senis et al., 2009).

Example platelet count = $2.487x10^8$/mL in 14mL

$$\frac{\text{Platelet concentration (platelets/mL)} \times \text{Volume (mL)}}{\text{Desired platelet concentration (platelets/mL)}} = \text{Volume of MTB (mL) to add to the platelet pellet}$$

$$\frac{2.487x10^8/\text{mL} \times 14\text{mL}}{2x10^8/\text{mL}} = 17.409 \text{ mL MTB}$$

Calculation 2.1: Example of washed platelet calculation (human platelet samples)

2.1.3.4 Human platelet aggregation

Human LTA experiments were primarily completed to compare the effects of $NaNO_2$ *vs* SNP (NO donor) in washed platelets from age-matched healthy volunteers, HFpEF-AF patients and CAF patients. Additional LTA experiments were also carried out to investigate $NaNO_2$'s mechanism of action in washed platelets from young *vs* old healthy volunteers. NO scavengers, oxyhaemoglobin (OxyHb) and 2-Phenyl-4,4,5,5-tetramethylimidazoline-1-oxyl 3-oxide (PTIO), were used to assess whether $NaNO_2$ was converted to NO under these experimental conditions, whilst the sGC inhibitor, 1-H-[1,2,4]oxadiazolo[4,3-a]quinoxalin-l-one (ODQ), was used to explore the involvement of sGC. BAYER 41-2272 was also used to investigate the potential for $NaNO_2$ to exhibit synergistic activity with an sGC stimulator in washed platelets from young *vs* old healthy volunteers.

The equipment required for the human LTA experiments was prepared during the one-hour platelet rest period. To start, the aggregometer (LUMI-DUAL aggregometer; CHRONO-LOG Corporation) was switched on and set to 37°C (the aggregometer took ~30 minutes to reach 37°C). Next, the cuvettes (CHRONO-LOG Corporation) were prepared. Firstly, magnetic stirrer bars (CHRONO-LOG Corporation) were placed into the cuvettes to enable future sample mixing within the stirring channels of the aggregometer. Each cuvette was also fitted with a spacer (CHRONO-LOG Corporation) to ensure that the platelet samples sat between the light source and the photo cell (light detector) within the stirring channels of the aggregometer. Washed platelet samples were then pipetted into the prepared cuvettes (300µL washed platelets at a concentration of $2x10^8$ platelets/mL/cuvette). Reference blanks containing 500µL MTB (Table 2.3) were also prepared (these cuvettes did not require a

stirrer or spacer) and placed into the 'blank' channels of the aggregometer (Jarvis et al., 2002; Pearce et al., 2004; Senis et al., 2009).

The compounds ($NaNO_2$, SNP, OxyHb, PTIO, ODQ and BAYER 41-2272; Tables 2.4 and 2.5) and collagen dilutions (Collagen Reagens HORM® Suspension, Takeda; agonist used to trigger platelet activation/aggregation; Table 2.6) required for the human LTA experiments were also prepared or appropriately diluted from previously made stock solutions (one exception was OxyHb, which was used at the stock concentration; Table 2.4) during the platelet rest period.

2.1.3.4.1 Oxyhaemoglobin preparation

OxyHb was prepared using a well-established protocol from Professor Martin Feelisch (Kelm et al., 1997; Salvemini et al., 1989). To start, 20mg of human haemoglobin containing a mixture of OxyHb and methemoglobin was dissolved in 1mL of distilled water. Next, >0.6mg of sodium dithionite ($Na_2S_2O_4$; equivalent to a 10-fold molar excess) was added to the haemoglobin solution, which was then stirred and left to air for approximately 10 minutes. During this period, haemoglobin was reduced to its pure oxy-form (excess $Na_2S_2O_4$ reduced methemoglobin to deoxyhaemoglobin, whilst airing facilitated the oxidation of deoxyhaemoglobin to OxyHb).

Excess reductant was then removed from the OxyHb solution by gel filtration through a PD-10 desalting column containing 8.3mL of Sephadex™ G-25 resin (GE Healthcare Life Sciences; column set-up is demonstrated by Figure 2.3). The PD-10 desalting column was first equilibrated with 25mL of distilled water (flow-through collected during the equilibration step was discarded). Next, the OxyHb solution was added to the column (1.5mL

of distilled water was also added to make a total volume of 2.5mL). The desalted/purified OxyHb was then eluted from the column with 3.5mL of distilled water and the middle run of the eluate (~800µL) was collected in a 15mL falcon tube.

The concentration of the OxyHb eluate was then determined spectrophotometrically (GE Healthcare/Amersham Biosciences Ultrospec 3100 Pro UV/Visible Spectrophotometer with a 1cm path length). A small proportion of the OxyHb eluate was first diluted (1:300; 10µL OxyHb in 2990µL distilled water) and the required cuvettes (Fisherbrand®) were then prepared (cuvette 1/reference blank; 1mL of distilled water, and cuvette 2/sample; 1mL of diluted OxyHb eluate). The amount of light absorbed by the reference blank/OxyHb sample was then measured by the spectrophotometer at two different wavelengths (510nm and 542nm; at each wavelength, three readings were taken per cuvette and averages were generated). Once the concentration of the OxyHb eluate had been calculated (Calculation 2.2; the OxyHb sample and reference blank were compared at each wavelength to account for any background absorbance), the OxyHb eluate was appropriately diluted to a stock concentration of 300µM (Calculation 2.2), before being aliquoted (100µL was pipetted into 0.6mL Eppendorf tubes) and stored at -80°C. On the day of experimentation, OxyHb was removed from the freezer, thawed on ice and used at the stock concentration (Table 2.4).

Reagents			**Stock Concentration** (μM)	**Volume Added to the Washed Platelet Samples** (μL)	**Final Concentration Within the Washed Platelet Samples** (μM)
Reagent *(Manufacturer)*	**Mass** (mg)	**Volume** (mL)			
Haemoglobin *(SIGMA-ALDRICH®)*	20	-	300 (100μL aliquots stored at -80°C)	10	10
$Na_2S_2O_4$ *(SIGMA-ALDRICH®)*	>0.6	-			
Distilled Water	-	~30 (* ~30mL distilled water was required for OxyHb preparation, however the final stock solution does not contain this much water).			

Table 2.4: OxyHb preparation (human LTA experiments)

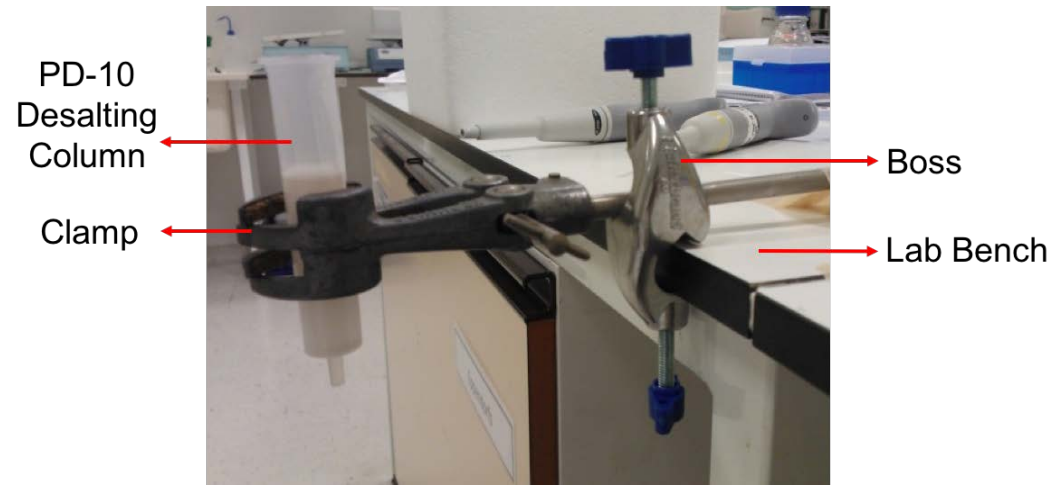

Figure 2.3: PD-10 desalting column setup for OxyHb preparation
The protective cap was first removed from the top of the PD-10 desalting column and the preservative liquid, which maintained the column quality during storage, was discarded. The column was then secured in a clamp in an upright position (the clamp was screwed into a boss attached to a lab bench). Flow-through was collected from the bottom of the column.

Concentration of OxyHb = $\frac{\Delta A_{542-510} * \text{dilution factor}}{\text{(extinction coefficient)}}$

Concentration of OxyHb = $\frac{(0.019-0.000)-(0.001-0.000)*300}{9.61 mM^{-1}cm^{-1}}$

= $\frac{0.018*300}{9.61 mM^{-1}cm^{-1}}$

= 0.561mM (561µM)

Concentration 1 x Volume 1 = Concentration 2 x Volume 2
561µM x 800µL = 300µM x XµL
~~561µM~~ x 800~~µL~~ = 300~~µM~~ x X~~µL~~ (x800)
448800 = 300 x X (÷300)
1496 = X = 1496 µL
1496 – 800 = 696µL

Add 696µL of distilled water to the 800µL OxyHb eluate sample to give a concentration of 300µM (total volume = 1496µL (14 aliquots (100µL)).

Calculation 2.2: Example of OxyHb eluate concentration calculation (human LTA experiments)

2.1.3.4.2 $NaNO_2$, SNP, PTIO, ODQ, BAYER 41-2272 and collagen preparation

To prepare $NaNO_2$, SNP, PTIO, ODQ and BAYER 41-2272 solutions (Table 2.5), the compounds were first weighed out into Eppendorf tubes and then solubilised in their relevant solvents (Eppendorf tubes were vigorously vortexed to dissolve the compounds; Table 2.5). PTIO, ODQ and BAYER 41-2272 solutions were prepared, diluted, aliquoted (into 0.6mL Eppendorf tubes; Table 2.5) and then stored at -20°C until the day of experimentation. When required, the stock solutions were removed from the freezer, thawed on ice and further diluted before use (Table 2.5). Alternatively, $NaNO_2$ and SNP solutions were prepared, appropriately diluted and then used on the day of experimentation (Table 2.5). Three collagen dilutions were also prepared on the day of experimentation. Collagen (taken from a 1mg/mL stock solution) and its diluent were pipetted into Eppendorf tubes, which were then vigorously vortexed to dissolve the collagen (Table 2.6).

All of the above compounds (including OxyHb) and collagen dilutions were stored on ice for the entirety of the human LTA experiments (the compounds/collagen dilutions were briefly removed for regular vortexing).

Compound	Reagents			Stock Concentration	Concentration Following Serial Dilutions (1:10) with MTB		Volume Added to the Washed Platelet Samples (µL)	Final Concentration Within the Washed Platelet Samples
	Reagent *(Manufacturer)*	Mass (mg)	Volume (mL)		Concentrations	Number of Serial Dilutions		
$NaNO_2$	$NaNO_2$ *(SIGMA-ALDRICH®)*	69.00	-	1M	1) 100mM 2) 10mM 3) 1mM	1) 1 2) 2 3) 3	3	1) 1mM 2) 100µM 3) 10µM
	MTB (see Table 4.3)	-	1					
SNP	SNP *(SIGMA-ALDRICH®)*	297.95	-	1M	1) 10µM 2) 1µM	1) 5 2) 6	3	1) 100nM 2) 10nM
	MTB *(see Table 4.3)*	-	1					
PTIO	PTIO *(SIGMA-ALDRICH®)*	23.329	-	100mM (20µL aliquots stored at -20℃)	1) 10mM	1) 1	3	1) 100µM
	100% Ethanol *(BDH PROLABO® VWR Chemicals)*	-	1					
ODQ	ODQ *(SIGMA-ALDRICH®)*	1.8715	-	10mM (50µL aliquots stored at -20℃)	1) 1mM	1) 1	3	1) 10µM
	Dimethyl Sulfoxide (DMSO) *(SIGMA-ALDRICH®)*	-	1					
BAYER 41-2272	Bayer Compound *(provided by Prof Adrian Hobbs, Queen Mary University of London)*	3.6	-	10mM (10µL aliquots stored at -20℃)	1) 10µM 2) 3µM 3) 1µM	1) 3 2) 3 followed by a 3:10 dilution with MTB 3) 4	3	1) 100nM 2) 30nM 3) 10nM
	Dimethyl Sulfoxide (DMSO) *(SIGMA-ALDRICH®)*	-	1					

Table 2.5: $NaNO_2$, SNP, PTIO, ODQ and BAYER 41-2272 preparation (human LTA experiments)

Dilution	**Volume of Collagen** (µL)	**Volume of Diluent** (µL)	**Ratio of Collagen to Diluent**	**Stock Concentration**	**Volume Added to the Washed Platelet Samples** (µL)	**Final Collagen Concentration Within the Washed Platelet Samples** (µg/mL)
1	5	45	1:10	100 µg/mL	3	1
2	30	70	3:10	300 µg/mL	3	3
3	5	-	-	1mg/mL	3	10

Table 2.6: Collagen preparations (human LTA experiments)

2.1.3.4.3 Human LTA experiments

On completion of the platelet rest period, aggregatory responses to collagen (platelet activator/agonist) were recorded under a variety of conditions (Borgognone et al., 2014; Borgognone et al., 2018).

Approximately 34 LTA experiments were completed per healthy volunteer (young and old):

- Collagen (1µg/mL, 3µg/mL ***or*** 10µg/mL) (collagen controls)
- $NaNO_2$ (10µM, 100µM ***or*** 1mM $NaNO_2$) + 3µg/mL collagen
- SNP (10nM ***or*** 100nM) + 3µg/mL collagen
- OxyHb (10µM) + 3µg/mL collagen
- OxyHb (10µM) + $NaNO_2$ (10µM, 100µM ***or*** 1mM $NaNO_2$) + 3µg/mL collagen
- OxyHb (10µM) + SNP (10nM ***or*** 100nM) + 3µg/mL collagen
- PTIO (100µM) + 3µg/mL collagen
- PTIO (100µM) + $NaNO_2$ (10µM, 100µM ***or*** 1mM $NaNO_2$) + 3µg/mL collagen
- PTIO (100µM) + SNP (10nM ***or*** 100nM) + 3µg/mL collagen
- ODQ (10µM) + 3µg/mL collagen
- ODQ (10µM) + $NaNO_2$ (10µM, 100µM ***or*** 1mM $NaNO_2$) + 3µg/mL collagen
- ODQ (10µM) + SNP (10nM ***or*** 100nM) + 3µg/mL collagen
- BAYER 41-2272 (10nM, 30nM ***or*** 100nM) + 3µg/mL collagen
- BAYER 41-2272 (30nM) + $NaNO_2$ (10µM, 100µM ***or*** 1mM $NaNO_2$) + 3µg/mL collagen
- BAYER 41-2272 (30nM) + SNP (10nM ***or*** 100nM) + 3µg/mL collagen

Approximately six LTA experiments were completed per patient (HFpEF-AF and CAF):

- Collagen (3µg/mL) (collagen control)
- $NaNO_2$ (10µM, 100µM ***or*** 1mM $NaNO_2$) + 3µg/mL collagen
- SNP (10nM ***or*** 100nM) + 3µg/mL collagen

When carrying out the collagen controls in healthy volunteers and patients, cuvettes containing washed human platelets were first placed into the incubating channels of the aggregometer, where the samples were heated for four minutes at 37°C. The cuvettes were then transferred to the stirring channels of the aggregometer, which functioned to reproduce vascular wall shear stress, and each contained a light source/photo cell to monitor light transmission through the samples during the LTA experiments (MTB reference blanks, which represented 100% light transmission/aggregation, were positioned behind the washed platelet samples for comparison). Whilst the samples were stirred for one minute at 37°C, the attached chart recorders (CHRONO-LOG Corporation) were set to run (e.g. at 10 squares/minute) and the aggregation baselines were then recorded (Figure 2.5). Next, 3µL of collagen (100µg/mL, 300µg/mL or 1mg/mL; Table 2.6) was pipetted into the washed platelets (300µL) to give a final concentration of 1µg/mL, 3µg/mL or 10µg/mL, respectively (the cuvettes were not removed from the aggregometer whilst collagen was added to the samples). The subsequent changes to light transmission (which were proportional to the extent of platelet aggregation induced by collagen) were monitored for five minutes and graphic readouts/traces of the aggregatory responses were produced in real-time by the chart recorders (Figure 2.5).

For the remainder of the human LTA experiments, washed platelets from healthy volunteers and patients were incubated with one or two of the prepared compounds (see list of LTA experiments above), before being activated with 3µL of 300µg/mL collagen (3µg/mL final concentration in 300µL washed platelet samples; Table 2.6). Firstly, 3µL of $NaNO_2$ (1mM, 10mM or 100mM solutions with final concentrations of 10µM, 100µM or 1mM, respectively; Table 2.5), 3µL of SNP (1µM or 10µM solutions with final concentrations of 10nM or 100nM, respectively; Table 2.5), 10µL of OxyHb (300µM solution with a final concentration of 10µM; Table 2.6) or 3µL of PTIO (10mM solution with a final concentration of 100µM; Table 2.5) was pipetted into the washed platelets as the cuvettes were placed into the incubating channels of the aggregometer (Figure 2.4A). These samples were then incubated for four minutes at 37°C, before being stirred for one minute at 37°C and then activated with collagen (Figure 2.4A). When simultaneously incubating OxyHb or PTIO with $NaNO_2$ (1mM final concentration; Table 2.5) or SNP (100nM final concentration; Table 2.5), the OxyHb/PTIO was pipetted into the cuvettes just prior to the $NaNO_2$/SNP (Figure 2.4A). Moreover, 3µL of ODQ (1mM solution with a final concentration of 10µM; Table 2.5) was incubated with the washed platelets for 19 minutes at 37°C (Figure 2.4B). These samples were also stirred for one minute at 37°C, before being activated with collagen (Figure 2.4B). When simultaneously incubating ODQ with $NaNO_2$ (1mM final concentration; Table 2.5) or SNP (100nM final concentration; Table 2.5), the $NaNO_2$/SNP was pipetted into the cuvettes 15 minutes into the 19-minute ODQ incubation period (Figure 2.4B). Finally, 3µL of BAYER 41-2272 (1µM, 3µM or 10µM solutions with final concentrations of 10nM, 30nM or 100nM, respectively; Table 2.5) was pipetted into the cuvettes as the incubated washed platelets were transferred to the stirring channels of the aggregometer (data published on BAYER 41-2272 was used to determine suitable final concentrations for the LTA

experiments (Roger et al., 2010)). These samples were also stirred for one minute at 37°C and then activated with collagen (Figure 2.4C). When simultaneously incubating BAYER 41-2272 (30nM final concentration; Table 2.5) with $NaNO_2$ (10μM, 100μM or 1mM final concentrations; Table 2.5) or SNP (10nM or 100nM final concentrations; Table 2.5), $NaNO_2$ or SNP was pipetted into the cuvettes four minutes before BAYER 41-2272 (Figure 2.4C).

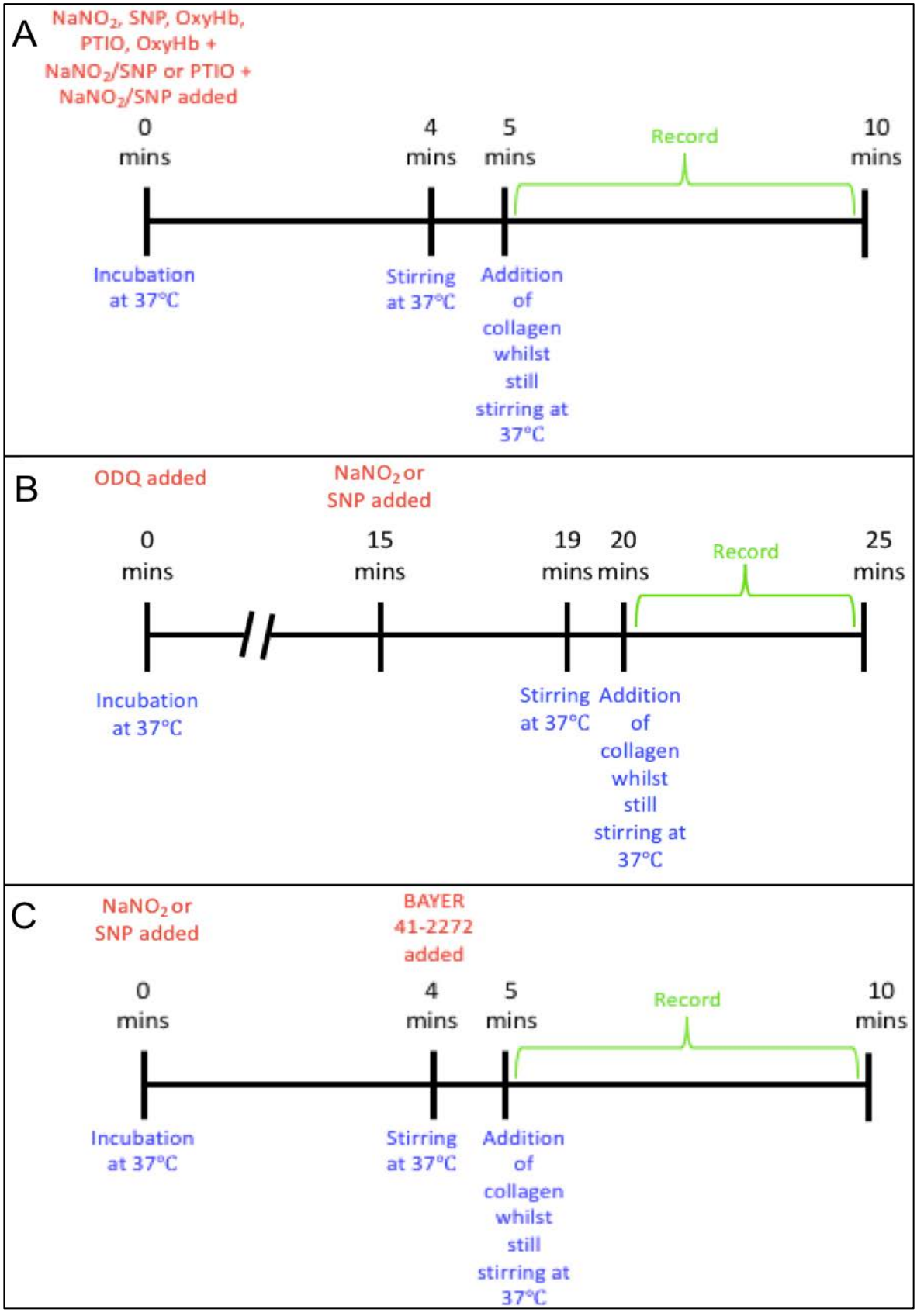

Figure 2.4: Aggregation protocols (human platelet samples)
Figure legend overleaf.

Figure 2.4: Aggregation protocols (human platelet samples)
A) Washed human platelets were incubated for four minutes at 37°C. $NaNO_2$ (at a final concentration of 10μM, 100μM or 1mM), SNP (at a final concentration of 10nM or 100nM), OxyHb (at a final concentration of 10μM) and PTIO (at a final concentration of 100μM) were added to the washed platelets as the cuvettes were placed into the incubating channels of the aggregometer. After one minute of stirring at 37°C, collagen (at a final concentration of 3μg/mL) was added to the samples and the response of the washed platelets to the agonist was recorded for five minutes.
B) Washed human platelets were incubated for 19 minutes at 37°C. ODQ (at a final concentration of 10μM) was added to the washed platelets as the cuvettes were placed into the incubating channels of the aggregometer, whilst $NaNO_2$ (at a final concentration of 1mM) and SNP (at a final concentration of 100nM) were added to the samples 15 minutes into the 19-minute ODQ incubation period. After one minute of stirring at 37°C, collagen (at a final concentration of 3μg/mL) was added to the samples and the response of the washed platelets to the agonist was recorded for five minutes.
C) Washed human platelets were incubated for four minutes at 37°C. $NaNO_2$ (at a final concentration of 1mM) and SNP (at a final concentration of 100nM) were added to the washed platelets as the cuvettes were placed into the incubating channels of the aggregometer, whilst BAYER 41-2272 (at a final concentration of 10nM, 30nM or 100nM) was added to the samples as the cuvettes were transferred to the stirring channels of the aggregometer. After one minute of stirring at 37°C, collagen (at a final concentration of 3μg/mL) was added to the samples and the response of the washed platelets to the agonist was recorded for five minutes.

2.1.3.5 Data analysis (human platelet aggregation)

To quantify the aggregatory responses produced during the human LTA experiments, each trace was analysed as shown in Figure 2.5, and percentage aggregation was then calculated (Calculation 2.3). This data was then transferred to Prism Version 7.0 (Graphpad Software, Inc., La Jolla, CA) for statistical analysis.

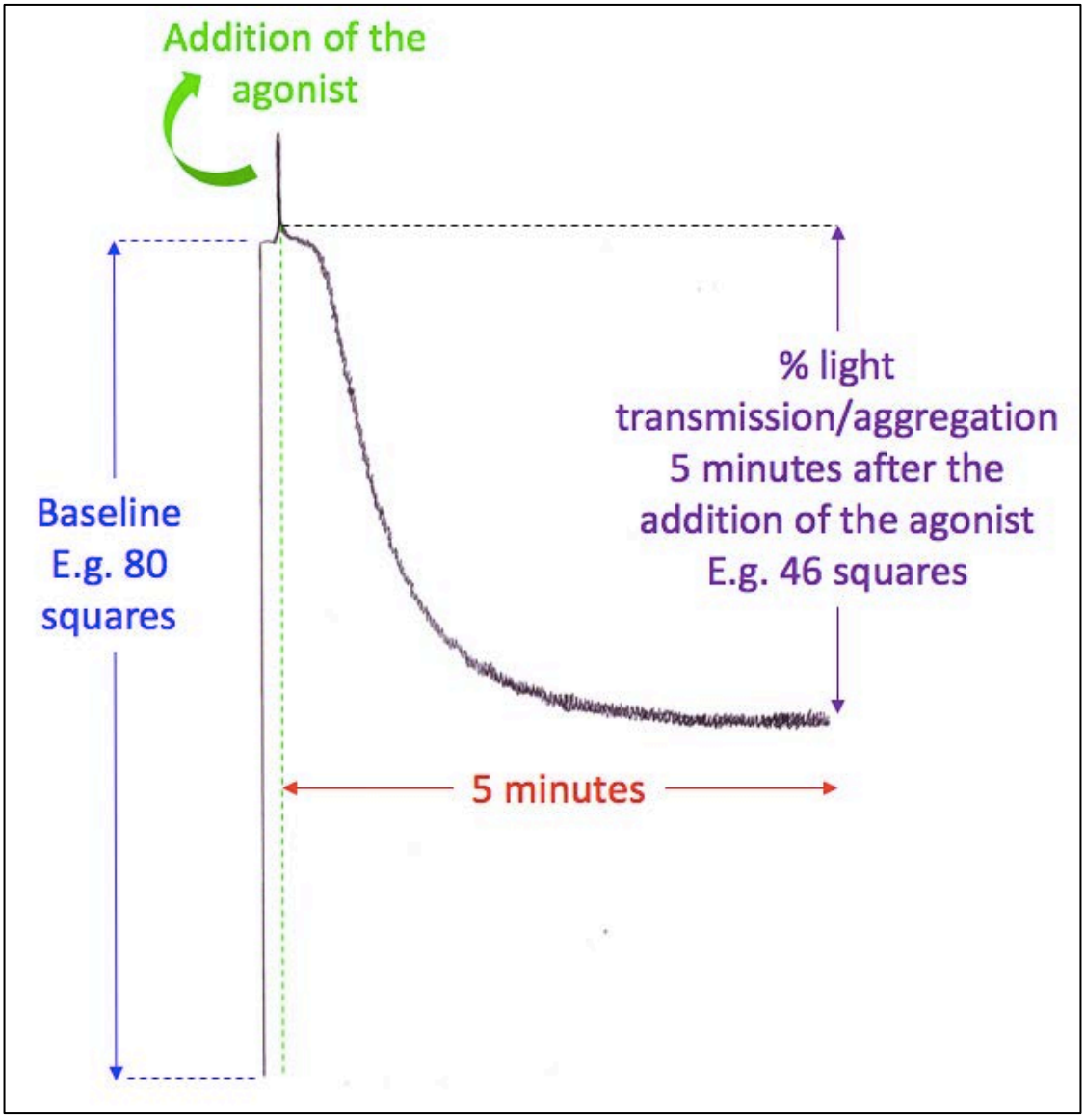

Figure 2.5: Trace analysis
To analyse each trace, the baseline and % light transmission recorded five minutes after the addition of the agonist were measured (grid squares were counted). Percentage aggregation was then established by carrying out the calculation shown below (Calculation 2.3).

$$\left[\frac{\text{\% light transmission 5 minutes after the addition of the agonist (number of squares)}}{\text{Baseline (number of squares)}}\right] \times 100 = \text{\% aggregation}$$

$$\left[\frac{46}{80}\right] \times 100 = 57.5\% = \text{\% aggregation}$$

Calculation 2.3: Example of percentage aggregation calculation for human washed platelet samples

2.1.4 Western blotting (human platelet samples)

2.1.4.1 Platelet homogenate preparation (human platelet samples)

To confirm the involvement of the sGC-cGMP-PKG pathway in $NaNO_2$-mediated inhibition of platelet aggregation, Western blotting analysis was carried out to explore the effects of $NaNO_2$ on the phosphorylation status of the downstream PKG substrate $VASPser^{239}$ (Borgognone et al., 2014; Borgognone et al., 2018). OxyHb, PTIO and ODQ were also used to establish whether the underlying mechanism of $NaNO_2$ was NO-dependent/independent.

To prepare the platelet homogenates, whole-blood samples were first obtained from young healthy volunteers (Section 2.1.3.1). Washed platelets were then prepared as described in Section 2.1.3.2, before being counted, diluted to a concentration of $5x10^8$ platelets/mL for biochemistry experiments (Western blotting) and then rested for one hour (Section 2.1.3.3). During the platelet rest period, the equipment and compounds required to produce the platelet homogenates were prepared. The aggregometer was switched on and set to 37°C, whilst the cuvettes (which contained 300µL of washed platelets at a concentration of $5x10^8$ platelets/mL and a stirrer bar), compound dilutions ($NaNO_2$, SNP, OxyHb, PTIO and ODQ; Sections 2.1.3.4.1 and 2.1.3.4.2) and the 5x reduced Laemmli sample buffer (Table 2.7) were all prepared.

On completion of the platelet rest period, up to 27 platelet homogenates were prepared per young healthy volunteer:

- Washed platelets only
- Washed platelets + 10μM $NaNO_2$ (5, 10, 25 ***or*** 45-minute incubation)
- Washed platelets + 100μM $NaNO_2$ (5, 10, 25 ***or*** 45-minute incubation)
- Washed platelets + 1mM $NaNO_2$ (5, 10, 25 ***or*** 45-minute incubation)
- Washed platelets + 10nM SNP (5, 10, 25 ***or*** 45-minute incubation)
- Washed platelets + 100nM SNP (5, 10, 25 ***or*** 45-minute incubation)
- Washed platelets + 10μM OxyHb
- Washed platelets + 10μM OxyHb + 1mM $NaNO_2$
- Washed platelets + 100μM PTIO
- Washed platelets + 100μM PTIO + 1mM $NaNO_2$
- Washed platelets + 10nM OQD
- Washed platelets + 10μM ODQ + 1mM $NaNO_2$

To prepare the human homogenates, cuvettes containing washed platelets were first placed into the incubating channels of the aggregometer, where the samples were heated for four minutes at 37°C. The cuvettes were then transferred to the stirring channels of the aggregometer, where the washed platelets were mixed for six minutes at 37°C. Once stirred, 75μL of 5x reduced Laemmli sample buffer (Table 2.7) was added to the cuvettes to lyse the washed platelets.

When incubating the samples with increasing concentrations of $NaNO_2$ or SNP, 3μL of $NaNO_2$ (1mM, 10mM or 100mM solutions with final concentrations of 10μM, 100μM or

1mM, respectively; Table 2.5) or SNP (1µM or 10µM solutions with final concentrations of 10nM or 100nM, respectively; Table 2.5) was pipetted into the washed platelets as the cuvettes were placed into the incubating channels of the aggregometer (Figures 2.6A and B). These samples were then incubated for one/four minutes at 37°C, before being stirred for 4, 6, 21 or 41 minutes at 37°C, and then lysed with 75µL of 5x reduced Laemmli sample buffer (Figures 2.6A and B).

OxyHb (10µL, 300µM solution with a final concentration of 10µM; Table 2.6), PTIO (3µL, 10mM solution with a final concentration of 100µM; Table 2.5) or ODQ (3µL, 1mM solution with a final concentration of 10µM; Table 2.5) was also pipetted into the washed platelets as the cuvettes were placed into the incubating channels of the aggregometer (Figures 2.7A and B). Once incubated at 37°C (OxyHb or PTIO; 4 mins, ODQ; 14 mins), the washed platelets were stirred for six minutes at 37°C and then lysed with 75µL of 5x reduced Laemmli sample buffer (Figures 2.7A and B). When simultaneously incubating OxyHb, PTIO or ODQ with $NaNO_2$ (1mM final concentration; Table 2.5), the OxyHb/PTIO was pipetted into the cuvettes just prior to $NaNO_2$, whilst $NaNO_2$ was pipetted into the washed platelets 10 minutes into the 14-minute ODQ incubation period (Figures 2.7A and B).

After the addition of 5x reduced Laemmli sample buffer (Table 2.7), all platelet homogenates were left to stir for a few seconds before being moved onto ice. Once thawed at room temperature, a long-tipped pipette was then used to transfer the platelet homogenates into labelled Eppendorf tubes. The platelet homogenates were stored at -20°C until further analysis.

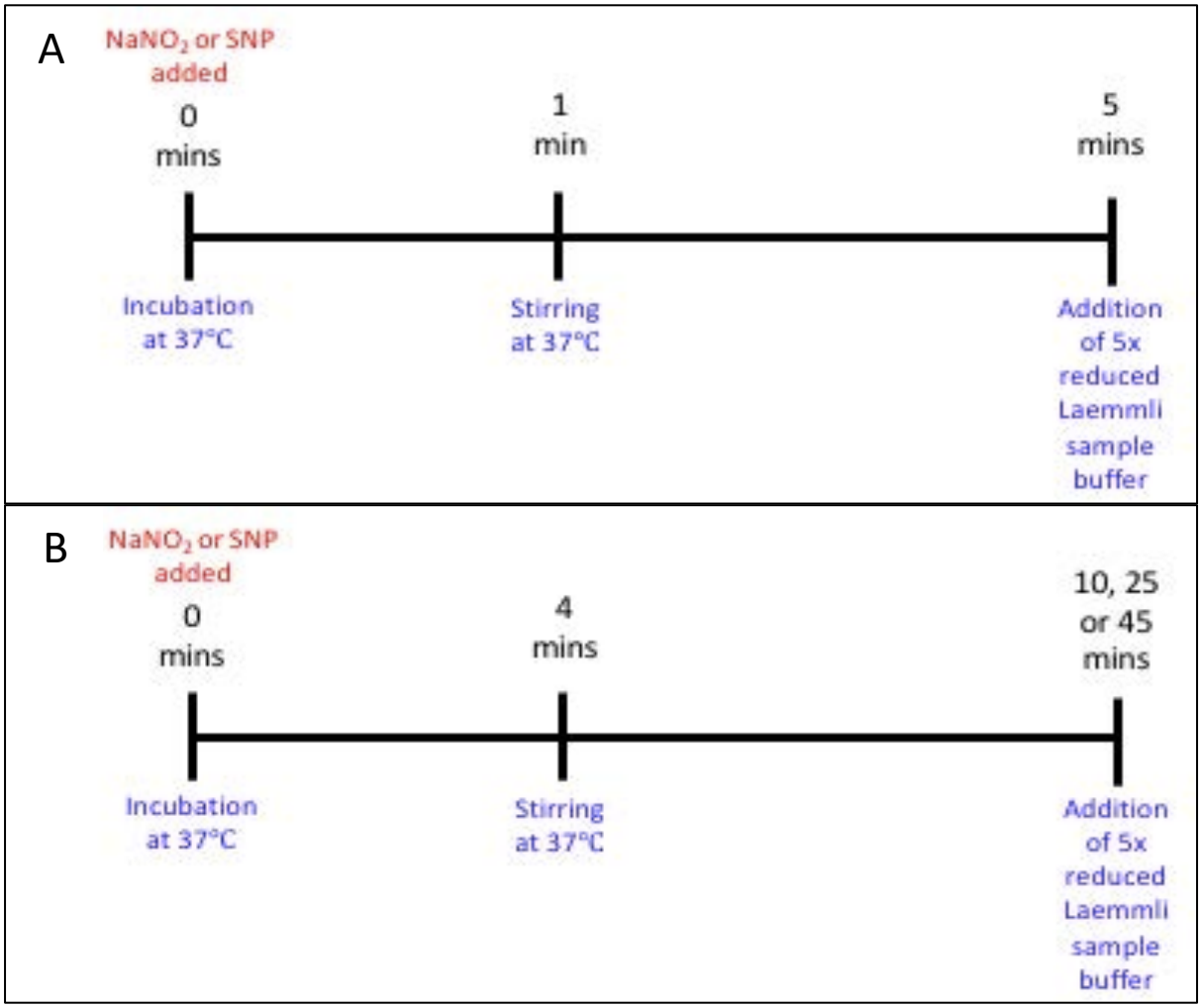

Figure 2.6: Preparation of platelet homogenates 1 (human samples)
A) Washed human platelets were incubated for one minute at 37°C. $NaNO_2$ (at a final concentration of 10µM, 100µM or 1mM) and SNP (at a final concentration of 10nM or 100nM) were also incubated with samples for one minute. The washed platelets were then stirred for four minutes at 37°C, before 5x reduced Laemmli sample buffer was added to the washed platelets to lyse the samples.
B) Washed human platelets were incubated for four minutes at 37°C. $NaNO_2$ (at a final concentration of 10µM, 100µM or 1mM) and SNP (at a final concentration of 10nM or 100nM) were also incubated with samples for four minutes. The washed platelets were then stirred for 6, 21 or 41 minutes at 37°C, before 5x reduced Laemmli sample buffer was added to the washed platelets to lyse the samples.

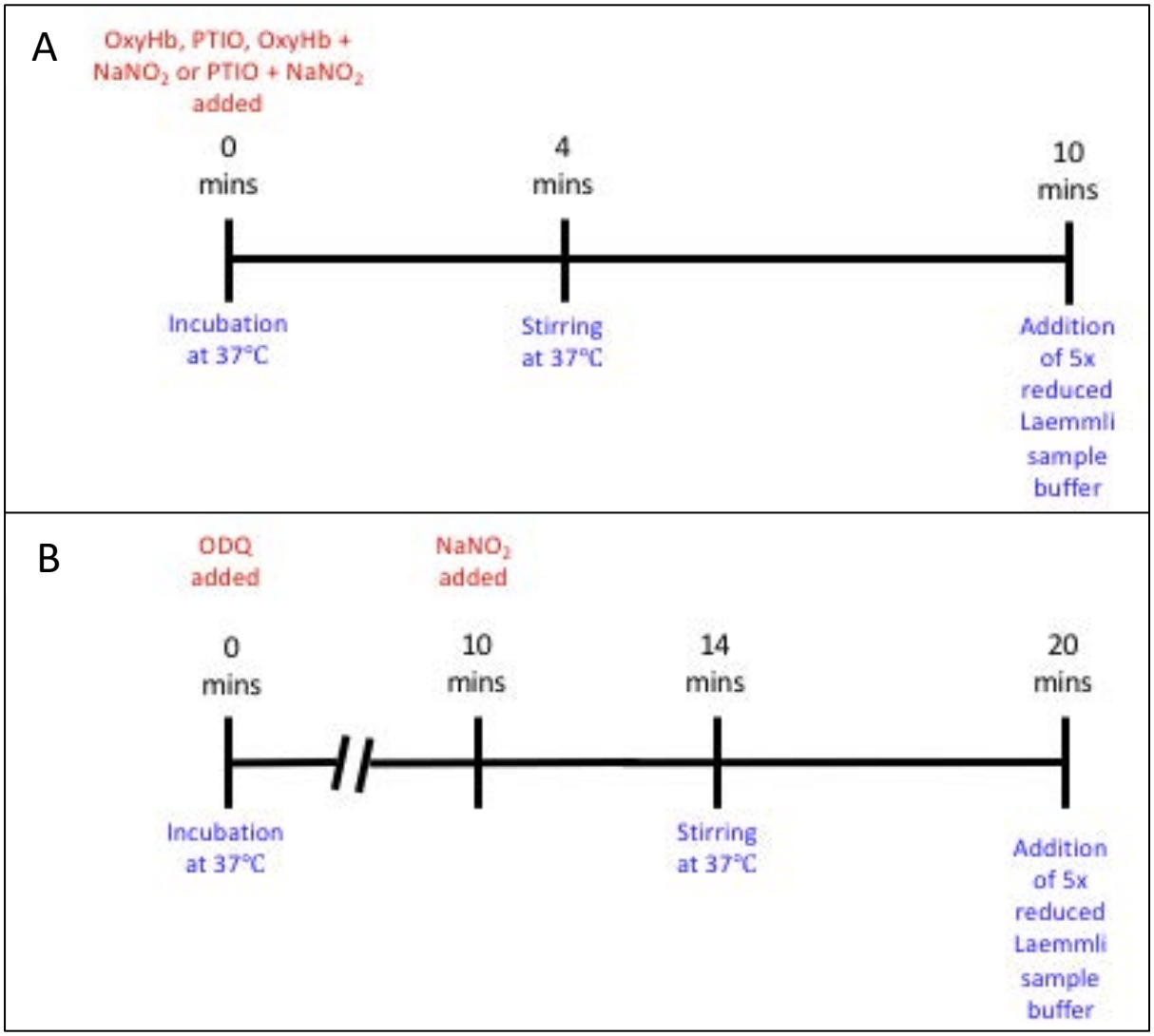

Figure 2.7: Preparation of platelet homogenates 2 (human samples)
A) Washed human platelets were incubated for four minutes at 37°C. $NaNO_2$ (at a final concentration of 1mM), OxyHb (at a final concentration of 10µM) and PTIO (at a final concentration of 100µM) were also incubated with samples for four minutes. The washed platelets were then stirred for six minutes at 37°C, before 5x reduced Laemmli sample buffer was added to the washed platelets to lyse the samples.
B) Washed human platelets were incubated with ODQ (at a final concentration of 10µM) for 14 minutes at 37°C. $NaNO_2$ (at a final concentration of 1mM) was added to the samples 10 minutes into the ODQ incubation period. The washed platelets were then stirred for six minutes at 37°C, before 5x reduced Laemmli sample buffer was added to the washed platelets to lyse the samples.

Reagents *(Manufacturer)*	**Final Concentration in the Reduced Laemmli Sample Buffer** (%)	**5x Laemmli Sample Buffer**		**Function**
		Mass (g)	**Volume** (mL)	
SDS *(SIGMA-ALDRICH®*	2	1	-	An anionic detergent that binds to and neutralises positive charges on sample proteins, to denature secondary/tertiary structures and enable protein separation by size, and not shape, during SDS-PAGE.
β-mercaptoethanol *(SIGMA-ALDRICH®)*	5	-	2.5 *on the day of the experiment β-mercaptoethanol (β-ME) was added to the aliquot of Laemmli sample buffer.	A disulfide reducing agent that disturbs both intra and inter-molecular disulfide bonds, to facilitate protein separation by size during SDS-PAGE.
Glycerol *(SIGMA-ALDRICH®)*	10	-	5	A simple polyol that increases sample density, to aid pipetting and prevent sample spill-over into the buffer.
1M Tris-HCL (pH 6.8) *(Trizma base =SIGMA-ALDRICH®, 37% HCL = VWR®)*	5	-	2.5	An effective buffer solution that regulates lysate acidity and osmolarity.
Brilliant Blue-R *(SIGMA-ALDRICH®)*	Add a trace amount	-	Add a trace amount	A methanol-based protein stain that is required for protein band detection after gel electrophoresis.

Table 2.7: Volumes (mL) and masses (g) of reagents used to make 5x reduced Laemmli sample buffer (10 mL)

2.1.4.2 Sodium dodecyl sulfate–polyacrylamide gel electrophoresis (SDS-PAGE)

Sodium dodecyl sulfate–polyacrylamide gel electrophoresis (SDS-PAGE) gels containing 8% acrylamide (Table 2.8) were constructed using numerous accessories, including casting stands, casting frames, short glass plates, glass spacer plates (1mm) and 10-well combs (Bio-Rad Mini-PROTEAN® Tetra handcast system). The gels produced contained two components: **1)** stacking gel and **2)** resolving gel. The stacking gel functioned to concentrate sample proteins into a single band and thus ensure all proteins started their migration through the resolving gel in unison, whilst the resolving gel separated sample proteins according to their molecular weight. SDS was added to the gels (Table 2.8) and the reservoir buffer (Table 2.9) to neutralise any charges present on the proteins.

Whilst the SDS-PAGE gels were setting, the human platelet homogenates were removed from the -20°C freezer and thawed on ice. Once thawed, the homogenates were lightly vortexed, boiled for five minutes at 95°C (Eppendorf ThermoMixer, C) to ensure complete protein denaturation and then centrifuged (Eppendorf Centrifuge, 5430R) at 1000 RPM for five minutes at room temperature. Long gel loading pipette tips were then used to load the Bio-Rad Precision Plus Protein™ ladder (5µL/well) and platelet homogenates (20µL/well) into the 8% acrylamide gels. Loaded gels were placed into Bio-Rad Mini-PROTEAN® Tetra Systems filled with reservoir buffer (Table 2.9), which were then supplied with 150 volts for one hour and 20 minutes to perform SDS-PAGE.

Reagents *(Manufacturer)*	**Volume** (µL)	
	Resolving Gel (8% Acrylamide)	Stacking Gel (8% Acrylamide)
30% Acrylamide *(National Diagnostics)*	$2.67x10^3$	$9.0x10^2$
Deionised Water	$3.38x10^3$	$4.00x10^3$
1M Tris-HCL (pH 8.8) *(Trizma base =SIGMA-ALDRICH®, 37% HCL = VWR®)*	$3.80x10^3$	-
1M Tris-HCL (pH 6.8) *(Trizma base =SIGMA-ALDRICH®, 37% HCL = VWR®)*	-	720
10% SDS *(SDS=SIGMA-ALDRICH®)*	100	60
TEMED *(SIGMA-ALDRICH®)*	10	10
APS *(SIGMA-ALDRICH®)*	100	100

Table 2.8: Volumes (µL) of reagents used to make 8% acrylamide SDS-PAGE gels (x2)

Reagents *(Manufacturer)*	**Volume** (µL)
10x Reservoir Buffer	$1.0x10^5$
10% SDS *(SDS=SIGMA-ALDRICH®)*	$1.0x10^4$
Distilled Water	$8.9x10^5$

Table 2.9: Volumes (µL) of reagents used to make SDS-PAGE reservoir buffer (1L)

2.1.4.3 Wet transfer

Following the completion of gel electrophoresis, wet transfer was then carried out to transfer the separated proteins from the 8% acrylamide gels onto Amersham™ Hybond™ polyvinylidene fluoride (PVDF) blotting membranes. The components necessary for the wet transfer process (two sponge pads, two pieces of blotting paper and one clamping cassette (Bio-Rad) per gel) were first soaked in ice-cold wet transfer buffer (Table 2.10) for approximately 15 minutes. At the same time, the PVDF blotting membranes were placed into methanol (BDH PROLABO® VWR Chemicals) and then soaked on the shaker for approximately 15 minutes. This process activated the membranes. The PVDF membranes were then removed from the methanol and stored in ice-cold wet transfer buffer for approximately five minutes.

Following apparatus soaking and membrane activation, gel sandwiches (Figure 2.8) were constructed under ice-cold wet transfer buffer to prevent gel dehydration. These sandwiches were then fitted into a Bio-Rad Mini Trans-Blot® Cell, which was filled with ice-cold wet transfer buffer (Table 2.10) and contained an ice pack. The tank was then supplied with 100 volts for one hour and 30 minutes to complete the wet transfer process.

Reagents *(Manufacturer)*	**Volume (µL)**	**Mass (g)**
Trizma Base *(SIGMA-ALDRICH®)*	-	6
Glycine *(SIGMA-ALDRICH®)*	-	28.8
Methanol *(VWR®)*	4.0×10^5	-
Distilled Water	$\sim 1.6 \times 10^6$	-

Table 2.10: Volumes (µL) and masses (g) of reagents used to make wet transfer buffer (2L)

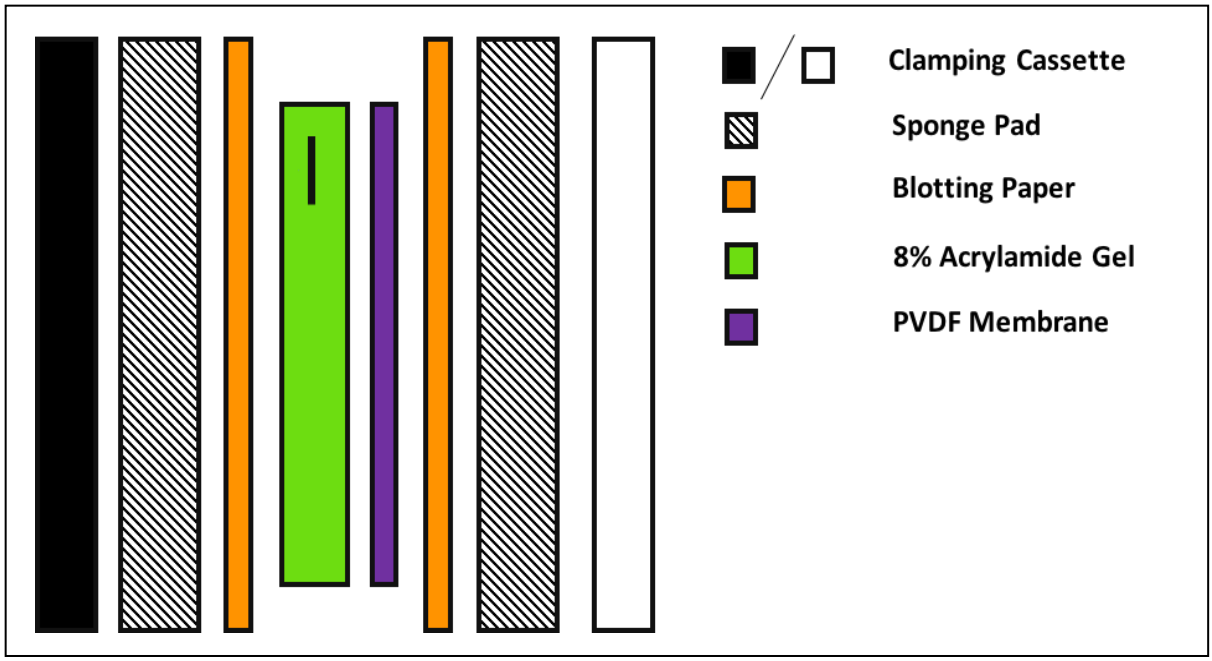

Figure 2.8: Gel sandwich
Gel sandwiches were constructed under wet transfer buffer. A clamping cassette was first opened out and placed into the wet transfer buffer. A sponge pad and piece of blotting paper were then positioned onto the back section (black side) of the cassette. An 8% acrylamide gel (which had been carefully released from its glass plates under distilled water) was then placed onto the blotting paper, ensuring that the ladder was observed on the right-hand side of the gel. Next, a PVDF membrane was positioned onto the gel and a small tube was rolled across the surface of the membrane to remove any air bubbles between the gel and the membrane. A piece of blotting paper and a sponge pad were then placed onto the membrane and the clamping cassette was closed to secure the gel sandwich.

2.1.4.4 Antibody incubation and film development (human platelet samples)

To evaluate the normal physiological $NaNO_2$ mechanism in washed platelets from young healthy volunteers, Western blot analysis was carried out to explore the phosphorylation status of VASPser^{239} (48 and 50 kDa) under a variety of conditions (Section 2.1.4.1).

Following wet transfer, 5% milk (Bio-Rad Blotting-Grade Blocker, non-fat dry milk) in Phosphate Buffered Saline 0.1% Tween (PBS-T) was used to block the PVDF membranes, for two hours at room temperature on a shaker. Once blocked, the PVDF membranes were probed with anti-Phospho-VASP (Ser293) (Table 2.11; Antibody 1) overnight at 4°C on a shaker. The next morning, the membranes were retrieved from the cold room and the primary antibodies were removed (anti-Phospho-VASP (Ser293) was stored at -20°C and used approximately three to five times before being discarded). The membranes were then washed thoroughly with PBS-T for one hour (PBS-T was changed every 15 minutes). Next, anti-Rb IgG (Table 2.11; Antibody 2) was added to the washed membranes and incubated for one hour at room temperature on a shaker. The secondary antibody was then discarded, and the membranes were washed thoroughly with PBS-T for another hour (PBS-T was changed every 15 minutes).

Pierce® Enhanced Chemiluminescence (ECL) Western Blotting Substrate (1mL) was then incubated on the washed membranes for three minutes on a shaker. The ECL was then discarded and the PVDF membranes were gently dabbed onto tissue paper to remove any excess solution, before being mounted into a Hypercassette™. Once within the darkroom, sheets of Amersham Hyperfilm™ were exposed to the membranes (film exposure times are

detailed in Table 2.12). An Xograph Compact X4 Automatic X-Ray Film Processor was then used to develop the films obtained.

Once blotting images had been captured, the membranes were rinsed with PBS-T to remove any residual ECL and then blocked with 5% milk in PBS-T, for two hours at room temperature on the shaker. To enable the reuse of the membranes and for the assessment of control loading, 10% sodium azide (50µl) was added to the milk after the first hour of blocking to inhibit any Horseradish Peroxidase (HRP)-conjugate secondary antibodies residing on the membranes. Next, the membranes were probed for the loading control, α-Tubulin, using Anti-α-Tubulin (Table 2.11; Antibody 3), which was incubated on the membranes overnight at 4°C on a shaker. The next morning, the membranes were retrieved from the cold room and the primary antibodies were removed (Anti-α-Tubulin was stored at -20°C and used approximately five times before being discarded). PBS-T was then used to thoroughly wash the membranes for one hour (PBS-T was changed every 15 minutes). Following washing, Anti-Ms IgG (Table 2.11; Antibody 4) was applied to the washed membranes and incubated for one hour at room temperature on a shaker. After the secondary antibody was discarded, the membranes were once again washed with PBS-T for one hour (PBS-T was changed every 15 minutes), before being incubated with ECL and then developed as described above. Film exposure times are detailed in Table 2.12.

	Antibody *(Antibody code, Antibody type)*	Manufacturer	Dilution factor used
1	Anti-Phospho-VASP (Ser293) Rb pAb *(3114, Primary Ab)*	Cell Signalling	1:1000 in 5% BSA/PBS-Tween
2	Anti-Rb IgG HRP-linked Gt pAb *(7074, Secondary Ab)*	Cell Signalling	1:10,000 in 1% Milk/PBS-Tween
3	Anti-α-Tubulin Ms mAb *(T6199, Primary Ab)*	SIGMA-ALDRICH®	1:5000 in 5% BSA/PBS-Tween
4	Anti-Ms IgG HRP-linked Gt pAb *(P0447, Secondary Ab)*	Dako	1:10,000 in 1% Milk/PBS-Tween

Table 2.11 Western blotting antibodies (human platelet samples)

For each antibody used during the human platelet study, this table details: their classification, their code, their manufacturer and the dilution at which they were used during Western blotting. Goat (Gt), Rabbit (Rb), Mouse (Ms), Antibody (Ab), Polyclonal Antibody (pAb), Monoclonal Antibody (mAb) and Horse Radish Peroxidase (HRP).

Primary Antibody	**Secondary Antibody**	**Exposure Time** (Seconds)
Anti-Phospho-VASP (Ser293)	Anti-Rb IgG	600
Anti-α-Tubulin	Anti-Ms IgG	20

Table 2.12: Optimum exposure time of the Amersham Hyperfilm™ to each membrane

2.1.4.5 Data analysis (Western blotting)

To quantify the protein bands on the VASP Western blot films, densitometric analysis was carried out using Adobe® Photoshop® CS Version 8.0. The densitometry data collected was then transferred to Prism Version 7.0 (Graphpad Software, Inc., La Jolla, CA) for statistical analysis.

2.2 Animal experiments

2.2.1 Animal ethics

Adult male ALDH2 wild type (WT) and knockout (KO) mice (25-30g, background C57BL/6 mice; supplied by RIKEN, Japan) were used throughout the research project. The experimental procedures performed on the mice had been approved by the UK Home Office and adhered to the UK Animals (Scientific Procedures) Act 1986. Cervical dislocation was used as a schedule one method for culling mice in the present study.

2.2.2 Genotyping

The ALDH2 breeding colony was maintained with heterozygous (HET) mice paired with either (i) HET, (ii) WT and/or (iii) KO mice. Regular genotyping was therefore necessary to identify male ALDH2 WT and KO mice for experimentation. The deoxyribonucleic acid (DNA) required for genotyping was obtained from mouse ear clippings, which were stored (at -20°C) until further analysis was possible (Section 2.2.2.1).

2.2.2.1 Sample digestion, DNA isolation and extraction

DNA AWAY™ surface decontaminant (ThermoFisher Scientific) was used to degrade traces of DNA contaminating the laboratory benches and equipment required for genotyping. DNA AWAY™ was sprayed before each major step in the genotyping protocol (Sections 2.2.2.1, 2.2.2.2 and 2.2.2.3) and left to stand for two minutes. The surfaces and equipment were then dried thoroughly using disposable paper towels.

An ISOLATE II genomic DNA Kit (BIOLINE) was used according to the manufacturer's guidelines to digest the tissue samples, and to isolate and extract their contained DNA.

Firstly, samples (a maximum of 11 at any one time) were removed from the -20°C freezer and allowed to defrost for a short period of time. Lysis buffer GL (180µL; BIOLINE) and the peptidase proteinase K (25µL; BIOLINE) were then added to each tissue sample. Next, the samples were thoroughly vortexed (WhirliMixer™, Fisons Scientific Equipment), before being heated at 56°C, 300rpm (Eppendorf ThermoMixer, C) for minimum of two hours. Each sample was completely immersed by the proteinase K/lysis buffer GL mixture to ensure that all proteins and cell membranes were effectively digested.

Following tissue digestion, the lysates were removed from the heating block and vigorously vortexed. Lysis buffer G3 (200µL; BIOLINE) was then added to the Eppendorf tubes and the lysates were vortexed, before undergoing a 10-minute incubation at 70°C to denature proteinase K. The lysates were then transferred back to room temperature and vortexed once again. Next, ethanol (200µL, 96-100%; BDH PROLABO® VWR Chemicals), which functioned to precipitate the DNA from the aqueous solutions, was added to the Eppendorf tubes and the lysates were vigorously vortexed.

The lysates were then transferred from the Eppendorf tubes to labelled genomic DNA spin columns containing silica gel membranes (BIOLINE). The lysate-filled spin columns were then centrifuged at 11,000xg for one minute at room temperature (Eppendorf Centrifuge, 5430R). This spinning process forced the lysates through the silica membranes, thus facilitating interactions between the DNA and the silica surface. The flow-through collected from each lysate was discarded from the collection tubes.

Impurities and enzyme inhibitors were then removed from the membrane-bound DNA with a three-stage washing and drying process. Firstly, wash buffer GW1 (500µL; BIOLINE) was pipetted into the spin columns, which were then centrifuged at 11,000xg for one minute at room temperature. The resultant flow-through was discarded. Wash buffer GW2 (600µL; BIOLINE) was then pipetted into the spin columns. Once again, the columns were centrifuged at 11,000xg for one minute at room temperature and the flow-through was discarded. Finally, a dry spin (11,000xg for one minute at room temperature) was carried out to eradicate any residual ethanol from the membrane-bound DNA. This step was essential due to the ability of the ethanol to significantly inhibit the polymerase chain reaction (PCR; Section 2.2.2.2).

The spin columns were then transferred from the collection tubes to autoclaved, labelled 1.5mL Eppendorf tubes. The isolated/purified DNA was then extracted from the silica membranes using elution buffer G (100µL; BIOLINE, a low ionic strength buffer), which had been previously heated to 70°C. The eluent was applied directly onto the silica membranes and left to incubate at room temperature for one minute. The spin columns were then centrifuged for a final time at 11,000xg for one minute at room temperature. The flow-through collected contained the purified DNA and was stored in the fridge prior to PCR (Section 2.2.2.2).

2.2.2.2 Polymerase chain reaction

PCR was then used to amplify specific fragments within the extracted DNA. This expansion process facilitated the detection of the DNA fragments, following the separation of the PCR products by gel electrophoresis (Section 2.2.2.3), and thus enabled the identification of mouse genotype. To avoid contamination, PCR reagents/samples were prepared under sterile conditions (safety cabinet; Thermo Scientific Holten Safe 2010). Firstly, master mix components (Tables 2.13 and 2.14) were pipetted into a 1.5mL Eppendorf tube and then thoroughly mixed by inversion. PCR samples, which contained 18.5µL of master mix and 1µL purified DNA, were then prepared in autoclaved, labelled PCR tubes. Three positive controls (18.5µL master mix + 1µL purified HET, WT or KO DNA from previously genotyped mice) and one negative control (18.5µL master mix) were also prepared. Once mixed by inversion, the PCR samples and controls were transferred to a thermocycler 48 PCR machine (SENSOQUEST) and the ALDH2 PCR programme (Figure 2.9) was initiated.

Reagents *(Manufacturer)*	**Volume per Sample** (µL)	**E.g. Volume for 10 Samples (5 samples, 3 positive controls, 1 negative control and 1 extra 'sample' to allow for any pipetting errors)** (µL*)*
Ready Mix PCR Master Mix (2x concentrated solution of Taq DNA polymerase, DNA nucleotide bases and all components required for PCR (e.g. buffer to ensure the right conditions for the reaction), excluding the DNA template and relevant primers) *(ThermoFisher SCIENTIFIC)*	10	100
Primer 1 (ALDH2_F1) *(SIGMA-ALDRICH®)*	1	10
Primer 2 (ALDH2_Int3_Rv) *(SIGMA-ALDRICH®)*	1	10
Primer 3 (ALDH2_R3) *(SIGMA-ALDRICH®)*	0.5	5
Hypure™ Cell Culture Grade Water *(Hyclone™)*	6	60

Table 2.13: Volumes of reagents (µL) used to produce the PCR master mix

Primer Name *(Manufacturer)*	**Primer Direction**	**Primer Sequence**	**Length** (bp)	**Bands Recognised** (bp)
ALDH2 _F1 *(SIGMA-ALDRICH®)*	Forward	*CCGTACTGACTGTCCCATGCAGTGCT*	26	WT band at 597 and KO band at 280
ALDH2_Int3_Rv *(SIGMA-ALDRICH®)*	Reverse	*GTTCACTCTGGTGACCACCATAGAG*	25	WT band at 597
ALDH2_R3 *(SIGMA-ALDRICH®)*	Reverse	*GGTGGATGTGGAATGTGTGCGAGGC*	25	KO band at 280

Table 2.14: ALDH2 primers used at a final concentration of 10µM during PCR

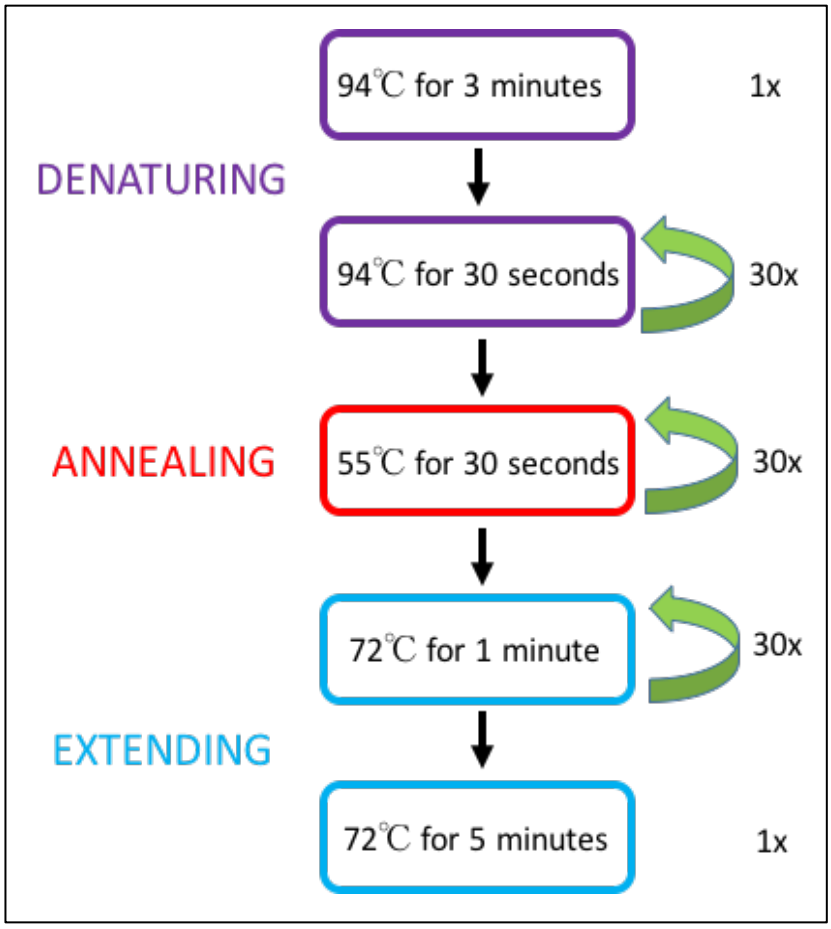

Figure 2.9: ALDH2 PCR programme (thermal cycling)
The one hour and 38 minute ALDH2 PCR programme comprised three stages: (i) a denaturing stage (two phases, 94°C for 3 minutes (1x) and 94°C for 30 seconds (30x)), (ii) an annealing stage (one phase, 55°C for 30 seconds (30x)) and (iii) an extending stage (two phases, 72°C for one minute (30x) and 72°C for five minutes (1x)). Firstly, the high temperature (94°C) maintained during the denaturing stage of the PCR programme functioned to break the hydrogen bonds between the base pairs of the template DNA, and thus led to the complete unwinding of the DNA double helix. DNA strand separation then enabled DNA primers (ALDH2_F1 (forward primer), ALDH2_Int3_Rv (reverse primer) and ALDH2_R3 (reverse primer)) to base pair, via hydrogen bonds, to the complementary regions of the template DNA. This base pairing process only commenced once the temperature had been significantly reduced during the annealing phase (55°C) of the PCR programme. Moreover, the rise in temperature during the extending stage (72°C) of the PCR programme then facilitated complementary base paring of DNA nucleotide bases (dNTPS: A, C, G and T) to the template DNA. dNTPs were one-by-one added to the template DNA by Taq polymerase (a thermostable enzyme with 5' to 3' polymerase and exonuclease activity), which attached at the primers in order to synthesise the complementary DNA strand. The three stages of the PCR cycle were repeated many times to produce numerous copies of the desired DNA sequences in a relatively short time frame.

2.2.2.3 Agarose gel electrophoresis

To determine the genotype of each ALDH2 mouse, PCR products were separated using agarose gel electrophoresis. Firstly, a 2% agarose gel was produced by combining agarose (2g; BIOLINE) and 1x Tris acetate-EDTA buffer (TAE) (100ml; SIGMA-ALDRICH®, made from a 10x TAE stock) in a 250ml beaker. This mixture was then heated intermittently for one minute in a microwave (PROline Micro Chef ST44, 950W) to dissolve the agarose crystals. Once the solution was completely transparent, SYBR® Safe DNA gel stain (5µL; Invitrogen) was added to the beaker. The agarose solution was then swirled to release any trapped air and left to cool for approximately five minutes, before being poured into an agarose gel casting tray (HU13). A cooler agarose solution resulted in a gel with a more constant pore size and averted gel apparatus warping from excessive heat. Sample wells were then formed with a 16-well comb (HU13), which was inserted into the agarose solution soon after pouring. Once set, the agarose gel was transferred to a gel electrophoresis unit (HU13 Mini-Plus Horizontal) filled with 1x TAE. The 16-well comb was then carefully removed. Next, the 100bp DNA ladder (5µL; PROMEGA), control PCR products (15µL; three positive controls (HET, KO and WT) and one negative control) and sample PCR products (15µL) were carefully pipetted into the wells of the agarose gel. The gel was then supplied with 100 volts for 40 minutes to separate the PCR products. After run completion, a GeneGenius gel imaging system (Syngene) containing a dark room, UV transilluminator, PC with GeneSnap software and thermal printer, was used to visualise and capture images of the DNA fragments. The genotype of each mouse was then determined from the printouts, with the positive controls acting as references (Figure 2.10). PCR and agarose gel electrophoresis were repeated when bands appeared in the negative control lane due to the potential for contamination to distort the genotyping results.

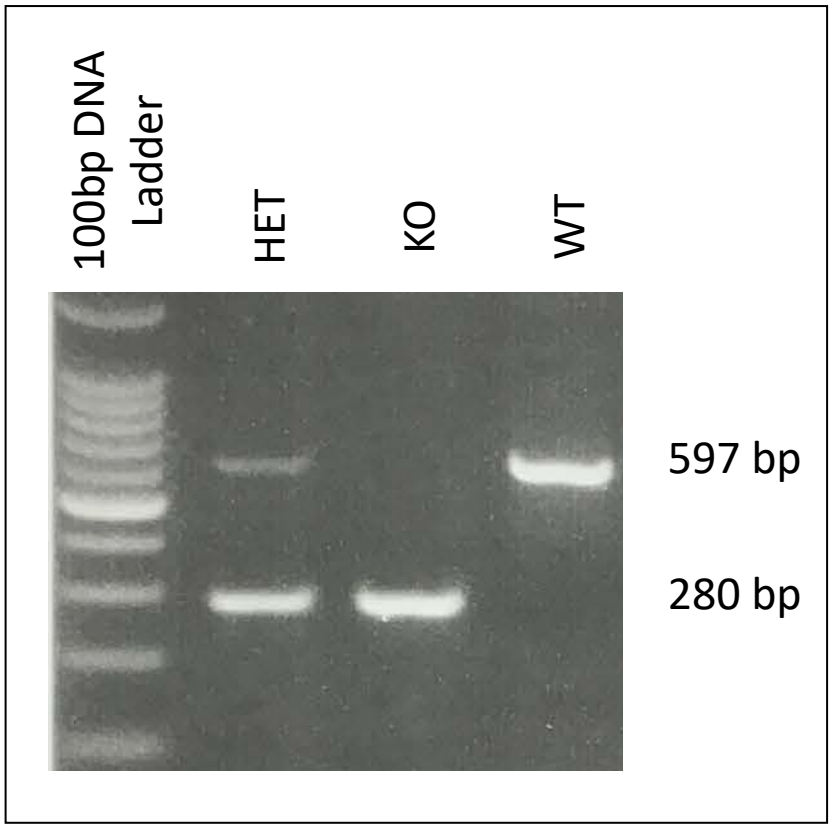

Figure 2.10: Identification of ALDH2 mouse genotype
DNA fragments were separated during agarose gel electrophoresis on the basis of their size (length in bp). Larger DNA fragments moved more slowly through the gel than smaller DNA fragments, thus larger DNA fragments could be seen to move a shorter distance through the gel and were visualised closer to the sample wells than smaller DNA fragments. The first lane in the gel contained the 100bp DNA ladder. The ladder was used for band identification and to establish DNA fragment size. The second lane in the gel comprised DNA from an ALDH2 HET mouse (HET control). The HET mice possessed one complete copy of the ALDH2 gene (demonstrated by the 597bp band) and one incomplete copy of the ALDH2 gene (demonstrated by the 280bp band). The third lane in the gel contained DNA from an ALDH2 KO mouse (KO control). The KO mice had two incomplete copies of the ALDH2 gene (demonstrated by the presence of the 280bp band only). The ALDH2 gene was knocked out by inserting a stop codon and neomycin selection cassette into exon three of the ALDH2 gene (these insertions disrupted the gene and thus prevented normal protein expression). The fourth lane in the gel comprised DNA from an ALDH2 WT mouse (WT control). The WT mice possessed two complete copies of the ALDH2 gene (demonstrated by the presence of the 597bp band only).

2.2.3 ALDH2 blood and tissue harvest

2.2.3.1 Collection of mouse blood

The blood samples required for the mouse washed platelet aggregation study (Section 2.2.4) and Western blotting investigations (Section 2.2.5) were collected from the inferior vena cava (IVC) as previously described (Adeghe and Cohen, 1986; Cazenave et al., 2004). Firstly, inhalation anaesthetics were used to anesthetise a male ALDH2 WT or KO mouse (25-30g) during terminal bleeding. A downdraft table (DDT; LEEC), comprising a source of oxygen (supplied at 1.5-2mL/min; Clinipath), flow meter, precision vaporizer, breathing circuit (non-rebreathing "Bain circuit") and scavenging system (PUREX), was used to deliver Isoflurane (a halogenated ether; IsoFlo®) to the mouse. Anaesthesia was first induced using an attached induction chamber (VetTech Solutions Ltd), which supplied isoflurane at a concentration of 4-5% + 0.8-1 L/min. Once sedated, and following cessation of the pedal withdrawal reflex, the mouse was quickly removed from the induction chamber, placed onto a dissection board and fitted with a face mask (Patterson Scientific). The face mask supplied isoflurane at a concentration of 1-3% + 0.8-1L/min to maintain anaesthesia for the remainder of the bleeding process.

The mouse was secured to the dissection board as shown in Figures 2.11A and B. The abdomen was then swabbed with 70% ethanol, before sterile surgical forceps and scissors (WEISS) were used to make a midline longitudinal incision approximately 3-4cm in length. The resultant skin flaps were then moved aside to enable the dissection of the peritoneum. Next, the viscera (e.g. intestines) was displaced from the abdomen to reveal the vertebral column and IVC (Figure 2.11A). A 1mL syringe with a 25G needle, containing 100µL of the anticoagulant ACD (Table 2.1), was then carefully inserted into the widest section of the IVC

(just above the confluence of the common iliac veins; Figure 2.11B). Once blood had entered the syringe (aided by capillary action), gentle suction was applied with the plunger until blood flow ceased. Approximately 1mL of blood was collected per mouse.

Following exsanguination, death was confirmed by cervical dislocation. The needle was then carefully removed from the syringe and discarded, before the collected blood was slowly transferred into a 1.5mL Eppendorf tube containing 200µL of MTB (on the day of experimentation 45mg glucose had been added to 50mL MTB and the pH had been adjusted (using a H12210 pH meter; HANNA Instruments) to 7.3 at 37°C; Table 2.3). The Eppendorf tube was gently inverted to mix the blood with the MTB.

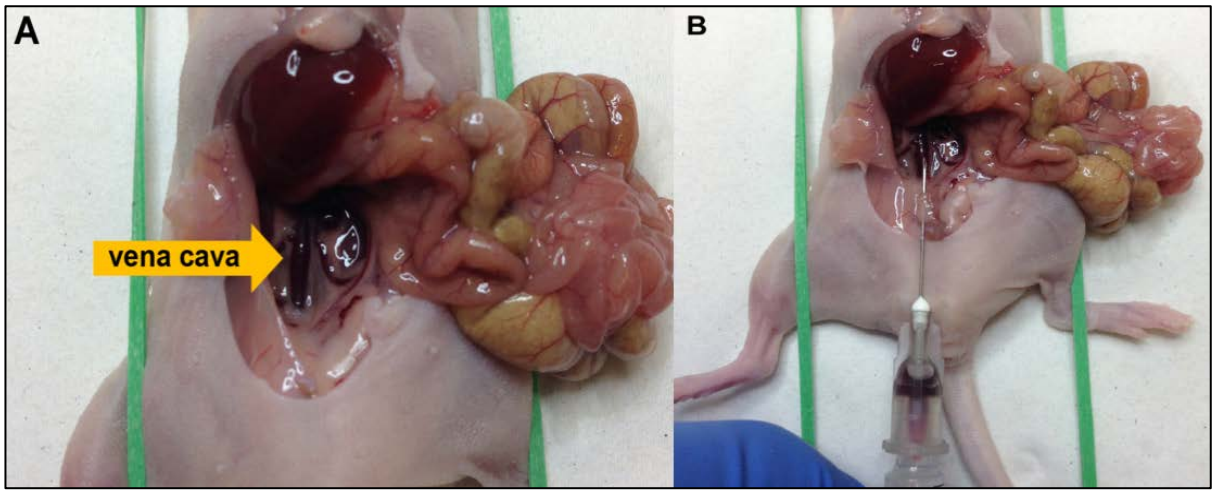

Figure 2.11: Blood collection via the IVC in ALDH2 WT and KO mice
A) This image demonstrates the anatomical position of the IVC within the mouse abdomen. To expose the inferior vena cava a 3-4cm midline longitudinal abdominal incision was carried out. This opening revealed the peritoneum, which was carefully dissected before the viscera was displaced from the abdomen to reveal the desired vessel.
B) This image details the 1mL syringe (25G needle, 100µL of ACD) inserted into the IVC ready for blood collection.

(Images taken from Im and Muschel, 2017)

2.2.3.2 Collection of mouse tissue

For the assessment of ALDH2 expression (Section 2.2.5) and/or lipid accumulation (Section 2.2.6), the median and left lateral liver lobes (liver tissue), quadriceps of the hind limb (skeletal muscle tissue) and heart (cardiac tissue) were all harvested from the ALDH2 WT and KO mice, following exsanguination (Section 2.2.3.1). After extraction, the tissues were briefly washed in ice-cold Krebs-Henseleit buffer (KHB; Table 2.15) and blotted dry, before being placed into previously labelled cryovials. The tissue samples were then immediately snap-frozen in liquid nitrogen and stored at -80°C until further processing.

Reagents *(Manufacturer)*	**Concentration (mM)**
NaCl (*SIGMA-ALDRICH®)*	118.5
$NaHCO_3$ *(Fisher Scientific UK)*	25
KCl *(VWR®)*	4.7
$MgSO_4.7H_2O$ (*VWR®)*	1.2
KH_2PO_4 *(VWR®)*	1.2
Glucose *(Fisher Scientific UK)*	1.1
$CaCl_2.H_2O$ *(VWR®)* (*the Krebs solution was gassed with 95%O_2/5%CO_2 for 10-15 minutes before $CaCl_2.H_2O$ was added)	1.4

Table 2.15: Concentration (mM) of reagents in the Krebs-Henseleit Buffer

2.2.4 Mouse washed platelet aggregation study

2.2.4.1 Preparation of washed mouse platelets

Washed mouse platelets were prepared as previously described (Cazenave et al., 2004). Firstly, Eppendorf tubes comprising blood samples from ALDH2 WT and KO mice (Section 2.2.3.1), were first centrifuged (MSE Micro Centaur) at 2000rpm (<200xg) for five minutes at room temperature, to fractionate the samples (Figure 2.2). The separated plasma and top two thirds of the erythrocyte layer were then aspirated and pipetted into sterile 1.5mL Eppendorf tubes. The plasma/erythrocyte mixtures were then centrifuged (Denley BS400 Centrifuge, Swinging Bucket) at 1000rpm (200xg) for six minutes at room temperature, to pellet any contaminating erythrocytes and leukocytes. The separated plasma was then aspirated (care was taken to avoid the buffy coat; Figure 2.2) and pipetted into sterile 1.5mL Eppendorf tubes. Next, 200µL MTB (Table 2.3) was added to the pellets, which were then gently mixed by inversion, before being centrifuged (Denley BS400 Centrifuge, Swinging Bucket) for a second time at 1000rpm (200xg) for six minutes at room temperature. The separated plasma was then carefully aspirated and pooled with the previously collected plasma.

The plasma volume was then standardised to 1mL with MTB (approximately 600-800µL of plasma was collected per mouse). Next, 1µL of 1mg/mL PGI_2 (Table 2.2) was added to the plasma to prevent platelet activation during high-speed centrifugation. The plasma was then centrifuged (Denley BS400 Centrifuge, Swinging Bucket) at 2800rpm (1000xg) for six minutes at room temperature, to pellet the platelets. The resultant supernatant was aspirated, and the washed platelets were re-suspended in 200µL MTB.

2.2.4.2 Mouse platelet count

The Z^{TM} Series COULTER COUNTER® was used to identify the number of platelets present in the ALDH2 WT and KO mouse platelet samples. As described in Section 2.1.3.3, the Coulter counter was first cleaned with ISOTON, before platelet samples were diluted (washed platelets; 5µL, ISOTON; 10mL) and then counted (platelets/mL) a total of three times. Once again, averages were calculated (platelets/mL).

The ALDH2 WT and KO mouse platelets were then further diluted in MTB to a concentration of $2x10^8$ platelets/mL for LTA experiments (Calculation 2.4 and Section 2.2.4.3). Before commencing these experiments, the washed platelets were rested for one hour to allow time for PGI_2 degradation (Cazenave et al., 2004).

Example of platelet count = $15.66x10^8$/mL in 200µL

Concentration 1 x Volume 1 = Concentration 2 x Volume 2
$15.66x10^8$/mL x 0.2mL = $2x10^8$/mL x (X + 0.2mL)
15.66~~$x10^8$/mL~~ x 0.2~~mL~~ = 2~~$x10^8$/mL~~ x (X + 0.2~~mL~~) **(÷2)**
15.66 x 0.1 = X + 0.2 **(x0.1)**
1.566 = X + 0.2 **(-0.2)**
1.566-0.2 = X = 1.366mL = 1366µL

Add 1366µL of MTB to the 200µL platelet sample to give a washed platelet concentration of $2x10^8$/mL for aggregation experiments (total volume = 1566µL).

Total volume of platelets = Number of possible aggregations
Volume of platelets
required for aggregation

1566µL = 5.22 = 5 aggregations
300uL

Calculation 2.4: Example of washed platelet calculation (mouse platelet samples)

2.2.4.3 Mouse platelet aggregation

Mouse LTA experiments were conducted to compare the effects of $NaNO_2$ *vs* SNP (NO donor) in washed platelets from ALDH2 WT and KO mice (Borgognone et al., 2014; Borgognone et al., 2018). During the one-hour platelet rest period, the aggregometer, cuvettes (samples; 300µL of washed ALDH2 WT or KO platelets at a concentration of $2x10^8$ platelets/mL, reference blanks; 500µL of MTB) and compounds ($NaNO_2$, SNP and collagen dilutions) required for the mouse LTA experiments were prepared as described in Section 2.1.3.4.

On completion of the platelet rest period, aggregatory responses to collagen were recorded under a variety of conditions.

A total of five LTA experiments were conducted per mouse:

- Collagen (3µg/mL) (collagen control)
- $NaNO_2$ (10µM, 100µM ***or*** 1mM $NaNO_2$) + 3µg/mL collagen
- SNP (100nM) + 3µg/mL collagen

Similar protocols were used for both the human (Section 2.1.3.4.3) and mouse LTA experiments.

2.2.4.4 Data analysis (mouse platelet aggregation)

The aggregatory responses produced during the mouse LTA experiments were analysed as described in Section 2.1.3.5.

2.2.5 Western blotting (mouse platelet and tissue samples)

2.2.5.1 Platelet homogenate preparation (mouse platelet samples)

To investigate ALDH2 expression in washed platelets and tissues (liver, skeletal muscle and cardiac tissue), Western blot analysis was conducted (Borgognone et al., 2014; Borgognone et al., 2018).

To prepare the platelet homogenates, blood was first collected from ALDH2 WT and KO mice (Section 2.2.3.1). Washed platelets were then prepared as described in Section 2.2.4.1, before being counted, diluted to a concentration of $5x10^8$ platelets/mL for Western blotting and then rested for one hour (Section 2.2.4.2). The aggregometer, cuvettes (which contained 300µL of ALDH2 WT or KO washed platelets at a concentration of $5x10^8$ platelets/mL and a stirrer bar) and 5x reduced Laemmli sample buffer (Table 2.7) were all prepared during this rest period.

Similar protocols were used to prepare the human (Section 2.1.4.1) and mouse platelet homogenates.

2.2.5.2 Tissue homogenate sample preparation (mouse liver, skeletal muscle and cardiac tissue samples)

On the day of homogenate preparation, liver, skeletal muscle and cardiac tissue samples collected from ALDH2 WT and KO mice (Section 2.2.3.2) were removed from the -80°C freezer and placed into liquid nitrogen. Each sample was then individually extracted from the liquid nitrogen dewar, before being crushed into a fine powder with a sterile mortar and pestle, whilst still under liquid nitrogen conditions. By processing one sample at a time, this prevented tissue thawing and therefore helped to maintain sample quality.

Once crushed, the tissue samples were immediately mixed with ice-cold homogenate buffer (HB; Table 2.16). Due to the variability in tissue mass, 250µL of HB was added to the skeletal muscle and cardiac tissue samples, whilst 500µL of HB was added to the liver tissue samples. As the tissues began to thaw, another volume of HB (skeletal muscle/cardiac tissue samples; 250µL, liver tissue samples; 500µL) was thoroughly stirred into each sample. The thawed homogenates were then pipetted into labelled Eppendorf tubes and snap-frozen in liquid nitrogen. To ensure each sample was entirely homogenised, a freeze-thawing process was then carried out. During this process, the homogenates were first removed from the liquid nitrogen and allowed to thaw on ice for 15 minutes. The homogenates were then snap-frozen for the second time, before being extracted from the liquid nitrogen and left to thaw on ice for approximately 30 minutes. Next, the thawed samples were centrifuged (13,000 RPM; Eppendorf Centrifuge, 5430R) for 15 minutes at 4°C, to pellet the debris. The supernatant was then pipetted into sterile Eppendorf tubes and the liver, skeletal muscle and cardiac tissue homogenates were stored on ice until the protein assay (Section 2.2.5.3) could be completed.

Reagents ***(Manufacturer)***	**Volume (µL)**	**Quantity**	**Function**	
100mM Tris Buffer (pH 7.4) *(Trizma base =SIGMA-ALDRICH®)*	$4.9x10^4$	-	An effective buffer solution that regulates sample acidity and osmolarity.	
200mM Sodium Orthovanadate Stock *(SIGMA-ALDRICH®)*	500	-	Following cell lysis, phosphatases, kinases and proteases, which are usually regulated, compartmentalised and trafficked within cells, move freely throughout the sample and can therefore target sample proteins.	A competitive inhibitor of protein tyrosine phosphatases, alkaline phosphatase, ATPase, adenosine kinase and phosphofructokinase, that maintains the phosphorylation state of proteins within the sample.
500mM Sodium Fluoride Stock *(SIGMA-ALDRICH®)*	500	-		An inhibitor of protein phosphoseryl and phosphothreonyl phosphatases, that maintains the phosphorylation state of proteins within the sample.
Protease Inhibitor Tablet *(ROCHE)*	-	1 tablet		Inhibitors of serine-proteases, cysteine-proteases, aspartic acid-proteases and aminopeptidases, that prevent proteolytic degradation of proteins within sample.

Table 2.16: Volumes (µL) of reagents used to make HB (50mL)

2.2.5.3 Protein assay

To determine the protein content of the ALDH2 WT and KO mouse tissue homogenates (liver, skeletal muscle and cardiac tissue; Section 2.2.5.2), a Bio-Rad DC™ protein assay (detergent compatible colorimetric assay for protein concentration) was carried out according to the manufacturer guidelines. Firstly, working reagent A was prepared by combining reagent S with reagent A (20µL of reagent S was added to each mL of reagent A; Calculation 2.5). Next, each sample was appropriately diluted (1:20 dilution in HB; Table 2.16) and bovine serum albumin (BSA; SIGMA-ALDRICH®) standards were prepared from a 1mg/mL BSA stock solution (Table 2.17). Both the standards and samples were stored on ice.

Triplicates (5µL per well) of the standards and samples were then pipetted into a sterile 96-well microtiter plate (FALCON®). Working reagent A (25µL) and Reagent B (200µL) were also loaded into the filled wells. To protect the UV sensitive reagents, the prepared microtiter plate was carefully covered with foil, before being left to incubate for 15 minutes at room temperature on a shaker. At the end of this incubation period, the foil was removed and a spectrophotometer (GE Healthcare/Amersham Biosciences Ultrospec 3100 Pro UV/Visible Spectrophotometer) was used to measure the absorbance of each well at 750nm. The absorbance readings were reliant on the development of colour, which resulted from the reaction between standard/sample proteins and reagent components, such as alkaline copper tartrate solution and Folin reagent. High levels of colour, and therefore high absorbance readings, were produced by wells with a high protein content, whereas low levels of colour/low absorbance readings resulted from wells with a low protein content. An average absorbance was calculated for each triplicate.

A BSA standard curve was then constructed to identify the protein content of the liver, skeletal muscle and cardiac tissue homogenates from their absorbance readings. The linear relationship between absorbance and concentration enabled this cross-referencing process. When sample absorbance correlated with the extreme top or bottom of the BSA standard curve, the protein assay was repeated at an alternative sample dilution (e.g. 1:10 or 1:50) due to the potential for reagent saturation and experimental error. Following the establishment of protein content, the tissue homogenates were diluted to a protein concentration of 25µg in Bio-Rad Laemmli Buffer with 5% β-mercaptoethanol, and then stored at -20°C for future Western blotting analysis.

E.g. 6 BSA standards and 6 samples

6 BSA standards x 3 wells = 18 wells
6 samples x 3 wells = 18 wells
18 wells + 18 wells = 36 wells

25µL of working reagent A per well
25µL x 36 wells = 900µL working reagent A required

For 900µL working reagent A
20µL of reagent S + 1000µL reagent A = 1020µL working reagent A (120µL spare)

Calculation 2.5: Reagent A/working reagent A requirement calculation

Concentration of the BSA Standard (µg/µL)	**Volume of 1µg/µL BSA Stock Solution** (µL)	**Volume of HB** (µL)
0	0	300
0.2	60	240
0.4	120	180
0.6	180	120
0.8	240	60
1.0	300	0

Table 2.17: Volumes (µL) of reagents used to make BSA standards (300µL)

2.2.5.4 SDS-PAGE

An SDS-PAGE gel containing 8% acrylamide was constructed as described in Section 2.1.4.2. The ALDH2 WT and KO mouse homogenates (platelets, liver tissue, skeletal muscle tissue and cardiac tissue) were also vortexed, boiled and centrifuged, prior to SDS-PAGE (Section 2.1.4.2). The prepared homogenates (20µL/well) and protein ladder were then loaded into the 8% acrylamide gel, which was ran as detailed in Section 2.1.4.2.

2.2.5.5 Wet transfer

Following gel electrophoresis, wet transfer was carried out as described in Section 2.1.4.3. This process transferred the separated proteins from the gel onto a PVDF membrane.

2.2.5.6 Antibody incubation and film development

To determine ALDH2 expression (52.6 kDa) in ALDH2 WT and KO mouse washed platelets and tissues (liver, skeletal muscle and cardiac tissue), Western blot analysis was carried out. Similar protocols were used to complete Western blotting in the human (Section 2.1.4.4) and mouse homogenates.

Following wet transfer, the PVDF membrane was blocked and then probed with anti-ALDH2 (Table 2.18; Antibody 1; stored at -20^{o}C and used approximately three to five times before being discarded) overnight at 4^{o}C on a shaker. Once washed, the membrane was probed with anti-Gt IgG (Table 2.18; Antibody 2) for one hour at room temperature on a shaker. After the secondary antibody had been discarded, the membrane was washed, incubated with ECL and then developed (film exposure times are detailed in Table 2.19).

The membrane was then rinsed and blocked with milk and sodium azide. Next, the membrane was probed for the loading controls, α-Tubulin and GAPDH, using Anti-α-Tubulin (Table 2.18; Antibody 3) and Anti-GAPDH (Table 2.18; Antibody 4), respectively. The membrane was first probed for α-Tubulin, before being blocked with milk and azide, and then probed for GAPDH. Following an overnight incubation at 4°C on a shaker, the primary antibodies were removed (Anti-α-Tubulin and Anti-GAPDH were stored at -20°C and used approximately five times before being discarded) and the membrane was washed. Anti-Ms IgG (Table 2.18; Antibody 5) was then applied to the membrane and incubated for one hour at room temperature on a shaker. Once the secondary antibody had been discarded, the membrane was washed, incubated with ECL and then developed (film exposure times are detailed in Table 2.19).

	Antibody *(Antibody code, Antibody type)*	Manufacturer	Dilution factor used
1	Anti-ALDH2 Gt pAb *(48837, Primary Ab)*	Santa Cruz Biotechnology	1:1000 in 5% BSA/PBS-Tween
2	Anti-Gt IgG HRP-linked Dk mAb *(2033, Secondary Ab)*	Santa Cruz Biotechnology	1:10,000 in 5% Milk/PBS-Tween
3	Anti-α-Tubulin Ms mAb *(T6199, Primary Ab)*	SIGMA-ALDRICH®	1:5000 in 5% BSA/PBS-Tween
4	Anti-GAPDH Ms mAb *(9484, Primary Ab)*	Abcam®	1:20,000 in 5% Milk/PBS-Tween
5	Anti-Ms IgG HRP-linked Gt pAb *(P0447, Secondary Ab)*	Dako	1:10,000 in 1% Milk/PBS-Tween

Table 2.18: Western blotting antibodies (ALDH2 WT and KO platelet and tissue samples)

For each antibody used during the mouse study, this table details: their classification, their code, their manufacturer and the dilution at which they were used during Western blotting. Goat (Gt), Mouse (Ms), Antibody (Ab), Polyclonal Antibody (pAb), Monoclonal Antibody (mAb) and Horse Radish Peroxidase (HRP).

Primary Antibody	**Secondary Antibody**	**Exposure Time** (Seconds)
Anti-ALDH2	Anti-Gt IgG	600
Anti-α-Tubulin	Anti-Ms IgG	20
Anti-GAPDH	Anti-Ms IgG	10

Table 2.19: Optimum exposure time of the Amersham Hyperfilm™ to each membrane

2.2.5.7 Data analysis (Western blotting)

To quantify the protein bands on the ALDH2 Western blot films, analysis was carried out as described in Section 2.1.4.5.

2.2.6 Oil red O staining

2.2.6.1 Tissue sectioning

A Bright Clinicut 60 Cryostat was used to section ALDH2 WT and KO mouse tissue (liver and skeletal muscle tissue; Section 2.2.3.2), prior to Oil Red O (ORO) staining and haematoxylin counterstaining. All tissue sections were cut as previously described (Mehlem et al., 2013).

Firstly, the liver and skeletal muscle samples were removed from the -80°C freezer and placed into liquid nitrogen. The tissue samples were then transferred to the cryostat chamber, which was maintained at a temperature of -40°C. Next, the tissues were carefully extracted from their cryovials and then mounted with optimum cutting temperature (OCT) compound (Tissue-Tek®), onto pre-cooled grooved specimen disks. Once the OCT compound had solidified, a specimen disk was fitted into the specimen head, which had been previously set at a 13° angle. The cutting handle was then rotated to move the specimen head towards the blade, and the sample was roughly trimmed at a cutting thickness of 30μM, until a cross-sectional tissue face was created. All liver samples were sectioned along the coronal plane, whilst skeletal muscle samples were sectioned along the transverse plane.

Traces of tissue and ice were removed from the blade with a stiff bristle paint brush. A few practice sections were completed at a cutting thickness of 6μM, to align the anti-roll plate with the edge of the blade and fine-tune the speed of handle rotation. Once the blade was clear, tissue sections were then cut and mounted, if undamaged, onto room temperature microscope slides (KLINIPATH; three sections were mounted onto each slide and two slides were prepared per sample). The anti-roll plate was carefully lifted for mounting and

repositioned before further sectioning. Any remaining tissue was prised from the specimen disk, trimmed and placed back into its cryovial for snap-freezing. The blade was thoroughly cleaned with the paintbrush, before trimming and sectioning the next sample. All tissue sections were left to dry at room temperature for 10-15 minutes, before being carefully wrapped in tin foil (two slides back to back) and stored at -20°C.

2.2.6.2 Oil red O staining

To enable the visualisation and quantification of fat cells and neutral lipids in sectioned ALDH2 WT and KO mouse liver and skeletal muscle tissue, ORO staining was completed (Mehlem et al., 2013). In the days leading up to staining, the ORO stock solution, which contained 0.5% ORO powder (SIGMA-ALDRICH®) in isopropanol (Fisher Scientific), was prepared. Approximately 30 minutes of simultaneous heating and shaking was required to dissolve the ORO powder in the isopropanol.

On the day of staining, the liver and skeletal muscle sections were first removed from the freezer, laid out on staining rods in a staining tray and then left to defrost for 30 minutes. Whilst the sections were thawing, the ORO working solution was prepared. After mixing the reagents (ORO stock solution; 30mL, distilled water; 20mL), the solution was left to stand for 10 minutes, before being filtered with Grade 1 Whatman filter paper (SIGMA-ALDRICH®) to remove any undissolved ORO powder. Next, a liquid blocking pen (Dako pen, Agilent Technologies) was used to draw around the liver and skeletal muscle sections. This provided a barrier to any liquids applied to the sections and therefore enabled uniform staining, whilst reducing reagent usage by preventing the need for constant reapplication.

To begin the staining process, 60% isopropanol was first incubated on the liver and skeletal muscle sections for five minutes (Figure 2.12). At the end of this incubation period, the slides were tilted to remove the solvent and ORO working solution was then incubated on the sections for 15 minutes (Figure 2.12). During this time, the slides were monitored to ensure that the liver and skeletal muscle sections remained completely covered with ORO working solution, to prevent the stain from drying and becoming uneven throughout the sections. Next, the ORO working solution was removed and 60% isopropanol was incubated on the sections for another five minutes (Figure 2.12). Isopropanol incubations encouraged ORO staining within the sections as ORO was more soluble in lipids than its solvent.

After removing the isopropanol, Mayer's haematoxylin counterstain (pfm medical UK Ltd) was applied to half of the slides to visualise tissue morphology and cell nuclei (per mouse; 4x slides stained with ORO working solution (2x liver and 2x skeletal muscle), 2x slides counterstained with Mayer's haematoxylin (1x liver and 1x skeletal muscle)). The sections were incubated with Mayer's haematoxylin for one minute (Figure 2.12). Following the removal of the counterstain, the slides were placed into a horizontal slide staining rack (TRAJAN) and rinsed with tap water for 15 minutes to remove excess stains (Figure 2.12). Once dry, a small amount of water-soluble mounting medium (IMMU-MOUNT, SHANDON) was applied to the slides in the region of the sections. Great care was taken to avoid the creation of bubbles in the mounting medium. Coverslips (Deckgläser) were then placed over the liver and skeletal muscle sections and the slides were left at room temperature until dry. The stained sections were stored in a cool dark place until imaging could be completed (Mehlem et al., 2013).

A Slide Scanner Axio Scan. Z1 (Zeiss) with brightfield and fluorescence imaging, set at a magnification of x20, was then used to capture high-quality virtual brightfield images of the ALDH2 WT and KO mouse sections stained with ORO and haematoxylin (Mehlem et al., 2013).

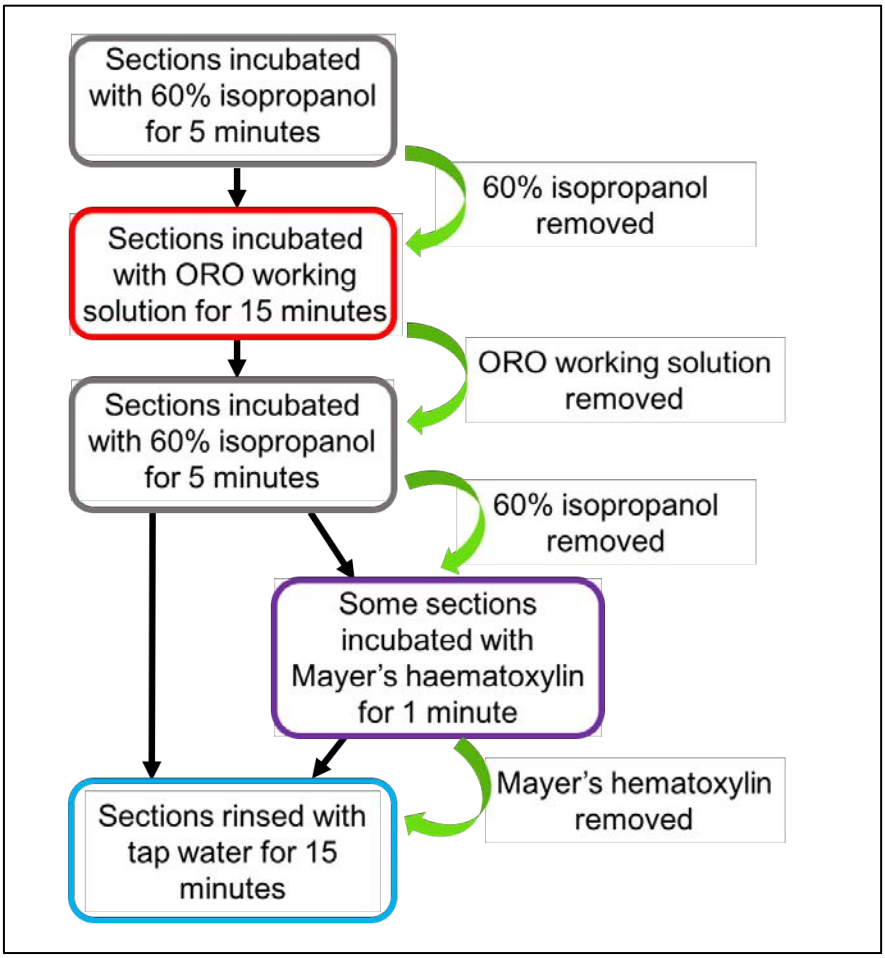

Figure 2.12: ORO and Mayer's haematoxylin staining protocol
ALDH2 WT and KO liver and skeletal muscle sections were incubated with: **1)** 60% isopropanol for five minutes, **2)** ORO working solution for 15 minutes, and then **3)** 60% isopropanol for five minutes (each stain was removed before applying the next). Half of the slides were also counterstained with Mayer's haematoxylin for 1 minute. Finally, all liver and skeletal muscle sections were rinsed with tap water for 15 minutes, to remove excess stains.

2.2.6.3 Data analysis (ORO staining in ALDH2 WT and KO tissue samples)

Zen 2 (blue edition) imaging software and ImageJ Fiji were used to quantify the level of ORO staining, and therefore lipid accumulation, within the ALDH2 WT and KO mouse liver and skeletal muscle tissue sections (Mehlem et al., 2013). Firstly, Zen 2 (blue edition) imaging software was used to capture 10 frames per brightfield image/tissue section. Each image was overlaid with a grid, before 10 frames were randomly selected and captured by another member of the lab to prevent selection bias. ImageJ Fiji was then used to quantify the percentage of ORO staining present in each frame. Each frame first underwent colour splitting (three channels; red, green and blue), before the red channel was analysed at a set threshold (previously established in control animals) to identify the percentage of red colouring and hence ORO staining in each frame. The data collected was then transferred to Prism Version 7.0 (Graphpad Software, Inc., La Jolla, CA) for statistical analysis.

2.3 Statistical analysis

Results are shown as a representative trace/blot or an average ± standard error of the mean (S.E.M.). Group differences were analysed using a variety of appropriate statistical tests, including one-way ANOVA or two-way ANOVA with a Bonferroni post-hoc test or Dunnett's test for multiple comparisons, Fisher's exact test, and unpaired t-test. $P<0.05$ was considered to be statistically significant. Prism Version 7.0 (Graphpad Software, Inc., La Jolla, CA) was used for the above analysis.

Chapter 3: Exploration of platelet function and nitrite in young *vs* old healthy volunteers.

3.1 Introduction

It is well-documented that platelet count decreases with age and previous studies have demonstrated that platelet count remains mostly stable during middle age (~25-60 years of age), but falls by approximately 8% (~20,000 platelets/μL) in the elderly (~60+ years of age) (Biino et al., 2013; Jones, 2016; Segal and Moliterno, 2006). Furthermore, it has been suggested that platelet reactivity increases almost linearly with age (Jones, 2016). Numerous studies have shown in middle-aged men and women (25-65 years) that there is a progressive increase in platelet responsiveness to a variety of agonists, such as ADP, adrenaline, collagen and AA (Kasjanovová and Baláz, 1986; Johnson et al., 1975; Jones, 2016). These changes in platelet function have been associated with alterations in mRNA/microRNA expression, oxidative stress and a reduction in PGI_2/5HT receptors on platelets (Dayal et al., 2013; Jones, 2016; Modesti et al., 1985; Simon et al., 2014). Although platelet reactivity has been thoroughly explored in middle-aged subjects, very little evidence exists on the changes in platelet responsiveness in the elderly (>70 years of age; Jones, 2016). However, a few studies have suggested that platelet function may in fact decrease in older age (Gilstad et al., 2009; O'Donnell et al., 2001).

Previous studies have reported decreased NO bioavailability with age, thus leading to the development of increased platelet activation and aggregation (Torregrossa et al., 2011). In particular, it has been revealed that endothelial function gradually declines with age, thus leading to significant reductions in NO production (Goubareva et al., 2007; Jones, 2016; Taddei et al., 2001). Moreover, the quantity of O_2^- generated by enzymes, such as NADPH oxidase, uncoupled eNOS and mitochondrial respiratory chain complexes, also increases with age (van der Loo et al., 2000). In the absence of compensatory antioxidant defences, NO is

readily scavenged by O_2^-, which in turn leads to reductions in NO bioavailability and the formation of $ONOO^-$ (Torregrossa et al., 2011; van der Loo et al., 2000). Oxidation of BH_4 by $ONOO^-$ contributes to the uncoupling of the eNOS dimer into single dysfunctional monomers, whilst excessive nitration/S-nitrosation of proteins, lipids and DNA by $ONOO^-$ can lead to further deleterious cardiovascular effects, including DNA strand breakage and poly-ADP-ribose polymerase activation (Abudukadier et al., 2013; Bailey et al., 2014; Bendall et al., 2005; Förstermann and Sessa, 2012).

In addition, platelet NO production and responsiveness are also thought to decrease with age (Goubareva et al., 2007; Torregrossa et al., 2011). Despite consistent observations regarding NO bioavailability, conflicting data from animal studies has demonstrated that eNOS expression and/or activation either decreases, remains unchanged or increases with age (Seals et al., 2011). In a recent platelet study involving young (<30 years of age) and middle-aged (>45 years of age) healthy volunteers, albuterol/collagen-mediated eNOS stimulation was absent from the older subjects, whilst eNOS phosphorylation was significantly greater in the younger subjects (Goubareva et al., 2007). Basal and albuterol/collagen-stimulated sGC expression and cGMP production were also greater in the younger subjects (Goubareva et al., 2007). Sverdlov and colleagues have also demonstrated increases in ADP-induced platelet aggregation and significant reductions in platelet responsiveness to the NO donor, SNP, over a 4-year study period in healthy subjects over the age of 55 (Sverdlov et al., 2014).

Despite the above findings, the lack of knowledge surrounding platelet function in older age is particularly concerning considering many anti-platelet therapies are prescribed to the elderly population (Jones, 2016). It has been suggested that the nitrate-nitrite-NO pathway is

not affected by age (Torregrossa et al., 2011), however nitrite still remains to be thoroughly investigated in the elderly population. Moreover, we have previously demonstrated that nitrite inhibits platelet aggregation and triggers cGMP production and VASPser^{239} phosphorylation in washed platelets from young healthy subjects, via NO-dependent and -independent mechanisms. The NO-independent effects of nitrite have been linked to an uncharacterised direct effect on sGC, however further research into the normal physiological nitrite mechanism in isolated platelets is still required (Borgognone et al., 2015). Furthermore, it has been revealed that the sGC stimulator, BAY 41-2272, does not require NO for its anti-platelet effects (Hobbs and Moncada, 2003), whilst the potential for nitrite to act synergistically with BAY 41-2272 in washed platelets remains to be explored across all age groups. Herein, platelet function, nitrite-mediated inhibition and the prospect for BAY 41-2272 to potentiate the effects of nitrite was compared in young *vs* old healthy volunteers. The involvement of NO and sGC in nitrite-mediated platelet inhibition and VASPser^{239} phosphorylation was also investigated in washed platelets obtained from healthy volunteers.

3.2 Hypothesis and specific aims

3.2.1 Hypothesis

$NaNO_2$ activates sGC independently of NO to inhibit platelet aggregation and cause $VASPser^{239}$ phosphorylation in washed platelets from healthy volunteers.

3.2.2 Specific aims

This study has five main aims:

1) To determine the collagen concentration for platelet aggregation to be used in young *vs* old healthy volunteers and for HFpEF-AF/CAF experiments in Chapter 4.
2) To compare platelet function and the effect of nitrite in young *vs* old healthy volunteers.
3) To investigate the involvement of NO and sGC in nitrite-mediated platelet inhibition in young *vs* old healthy volunteers.
4) To determine whether the sGC stimulator, BAY 41-2272, potentiates the effects of nitrite in young *vs* old healthy volunteers.
5) To investigate the involvement of NO and sGC in nitrite-mediated $VASPser^{239}$ phosphorylation in washed platelets from young healthy volunteers.

3.3 Research methods

Blood samples were obtained from young and old healthy volunteers as previously described in Section 2.1.3. To evaluate the effects of nitrite and BAY 41-2272 on platelet aggregation, washed platelets were prepared and counted for LTA experiments as described in Section 2.1.3. Aggregatory responses were then quantified as discussed in Section 2.1.3. To investigate the effects of nitrite on platelet VASPser^{239} phosphorylation, platelet homogenates for Western blotting were also prepared and analysed as described in Section 2.1.4.

3.4 Results

3.4.1 Subject characteristics

Table 3.1 shows the subject characteristics. Gender was well matched in the young and old healthy volunteers (P=0.61; Fisher's exact test). There was a significant difference between the mean age of the young healthy volunteers, when compared with the mean age of the old healthy volunteers (P<0.001; unpaired t-test).

Parameter	**Young Healthy Volunteers (YHV)** (n=13)	**Old Healthy Volunteers (OHV)** (n=11)
Sex (M/F)	9/4	8/3
Age, y (Mean ±SD)	28.0±5.8	72.3±5.0

Table 3.1: Subject characteristics

3.4.2 Determining the concentration response to collagen on platelet aggregation in young and old healthy volunteers

To determine a suitable collagen concentration for platelet aggregation experiments, a dose-response to collagen (1μg/mL, 3μg/mL or 10μg/mL) was conducted in the young and old healthy volunteers. Representative traces are shown in Figures 3.1A and C, respectively. As depicted in Figure 3.1B, 3μg/mL and 10μg/mL collagen caused approximately 57.53% and 64.47% aggregatory responses in platelets from young healthy volunteers, whilst 1μg/mL collagen induced approximately 29.00% platelet aggregation. Analysis revealed that there was no significant difference between the 3 μg/mL and 10μg/mL collagen doses. A similar trend was also observed in the older healthy volunteers (Figure 3.1D). Approximately 41.08% platelet aggregation was induced by 1μg/mL collagen, whilst there was no significant difference between the aggregatory responses caused by the 3μg/mL (58.39%) and 10μg/mL (66.12%) collagen doses. Since 3μg/mL collagen achieved a 50% aggregatory response in both groups of healthy volunteers, this dose was selected for the present study.

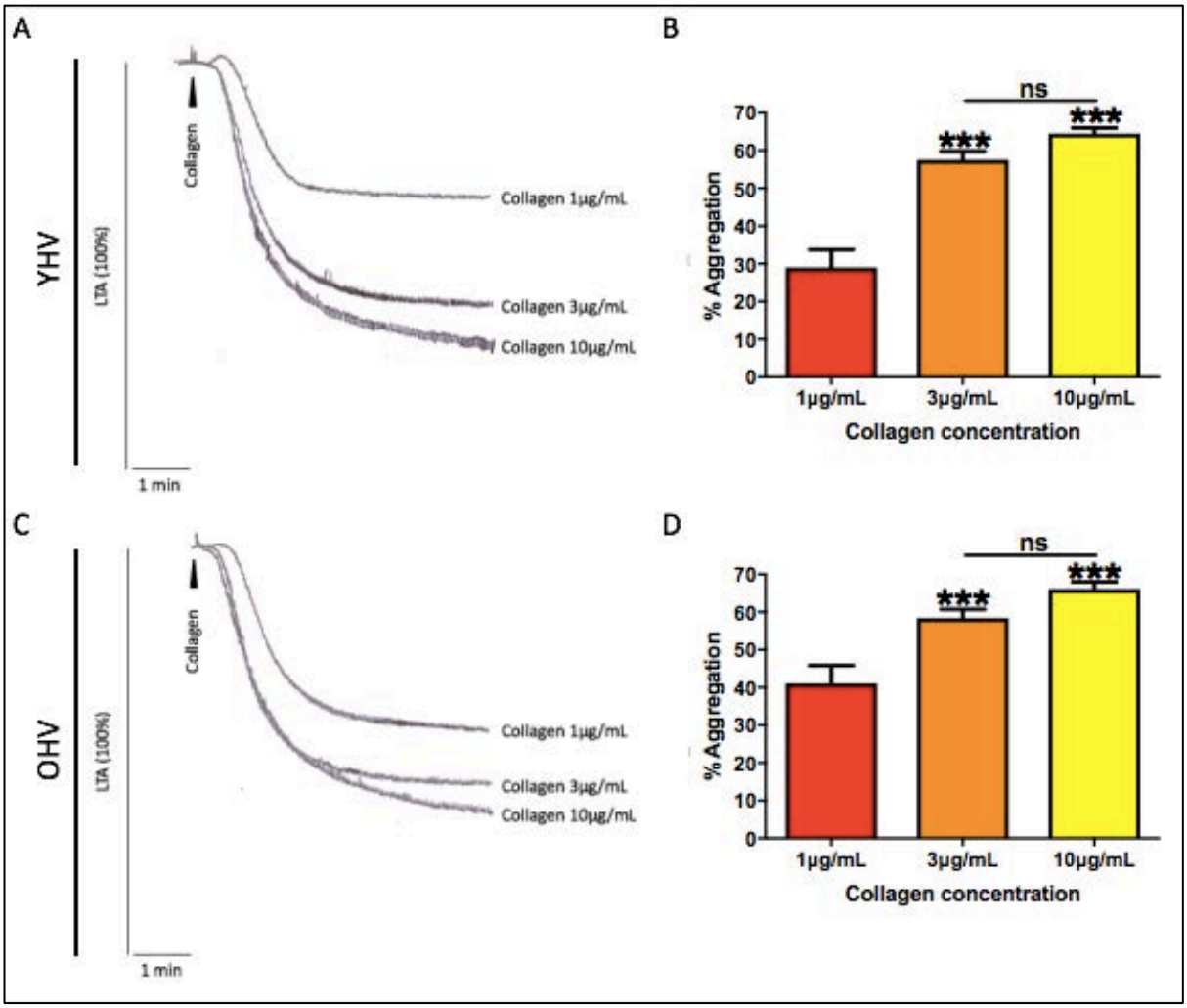

Figure 3.1: <u>Platelet aggregation responses to 1, 3 and 10µg/mL collagen in young and old healthy volunteers</u>

Washed platelets at a concentration of $2x10^8$/mL from young (YHV) and old healthy volunteers (OHV) were activated with either 1µg/mL, 3µg/mL or 10µg/mL collagen and then studied by light transmission aggregometry (LTA) for 5 minutes.

A/C: Representative traces demonstrating the influence of collagen concentration on platelet aggregation responses in young and old healthy volunteers.
B/D: Quantitative analysis of repeat aggregation responses (% aggregation at 5 minutes). Bars represent means ± S.E.M. n=10-11. Statistical differences were determined using a repeated measures one-way ANOVA with a Bonferroni post-hoc test (*P<0.05, **P<0.01 and ***P<0.001 (*'s compare to 1µg/mL collagen)).

3.4.3 $NaNO_2$ inhibits platelet aggregation in young and old healthy volunteers

The effects of $NaNO_2$ on washed platelet aggregation responses to 3μg/mL collagen were compared in young *vs* old healthy volunteers. Representative traces are shown in Figures 3.2A and B, respectively. In the young healthy volunteers, incubation with $NaNO_2$ (10μM, 100μM or 1mM) significantly attenuated collagen-induced platelet aggregation in a dose-dependent manner, when compared to the control group (Figure 3.2C). As shown in Figure 3.2C, $NaNO_2$ also inhibited collagen-induced platelet aggregation in a concentration-dependent manner in the older healthy volunteers. We observed a significant attenuation with both the 100μM and 1mM doses, when compared to the control group. Furthermore, there was not a significant interaction between the young and old healthy volunteers.

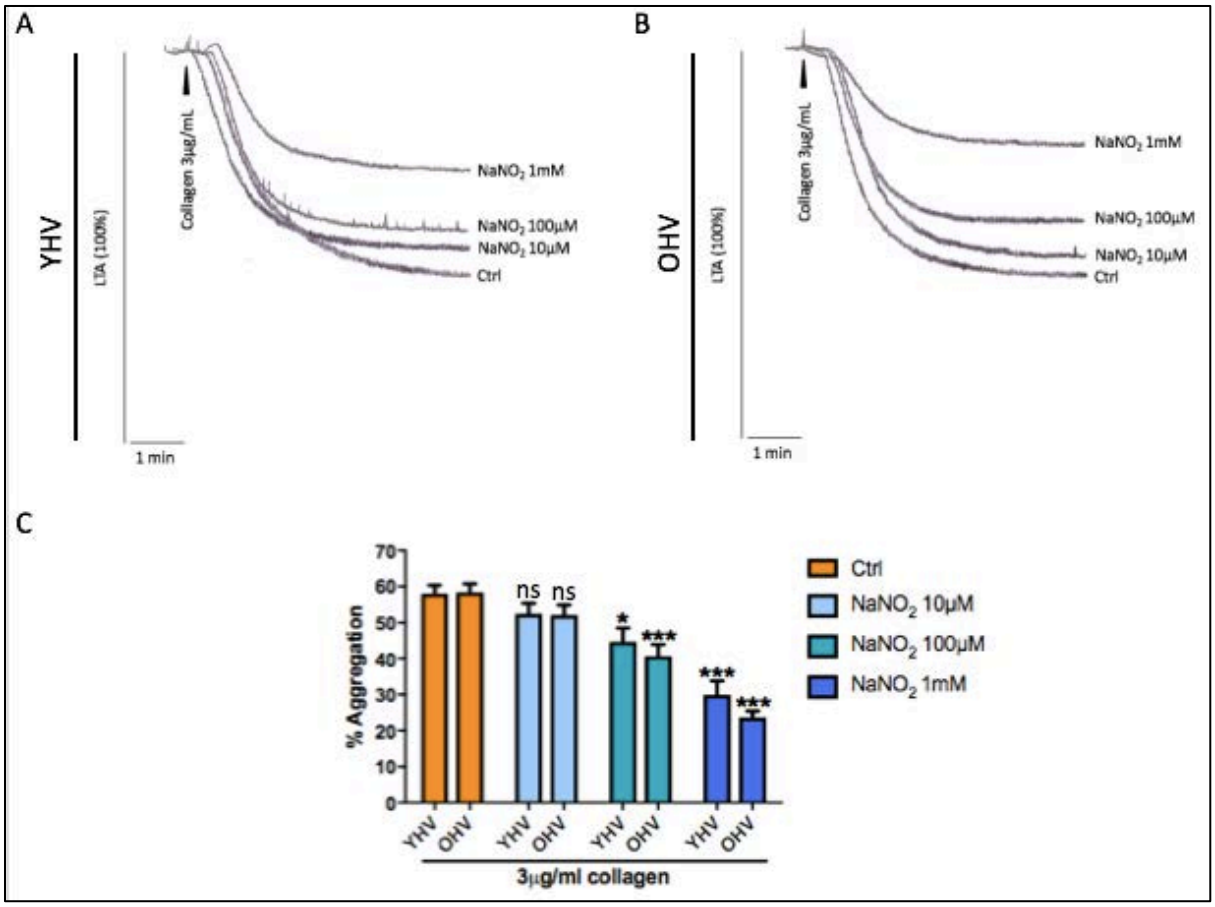

Figure 3.2: <u>Platelet aggregation responses in young and old healthy volunteers following $NaNO_2$ incubation</u>

Washed platelets at a concentration of $2x10^8$/mL from young (YHV) and old healthy volunteers (OHV) were incubated with increasing concentrations of $NaNO_2$ (10µM, 100µM or 1 mM) for 5 minutes, before being activated with 3µg/mL collagen and studied by light transmission aggregometry (LTA) for 5 minutes.

A/B: Representative traces demonstrating the influence of $NaNO_2$ incubation on platelet aggregation responses in young and old healthy volunteers.
C: Quantitative analysis of repeat aggregation responses (% aggregation at 5 minutes). Bars represent means ± S.E.M. n=11. Statistical differences were determined using a repeated measures two-way ANOVA with Dunnett's test for multiple comparisons (*P<0.05, **P<0.01 and ***P<0.001).

3.4.4 SNP inhibits platelet aggregation in young and old healthy volunteers

The NO donor, SNP, was used as a positive control in the present study. The representative traces shown in Figures 3.3A and B, illustrate the effects of SNP on washed platelet aggregation responses to 3μg/mL collagen in the young and old healthy volunteers, respectively. In the young healthy volunteers, incubation with SNP (10nM or 100nM) led to significantly lower collagen-induced platelet aggregation responses, when compared to the control group (Figure 3.3C). A similar trend was also observed in the older healthy volunteers (Figure 3.3C). Incubation with SNP attenuated platelet aggregation in response to collagen in a dose-dependent manner, when compared to the control group. Analysis demonstrated that there was not a significant interaction between the young and old healthy volunteers with SNP treatment.

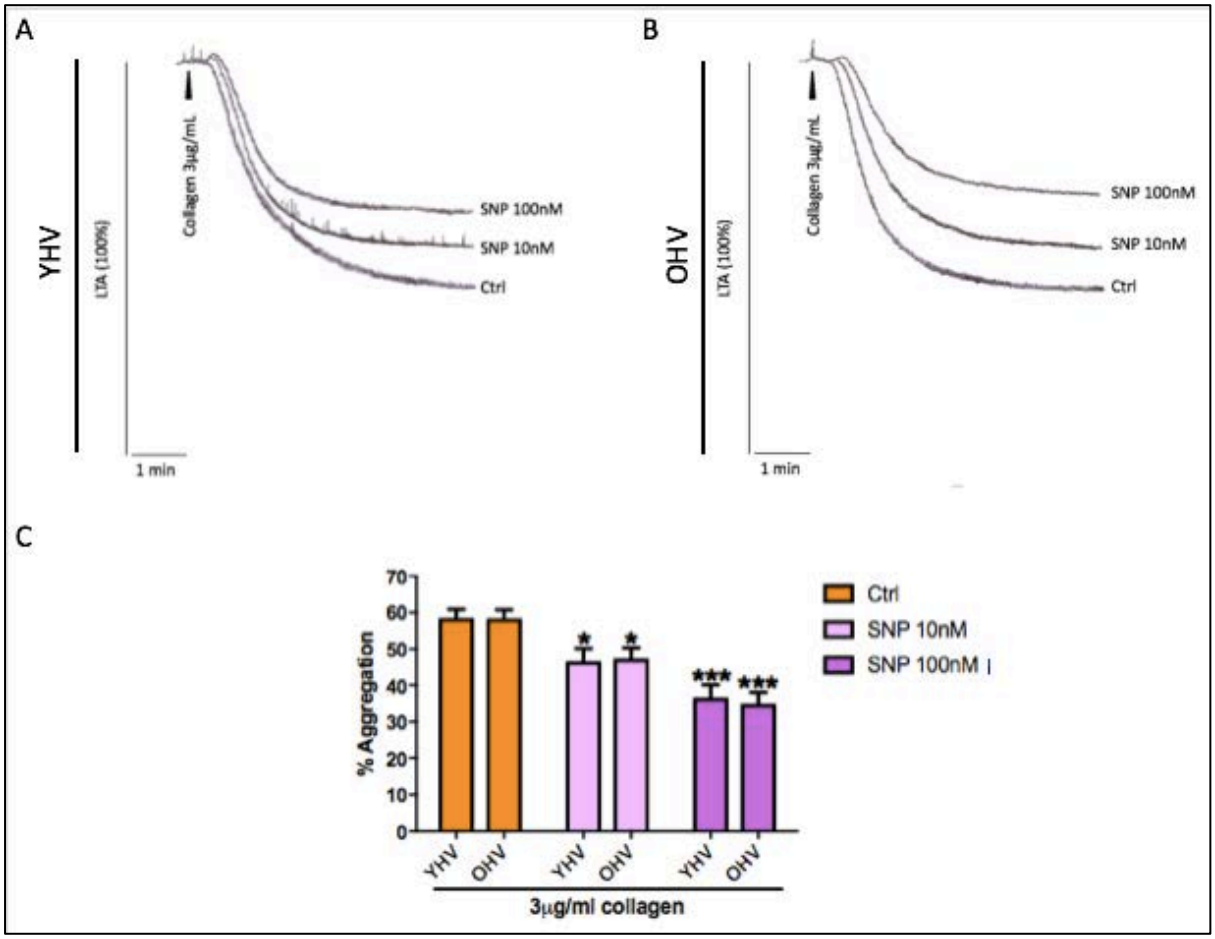

Figure 3.3: <u>Platelet aggregation responses in young and old healthy volunteers following SNP incubation</u>

Washed platelets at a concentration of $2x10^8$/mL from young (YHV) and old healthy volunteers (OHV) were incubated with increasing concentrations of SNP (10nM or 100nM) for 5 minutes, before being activated with 3µg/mL collagen and studied by light transmission aggregometry (LTA) for 5 minutes.

A/B: Representative traces demonstrating the influence of SNP incubation on platelet aggregation responses in young and old healthy volunteers.
C: Quantitative analysis of repeat aggregation responses (% aggregation at 5 minutes). Bars represent means ± S.E.M. n=11. Statistical differences were determined using a repeated measures two-way ANOVA with Dunnett's test for multiple comparisons (*P<0.05, **P<0.01 and ***P<0.001).

3.4.5 $NaNO_2$ inhibits platelet aggregation via NO-independent pathway in young and old healthy volunteers

To assess whether $NaNO_2$ inhibits platelet aggregation via a NO-dependent or -independent pathway in young and old healthy volunteers, the washed platelets were incubated with two different NO scavengers (OxyHb and PTIO), respectively. To test the efficacy of these NO scavengers, platelet aggregation in response to 3μg/mL collagen was also investigated in the presence of the NO donor, SNP. The representative traces shown in Figures 3.4A and C, demonstrate the effects of OxyHb (10μM; extracellular NO scavenger) on platelet aggregation in the absence and presence of SNP (100nM) or $NaNO_2$ (1mM). In the young healthy volunteers, OxyHb incubations were able to revert the attenuation to platelet aggregation caused by SNP incubations (Figure 3.4B). However, the inhibition to platelet aggregation resulting from $NaNO_2$ incubations, could not be reversed with OxyHb incubations (Figure 3.4B). A similar trend was also observed in the older healthy volunteers (Figure 3.4D). OxyHb reversed the inhibition to platelet aggregation resulting from SNP, whilst OxyHb could not revert the attenuation to platelet aggregation caused by $NaNO_2$.

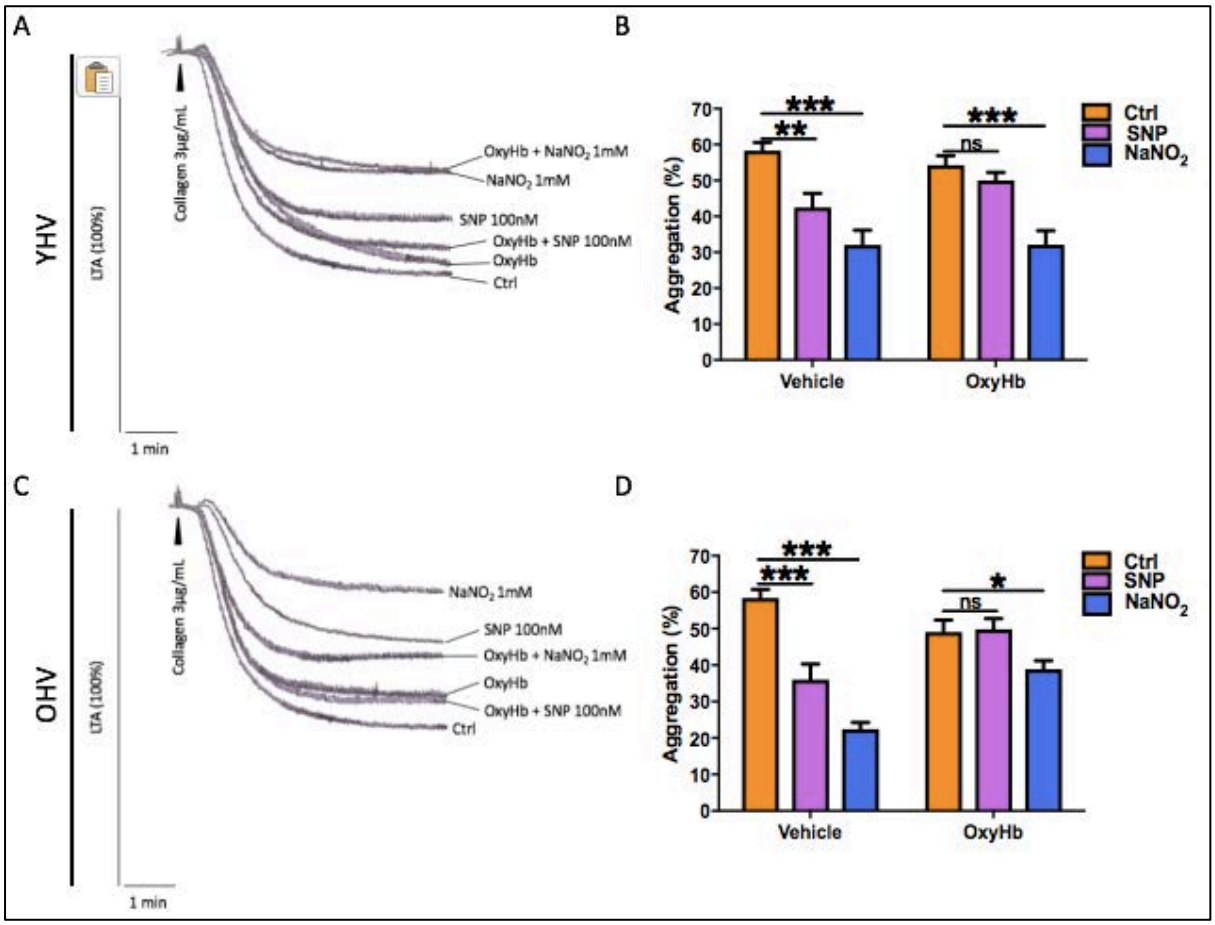

Figure 3.4: <u>Platelet aggregation responses in young and old healthy volunteers following: a) SNP, b) $NaNO_2$, c) OxyHb, d) OxyHb + SNP or e) OxyHb + $NaNO_2$ incubations</u>

Washed platelets at a concentration of $2x10^8$/mL from young (YHV) and old healthy volunteers (OHV) were incubated with: **a)** 100nM SNP, 1mM $NaNO_2$ or 10µM OxyHb for 5 minutes, or **b)** 10µM OxyHb + 100nM SNP or 1mM $NaNO_2$ for 5 minutes (OxyHb was added immediately before the SNP or $NaNO_2$). The washed platelets were activated with 3µg/mL collagen and studied by light transmission aggregometry (LTA) for 5 minutes.

A/C: Representative traces demonstrating the influence of SNP, $NaNO_2$, OxyHb, OxyHb + SNP or OxyHb + $NaNO_2$ incubation on platelet aggregation responses in young and old healthy volunteers.

B/D: Quantitative analysis of repeat aggregation responses (% aggregation at 5 minutes). Bars represent means ± S.E.M. n=8. Statistical differences were determined using a repeated measures one-way ANOVA with Dunnett's test for multiple comparisons (*P<0.05, **P<0.01 and ***P<0.001).

To determine whether $NaNO_2$ inhibited platelet aggregation in young and old healthy volunteers via an intracellular NO-dependent or –independent pathway, we next used PTIO (intracellular NO scavenger). The representative traces shown in Figures 3.5A and C, reveal the influence of PTIO (100μM) on platelet aggregation in the absence and presence of SNP (100nM) or $NaNO_2$ (1mM). In the young healthy volunteers, PTIO incubations were also able to reverse the inhibition to platelet aggregation caused by SNP incubations (Figure 3.5B). However similarly to OxyHb, PTIO incubations could not reverse the attenuation to platelet aggregation resulting from $NaNO_2$ incubations (Figure 3.5B). Once again, the trend observed in the older healthy volunteers was not dissimilar (Figure 3.5D). PTIO reverted the inhibition to platelet aggregation resulting from SNP incubations, but could not reverse the attenuation to platelet aggregation caused by $NaNO_2$.

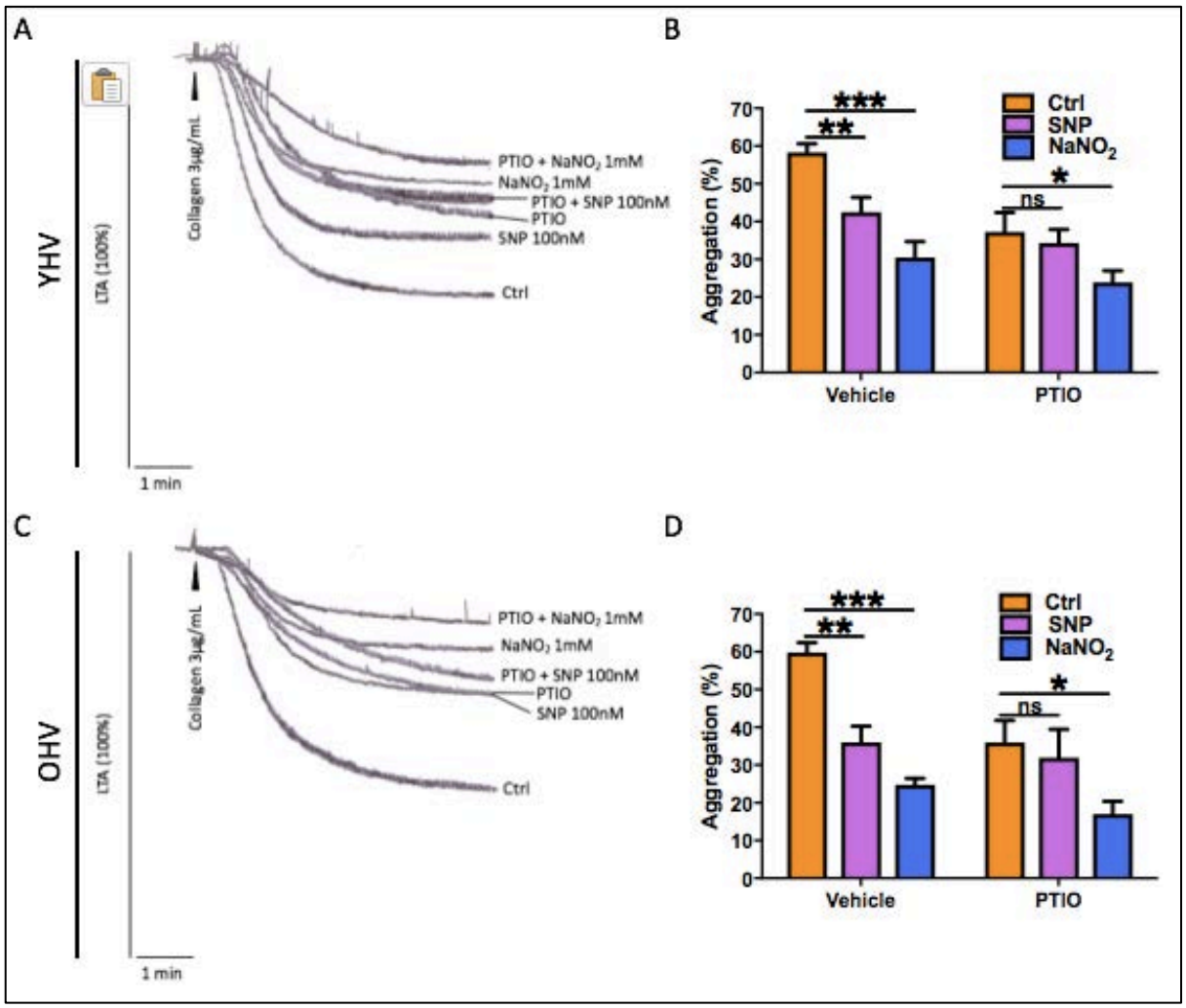

Figure 3.5: <u>Platelet aggregation responses in young and old healthy volunteers following: a) SNP, b) $NaNO_2$, c) PTIO, d) PTIO + SNP or e) PTIO + $NaNO_2$ incubations</u>

Washed platelets at a concentration of $2x10^8$/mL from young (YHV) and old healthy volunteers (OHV) were incubated with: **a)** 100nM SNP, 1mM $NaNO_2$ or 100µM PTIO for 5 minutes, or **b)** 100µM PTIO + 100nM SNP or 1mM $NaNO_2$ for 5 minutes (PTIO was added immediately before the SNP or $NaNO_2$). The washed platelets were activated with 3µg/mL collagen and studied by light transmission aggregometry (LTA) for 5 minutes.

A/C: Representative traces demonstrating the influence of SNP, $NaNO_2$, PTIO, PTIO + SNP or PTIO + $NaNO_2$ incubation on platelet aggregation responses in young and old healthy volunteers.

B/D: Quantitative analysis of repeat aggregation responses (% aggregation at 5 minutes). Bars represent means ± S.E.M. n=8. Statistical differences were determined using a repeated measures one-way ANOVA with Dunnett's test for multiple comparisons (*P<0.05, **P<0.01 and ***P<0.001).

3.4.6 $NaNO_2$ inhibits platelet aggregation via the sGC pathway in young and old healthy volunteers

To further dissect the mechanism by which $NaNO_2$ attenuated platelet aggregation in both young and old healthy volunteers, we then assessed the possible role for sGC. As depicted in Figures 3.6A and C, washed platelets were incubated in the presence and absence of the sGC inhibitor (ODQ; 10μM), before being activated with 3μg/mL collagen. In the young healthy volunteers, ODQ was able to reverse the attenuation to platelet aggregation caused by 100nM SNP (Figure 3.6B). A similar effect was also observed with 1mM $NaNO_2$ incubations (Figure 3.6B). ODQ successfully reverted $NaNO_2$-mediated inhibition of platelet aggregation, when compared to the vehicle treatment group. A similar trend was also observed in the older healthy volunteers (Figure 3.6D). ODQ reverted both SNP- and $NaNO_2$-mediated inhibition of platelet aggregation, when compared to the vehicle treatment groups.

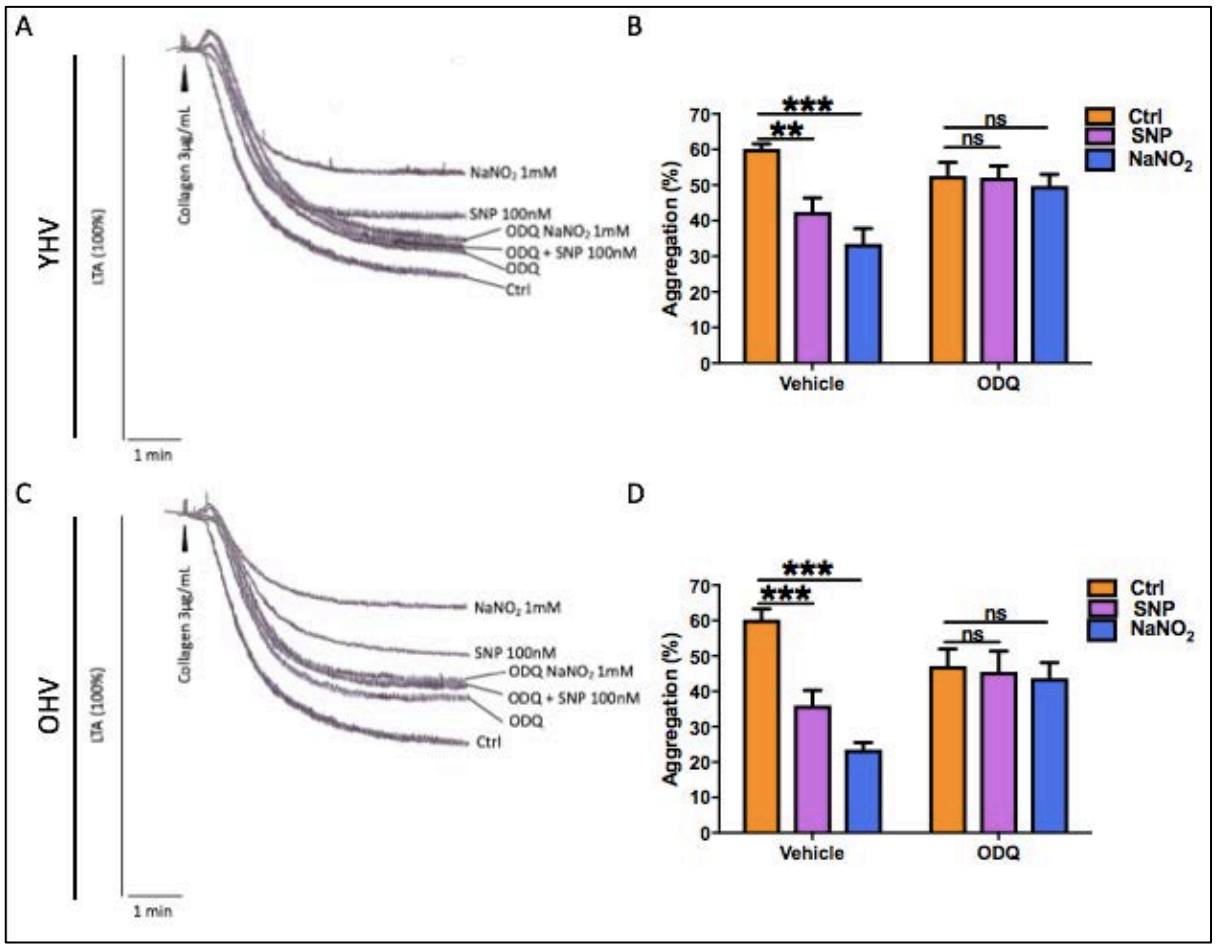

Figure 3.6: <u>Platelet aggregation responses in young and old healthy volunteers following: a) SNP, b) $NaNO_2$, c) ODQ, d) ODQ + SNP or e) ODQ + $NaNO_2$ incubations</u>

Washed platelets at a concentration of $2x10^8$/mL from young (YHV) and old healthy volunteers (OHV) were incubated with: **a)** 100nM SNP or 1mM $NaNO_2$ for 5 minutes **b)** 10µM ODQ for 20 minutes, or **c)** 10µM ODQ + 100nM SNP or 1mM $NaNO_2$ for 5 minutes (ODQ was added 15 minutes before the SNP or $NaNO_2$). The washed platelets were activated with 3µg/mL collagen and studied by light transmission aggregometry (LTA) for 5 minutes.

A/C: Representative traces demonstrating the influence of SNP, $NaNO_2$, ODQ, ODQ + SNP or ODQ + $NaNO_2$ incubation on platelet aggregation responses in young and old healthy volunteers.
B/D: Quantitative analysis of repeat aggregation responses (% aggregation at 5 minutes). Bars represent means ± S.E.M. n=8. Statistical differences were determined using a repeated measures one-way ANOVA with Dunnett's test for multiple comparisons (*P<0.05, **P<0.01 and ***P<0.001).

3.4.7 BAY 41-2272 (sGC stimulator) has a synergistic effect on $NaNO_2$ platelet aggregation responses in young and old healthy volunteers

As shown in Figures 3.7A and C, the sGC stimulator, BAY 41-2272 (10nM, 30nM or 100nM), inhibited platelet aggregation in response to 3µg/mL collagen in a dose-dependent manner, when compared to the young healthy volunteer control group. A similar trend was also observed in the older healthy volunteers (Figures 3.7B and C). Incubations with BAY 41-2272 inhibited collagen-induced platelet aggregation in a concentration-dependent manner, with significant attenuation at 30nM and 100nM, when compared to the control group. Furthermore, there was not a significant interaction between the young and old healthy volunteers with BAY 41-2272 treatment.

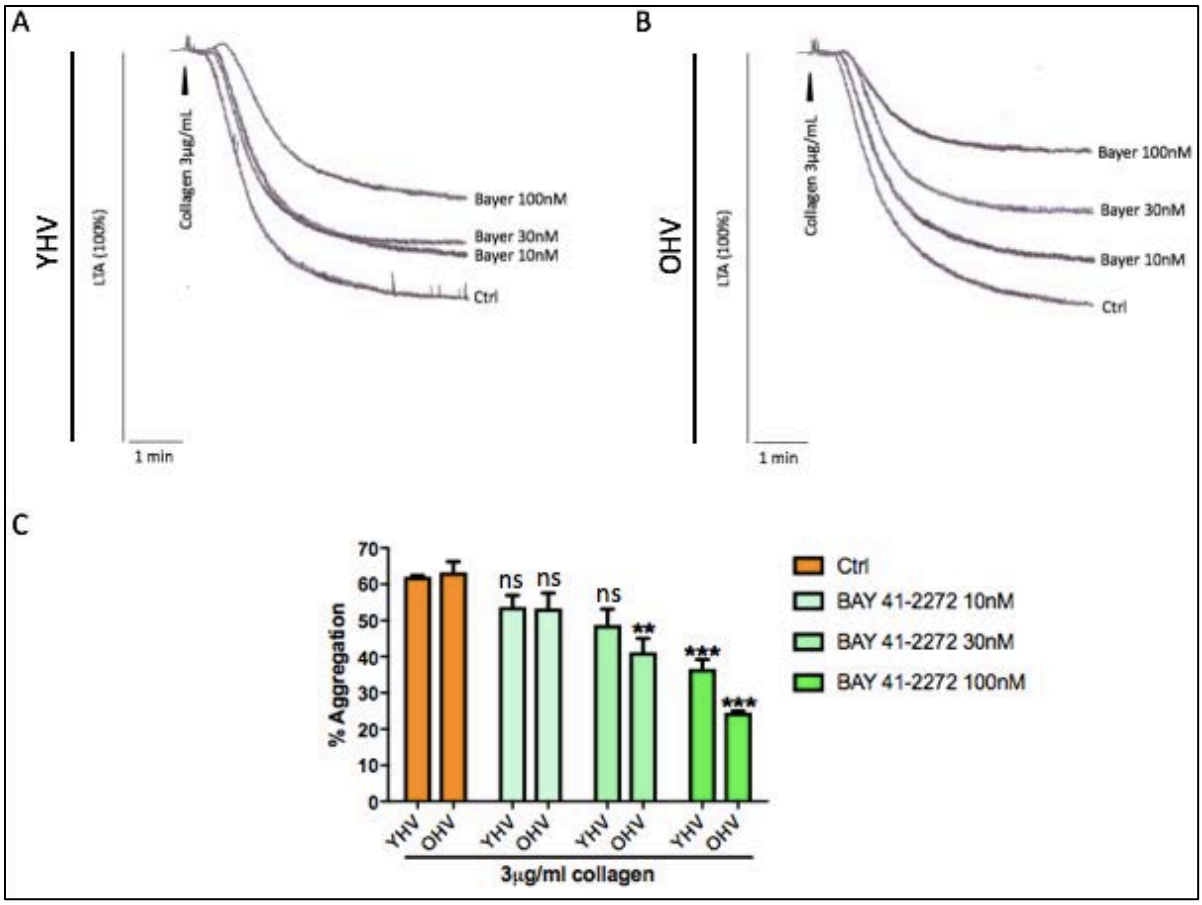

Figure 3.7: <u>Platelet aggregation responses in young and old healthy volunteers following incubations with BAY 41-2272</u>

Washed platelets at a concentration of $2x10^8$/mL from young (YHV) and old healthy volunteers (OHV) were incubated with increasing concentrations of BAY 41-2272 (10nM, 30nM or 100nM) for 1 minute, before being activated with 3µg/mL collagen and studied by light transmission aggregometry (LTA) for 5 minutes.

A/B: Representative traces demonstrating the influence of BAY 41-2272 on platelet aggregation responses in young and old healthy volunteers.
C: Quantitative analysis of repeat aggregation responses (% aggregation at 5 minutes). Bars represent means ± S.E.M. n=3. Statistical differences were determined using a repeated measures two-way ANOVA with Dunnett's test for multiple comparisons (*P<0.05, **P<0.01 and ***P<0.001).

To determine whether $NaNO_2$ exhibited synergistic activity with BAY 41-2272, we chose to use the intermediate dose of BAY 41-2272 to inhibit platelet aggregation. In both the young and old healthy volunteers, 30nM BAY 41-2272 caused a significant inhibition of 3µg/mL collagen by approximately 13.70% and 14.93% aggregation, respectively (Figures 3.8B and D). In the young healthy volunteers, $NaNO_2$ (10µM, 100µM or 1mM) produced a concentration-dependent inhibition of collagen-induced platelet aggregation (Figure 3.8A). However, in the presence of BAY 41-2272, the potency of $NaNO_2$ was significant in a synergistic fashion when compared to $NaNO_2$ alone (Figure 3.8B). Analysis showed that there was a significant difference between $NaNO_2$ alone and BAY 41-2272 + $NaNO_2$ at all concentrations. A similar trend was also observed in the older healthy volunteers (Figures 3.8C and D). Incubation with both $NaNO_2$ and BAY 41-2272 further inhibited collagen-induced platelet aggregation when compared with $NaNO_2$ alone.

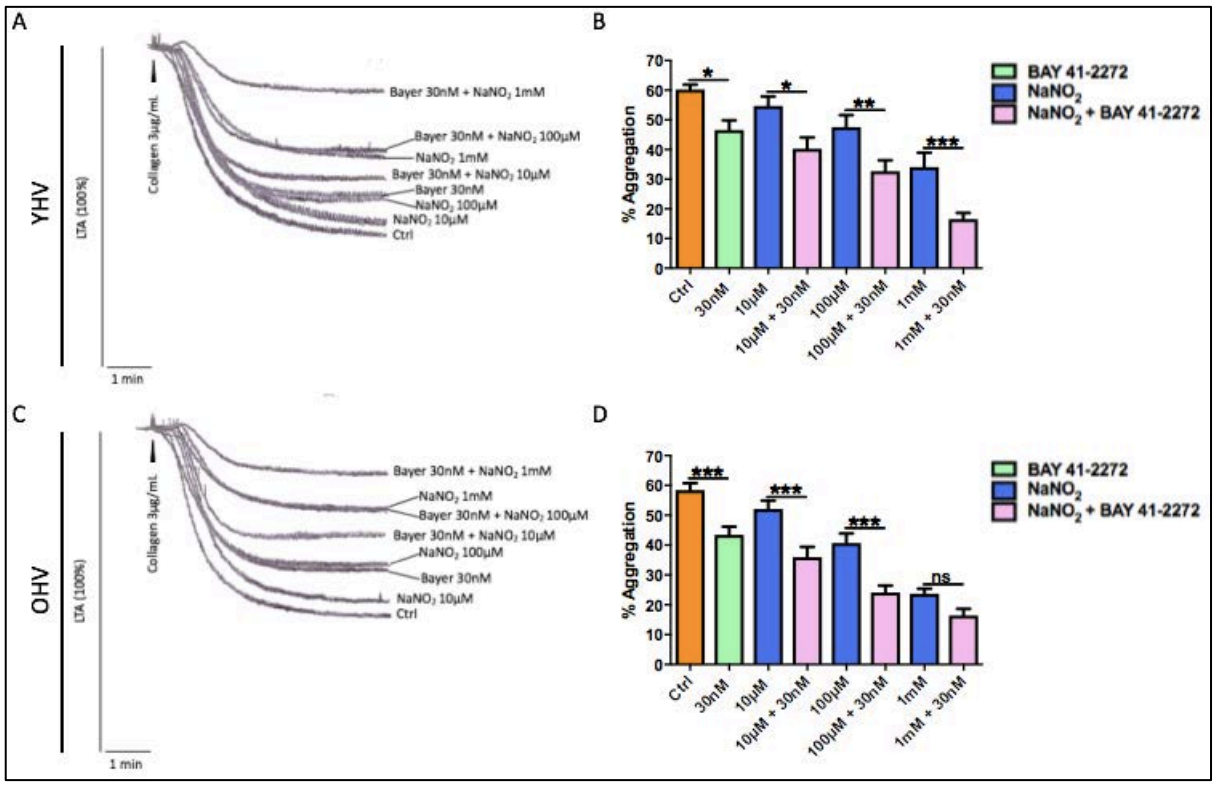

Figure 3.8: <u>Platelet aggregation responses in young and old healthy volunteers following: a) BAY 41-2272, b) $NaNO_2$ or c) $NaNO_2$ + BAY 41-2272 incubations</u>
Washed platelets at a concentration of $2x10^8$/mL from young (YHV) and old healthy volunteers (OHV) were incubated with: **a)** 30nM BAY 41-2272 for 1 minute, **b)** an increasing concentration of $NaNO_2$ (10µM, 100µM or 1 mM) for 5 minutes or **c)** an increasing concentration of $NaNO_2$ (10µM, 100µM or 1 mM) + 30nM BAY 41-2272 for 1 minute ($NaNO_2$ was added 4 minutes before BAY 41-2272). The washed platelets were activated with 3µg/mL collagen and studied by light transmission aggregometry (LTA) for 5 minutes.

A/C: Representative traces demonstrating the influence of BAY 41-2272, $NaNO_2$ or $NaNO_2$ + BAY 41-2272 incubation on platelet aggregation responses in young and old healthy volunteers.
B/D: Quantitative analysis of repeat aggregation responses (% aggregation at 5 minutes). Bars represent means ± S.E.M. n=8-11. Statistical differences were determined using a repeated measures one-way ANOVA with a Bonferroni post-hoc test to make comparisons (*P<0.05, **P<0.01 and ***P<0.001).

To validate the effects of $NaNO_2$ with the sGC stimulator, the experiments were also repeated with SNP (NO donor) as a positive control. As shown in Figures 3.9A and C, the washed platelets from both young and old healthy volunteers were incubated with either BAY 41-2272, SNP or SNP + BAY 41- 2272. In both the young and old healthy volunteers, 30nM BAY 41-2272 significantly inhibited platelet aggregation in response to 3µg/mL collagen by approximately 13.14% and 14.93% aggregation, respectively (Figures 3.9B and D). SNP (10nM or 100nM) also produced a concentration-dependent inhibition of platelet aggregation in response to collagen in the young healthy volunteers (Figure 3.9A). However, in the presence of BAY 41-2272, there was a significant inhibition of platelet aggregation in response to collagen when compared to SNP alone (Figure 3.9B). A similar trend was also observed in the older healthy volunteers (Figures 3.9C and D). Comparisons revealed that incubations with both SNP and BAY 41-2272 increased the inhibition to collagen-induced platelet aggregation, when compared to SNP alone.

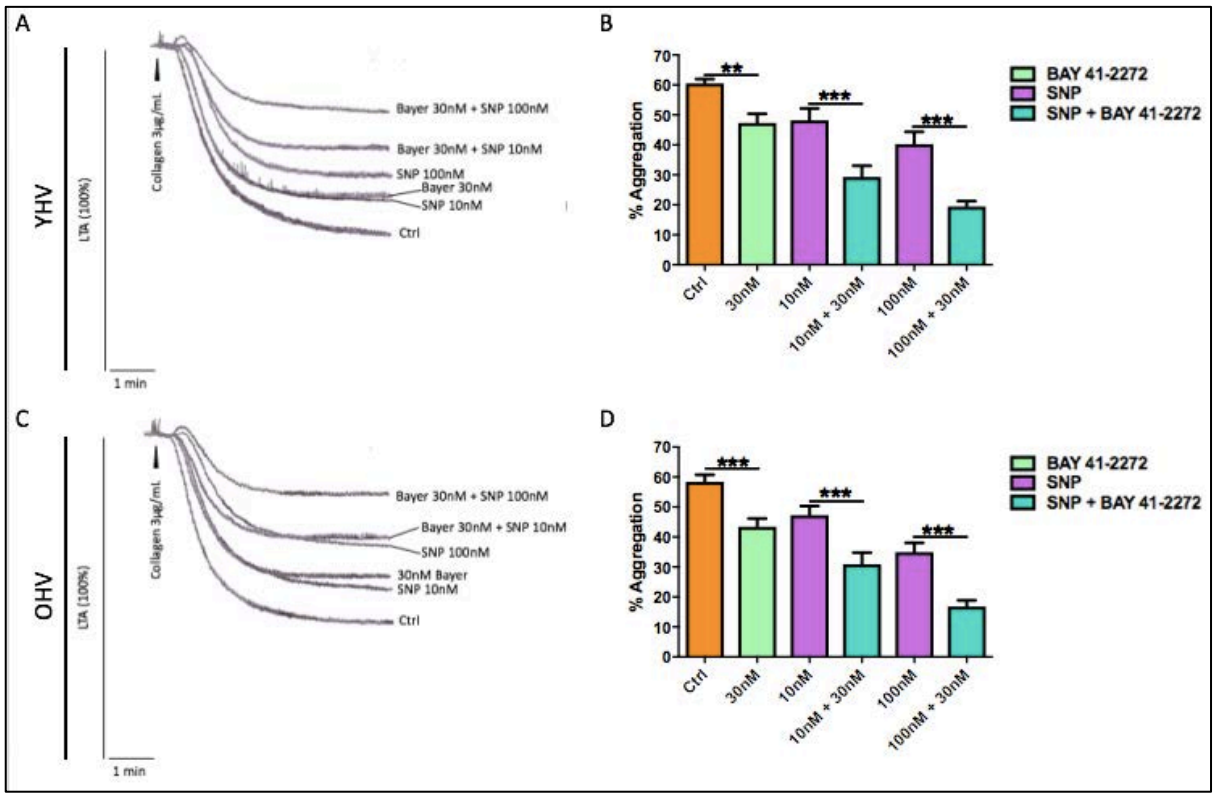

Figure 3.9: <u>Platelet aggregation responses in young and old healthy volunteers following: a) BAY 41-2272, b) SNP or c) SNP + BAY 41-2272 incubations</u>

Washed platelets at a concentration of $2x10^8$/mL from young (YHV) and old healthy volunteers (OHV) were incubated with: **a)** 30nM BAY 41-2272 for 1 minute, **b)** an increasing concentration of SNP (10nM or 100nM) for 5 minutes or **c)** an increasing concentration of SNP (10nM or 100nM) + 30nM BAY 41-2272 for 1 minute (SNP was added 4 minutes before BAY 41-2272). The washed platelets were activated with 3µg/mL collagen and studied by light transmission aggregometry (LTA) for 5 minutes.

A/C: Representative traces demonstrating the influence of BAY 41-2272, SNP or SNP + BAY 41-2272 incubation on platelet aggregation responses in young and old healthy volunteers.

B/D: Quantitative analysis of repeat aggregation responses (% aggregation at 5 minutes). Bars represent means ± S.E.M. n=9-11. Statistical differences were determined using a repeated measures one-way ANOVA with a Bonferroni post-hoc test to make comparisons (*P<0.05, **P<0.01 and ***P<0.001).

3.4.8 $NaNO_2$ phosphorylates $VASPser^{239}$ in platelets from young healthy volunteers

In order to understand the normal physiological $NaNO_2$ mechanism in washed platelets, we next investigated the effects of $NaNO_2$ on the phosphorylation status of the downstream PKG substrate $VASPser^{239}$. Representative $pVASPser^{239}$ Western blots are shown in Figure 3.10A. As depicted in Figure 3.10B, $VASPser^{239}$ phosphorylation increased in a concentration-dependent manner following $NaNO_2$ treatment as compared to the NO donor, SNP. Moreover, with all concentrations of $NaNO_2$ and SNP, $VASP^{ser239}$ phosphorylation peaked at 10 minutes, before falling to low levels at 45 minutes of incubation (Figure 3.10B). The levels of $VASPser^{239}$ phosphorylation observed with 100μM and 1mM $NaNO_2$ treatments were also similar to those triggered by 10nM and 100nM SNP, respectively (Figure 3.10B).

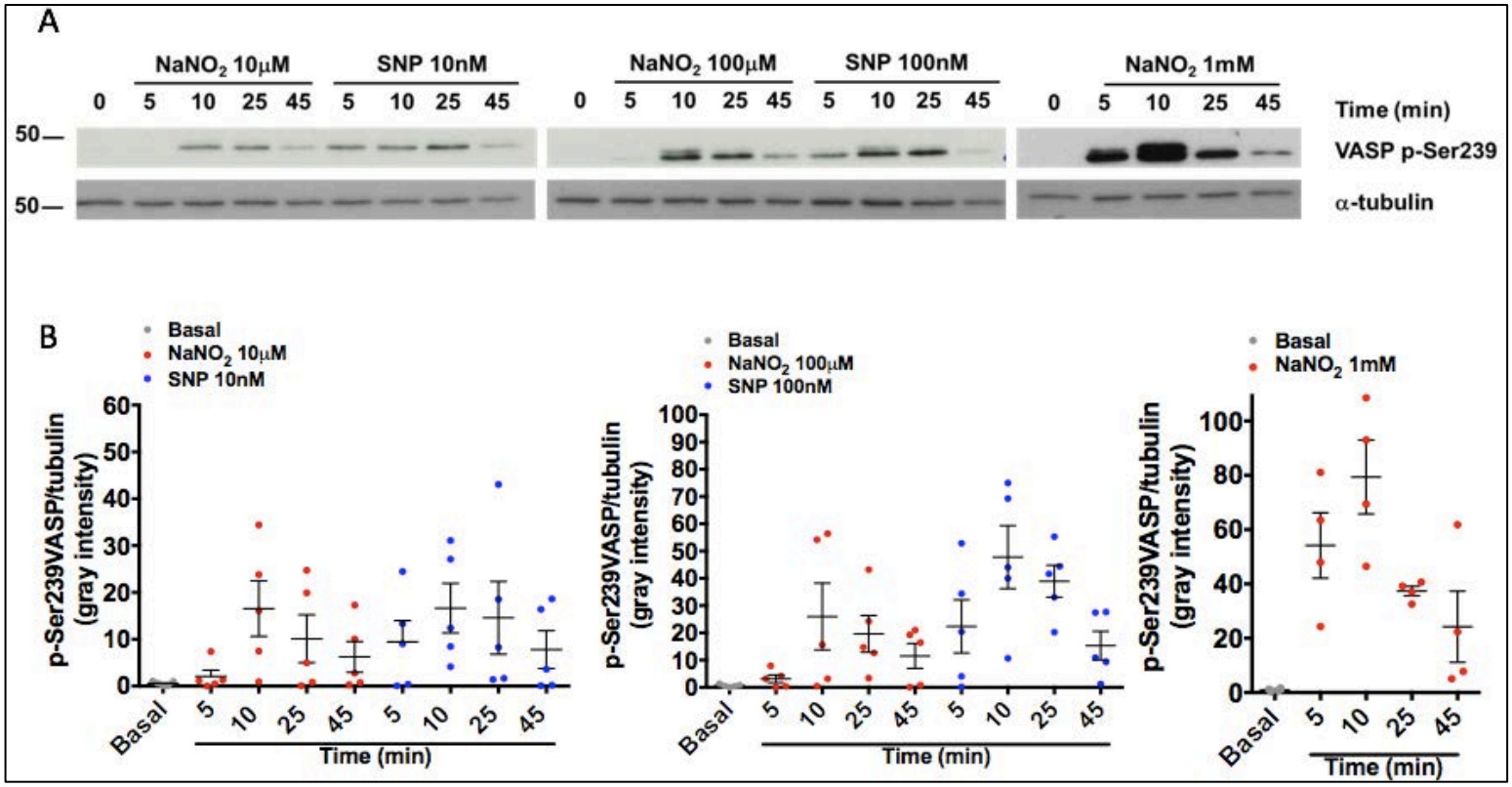

Figure 3.10: <u>Time profile of VASP^{ser239} phosphorylation in platelets from young healthy volunteers following $NaNO_2$ or SNP incubations</u>

$5x10^8$/mL washed platelets obtained from young healthy volunteers were incubated with increasing concentrations of $NaNO_2$ (10μM, 100μM or 1mM) or SNP (10nM or 100nM), before being lysed with 5x sample buffer at the specified time points (5, 10, 24 or 45 mins). The homogenates were then used for SDS-PAGE (8%) and Western blot. The blots were exposed to anti-pVASP^{ser239} (1:1000) or anti-α-Tubulin (1:5000), and the appropriate secondary antibodies (anti-rabbit or anti-mouse; 1:10,000).

A: Representative Western blots demonstrating the effect of $NaNO_2$ (10μM, 100μM or 1mM) or SNP (10nM or 100nM) incubations (5, 10, 25 or 45 mins) on the level of VASP^{ser239} phosphorylation in platelets obtained from young healthy volunteers. α-Tubulin was used as a loading control.

B: Quantitative analysis of repeat experiments (pVASP^{ser239}/α-Tubulin; grey intensity). Bars represent means ± S.E.M. n=4-5.

3.4.9 $NaNO_2$ activates the sGC-cGMP-PKG-VASP signalling cascade via NO-independent pathway in platelets from young healthy volunteers

To establish whether the effect of $NaNO_2$ on sGC was NO-dependent or independent, we next assessed pVASPser^{239} in the absence and presence of NO scavengers, OxyHb and PTIO (Figure 3.11A). As shown in Figure 3.11B, 1mM $NaNO_2$ treatment phosphorylated VASPser^{239} in the presence of the NO scavengers. To confirm whether $NaNO_2$ directly activated the sGC we next pre-incubated young healthy washed platelets with sGC inhibitor, ODQ. Under these conditions, $NaNO_2$ did not phosphorylate VASPser^{239} (Figure 3.11B).

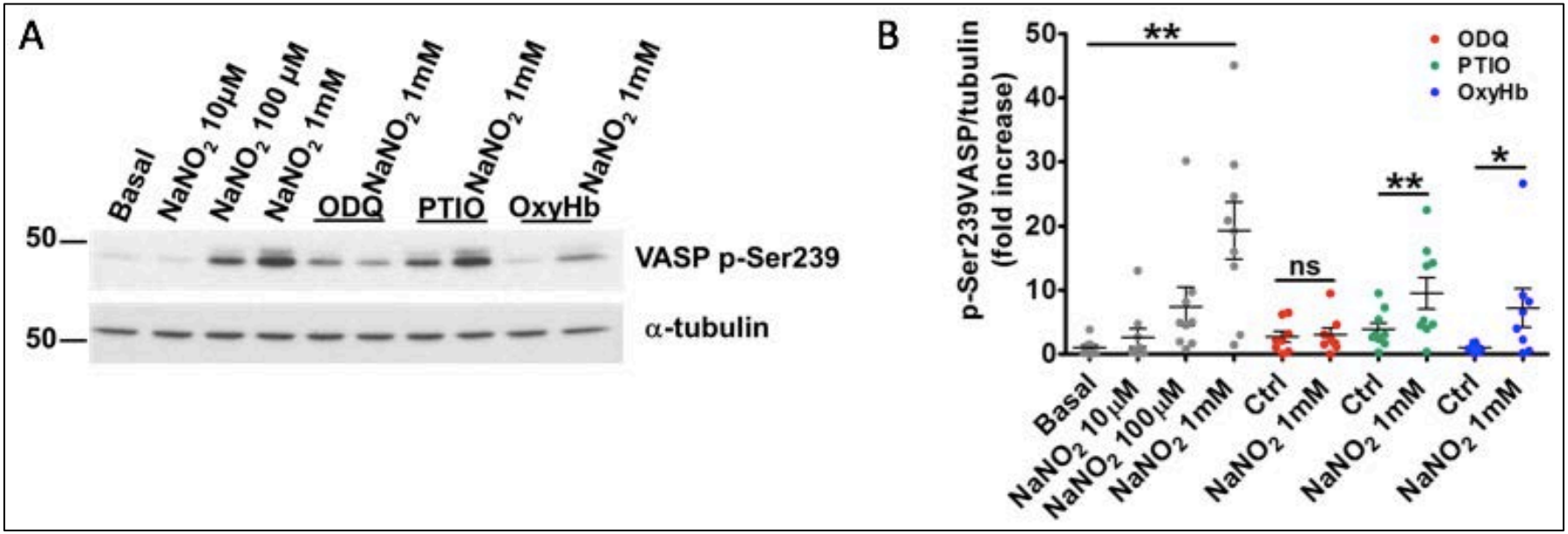

Figure 3.11: <u>VASPser^{239} phosphorylation in platelets from young healthy volunteers following: a) $NaNO_2$ b) ODQ, c) ODQ + $NaNO_2$, d) PTIO, e) PTIO + $NaNO_2$, f) OxyHb or g) OxyHb + $NaNO_2$ incubations</u>

$5x10^8$/mL washed platelets obtained from young healthy volunteers were incubated with: **a)** increasing concentrations of $NaNO_2$ (10µM, 100µM or 1mM), **b)** 10µM ODQ, **c)** 10µM ODQ + 1mM $NaNO_2$, **d)** 100µM PTIO, **e)** 100µM PTIO + 1mM $NaNO_2$, **f)** 10µM OxyHb and **e)** 10µM OxyHb + 1mM $NaNO_2$ for 10 minutes (OxyHb/PTIO were added immediately before $NaNO_2$, whilst ODQ was added 15 minutes before $NaNO_2$), before being lysed with 5x sample buffer. The homogenates were then used for SDS-PAGE (8%) and Western blot. The blots were exposed to anti-pVASPser^{239} (1:1000) or anti-α-Tubulin (1:5000), and the appropriate secondary antibodies (anti-rabbit or anti-mouse; 1:10,000).

A: Representative Western blots demonstrating the effect of $NaNO_2$, ODQ, ODQ + $NaNO_2$, PTIO, PTIO + $NaNO_2$, OxyHb and OxyHb + $NaNO_2$ incubations on the level of VASPser^{239} phosphorylation in platelets obtained from young healthy volunteers. α-Tubulin was used as a loading control.

B: Quantitative analysis of repeat experiments (pVASPser^{239}/α-Tubulin; grey intensity). Bars represent means ± S.E.M. n=8-9. Statistical differences were determined using a repeated measures one-way ANOVA with a Bonferroni post-hoc test to make comparisons (*P<0.05, **P<0.01 and ***P<0.001).

3.5 Discussion

Although platelet reactivity and NO production/responsiveness are thought to decrease with age (Gilstad et al., 2009; Goubareva et al., 2007; O'Donnell et al., 2001; Torregrossa et al., 2011), the effect of aging on platelet function still remains to be explored in the elderly population (>70 years of age). Further, the potential for nitrite to be used as an anti-platelet agent in older healthy volunteers also requires investigation, whilst the combined effect of nitrite and BAY 41-2272 (sGC stimulator) remains to be explored across all age groups.

Numerous experimental studies have demonstrated nitrite to inhibit platelet aggregation following its conversion to NO by the reductase activity of partially deoxygenated haemoglobin (Parakaw et al., 2017; Srihirun et al., 2012). However, the majority of these experiments have been conducted in either whole-blood or PRP (Corti et al., 2013; Dautov et al., 2014; Parakaw et al., 2017), and the precise mechanism(s) of nitrite still remains unclear. Therefore, to determine the mechanism by which nitrite inhibits aggregation and to minimise contributions from other blood cells and proteins, we chose to use washed platelets for the present study. By using isolated platelets this also prevented interference from the well-known NO scavenger, OxyHb, which is found in erythrocytes.

Firstly, Figure 3.1 demonstrates that there was not a significant difference between the platelet responses to collagen in the young *vs* old healthy volunteers, who were well matched in terms of gender, but significantly separated by age. The aggregatory responses were also slightly higher in the old healthy volunteers for all three collagen concentrations. These observations are surprising and contradict previous findings by O'Donnell and colleagues, who suggested the effect of age on platelet function was not linear and that aggregability

decreases with increasing old age (>75 years) (O'Donnell et al., 2001). Conversely, a study in healthy individuals revealed that platelet activation and the stability of platelet adhesions increase with age. These findings indicate that platelet function may actually increase in older age, however only a small proportion of the participants were over the age of 65 (Cowman et al., 2015).

In the present study, $NaNO_2$ significantly attenuated collagen-induced platelet aggregation in a dose-dependent manner in both the young and old healthy volunteers (Figure 3.2). These trends demonstrate that nitrite-mediated platelet inhibition is not dependent upon other cell types or plasma proteins, as previously suggested (Corti et al., 2013). Both the 100μM and 1mM $NaNO_2$ concentrations also inhibited platelet aggregation to a greater degree in the older volunteers, however there was not a significant interaction between the two age groups. These findings suggest that higher concentrations of nitrite are just as effective in the elderly population and thus highlight the potential for nitrite to be used as an anti-platelet therapy across all ages.

A significant concentration-dependent inhibition of collagen-induced platelet aggregation was also observed in both the young and old healthy volunteers with the NO donor and positive control, SNP (Figure 3.3). Whilst there was not a significant interaction between the two age groups, the 100nM SNP dose also inhibited platelet aggregation to a greater degree in the older volunteers. These findings suggest that NO responsiveness is in fact maintained in older age and therefore contradict previous observations by Goubareva/Sverdlov and colleagues (Goubareva et al., 2007; Sverdlov et al., 2014).

Moreover, the NO scavengers, OxyHb and PTIO, were not able to revert the attenuation to collagen-induced platelet aggregation caused by 1mM $NaNO_2$ in both the young and old healthy volunteers (Figures 3.4 and 3.5). However, the inhibition provided by 100nM SNP was reversed by OxyHb and PTIO in both age groups (Figures 3.4 and 3.5). Since nitrite-mediated inhibition was not reversed by the two NO scavengers this suggests that nitrite was not converted to NO in the washed platelets. Furthermore, the inhibition to collagen-induced platelet aggregation caused by 1mM $NaNO_2$ and 100nM SNP was successfully reverted by the sGC inhibitor, ODQ, in both the young and old healthy volunteers (Figure 3.6). These findings indicate that nitrite activates sGC in the washed platelets and corroborate a recent study in healthy volunteers (Parakaw et al., 2017). Parakaw and colleagues documented decreases in platelet aggregation, P-selectin expression and platelet-monocyte/-lymphocyte interactions following $NaNO_2$ inhalation, whilst nitrite-mediated increases in $VASPser^{239}$ phosphorylation were shown to be inhibited by ODQ in deoxygenated whole-blood (Parakaw et al., 2017). These observations suggest that nitrite may prove beneficial in conditions of platelet hyperaggregability, whilst also demonstrating the importance of sGC in the normal physiological nitrite mechanism. However, it is important to acknowledge that the experiments were conducted in whole-blood (oxygenated; *in vivo*, and deoxygenated; *in vitro*) and not isolated platelets (Parakaw et al., 2017). Therefore, our data (OxyHb, PTIO and ODQ) corroborates with their findings.

The sGC stimulator, BAY 41-2272, has previously been shown to cause dose-dependent non-NO-dependent anti-platelet effects in PRP/washed platelets from healthy humans and *in vivo* blood pressure measurements in rats (Hobbs and Moncada, 2003). In the present study, BAY 41-2272 alone significantly attenuated collagen-induced platelet aggregation in a dose-

dependent manner in both the young and old healthy volunteers (Figure 3.7). These findings indicate that the anti-aggregatory effects of BAY 41-2272 do not require NO, as recently suggested by Roger and colleagues (Roger et al., 2010), and therefore corroborate the study by Hobbs and colleagues, who also investigated 10nM, 30nM and 100nM BAY 41-2272 concentrations (Hobbs and Moncada, 2003). In the present study, we also observed that both 30nM and 100nM BAY 41-2272 concentrations inhibited platelet aggregation to a greater degree in the older healthy volunteers, however there was not a significant interaction between the two age groups. These findings suggest that BAY 41-2272 remains effective in the elderly population, thus highlighting the potential for BAY 41-2272 to be used to treat conditions hyperaggregability across all ages.

The sGC-dependent effects of nitrite also exhibited synergistic activity with 30nM BAY 41-2272 in both the young and old heathy volunteers (Figure 3.8). We show for the first time the effects of nitrite with BAY 41-2272 in washed platelets, thus these novel findings suggest that BAY 41-2272 could be used to potentiate the sGC-dependent effects of nitrite across all age groups in the future. The NO donor and positive control, SNP, also exhibited synergistic activity with 30nM BAY 41-2272 (Figure 3.9). Synergistic activity between BAY 41-2272 and an alternate NO donor, GSNO, has previously been observed in human PRP and washed platelets by Hobbs and colleagues (Hobbs and Moncada, 2003). In addition, our findings also corroborate with an *in vivo* rabbit model, where BAY 41-2272 was shown to potentiate the effects of SNP, thus leading to stronger penile erections (Bischoff et al., 2003).

We and others have previously shown that nitrite increases VASPser^{239} phosphorylation in both washed platelets and PRP in the presence of deoxygenated erythrocytes (Borgognone et

al., 2015; Srihirun et al., 2018). In the present study, we also observed nitrite to increase VASPser^{239} phosphorylation in washed platelets from young healthy volunteers (Figure 3.10), thus suggesting that nitrite inhibits platelet aggregation in the absence of other cells and proteins. Interestingly, VASPser^{239} phosphorylation also occurred in the presence of NO scavengers, OxyHb and PTIO, but not when washed platelets from the young healthy volunteers were incubated with the sGC inhibitor, ODQ (Figure 3.11). This data further supports the notion that the underlying mechanism of nitrite in washed platelets acts through sGC-PKG-VASPser239 independently of NO.

3.5.1 Study limitations and future considerations

In the present chapter, there are a number of study limitations in relation to both the LTA experiments and Western blotting analysis. Firstly, as collagen was the only agonist used throughout the LTA experiments, it cannot be assumed that platelet dysfunction was absent from both the young and old healthy volunteers (Dovlatova, 2015). Platelet dysfunction is caused by a plethora of factors, thus several agonists targeting a variety of receptors may be required to perceive certain defects (Dovlatova, 2015). Recently, it has been established that the use of five agonists, including ADP, AA, collagen, adrenaline and TXA_2, at a single concentration, is sufficient to detect the majority of platelet function defects (Hayward et al., 2009).

Furthermore, pharmacological (10μM, 100μM and 1mM) and not physiological (200-600nM) concentrations of nitrite were used in both the LTA experiments and Western blotting analysis, thus modulation of platelet function by normal plasma nitrite concentrations cannot be assumed from the above findings (Kevil et al., 2011; Srihirun et al., 2018). Despite

this, previous studies by other research groups have shown either 1-10μM $NaNO_2$ to inhibit ADP-induced platelet aggregation in PRP+erythrocytes or 500μM $NaNO_2$ to inhibit ADP-induced platelet aggregation in plasma (Laustiola et al., 1991; Srihirun et al., 2018). Therefore, implicating that the pharmacological concentrations of nitrite may have the potential to be used as an anti-platelet therapy for all ages in the future (Laustiola et al., 1991; Srihirun et al., 2018).

Moreover, whilst interference from other blood cell types and plasma proteins was prevented by experimentation in washed platelets, heme-containing components of the mitochondrial respiratory chain (e.g. cytochrome C) may have contributed to nitrite-mediated attenuation by converting nitrite to NO within the platelets (Kevil et al., 2011). Reduction of nitrite inside the platelet would certainly circumvent scavenging by the extracellular NO scavenger, OxyHb, whilst potentially influencing the efficacy of the intracellular NO scavenger, PTIO. Since the NO scavengers are limited by both the relative rate and location of NO production, further studies are therefore warranted to assess the involvement of heme-containing components in nitrite-mediated platelet attenuation.

In addition, it is well-known that OxyHb absorbs light. As such, the addition of OxyHb to washed platelet samples could influence the aggregation traces. To control the effect of OxyHb on light transmission, the impact of the NO scavenger on the aggregation baseline was first tested. A consistent baseline was observed in the presence of OxyHb due to the low final concentration of the NO scavenger (10μM in 300μL washed platelets).

Furthermore, nitrite-mediated VASPser^{239} phosphorylation was only investigated in washed platelets from young healthy volunteers. To ensure that the underlying mechanism of nitrite in washed platelets is consistent across all age groups, it is important to investigate VASPser^{239} phosphorylation under the same conditions in old healthy volunteers.

In addition, PKG activity was indirectly measured via VASPser^{239} phosphorylation status by Western blotting analysis. For instance, the increases in VASPser^{239} phosphorylation observed following $NaNO_2$ treatment in washed platelets obtained from young healthy volunteers, suggested an increase in PKG activity under these conditions. Therefore, a PKG colorimetric activity assay would further support the notion that nitrite activates the VASP-PKG pathway in both young and old healthy volunteers (Das et al., 2008).

Finally, a longitudinal study (e.g. involving the same volunteers 2, 4 and 6 years later) would also help to demonstrate any changes to platelet function over time, in the elderly population (Jones, 2016). However, a study of this sort would not be without difficulties, due to the potential for old healthy volunteers to rapidly deteriorate and subsequently require medication.

3.5.2 Conclusions

The results of this study reveal that $NaNO_2$ activates sGC independently of NO to inhibit washed platelet aggregation in both young and old healthy volunteers, thus supporting the potential for nitrite to be used as an anti-platelet therapy across all ages. The synergistic activity observed between nitrite and BAY 41-2272 also alludes towards the prospect of a nitrite-based combination therapy to address conditions of hyperaggregability in the future. Overall, this study demonstrates that with the right application, nitrite may have the potential to inhibit platelet aggregation across all ages and possibly disease states.

Chapter 4: Evaluation of the phenomenon of “platelet NO resistance” and nitrite in patients with HFpEF-AF and CAF only.

4.1 Introduction

It is well known that "platelet NO resistance" exists in patients with HFrEF (Anderson et al., 2004), but whether this occurs in HFpEF still remains to be elucidated. It was demonstrated by Anderson and colleagues, that both the platelets and vasculature of the HFrEF patients are significantly less responsive to NO donors (e.g. SNP), when compared to healthy controls (Anderson et al., 2004; Chirkov and Horowitz, 2007, Procter et al., 2016). As such, it was implicated from this study that this may reduce the effectiveness of some NO-mediated HF therapies and thus may subsequently contribute to the pro-thrombotic state in HF patients (Chirkov and Horowitz, 2007). Therefore, HF patients would benefit from a novel treatment that circumvents the "platelet NO resistance" phenomenon.

Recent studies by our research group and others have demonstrated nitrite as a potential therapeutic agent for HF (Borgognone et al., 2015; Borlaug et al., 2015; Ormerod et al., 2015). Nitrite has been shown to have both NO-dependent and -independent beneficial effects in various physiological and pathophysiological conditions, such as MI, pulmonary hypertension, HFrEF and HFpEF. Furthermore, nitrite has also been shown to inhibit platelet aggregation in healthy volunteers (Kadan et al., 2015) and may potentially improve platelet function in patients with HFpEF.

CAF often coexists with HFpEF and HFrEF (~40% and ~35%, respectively) and is also associated with intra-arterial thrombosis and thromboembolism (Lam et al., 2017; Linssen et al., 2011; Procter et al., 2015; Sartipy et al., 2017). Numerous research groups have observed an impaired platelet NO response in patients with AF, stable angina and acute coronary syndromes, and recently it has been revealed that this impairment contributes to platelet

hyperaggregability in patients with early onset AF (Chirkov et al., 2001; Chung and Lip, 2006; Procter et al., 2015). Herein, "platelet NO resistance" and nitrite was investigated in both HFpEF-AF and CAF, due to the close association between the two disease states (Lam et al., 2017; Sartipy et al., 2017).

4.2 Hypothesis and specific aims

4.2.1 Hypothesis

Nitrite circumvents the phenomenon of "platelet NO resistance" in washed platelets from patients with HFpEF-AF but not CAF alone.

4.2.2 Specific aims

This study has two main aims:

1) To determine whether the phenomenon of "platelet NO resistance" exists in patients with: **1)** HFpEF-AF and **2)** CAF only.
2) To compare the effects of nitrite in patients with HFpEF-AF or CAF and evaluate whether nitrite circumvents the phenomenon of "platelet NO resistance" in HFpEF patients.

4.3 Research methods

Blood was obtained from patients with HFpEF-AF and CAF alone as previously described in Section 2.1.3. To evaluate the effects of nitrite and BAY 41-2272 on platelet aggregation, washed platelets were prepared and counted for LTA experiments as described in Section 2.1.3. Aggregatory responses were then quantified as discussed in Section 2.1.3.

4.4 Results

4.4.1 Subject characteristics

Table 4.1 shows the subject characteristics and drug therapies. The old healthy volunteers, HFpEF-AF patients and CAF patients were all age- (P>0.05; one-way ANOVA) and gender-matched (P=0.22-0.65; Fisher's exact test).

Parameter	**Old Healthy Volunteers (OHV)** (n=11)	**Heart Failure with Preserved Ejection Fraction with Chronic Atrial Fibrillation (HFpEF-AF)** (n=29)	**Chronic Atrial Fibrillation (CAF)** (n=8)
Sex (M/F)	8/3	21/8	4/4
Age, y (Mean ±SD)	72.3±5.0	74.3±6.2	73.9±7.9
NYHA-Class I/II/III/	-	23/11/2	-
Diabetes Mellitus	-	2	2
ACE-inhibitors	-	10	2
Angiotensin II receptor blocker	-	2	2
Diuretics	-	2	4
β-adrenoceptor antagonists	-	8	6
α-adrenoceptor antagonist	-	2	-
Calcium channel blocker	-	9	1
Statins	-	10	2
Cardiac glycoside	-	-	-
Digoxin	-	4	2
Anti-arrhythmic	-	-	1
Anti-diabetic	-	2	2
Anti-coagulant	-	26	8

Table 4.1: Subject characteristics

4.4.2 $NaNO_2$ circumvents the phenomenon of "platelet NO resistance" in HFpEF-AF patients

In order to investigate whether $NaNO_2$ circumvented "platelet NO resistance" in HFpEF-AF patients, the effects of $NaNO_2$ on washed platelet aggregation responses to 3μg/mL collagen were first compared in old healthy volunteers *vs* HFpEF-AF patients. Representative traces are shown in Figures 4.1A and B, respectively. In the old healthy volunteers, $NaNO_2$ (10μM, 100μM or 1mM) attenuated platelet aggregation in a dose-dependent manner in response to collagen, when compared to the control group (Figure 4.1D). However, in HFpEF-AF patients, 10μM and 100μM $NaNO_2$ treatment had no effect on platelet aggregation, whilst 1mM $NaNO_2$ significantly attenuated platelet aggregation responses to collagen, when compared to the control group (Figure 4.1D).

To determine whether the responses observed in HFpEF-AF patients were caused by HF, CAF or a combination of both, the effects of $NaNO_2$ on washed platelet aggregation responses to 3μg/mL collagen were also explored in patients with CAF only. Representative traces are shown in Figure 4.1C. In this sub-group of patients, $NaNO_2$ also significantly attenuated platelet aggregation at the highest concentration (1mM), with modest attenuation at the lower concentrations (10μM and 100μM), when compared to the control group (Figure 4.1D).

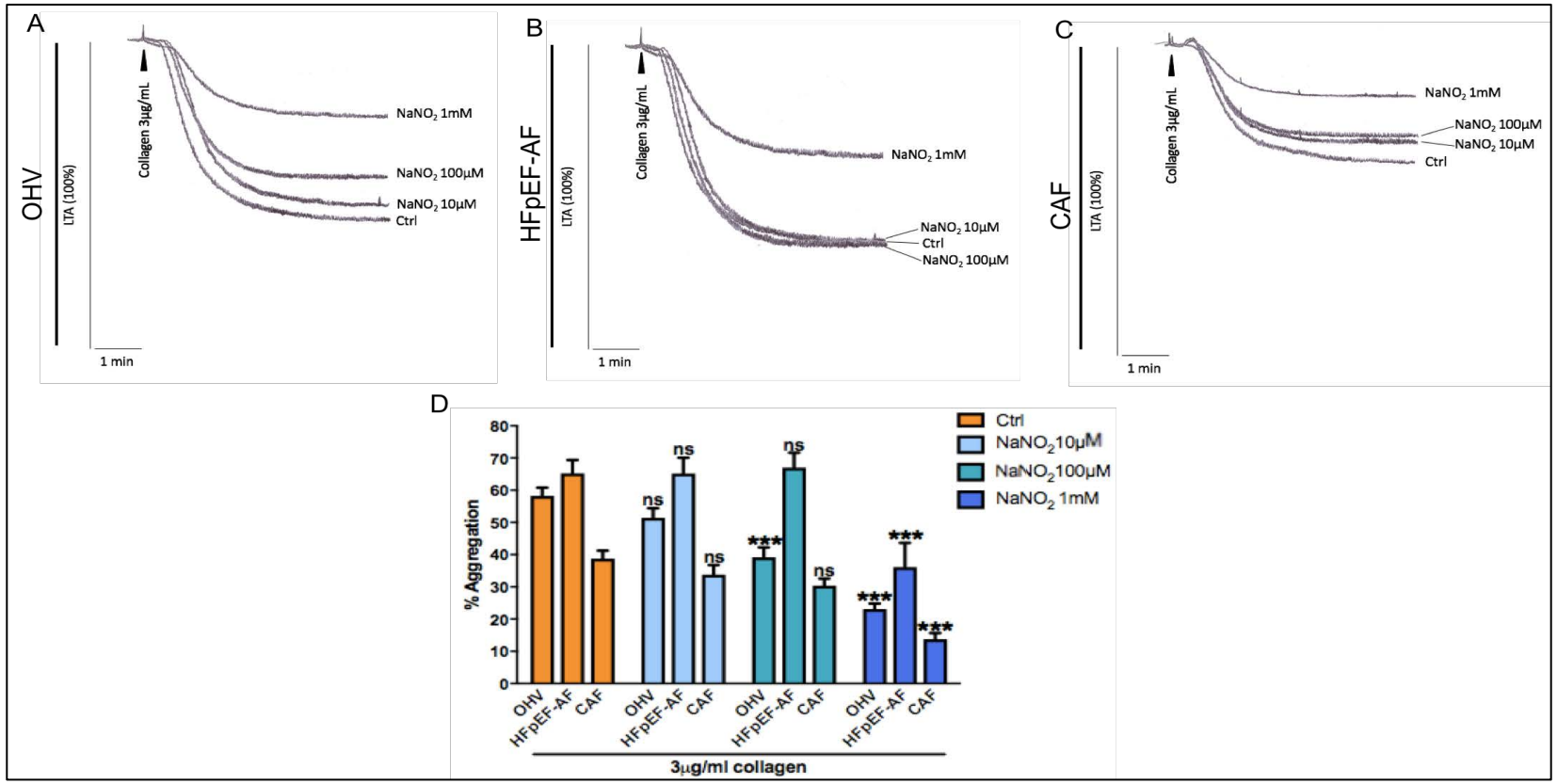

Figure 4.1: <u>Platelet aggregation responses in old healthy volunteers, HFpEF-AF patients and CAF patients following $NaNO_2$ incubation</u>

Washed platelets at a concentration of $2x10^8$/mL from old healthy volunteers (OHV), HFpEF-AF patients and CAF patients were incubated with increasing concentrations of $NaNO_2$ (10µM, 100µM or 1 mM) for 5 minutes, before being activated with 3µg/mL collagen and studied by light transmission aggregometry (LTA) for 5 minutes.

A/B/C: Representative traces demonstrating the influence of $NaNO_2$ incubation on platelet aggregation responses in old healthy volunteers, HFpEF-AF patients and CAF patients.

D: Quantitative analysis of repeat aggregation responses (% aggregation at 5 minutes). Bars represent means ± S.E.M. n=8-10. Statistical differences were determined using a repeated measures two-way ANOVA with Dunnett's test for multiple comparisons (*P<0.05, **P<0.01 and ***P<0.001).

The effects of SNP on platelet aggregation responses to 3μg/mL collagen were also compared as a positive control in the old healthy volunteers, HFpEF-AF patients and CAF patients. Representative traces are shown in Figures 4.2A, B and C, respectively. As shown in Figure 4.2D, SNP (10nM and 100nM) significantly attenuated platelet aggregation in a dose-dependent manner, when compared to the old healthy volunteer control group. Furthermore, SNP also produced a concentration-dependent inhibition of collagen-induced platelet aggregation in the CAF patients. As depicted in Figure 4.2D, we observed a significant attenuation with both the 10nM and 100nM doses, when compared to the control group. Interestingly, in the HFpEF-AF group, SNP treatment had no effect on platelet aggregation, when compared to the control group (Figure 4.2D).

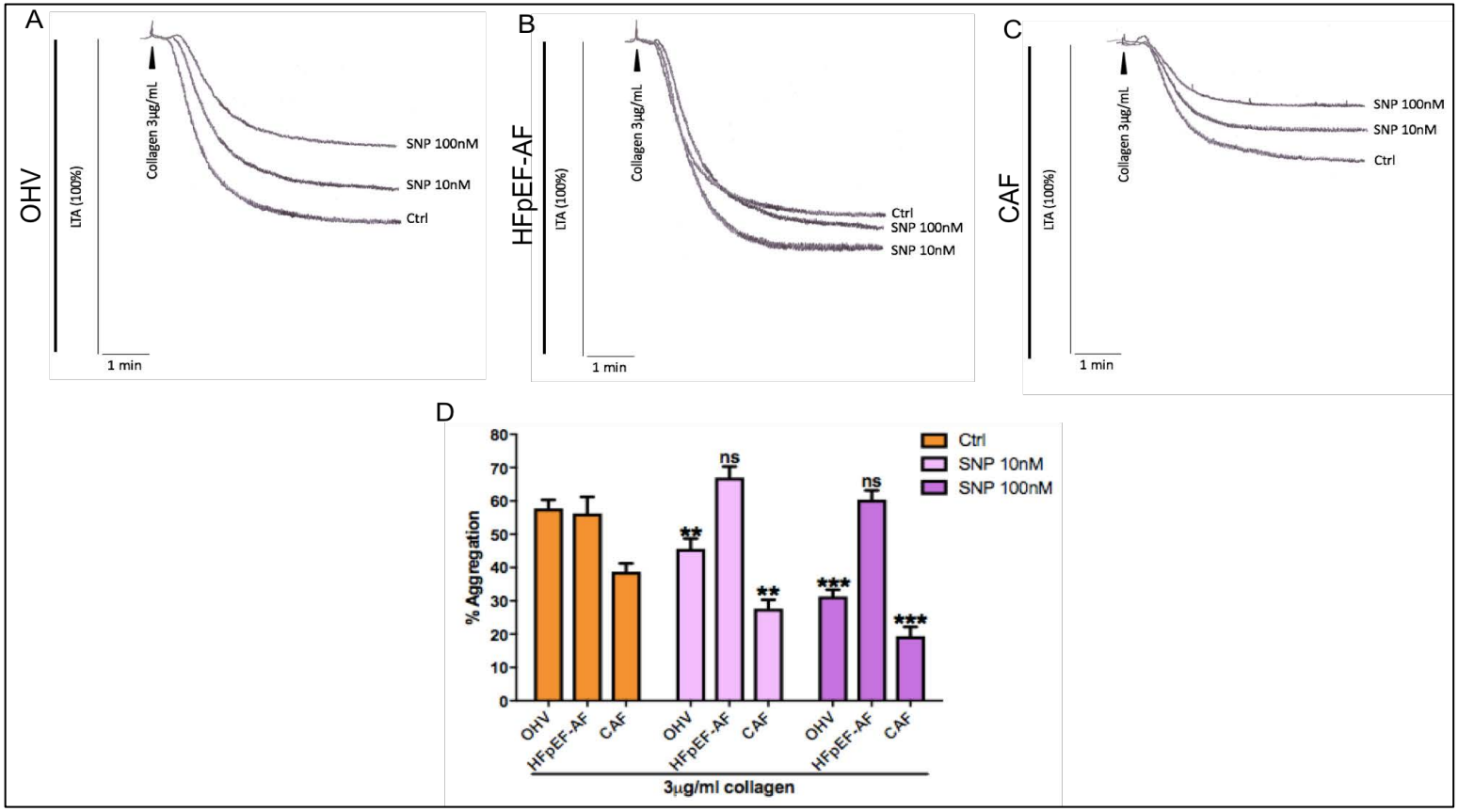

Figure 4.2: <u>Platelet aggregation responses in old healthy volunteers, HFpEF-AF patients and CAF patients following SNP incubation</u>

Washed platelets at a concentration of $2x10^8$/mL from old healthy volunteers (OHV), HFpEF-AF patients and CAF patients were incubated with increasing concentrations of SNP (10nM or 100nM) for 5 minutes, before being activated with 3µg/mL collagen and studied by light transmission aggregometry (LTA) for 5 minutes.

A/B/C: Representative traces demonstrating the influence of SNP incubation on platelet aggregation responses in old healthy volunteers, HFpEF-AF patients and CAF patients.

D: Quantitative analysis of repeat aggregation responses (% aggregation at 5 minutes). Bars represent means ± S.E.M. n=8-10. Statistical differences were determined using a repeated measures two-way ANOVA with Dunnett's test for multiple comparisons (*P<0.05, **P<0.01 and ***P<0.001).

4.5 Discussion

The phenomenon of "platelet NO resistance" has been shown to exist in patients with HFrEF (Anderson et al., 2004), but its occurrence in HFpEF remains to be defined. "Platelet NO resistance" is thought to reduce the effectiveness of some NO-mediated HF therapies, in addition to contributing to the pro-thrombotic state in HF (Chirkov and Horowitz, 2007). As such, HF patients would benefit from a novel treatment that circumvents "platelet NO resistance". Nitrite has been shown to inhibit platelet aggregation in heathy volunteers (Borgognone et al., 2015; Kadan et al., 2015), however the potential for nitrite to address "platelet NO resistance" in HFpEF or CAF, which often coexist together, is yet to be investigated.

In the present study, a diminished response to the NO donor, SNP, was observed in washed platelets from HFpEF-AF patients, when compared to the healthy volunteers and CAF patient group (Figure 4.2). These findings reveal that the phenomenon of "platelet NO resistance" may also exist in HFpEF. This novel concept has not yet been documented, however the identification of this underlying phenomenon may enable upcoming HFpEF therapies to be better tailored to the disease state and therefore help to improve future patient survival. Furthermore, a significant attenuation to platelet aggregation was observed following treatment with 1mM $NaNO_2$ in HFpEF-AF patients (Figure 4.1). These original findings suggest that high concentrations of nitrite may be able to circumvent "platelet NO resistance" in HFpEF-AF and hence highlight the potential for nitrite to address hyperaggregability in HFpEF in the future. In addition, since both $NaNO_2$ and SNP triggered concentration-dependent attenuation of platelet aggregation in CAF patients, this suggests that "platelet NO resistance" is primarily associated with HFpEF and not CAF (Figures 4.1 and 4.2). Once

again, the identification of underlying phenomenon or phenotyping subsequently enables pharmacological treatment to be tailored to the individual and disease state (e.g. personalised medicine), depending upon their response to NO donors.

As previously mentioned in Chapter 3, all experiments conducted in washed platelets to eliminate interference from other blood cell types and plasma proteins in nitrite-mediated effects. It is well known that O_2^- production by neutrophils contributes to a reduction in NO bioavailability and "platelet NO resistance" in HF (Anderson et al., 2004; Rajendran and Chirkov, 2008). However, since the phenomenon was observed in isolated platelets, this suggests that the production of O_2^- is not solely responsible for "platelet NO resistance" in HFpEF-AF.

Furthermore, our group have extended the findings observed in the present study by investigating the underlying mechanisms of nitrite in washed platelets from HFpEF-AF patients (Borgognone et al., 2018). LTA experiments revealed that NO scavengers (OxyHb or PTIO) could not revert nitrite-mediated attenuation of collagen-induced platelet aggregation in HFpEF-AF patients, whilst the sGC inhibitor, ODQ, reversed nitrite-dependent platelet inhibition in this patient group. However, SNP-mediated inhibition was shown to be reverted by OxyHb, PTIO and ODQ in HFpEF-AF patients (Borgognone et al., 2018). These findings therefore suggest that nitrite acts through sGC independently of NO to cause an attenuation of platelet aggregation in HFpEF-AF patients (Borgognone et al., 2018), and thus corroborate with our findings in heathy volunteers (Chapter 3).

Nitrite was also shown to increase VASPser^{239} phosphorylation in washed platelets from HFpEF-AF patients (Borgognone et al., 2018). VASPser^{239} phosphorylation occurred in the presence of NO scavengers, OxyHb and PTIO, but not when washed platelets from the HFpEF-AF patients were incubated with the sGC inhibitor, ODQ (Borgognone et al., 2018). These findings therefore indicate that nitrite acts through sGC-PKG-VASPser239 independently of NO in washed platelets from HFpEF-AF patients (Borgognone et al., 2018), and hence corroborate with the results of the LTA experiments and our findings in healthy volunteers (Chapter 3).

4.5.1 Study limitations and future considerations

This study also has a few limitations which will now be addressed. Firstly, the only platelet agonist used during the LTA experiments was collagen. As discussed in Chapter 3, this is a key limitation as the presence or absence of platelet dysfunction in the healthy volunteers, HFpEF-AF patients and CAF patients cannot be assumed from one agonist (Dovlatova, 2015; Hayward et al., 2009). A decreased platelet aggregation response to collagen was observed in washed platelets obtained from CAF patients, when compared to the healthy volunteers and HFpEF-AF patient group. To our knowledge the effect of collagen on washed platelets from CAF has not been investigated before, but our group have previously reported PRP aggregation in response to 2mg/mL collagen to be inhibited by approximately 24% in patients with CAF on no anti-thrombotic therapy (Kamath et al., 2002). Furthermore, the complexity of events of platelet activation in AF have been documented (Kamath et al., 2002; Kamath et al., 2003) and therefore further studies involving multiple agonists (e.g. ADP, AA, collagen, adrenaline and TXA_2) are required to explore platelet function and the role of NO donors/nitrite in this disease state.

Furthermore, high concentrations of nitrite (1mM) were used in the present study. As discussed in Chapter 3, this is a major drawback as any modulation of platelet function by normal plasma nitrite concentrations cannot be assumed when using non-physiological concentrations of $NaNO_2$ (Kevil et al., 2011; Srihirun et al., 2018).

Moreover, a number of the HFpEF-AF (10/29) and CAF patients (2/8) were taking ACE-inhibitors, which have previously been linked to reductions in "platelet NO resistance". Despite this, the ACE-inhibitors seemed not to influence "platelet NO resistance" under these circumstances as the phenomenon appeared in all HFpEF-AF patients.

Finally, the potential for nitrite to exhibit synergistic activity with BAY 41-2272 also remains to be investigated in HFpEF-AF patients. To determine whether the applications of BAY 41-2272 exceed healthy volunteers and establish whether nitrite can circumvent "platelet NO resistance" more effectively in the presence of BAY 41-2272, further studies are warranted.

4.5.2 Conclusions

The results of this study demonstrate that nitrite circumvents the phenomenon of "platelet NO resistance" in washed platelets from patients with HFpEF-AF but not CAF alone. Therefore, highlighting the potential for nitrite therapy to address hyperaggregability in HFpEF in the future. Additional studies by our research group suggest that nitrite acts through sGC-PKG-VASPser239 independently of NO, to cause an attenuation of platelet aggregation in HFpEF-AF patients. Further, HFpEF-AF patient phenotyping and subsequent stratification of pharmacological treatment according to NO response, may also help to reduce the morbidity and mortality of HFpEF in the future.

Chapter 5: Exploration of nitrite, lipid content and tissue morphology in ALDH2 WT and KO mice.

5.1 Introduction

Over the last 30 years, the role of ALDH2 in the two-stage process of ethanol metabolism has been thoroughly explored (Chen et al., 2014). ALDH2 belongs to a superfamily of detoxifying enzymes which function to maintain cellular haemostasis by oxidising reactive aldehydes to non-toxic carboxylic acids (Budas et al., 2009). These tetrameric enzymes are found in the mitochondrial matrix of most tissues, but ALDH2 is present at the highest concentration in the liver (Budas et al., 2009; Chen et al., 2014).

Mitochondrial ALDH2 has also emerged as an important mediator of cardioprotection (Budas et al., 2009). There is increasing evidence to suggest that myocardial ALDH2 enzymes mediate the detoxification of reactive aldehydes, such as acetaldehyde or 4-hydroxynonenal (4-HNE)/malondialdehyde (MDA), and protect the heart from oxidative stress (Budas et al., 2009; Chen et al., 2014). During HF and myocardial ischaemia reperfusion injury (IRI), excessive ROS production exacerbates the peroxidation of polyunsaturated fatty acids, including AA, linoleic acid and cardiolipin, which are present in the mitochondrial and plasma membranes. Lipid hydroperoxides formed by this process subsequently give rise to toxic end-products, 4-HNE and MDA, which then go on to form adducts and cause myocardial damage (Bolli et al., 1989; Roede and Jones, 2010; Uchida and Stadtman, 1992). 4-HNE is the most reactive of the endogenous aldehydes generated during lipid peroxidation and due to its amphiphilic nature, 4-HNE can easily diffuse across membranes and react with cysteine, histidine and lysine residues to form protein adducts via Michael addition (>99%) and Schiff base (<1%) reactions (Chen et al., 2014; Uchida and Stadtman, 1992). During IRI, a build-up of 4-HNE adducts within the myocardium impairs cardiac contractility and promotes cardiac cell damage/death by: **1)** increasing mitochondrial

permeability and dysfunction, **2)** inhibiting the electron transport chain and Krebs cycle, **3)** inhibiting ALDH2 activity, **4)** reducing membrane integrity, **5)** inhibiting proteasomal function, **6)** triggering unfolded protein accumulation, and **7)** causing DNA damage (Chen et al., 2014). Accumulation of 4-HNE and its adducts, has also been linked to the development of HF, cardiomyopathies, hypertension, peripheral artery disease, stroke and atherosclerosis (Chen et al., 2014; Gueldner et al., 2016; Guo et al., 2013).

Furthermore, the contribution of the mitochondrial ALDH2 enzyme in cardioprotection was originally discovered downstream of mitochondrial protein kinase C type ϵ (PKCϵ) activation (Budas et al., 2010; Chen et al., 2008; Chen et al., 2014). A broad range of stimuli, including PKCϵ-/PI3K-dependent phosphorylation (endogenous stimuli) and aldehyde dehydrogenase activators (Aldas; exogenous stimuli) have also been shown to activate ALDH and protect the heart against myocardial IRI. These findings both allude towards a fundamental role for ALDH2 in cardioprotection (Garlid et al., 2009).

Moreover, aldehyde detoxification occurs rapidly in individuals with fully functioning ALDH2 enzymes (e.g. individuals with two WT ALDH2*1 alleles), whilst individuals with reduced ALDH2 activity (e.g. carriers of the ALDH2*2 allele) experience an accumulation of toxic aldehydes, such as acetaldehyde and 4-HNE (Chen et al., 2014; Dandre et al., 1995; Goedde et al., 1992; Li et al., 2006). The ALDH2*2 polymorphism is characterised by a single base mutation resulting in the replacement of the amino acid glutamate with lysine and is found in approximately 35-40% of East Asians (e.g. Chinese, Korean, Japanese and Taiwanese people) (Budas et al., 2009; Chen et al., 2014; Yoshida et al., 1984). Moreover, the mutant ALDH2*2 allele has recently been shown to exert a dominant effect over its WT

ALDH2*1 allele. Much less than 50% of the WT enzymatic activity has been observed in heterozygous individuals (ALDH2*1/*2), whilst only ~1-4% of the WT ALDH2 activity has been seen in homozygous individuals (ALDH2*2/*2) (Chen et al., 2014; Farres et al., 1994; Ferencz-Biro and Pietruszko, 1984; Zhou and Weiner, 2000).

Human epidemiological studies have also revealed that ALDH2*2 carriers exhibit increased susceptibility to cardiac disease, including MI, atherosclerosis and pulmonary arterial hypertension (Chen et al., 2014; Gueldner et al., 2016; Xu et al., 2017). Whilst, experimental studies in ALDH2*2 mice have shown increased ROS production, endothelial dysfunction and exacerbated cardiac damage following IRI (Chen et al., 2014). Experimental approaches to enhance ALDH2 activity through genetic overexpression or pharmacological activation of ALDH2 have demonstrated improved 4-HNE detoxification and subsequent protection against both acute (e.g. IRI and stroke) and chronic (e.g. HF) CVDs (Chen et al., 2014).

In addition, carriers of the mutant ALDH2*2 allele have a diminished response to organic nitrates, such as GTN, which are currently used to treat angina, acute MI and HF (Bailey et al., 2014; MacAllister, 2000; Mackenzie et al., 2005). ALDH2 is considered to be the principle enzyme responsible for vascular GTN bioactivation and NO release, thus the mitochondrial enzyme plays a pivotal role in the vasodilatory and anti-platelet effects of organic nitrates (Li et al., 2006; Mackenzie et al., 2005; Mollace et al., 2014). Oxidative stress resulting from the production of free radicals, O_2^- and $ONOO^-$, has been linked to the development of nitrate tolerance (Daiber and Münzel, 2015; D'Souza et al., 2011; Mollace et al., 2014). In a recent study by Mollace and colleagues, prolonged GTN incubation was shown to reverse GTN-mediated attenuation of thrombin-induced platelet aggregation, whilst

also reducing cGMP levels in washed platelets (Mollace et al., 2014). These effects were associated with a reduction in GTN-induced nitrite formation and the nitration of ALDH2 at tyrosine residues, thus indicating that GTN tolerance resulted from a reduction in NO production associated with ALDH2 impairment (Mollace et al., 2014). Co-incubation of the platelets with the SOD mimetic/$ONOO^-$ scavenger, Mn(III) tetrakis (4-benzoic acid) porphyrin (MnTBAP), was also shown to reverse nitrate tolerance in washed platelets. These findings therefore confirmed the role of O_2^- and $ONOO^-$ in ALDH2 inactivation and the development of nitrate tolerance (Mollace et al., 2014).

A few studies have also revealed interactions between mitochondrial ALDH2 and nitrite. Firstly, ALDH2 plays a critical role in the reduction of nitrite to NO in the 'nitrate-nitrite-NO pathway' (Li et al., 2008). This process is regulated by oxygen tension, pH and a reduction in substrate concentrations, and has been shown to be much more prominent in tissues than in the blood (Li et al., 2008). Furthermore, in a recent study of ischaemia in the human forearm, the administration of nitrite during the second window of pre- and post-conditioning was shown to reduce endothelial dysfunction in ALDH2*2 carriers (Ormerod et al., 2017). Since reductions in IRI were absent from individuals homozygous for the ALDH2*1 allele, these findings indicate that the effects of nitrite-mediated pre/post-conditioning may be dependent on ALDH2 genotype (Ormerod et al., 2017). ALDH2 has also emerged as an important mediator of hypoxic vasodilation in HF (Arif et al., 2015). Nitrite-mediated dilation diminished in rat aorta and human resistance vessels following the inhibition of ALDH2 by cyanamide or propionaldehyde, especially under hypoxic conditions (Arif et al., 2015). Finally, in a recent metabolomic/proteomic study, nitrite-dependent phosphorylation of ALDH2 at Thr^{431} was observed in rat hearts (Perlman et al., 2009). Phosphorylation of

ALDH2 at Thr^{431} is also mediated by PKCϵ and has been shown to cause cardioprotective increases in enzyme activity, thus these findings suggest that interactions between nitrite and ALDH2 may be important for nitrite-mediated cardioprotection (Chen et al., 2008; Perlman et al., 2009).

Since a number of recent studies propose a role for mitochondrial ALDH2 in nitrite-mediated effects of vascular and cardiac disease, this suggests that this mechanism may have some benefits on platelet function. We have previously shown that nitrite significantly attenuates platelet aggregation in both healthy volunteers (Chapter 3) and patients with HFpEF-AF (Chapter 4), but the mechanism of nitrite in platelet aggregation remains to be fully elucidated. As such, further research is warranted to assess whether ALDH2 contributes to nitrite-mediated attenuation of platelet aggregation.

Finally, the mutant ALDH2*2 allele is thought to be a novel risk factor for the development of non-alcoholic fatty liver disease (NAFLD), which is characterised by the deposition of fat in the liver (Oniki et al., 2016). A recent study examining the association of hepatic steatosis with common subclinical/clinical CVD outcomes, has revealed a link between hepatic steatosis and CVD (Mellinger et al., 2015). As such, further research into the relationship between tissue lipid content (e.g. liver and skeletal muscle tissue) and ALDH2 expression/activity is warranted.

Herein, the contribution of ALDH2 to nitrite-mediated attenuation of washed platelet aggregation will first be explored in ALDH2 WT and KO mice. The influence of the ALDH2

expression, and therefore activity, on neutral lipid accumulation and tissue morphology will also be compared in ALDH2 WT *vs* KO tissues (e.g. liver and skeletal muscle tissue).

5.2 Hypothesis and specific aims

5.2.1 Hypothesis

ALDH2 plays an essential role in nitrite-mediated attenuation of collagen-induced platelet aggregation in mouse washed platelets, whilst inactivation of the ALDH2 gene increases the lipid content of mouse liver and skeletal muscle tissue.

5.2.2 Specific aims

This study has three main aims:

1) To determine ALDH2 expression in washed platelets and tissues (liver, skeletal muscle and cardiac tissue) obtained from ALDH2 WT and KO mice, respectively.
2) To compare the effects of nitrite in ALDH2 WT *vs* KO mice, and determine the contribution of ALDH2 to nitrite-mediated attenuation of platelet aggregation.
3) To compare the lipid accumulation/tissue morphology of liver and skeletal muscle tissue sections from ALDH2 WT *vs* KO mice.

5.3 Research methods

Blood and tissue (liver, skeletal muscle and cardiac tissue) samples were obtained from ALDH2 WT and KO mice as previously described in Section 2.2.3. To evaluate the effects of ALDH2 and nitrite on platelet aggregation, washed platelets were prepared and counted for LTA experiments as described in Section 2.2.4. Aggregatory responses were then quantified as discussed in Section 2.2.4. Platelet and tissue homogenates for Western blotting were also prepared and analysed as described in Section 2.2.5. To compare lipid accumulation and tissue morphology in ALDH2 WT and KO mice, liver and skeletal muscle tissue samples were first sectioned and stained with ORO, before counterstaining with Mayer's haematoxylin, as previously described Section 2.2.6. The extent of lipid accumulation revealed by ORO staining was analysed as discussed in Section 2.2.6.

5.4 Results

5.4.1 ALDH2 expression in ALDH2 WT and KO mice

To determine whether ALDH2 is expressed in washed platelets, liver, skeletal muscle and cardiac tissue, Western blot analysis was conducted. As depicted in Figures 5.1A and B, ALDH2 was expressed in all of the ALDH2 WT samples, but the level of ALDH2 expression varied between the sample types. Densitometric analysis revealed that ALDH2 expression was 18-fold higher in the WT liver tissue and 3-fold higher in the WT cardiac tissue, when compared with ALDH2 expression in the WT platelets (Figure 5.1B). Whilst there was a 0.6-fold decrease in ALDH2 expression in the WT skeletal muscle tissue, when compared to the WT platelets. Conversely, ALDH2 was not expressed in any of the KO samples (Figures 5.1A and B).

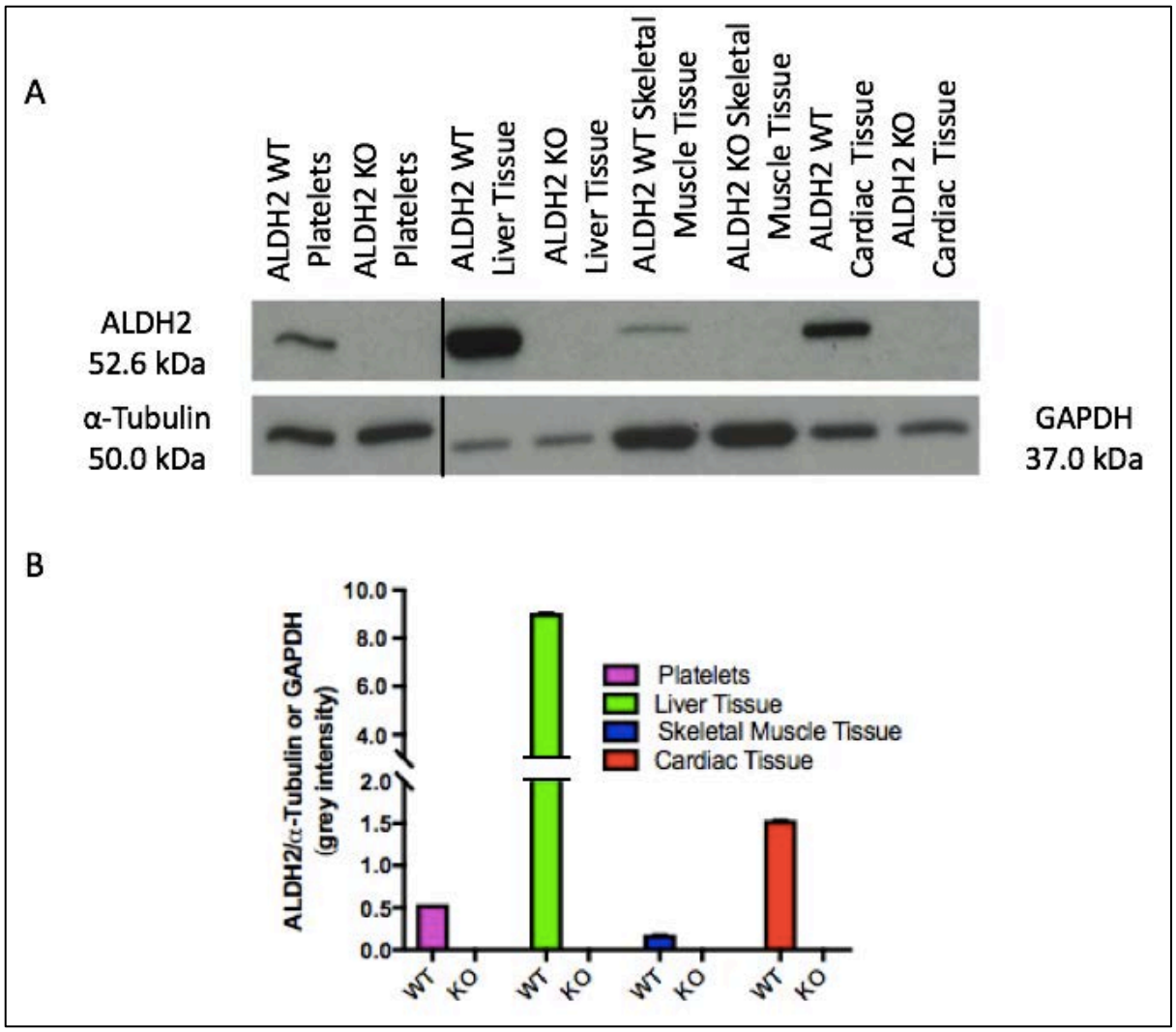

Figure 5.1: <u>ALDH2 expression in platelets and tissues obtained from ALDH2 WT and KO mice</u>

$5x10^8$/mL washed platelets obtained from ALDH2 WT and KO mice were incubated for 10 minutes before being lysed with 5x sample buffer. ALDH2 WT and KO tissue (liver, skeletal muscle and cardiac tissue) homogenates, containing ~25µg of protein, were also prepared. The platelet and tissue homogenates were then used for SDS-PAGE (8%) and Western blot. The blot was probed with anti-ALDH2 (1:1000), anti- α-Tubulin (1:5000) or anti-GAPDH (1:20,000), and the appropriate secondary antibodies (anti-goat or anti-mouse; 1:10.000).

A: Representative Western blot demonstrating ALDH2 expression in platelets and tissues (liver, skeletal muscle and cardiac tissue) harvested from ALDH2 WT and KO mice. α-Tubulin and GAPDH were used as loading controls.
B: Quantitative analysis of the representative Western blot (ALDH2/α-Tubulin (platelets) or GAPDH (liver, skeletal muscle and cardiac tissue); grey intensity). n=1.

5.4.2 Does $NaNO_2$ inhibit platelet aggregation via ALDH2?

To determine the contribution of ALDH2 to nitrite-mediated platelet inhibition, washed platelet aggregation was compared in ALDH2 WT *vs* KO mice. As shown in Figures 5.2A and B, the NO donor, SNP, was used as a positive control for the present study. In the ALDH2 WT mice, 100nM SNP significantly attenuated washed platelet aggregation to 3µg/mL collagen, when compared to the control group (Figure 5.2C). $NaNO_2$ (10µM, 100µM or 1mM) also inhibited collagen-induced platelet aggregation in a concentration-dependent manner, when compared to the control group (Figure 5.2C). In contrast, neither SNP nor $NaNO_2$ significantly inhibited collagen-induced platelet aggregation in the ALDH2 KO washed platelets, when compared to the control group. SNP inhibited platelet aggregation by approximately 11.80%, whilst there was no apparent platelet inhibition with 10µM, 100µM or 1mM $NaNO_2$ (Figure 5.2C), when compared to the control. However, comparisons between the genotypes revealed that there was not a significant difference between the effects of SNP in ALDH2 WT and KO platelets (Figure 5.2C).

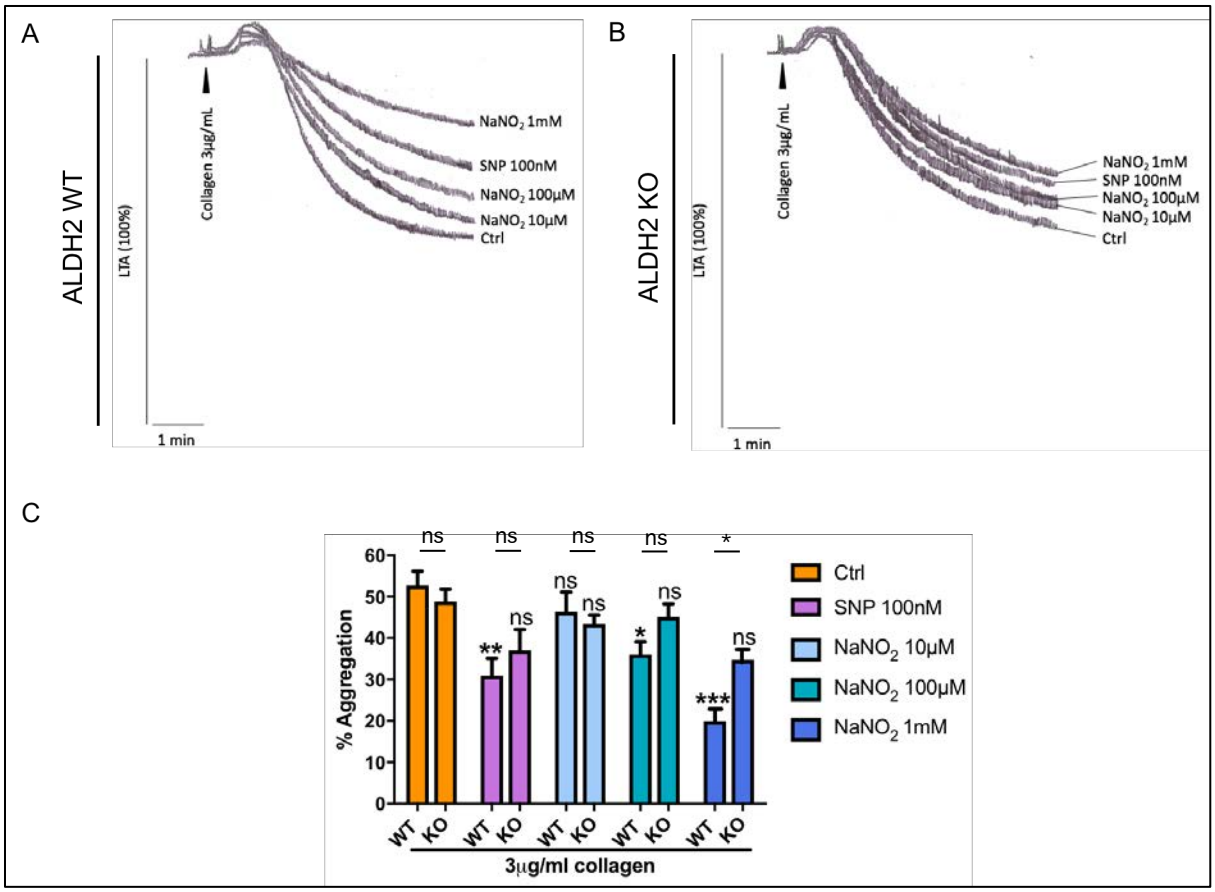

Figure 5.2: <u>Platelet aggregation responses in ALDH2 WT and KO mice following SNP or $NaNO_2$ incubation</u>

Washed platelets at a concentration of $2x10^8$/mL from ALDH2 WT and KO mice were incubated with 100nM SNP or increasing concentrations of $NaNO_2$ (10µM, 100µM or 1 mM) for 5 minutes, before being activated with 3µg/mL collagen and studied by light transmission aggregometry (LTA) for 5 minutes.

A: Representative traces demonstrating the influence of SNP or $NaNO_2$ incubation on platelet aggregation responses ALDH2 WT and KO mice.
B/: Quantitative analysis of repeat aggregation responses (% aggregation). Bars represent means ± S.E.M. n=6-7. Statistical differences were determined using repeated measures two-way ANOVA with Dunnett's test for multiple comparisons and unpaired t-tests (*P<0.05, **P<0.01 and ***P<0.001).

5.4.3 ALDH2 WT and KO tissue staining

5.4.3.1 ORO staining in liver tissue

ORO staining was used to visualise neutral lipid accumulation within ALDH2 WT and KO mouse livers. Figure 5.3A shows representative images of ORO stained ALDH2 WT and KO liver sections, respectively. The variation in ORO staining in the ALDH2 WT and KO liver tissue is highlighted by the magnified insets shown at the bottom right corner of the images in Figure 5.3A. As shown in Figure 5.3B, there was a significant increase in the % of ORO staining in ALDH2 KO liver sections, when compared to the ALDH2 WT liver sections.

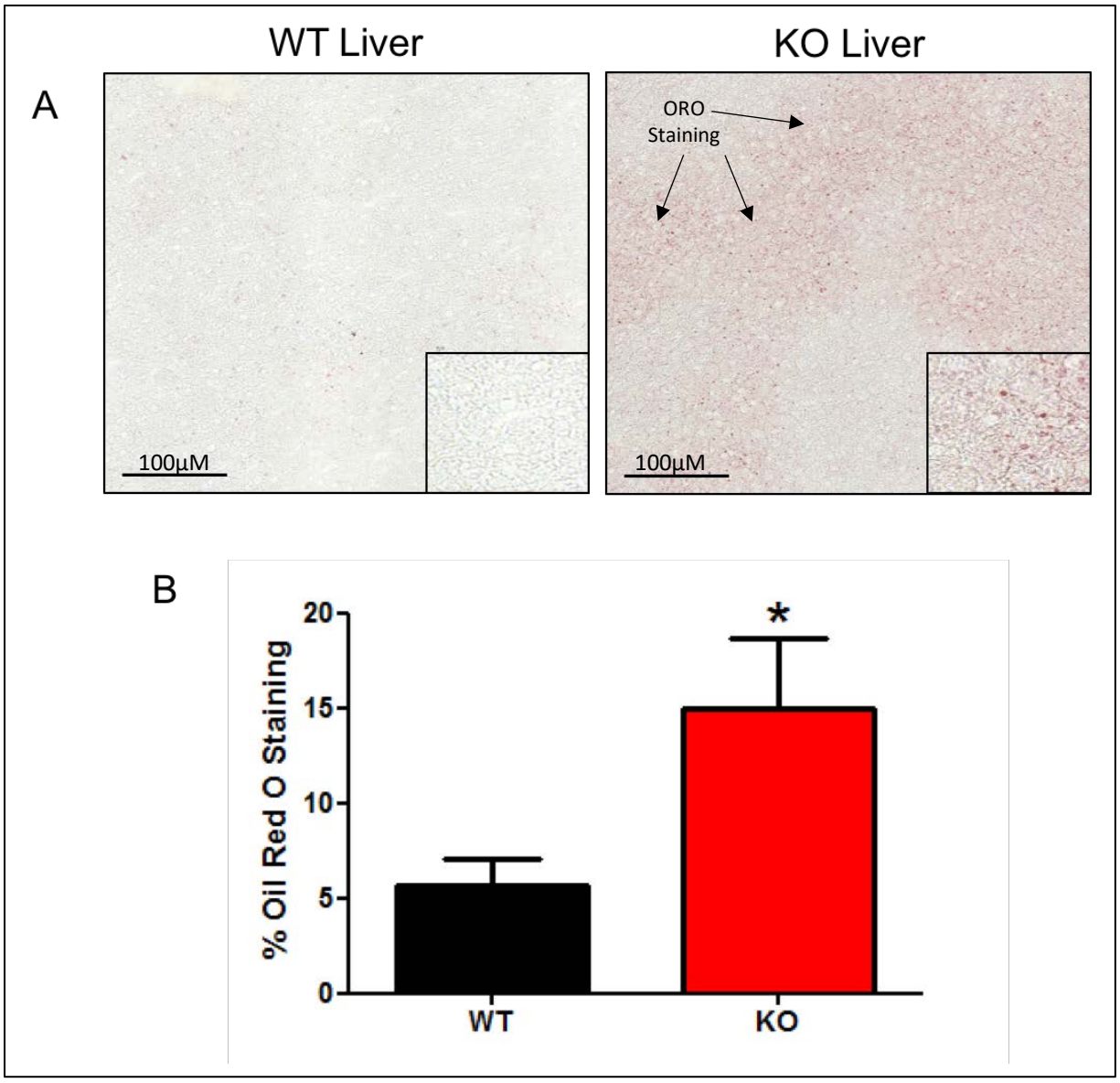

Figure 5.3: <u>ORO staining in ALDH2 WT and KO liver tissue sections</u>
Liver tissue samples obtained from ALDH2 WT and KO mice were sectioned using a cryostat. The 6µM liver tissue sections were then stained with ORO to enable the visualisation and quantification of the contained lipids.
A: Representative images demonstrating fat cell and neutral lipid accumulation in liver tissue sections from ALDH2 WT and KO mice. Scale bars represent 100µM and the magnification is x20. To highlight tissue morphology, insets from the images have been magnified 3x.
B: Quantitative analysis of repeat ORO staining (% ORO staining). Bars represent means ± S.E.M. n=7. Statistical differences were determined using an unpaired t-test (*P<0.05).

5.4.3.2 ORO staining in skeletal muscle tissue

ORO staining was also analysed in ALDH2 WT and KO mouse skeletal muscle. Representative images are shown in Figure 5.4A. As depicted in Figure 5.4B, there was a significant rise in the % of ORO staining in ALDH2 KO skeletal muscle sections, when compared to the ALDH2 WT liver sections. Once again, the variation in ORO staining is highlighted by the magnified insets shown at the bottom right corner of the images in Figure 5.4A.

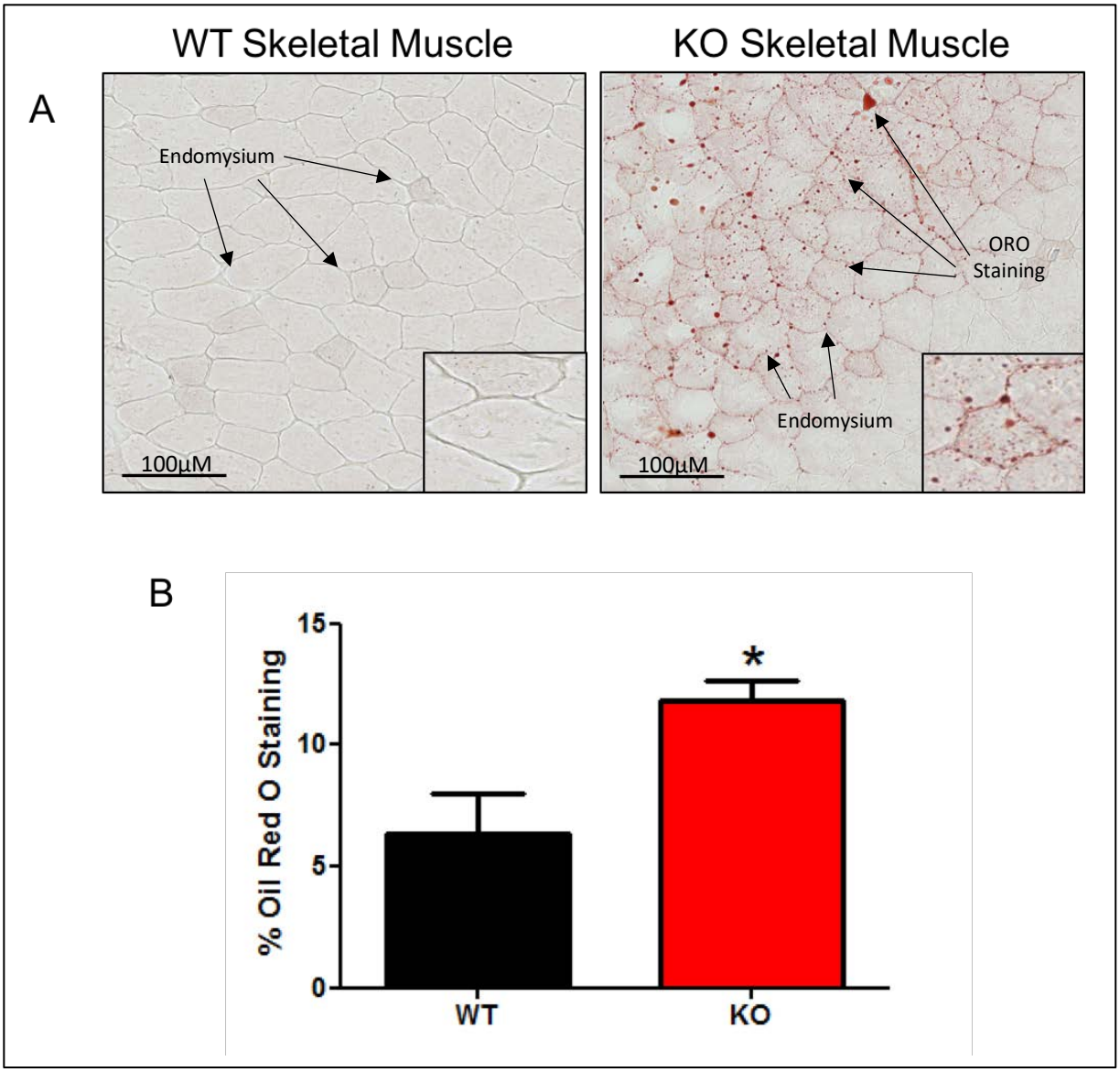

Figure 5.4: <u>ORO staining in ALDH2 WT and KO skeletal muscle tissue sections</u>
Skeletal muscle tissue samples obtained from ALDH2 WT and KO mice were sectioned using a cryostat. The 6µM skeletal muscle tissue sections were then stained with ORO to enable the visualisation and quantification of the contained lipids.
A: Representative images demonstrating fat cell and neutral lipid accumulation in skeletal muscle tissue sections from ALDH2 WT and KO mice. Scale bars represent 100µM and the magnification is x20. To highlight tissue morphology, insets from the images have been magnified 3x.
B: Quantitative analysis of repeat ORO staining (%ORO staining). Bars represent means ± S.E.M. n=6. Statistical differences were determined using an unpaired t-test (*P<0.05).

5.4.3.3 Mayer's haematoxylin counterstaining in liver and skeletal muscle tissue

Liver sections that had been previously stained with ORO were then counterstained with Mayer's haematoxylin. This staining enabled tissue morphology and cell nuclei to be visualised. Figures 5.5A and B show representative images of Mayer's haematoxylin stained ALDH2 WT and KO liver (Figure 5.5A) and skeletal muscle (Figure 5.5B) sections. As depicted in Figures 5.5A and B, both ALDH2 WT and KO liver and skeletal muscle had a normal morphology. The normal morphology is also highlighted by the magnified insets shown at the bottom right corner of these images.

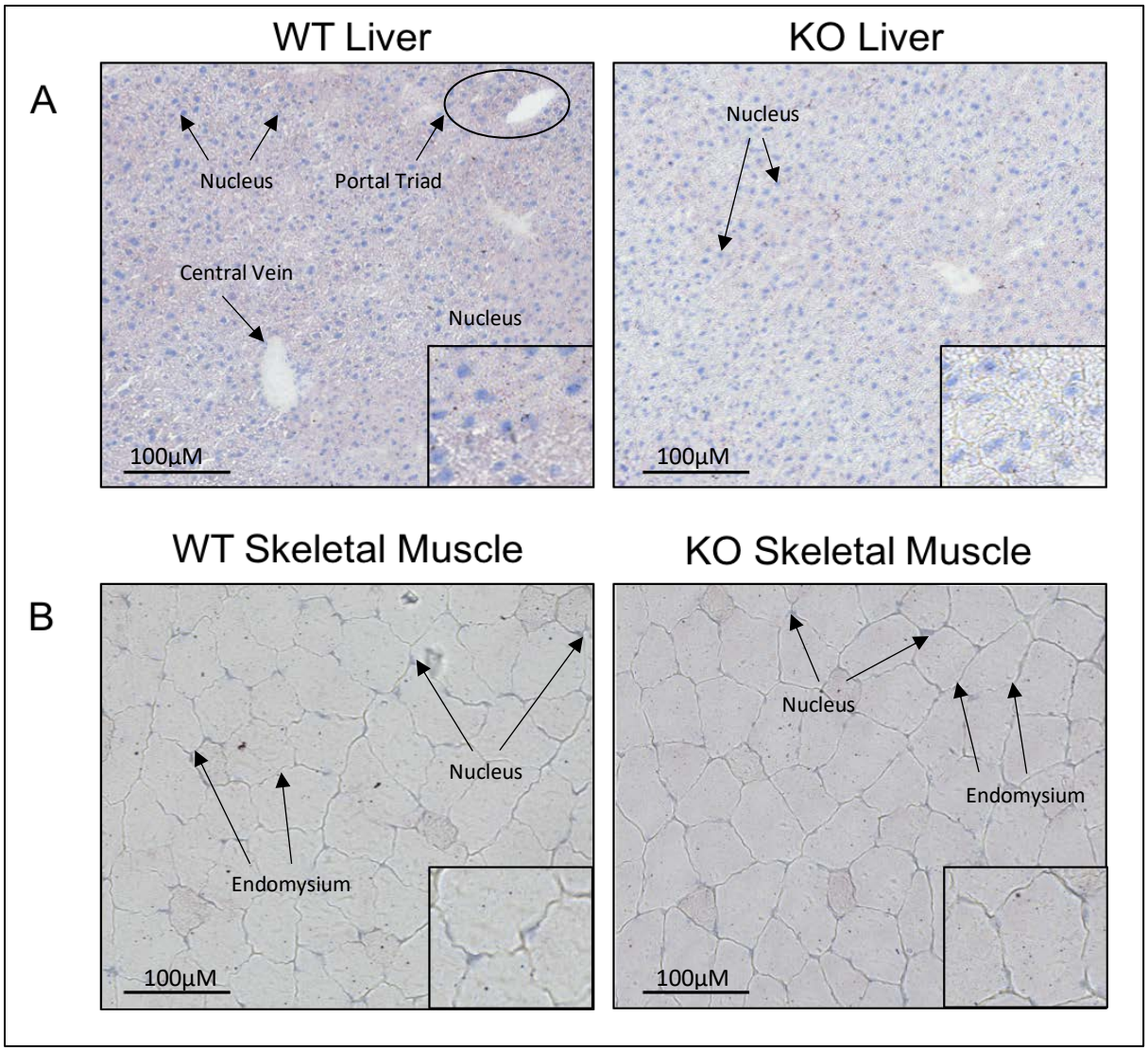

Figure 5.5: <u>Mayer's haematoxylin counterstaining in ALDH2 WT and KO liver and skeletal muscle tissue</u>

Liver and skeletal muscle tissue samples obtained from ALDH2 WT and KO mice were sectioned using a cryostat. The 6µM liver and skeletal muscle tissue sections were stained with ORO, before being counterstained with Mayer's haematoxylin to enable the tissue morphology and cell nuclei to be visualised.

A/B: Representative images demonstrating the tissue morphology of liver and skeletal muscle tissue sections from ALDH2 WT and KO mice. Scale bars represent 100µM and the magnification is x20. To further highlight tissue morphology, insets from the images have been magnified 3x.

5.5 Discussion

It is widely recognised that ALDH2 plays an essential role in cardioprotection and is thought to be associated with the detoxification of reactive aldehydes, such as acetaldehyde and 4-HNE (Budas et al., 2009; Chen et al., 2014). Furthermore, studies have revealed an interaction between ALDH2 and GTN, which is largely responsible for vascular GTN bioactivation and NO release, and therefore fundamentally involved in the anti-platelet effects of organic nitrates (Mackenzie et al., 2005; Mollace et al., 2014). A role for ALDH2 in nitrite-mediated cardioprotection and vasodilatation have also been suggested (Arif et al., 2015; Ormerod et al., 2017). In addition, our group have very recently reported that nitrite inhibits platelet aggregation in both healthy and HFpEF-AF patients (Borgognone et al., 2018). However, the mechanism of nitrite in platelet aggregation remains to be fully elucidated, and to the best of our knowledge the role of ALDH2 in nitrite-mediated platelet aggregation has not been investigated. Herein, we show for the first time that nitrite inhibits platelet aggregation in the presence of ALDH2.

We first validated the ALDH2 expression in the platelet and tissue samples. As expected, Western blot analysis revealed that ALDH2 was expressed in the WT mouse liver, skeletal muscle and cardiac tissue, and interestingly in the washed platelets (Figure 5.1). The ALDH2 enzyme was not expressed in any of the KO samples (Figure 5.1). Our findings are supported by a recent mouse study, where ALDH2 was expressed in the liver and heart of ALDH2 WT mice (Oyama et al., 2005). Oyama and colleagues also suggested that the tissue-distribution of the enzyme was very similar in mice and humans, thus adding translatability and relevance to our mouse study (Oyama et al., 2005). Whilst ALDH2 has also been shown to be

expressed in mouse skeletal muscle (Zhang et al., 2017), ALDH2 expression has not previously been demonstrated in isolated platelets from mice.

Numerous whole-blood and PRP aggregation studies from healthy subjects and mice have shown nitrite to inhibit platelet aggregation following its conversion to NO by the reductase activity of partially deoxygenated haemoglobin (Corti et al., 2013; Parakaw et al., 2017; Park et al., 2013; Srihirun et al., 2012). It has been revealed that a reduction of nitrite via nitrite reductases, such as deoxyhaemoglobin, XOR and ALDH2, helps to maintain NO production during hypoxia and acidosis (Calvert and Lefer, 2009; Vitturi and Patel, 2011). The XOR inhibitor, febuxostat, was also shown to partially reverse the anti-thrombotic effects of $NaNO_2$ in rats (Kramkowski et al., 2016). Furthermore, our research group have very recently demonstrated that nitrite acts through sGC-PKG-VASPser239 independently of NO, to cause an attenuation of platelet aggregation in healthy volunteers and HFpEF-AF patients (Chapters 3 and 4). Despite these findings, aspects of the platelet nitrite-mechanism remain unclear. Numerous interactions between mitochondrial ALDH2 and nitrite have been documented, thus suggesting that nitrite may also interact with ALDH2 to mediate an attenuation of platelet aggregation.

In the present study, we demonstrate that active ALDH2 is required for nitrite-mediated attenuation of washed platelet aggregation in response to collagen (Figure 5.2). The effects of the NO donor, SNP, were shown to be almost identical in the ALDH2 WT and KO washed platelets, however a more significant attenuation of platelet aggregation was observed with higher concentrations of $NaNO_2$ (Figure 5.2). These novel findings therefore suggest that nitrite may in fact interact with ALDH2 to inhibit platelet aggregation, since mutant ALDH2

mice abolished nitrite's effect on platelet function. By developing our understanding of ALDH2-/nitrite-mediated platelet function this could help to improve the efficacy of anti-platelet therapies and additional treatments in HF and other CVDs in the future.

Tissues with a high energy demand and therefore mitochondrial content, such as the liver and skeletal muscle, are more severely affected by mitochondrial dysfunction (Boengler et al., 2017). Recent studies have reported that the ALDH2*2 allele may be a risk factor for liver steatosis and NAFLD development (Oniki et al., 2016). The effect of ALDH2 deficiency on skeletal muscle lipid content still remains to be investigated, however the accumulation of triglycerides within skeletal muscle has been linked to obesity, insulin resistance and type 2 diabetes (Goodpaster and Wolf, 2004). In the present study, we demonstrated that the lipid content was significantly increased in the ALDH2 mouse KO liver and skeletal muscle tissue, when compared to their respective WT controls (Figures 5.3 and 5.4). These findings suggest that the ALDH2*2 allele may also be a risk factor for lipid accumulation in skeletal muscle tissue. Further research into the effect of ALDH2 deficiency on tissue lipid content is therefore warranted, especially as hepatic steatosis has now been associated with CVD, (Mellinger et al., 2015), whilst lipid accumulation within skeletal muscle was previously linked to obesity, insulin resistance and type 2 diabetes (Goodpaster and Wolf, 2004).

Finally, despite increases in lipid content in ALDH2 KO liver and skeletal muscle tissue, all ALDH2 WT and KO tissues sections had a normal morphology (Figure 5.5). It is well recognised that morphological changes only occur during the development of fatty vacuoles in the liver (Gerspach et al., 2017). Since morphological changes were not observed in

ALDH2 KO sections, this suggests that extensive lipid infiltration does not occur in liver and skeletal muscle tissue with ALDH2 deficiency.

5.5.1 Study limitations and future considerations

In the present chapter, there are a couple of study limitations in relation to the LTA experiments and ORO tissue staining. Firstly, collagen was the only agonist used to trigger washed platelet aggregation. As discussed in Chapters 3 and 4, this limitation restricts the evaluation of platelet function. Additional experiments involving multiple agonists are therefore required to investigate platelet function in both ALDH2 WT and KO mice (Dovlatova, 2015; Hayward et al., 2009).

In addition, as previously explained in Chapters 3 and 4, non-physiological concentrations of nitrite were used in the LTA experiments. The use of pharmacological $NaNO_2$ concentrations is a major disadvantage as changes to platelet function by normal plasma nitrite concentrations cannot be assumed from these studies (Kevil et al., 2011; Srihirun et al., 2018).

Furthermore, whilst the present study has revealed the importance of ALDH2 in nitrite-mediated attenuation of washed platelet aggregation in mice, further studies are warranted to confirm these findings in man. In ALDH2 KO mice, gene disruption prevents all ALDH2 expression. However, in the human population ALDH2 KOs do not exist and heterozygous (ALDH2*1/*2; less than 50% enzyme activity)/homozygous individuals (ALDH2*2/*2: approximately 1-4% enzyme activity) can be seen to express varying levels of WT enzymatic activity (Chen et al., 2014; Farres et al., 1994; Ferencz-Biro and Pietruszko, 1984; Zhou and

Weiner, 2000). As such, a genetic mouse ALDH2*2 strain could be used to give a more accurate representation of the interactions between ALDH2 and nitrite in the human population (Jin et al., 2015).

Moreover, it is well known that ALDH2 functions as a nitrite reductase, to reduce nitrite and hence cause NO release, in conditions such as hypoxia and acidosis (Calvert and Lefer, 2009; Vitturi and Patel, 2011). As such, active ALDH2 may have contributed to nitrite-mediated attenuation of washed platelet aggregation in mice through a NO-dependent mechanism. The potential involvement of NO is somewhat contradictory to our findings in human platelets, where $NaNO_2$ was shown to activate sGC independently of NO to inhibit washed platelet aggregation (Chapters 3 and 4). To further explore the underlying nitrite mechanism in mouse washed platelets, additional experiments in the presence of NO scavengers, OxyHb and PTIO, and the sGC inhibitor, ODQ, are warranted in ALDH2 WT and KO platelets. These investigations would reveal whether nitrite activates sGC independently of NO in mouse washed platelets and potentially corroborate with our findings in human platelets. The importance of ALDH2-nitrite interactions in nitrite-mediated sGC activation and the attenuation of platelet aggregation could also be explored under these circumstances to further delineate the cardioprotective mechanisms of ALDH2 and nitrite.

Whilst Mollace and colleagues have previously reported ALDH2 to play a pivotal role in organic nitrate (GTN) tolerance in platelets, and since our group have very recently shown nitrite to circumvent the phenomenon of platelet NO resistance (Borgognone et al., 2018; Mollace et al., 2014). It would be essential to assess whether nitrite induces tolerance following long-term treatment *in vivo* in ALDH2 KO and WT mice, respectively.

Furthermore, ORO staining may not provide the most accurate representation of lipid accumulation in tissues. Polar lipids, such as phospholipids, are not stained by ORO, whilst tissues with low lipid contents are very difficult to stain. Moreover, ORO staining can only be used to quantify the general accumulation of lipids in tissues and not specific lipid types. Quantification of the staining is also very laborious and time consuming, as a result of the computer software used. Finally, large data sets are preferable for this type of analysis, therefore a larger sample size of n>8 is required (Mehlem et al., 2013).

5.5.2 Conclusions

We show two major findings in this study, firstly that nitrite requires ALDH2 to inhibit platelet aggregation. Secondly, that inactivation of ALDH2 increases the lipid content of mouse liver and skeletal muscle tissue without affecting tissue morphology. Further studies are warranted to evaluate the impact of ALDH2 in nitrite anti-platelet therapy, and develop our understanding of ALDH2 in skeletal muscle. Especially when approximately 40% of the East Asian population have ALDH2 deficiency and is associated with high prevalence of cardiovascular disease.

Chapter 6: General discussion

6.1 Introduction summary

Since the discovery of NO in vasculature, a substantial amount of research has been undertaken to investigate the role of NO in platelets. It is well established that NO bioavailability and responsiveness decrease with age, thus leading to increases in platelet activation and aggregation (Goubareva et al., 2007; Jones, 2016; Torregrossa et al., 2011). However, very little evidence exists on the changes to platelet function in the elderly (>70 years of age; Jones, 2016). Furthermore, the phenomenon of "platelet NO resistance" has been demonstrated in patients with HFrEF (Anderson et al., 2004), but whether this exists in HFpEF patients still remains to be elucidated. As such, the pro-thrombotic state in HF is likely to be exacerbated by this phenomenon, whilst the effectiveness of some NO-mediated HF therapies may also be reduced (Chirkov and Horowitz, 2007). Pharmacotherapeutic agents, such as ACE inhibitors, Beta-blockers and Digoxin, are frequently used in HFrEF to target associated neurohormonal dysregulation and haemodynamic instability. However, these drugs remain ineffective in HFpEF (Loudon et al., 2016) and the discovery of a novel agent that circumvents "platelet NO resistance" in HFpEF is therefore desirable. Currently, nitrite is being investigated with the potential of becoming a novel therapeutic agent for many CVDs and has been shown to have numerous protective effects in HF (Borlaug et al., 2015; Ormerod et al., 2015), whilst also inhibiting platelet aggregation in healthy volunteers (Borgognone et al., 2015). A few studies have also revealed interactions between nitrite and the mitochondrial enzyme, ALDH2, which has previously emerged as an important mediator for hypoxic vasodilator in HF patients (Arif et al., 2015) and very recently in second window pre-/post-conditioning (Ormerod et al., 2017). Whether ALDH2 plays a role in nitrite-mediated inhibition of platelet aggregation remains to be fully elucidated. Therefore, in the present thesis the aim was to develop our understanding of the following: **1)** platelet function

in young *vs* old healthy subjects (Chapter 3), **2)** the potential for nitrite to be used as an anti-platelet agent in patients with HFpEF-AF and CAF alone (Chapter 4), and **3)** the role of ALDH2 on nitrite responses to platelet aggregation (Chapter 5).

6.2 Discussion

Numerous whole blood and platelet rich plasma (PRP) aggregation studies from healthy subjects and animals have shown that nitrite inhibits platelet aggregation through an erythrocyte-dependent mechanism (Corti et al., 2013; Dautov et al., 2014; Parakaw et al., 2017). Under these conditions, nitrite inhibits platelet aggregation via the conversion to NO by the reductase activity of partially deoxygenated haemoglobin, and increases VASP phosphorylation at the Ser^{239} site in platelets (Parakaw et al., 2017; Srihirun et al., 2012). To determine whether nitrite inhibits platelet aggregation independently of haemoglobin and other plasma proteins, we conducted our experiments in washed platelets and to the best of our knowledge, we are the only research group to date to have investigated nitrite in washed platelets.

In the present study we show that nitrite activates sGC independently of NO to inhibit washed platelet aggregation in both young and old healthy volunteers, whilst also demonstrating synergistic activity between nitrite and BAY 41-2272 in both age groups. The sGC stimulator, BAY 41-2272, was also shown to have NO-independent anti-aggregatory effects. These novel findings therefore highlight the potential for nitrite to be used, both alone and in combination with BAY 41-2272, as an anti-platelet therapy across all ages in the future.

Since our results show that nitrite inhibits platelet aggregation in the elderly healthy subjects, we next evaluated the effects of nitrite on platelet function in patients with HFpEF-AF. We demonstrated a diminished response to the NO donor, SNP, in washed platelets from HFpEF-AF patients, when compared to the healthy volunteers and CAF patient group, whilst revealing a significant attenuation to platelet aggregation following 1mM $NaNO_2$ treatment in HFpEF-AF patients. With these findings we show for the first time that "platelet NO resistance" exists in HFpEF-AF and that high concentrations of nitrite circumvent this phenomenon in HFpEF-AF patients. Since $NaNO_2$ and SNP both triggered concentration-dependent attenuation of platelet aggregation in CAF patients, we also show that "platelet NO resistance" is primarily associated with HFpEF and not CAF. Additional experiments completed by our research group demonstrate that nitrite also activates sGC independently of NO to inhibit washed platelet aggregation in HFpEF-AF patients. (Borgognone et al., 2018). Overall, these innovative findings highlight the potential for nitrite therapy to address conditions of hyperaggregability in the future, especially in patients with HFpEF-AF.

Since a number of recent studies propose a role for mitochondrial ALDH2 in nitrite-mediated effects of vascular and cardiac disease, this suggests that this mechanism may have some benefits on platelet function. We have previously shown that nitrite significantly attenuates platelet aggregation in both healthy volunteers and patients with HFpEF-AF, however the mechanism of nitrite in platelet aggregation remains to be fully elucidated. Our data shows for the first time that activate ALDH2 is required for nitrite to inhibit platelet aggregation and to prevent lipid accumulation in the liver and skeletal muscle tissue of ALDH2 mice. The effect of ALDH2 deficiency on skeletal muscle lipid content still remains to be investigated, however recent studies have reported that the ALDH2*2 allele as a risk factor for liver

steatosis and NAFLD development (Oniki et al., 2016). These novel findings contribute to our understanding of nitrite- and ALDH2-mediated cardioprotection, thus may help to improve the effectivity of anti-platelet therapies in the future.

6.3 Study limitations and future directions

There are a couple of major limitations regarding the LTA experiments, Western blotting analysis and ORO staining in the present project. Firstly, heme-containing components of the mitochondrial respiratory chain (e.g. cytochrome C) may have contributed to nitrite-mediated inhibition by converting nitrite to NO within the washed platelets (Kevil et al., 2011). It is likely that intraplatelet nitrite reduction circumvents NO scavenging by OxyHb and PTIO, therefore further studies are warranted to investigate the influence of heme-containing components on nitrite-mediated platelet inhibition.

Furthermore, the underlying nitrite mechanism and potential for BAY 41-2272 to act synergistically with nitrite was only investigated in washed platelets obtained from healthy volunteers. Therefore, further studies are essential to determine whether the synergistic effect of nitrite and BAY 41-2272 (sGC stimulator) would be of benefit in patients with HFpEF-AF and/or CAF patients.

Moreover, whilst the present study has revealed the importance of ALDH2 in nitrite-mediated attenuation of washed platelet aggregation in mice, further studies in a genetic mouse ALDH2*2 strain are warranted to confirm these findings in man. (Jin et al., 2015). Additional experiments in the presence of NO scavengers, OxyHb and PTIO, and the sGC inhibitor, ODQ, are also warranted in ALDH2 WT and KO platelets to determine whether

ALDH2-nitrite interactions activate sGC independently of NO to cause the attenuation of washed platelet aggregation.

6.4 Conclusion

In summary, we show for the first time in man that nitrite attenuates platelet aggregation in healthy volunteers and patients with HFpEF-AF. Furthermore, we demonstrate for the first time that the phenomenon of “platelet NO resistance” exists in HFpEF-AF, whilst also revealing that high concentration nitrite is able to circumvent “platelet NO resistance” in washed platelets independently of NO. We also show that ALDH2 is required for nitrite to inhibit platelet aggregation in mice. Overall, these novel findings highlight the potential for nitrite to be used as an anti-platelet therapy in the future, especially in patients with HFpEF-AF, however further research into the influence of heme-containing components on nitrite-mediated platelet inhibition, nitrite-BAY 41-2272 combination therapy in HFpEF-AF patients and ALDH2-nitrite interactions in a genetic mouse ALDH2*2 strain is warranted.

Chapter 7: References

Abudukadier, A., Fujita, Y., Obara, A. et al. (2013). Tetrahydrobiopterin has a glucose-lowering effect by suppressing hepatic gluconeogenesis in an endothelial nitric oxide synthase-dependent manner in diabetic mice. **Diabetes**, 62 (9): 3033-3043.

Adeghe, A.J. and Cohen, J. (1986) A better method for terminal bleeding of mice. **Lab Anim.**, 20 (1): 70-72.

Anderson, R.A., Ellis, G.R., Chirkov, Y.Y. et al. (2004) Determinants of platelet responsiveness to nitric oxide in patients with chronic heart failure. **Eur J Heart Fail,** 6: 47-54.

Apostoli, G.L., Solomon, A., Smallwood, M.J. et al. (2014) Role of inorganic nitrate and nitrite in driving nitic-oxide-cGMP-mediated inhibition of platelet aggregation *in vitro* and *in vivo*. **J Thrombosis Haemost**, 12 (11): 1880-1889.

Arimura, K., Egashira, K., Nakamura, R. et al. (2001) Increased inactivation of nitric oxide is involved in coronary endothelial dysfunction in heart failure. **Am J Physiol Heart Circ Physil**, 280 (1): 68-75.

Arif, S., Borgognone, A., Lin, E.L. et al. (2015) Role of aldehyde dehydrogenase in hypoxic vasodilator effects of nitrite in rats and humans. **Br J Pharmacol**, 172 (13): 3341-3352.

Bailey, J.C., Feelisch, M., Horowitz, J.D. et al (2014) Pharmacology and therapeutic role of inorganic nitrite and nitrate in vasodilation. **Pharmacol Ther**, 144: 303-320.

Balsinde, J., Winstead, M., Dennis, E.A. (2002) Phospholipase A_2 regulation of arachidonic acid mobilisation. **FEBS**, 531: 2-6.

Bauersachs, J. and Widder, J.D. (2008) Endothelial dysfunction in heart failure. **Pharmacol Rep**, 60 (1): 119-126.

Bauersachs, J., Fleming, I., Fraccarollo, D. et al. (2001) Prevention of endothelial dysfunction in heart failure by vitamin E: attenuation of vascular superoxide anion formation and increase in soluble guanylyl cyclase expression. **Cardiovasc Res**, 51 (2): 344-350.

Bell, S.E., Shan, C.M. and Gordge, M.P. (2007) Protein disulfide-isomerase mediates delivery of nitric oxide derivatives into platelets. **Biochem J**, 403 (2): 283-288.

Bendall, J. K., Alp, N. J., Warrick, N. et al. (2005). Stoichiometric relationships between endothelial tetrahydrobiopterin, endothelial NO synthase (eNOS) activity, and eNOS coupling in vivo: insights from transgenic mice with endothelial-targeted GTP cyclohydrolase 1 and eNOS overexpression. **Circ Res**, 97 (9): 864-871.

Benz, P.M., Laban, H., Zink. J. et al. (2016) Vasodilator-stimulated phosphoprotein (VASP)-dependent and –independent pathways regulate thrombin-induced activation of Rap1b in platelets. **Cell Commun Signal**, 14 (1): 21-33.

Bhatnagar, P., Wickramasinghe, K., Williams, J. et al. (2015) The epidemiology of cardiovascular disease in the UK 2014. **Heart**, 101 (15): 1182-1189.

Biino, G., Santimone, I., Minelli, C. et al. (2013) Age- and sex-related variations in platelet count in Italy: a proposal of reference ranges based on 40987 subjects' data. **PLoS One**, 8 (1): 1-7.

Bischoff, E., Schramm, M., Straub, A. et al. (2003) BAY 41-2272: a stimulator of soluble guanylyl cyclase induces nitric oxide-dependent penile erection in vivo. **Urology**, 61 (2): 464-467.

Boengler, K., Kosiol, M., Mayr, M. et al. (2017) Mitochondria and ageing: role in heart, skeletal muscle and adipose tissue. **JCSM**, 8 (3): 349-369.

Bolli, R., Jeroudi, M.O. and Patel, B.S. (1989) Direct evidence that oxygen-derived free radicals contribute to post-ischemic myocardial dysfunction in the intact dog. **Proc Natl Acad Sci U S A**, 86 (12): 4695-4699.

Borgognone, A., Loka, T., Rainger, E. et al. (2015) Nitrite is a cGMP generator in isolated platelets. **BMC Pharmacol Toxicol**, 16 (1): 65.

Borgognone, A., Lowe, K.L., Watson, S.P. et al. (2014) Natriuretic peptides induce weak VASP phosphorylation at Serine 239 in platelets. **Platelets**, 25 (1): 1-7.

Borgognone, A., Shantsila, E., Worrall, S.M. et al. (2018) Nitrite circumvents platelet resistance to nitric oxide in patients with heart failure preserved ejection fraction and chronic atrial fibrillation. **Cardiovasc Res**, 114 (10): 1313-1323.

Borlaug, B.A. (2013) Heart failure with preserved and reduced ejection fraction: different risk profiles for the different diseases. **Eur Heart J**, 34 (19): 1393-1395.

Borlaug, B.A., Koepp, K.E. and Melenovsky, V. (2015) Sodium nitrite improves exercise hemodynamics and ventricular performance in heart failure with preserved ejection fraction. **J Am Coll Cardiol**, 66 (15): 1672-1682.

Borlaug, B.A., Melenovsky, V. and Koepp, K.E. (2016) Inhaled sodium nitrite improves rest and exercise hemodynamics in heart failure with preserved ejection fraction. **Circ Res**, 119: 880-886.

Boulos, C., Jiang, H. and Balazy, M. (2000) Diffusion of peroxynitrite into the human platelet inhibits cyclooxygenase via nitration of tyrosine residues. **J Pharmacol Exp Ther**, 293 (1): 222-229.

Budas, G.R., Disatnik, M.H., Chen, C.H. et al. (2010) Activation of aldehyde dehydrogenase 2 (ALDH2) confers cardioprotection in protein kinase C epsilon (PKCvarepsilon) knockout mice. **J Mol Cell Cardiol,** 48 (4): 757-764.

Budas, G.R., Disatnik, M.H. and Mochly-Rosen, D. (2009) Aldehyde dehydrogenase 2 in cardiac protection: a new therapeutic target? **Trends Cardiovasc Med**, 19 (5): 158-164.

Bui, A.L., Horwich, T.B. and Fonarow, G.C. (2011) Epidemiology and risk profile of heart failure. Nature Reviews: **Nat Rev Cardiol**, 8 (1): 30-41.

Burkhoff, D. (2012) Mortality rate in heart failure with preserved ejection fraction: an unacceptably high rate. **Eur Heart J**, 33 (14): 1718-1720.

Busse, R. and Mülsch, A. (1990) Calcium-dependent nitric oxide synthesis in endothelial cytosol is mediated by calmodulin. **FEBS Lett**, 265 (1): 133-136.

Butler, A.R. and Feelisch, M. (2008). Therapeutic uses of inorganic nitrite and nitrate: from the past to the future. **Circulation**, 117: 2151–2159.

Calvert, J.W. and Lefer, D.J. (2009) Myocardial protection by nitrite. **Cardiovasc Res**, 83: 195-203.

Camm, A.J., Kirchhof, P., Lip, G.Y. et al. (2010) Guidelines for the management of atrial fibrillation: the Task Force for the Management of Atrial Fibrillation of the European Society of Cardiology (ESC). **Eur Heart J**, 31 (19): 2369-2429.

Cazenave, J.P., Ohimann, P., Cassel, D. et al. (2004) Preparation of washed platelet suspensions from human and rodent blood. **Methods Mol Biol**, 272: 13-28.

Celikel, R., McClintock, R.A., Roberts, J.R. et al. (2003) Modulation of alpha-thrombin function by distinct interactions with glycoprotein Ibalpha. **Science**, 301 (5630): 218-221.

Chen, C.H., Budas, G.R., Churchill, E.N. et al. (2008) Activation of aldehyde dehydrogenase-2 reduces ischemic damage to the heart. **Science**, 321 (5895): 1493-1495.

Chen, C.H., Ferreira, J.C.B., Gross, E.R. et al. (2014) Targeting aldehyde dehydrogenase 2: new therapeutic opportunities. **Physiol Rev**, 94 (1): 1-34.

Chen, Z., Foster, M.W., Zhang, J. et al. (2005) An essential role for mitochondrial aldehyde dehydrogenase in nitroglycerin bioactivation. **Proc Natl Acad Sci U S A**, 102 (34): 12159-12164.

Chirkov, Y.Y. and Horowitz, J.D. (2007) Impaired tissue responsiveness to organic nitrate and nitric oxide: a new therapeutic frontier? **Pharmacol Ther**, 116: 287-305.

Chirkov, Y.Y., Holmes, A.S., Willoughby, S.R. et al. (2001) Stable angina and acute coronary syndromes are associated with nitric oxide resistance in platelets. **J Am Coll Cardiol**, 37 (7): 1851-1857.

Chung, I. and Lip, G.Y.H. (2006) Platelets and heart failure. **Eur Heart J**, 27 (22): 2623-2631.

Comini, L., Bachetti, T., Gaia, G. et al. (1996) Aorta and skeletal muscle NO synthase expression in experimental heart failure. **J Mol Cell Cardiol**, 28 (11): 2241–2248.

Cook, C., Cole, G., Asaria, P. et al. (2014) The annual global economic burden of heart failure. **Int J of Cardiol**, 171 (3): 368-379.

Corti, P., Tejero, J. and Gladwin, M.T. (2013) Evidence mounts that red cells and deoxyhemoglobin can reduce nitrite to bioactive NO to mediate intravascular endocrine NO signaling: commentary on "Anti-platelet effects of dietary nitrate in healthy volunteers: involvement of cGMP and influence of sex". **Free Radic Biol Med**, 65: 1518-1520.

Cowman, J., Dunne, E., Oglesby, I. et al. (2015) Age-related changes in platelet function are more profound in women than men. **Sci Rep**, 5:1-7.

D'Souza, Y., Dowlatshahi, S. and Bennett, B.M. (2011) Changes in aldehyde dehydrogenase 2 expression in rat blood vessels during glyceryl trinitrate tolerance development and reversal. **Br J Pharmacol**, 164 (2): 632-643.

Daiber, A. and Münzel, T. (2015) Organic nitrate therapy, nitrite tolerance, and nitrate-induced endothelial dysfunction: emphasis on redox biology and oxidative stress. **Antioxid Redox Signal**, 23 (11): 899-942.

Daly, M.E. (2011) Determinants of platelet count in humans. **Haematologica**, 96 (1): 10-13.

Dandre, F., Cassaigne, A. and Iron, A. (1995) The frequency of the mitochondrial aldehyde dehydrogenase I2 (atypical) allele in Caucasian, Oriental and African black populations determined by the restriction profile of PCR-amplified DNA. **Mol Cell Probes**, 9 (3): 189-193.

Das, A., Xi, L. and Kukreja, R.C. (2008) Protein kinase G-dependent cardioprotective mechanism of phosphodiesterase-5 inhibition involved phosphorylation of ERK and GSK3β. **J Biol Chem**, 283: 29572-29585.

Dautov, R.F., Stafford, I., Liu, S. et al. (2014) Hypoxic potentiation of nitrite effects in human vessels and platelets. **Nitric Oxide**, 40: 36-44.

Dayal, S., Wilson, K.M., Motto, D.G. et al. (2013) Hydrogen peroxide promotes aging-related platelet hyperactivation and thrombosis. **Circulation**, 127 (12): 1308-1316.

den Dekker, E., Gorter, G., Heemskerk, J.W. et al. (2002) Development of platelet inhibition by cAMP during megakaryocytopoiesis. **J Biol Chem**, 277 (32): 29321-29329.

Dimmeler, S., Fleming, I., Fisslthaler, B. et al. (1999) Activation of nitric oxide synthase in endothelial cells by Akt-dependent phosphorylation. **Nature**, 399 (6736): 601-605.

Doel, J.J., Benjamin, N., Hector, M. P. et al. (2005). Evaluation of bacterial nitrate reduction in the human oral cavity. **Eur J Oral Sci**, 113 (1): 14–19.

Dovlatova, N. (2015) Current status and future prospects for platelet function testing in diagnosis of inherited bleeding disorders. **Br J Haematol**, 170 (2): 150-61.

Dumas, J.J., Kumar, R., Seehra, J. et al. (2003) Crystal structure of the GpIbalpha-thrombin complex essential for platelet aggregation. **Science**, 301 (5630): 222-226.

Eggebeen, J., Kim-Shapiro, D. B., Haykowsky, M. et al. (2016) One week of daily dosing with beetroot juice improves submaximal endurance and blood pressure in older patients with heart failure and preserved ejection fraction. **JACC Heart Fail**, 4*:* 428-437.

Elahi, M.M, Kong, Y.X. and Matata, B.M. (2009) Oxidative stress as a mediator of cardiovascular disease. **Oxid Med Cell Longev**, 2 (5): 259-269.

ElGuindy, A. and Yacoub, M.H. (2012) Heart failure with preserved ejection fraction. **Glob Cardiol Sci Pract**, 10: 1-19.

Essex, D.W., Chen, K. and Swiatkowska, M. (1995) Localization of protein disulfide isomerase to the external surface of the platelet plasma membrane. **Blood**, 86 (6): 2168-2173.

Farres, J., Wang, X., Takahashi, K. et al. (1994) Effects of changing glutamate 487 to lysine in rat and human liver mitochondrial aldehyde dehydrogenase. A model to study human (Oriental type) class 2 aldehyde dehydrogenase. **J Biol Chem**, 269 (19): 13854-13860.

Feng, C. and Tollin, G. (2009) Regulation of interdomain electron transfer in the NOS output state for NO production. **Dalton Trans**, 14 (34): 6629-6700.

Ferencz-Biro, K. and Pietruszko, R. (1984) Human aldehyde dehydrogenase: catalytic activity in oriental liver. **Biochem Biophy Res Commun**, 118 (1): 97-102.

Fischer, D., Rossa, S., Landmesser, S. et al. (2005) Endothelial dysfunction in patients with chronic heart failure is independently associated with increased incidence of hospitalization, cardiac transplantation, or death. **Eur Heart J**, 26 (1): 65-69.

Fleming, I., Fisslthaler, B., Dimmeler, S. et al. (2001) Phosphorylation of Thr(495) regulates Ca(2+)/calmodulin-dependent endothelial nitric oxide synthase activity. **Circ Res**, 88 (11): 68-75.

Förstermann, U. (2008) Oxidative stress in vascular disease: causes, defence mechanisms and potential therapies. **Nat Clin Prac Cardiovasc Med**, 5 (6): 338-349.

Förstermann, U. and Sessa, W.C. (2012) Nitric oxide synthases: regulation and function. **Eur Heart J**, 33 (7): 829-837.

Fulton, D., Gratton, J.P., McCabe, T.J. et al. (1999) Regulation of endothelium-derived nitric oxide production by protein kinase Akt. **Nature**, 399 (6736): 597-601.

Gachet, C. (2008) P2 receptors, platelet function and pharmacological implications. **J Thrombosis Haemost**, 99 (3): 466-472.

Gale, A.J. (2011) Current understanding of hemostasis. **Toxicol Path**, 39 (1): 273-280.

Garlid, K.D., Costa, A.D., Quinlan, C.L. et al. (2009) Cardioprotective signaling to mitochondria. **J Mol Cell Cardiol**, 46 (6): 858-866.

Gerspach, C., Imhasly, S., Klingler, R. et al. (2017) Variation in fat content between liver lobes and comparison with histopathological scores in dairy cows with fatty liver. **BMC Vet Res**, 13 (1): 98.

Gilstad, J.R., Gurbel, P.A. and Andersen, R.E. (2009) Relationship between age and platelet activation in patients with stable and unstable angina. **Arch Gerontol Geriatr**, 48 (2): 155-159.

Gkaliagkousi, E. and Ferro, A. (2011) Nitric oxide signalling in the regulation of cardiovascular and platelet function. **Fronti Biosci (Landmark Ed)**, 1 (16): 1873-1897.

Goedde, H.W., Agarwal, D.P., Fritze, G et al. (1992) Distribution of ADH2 and ALDH2 genotypes in different populations. **Hum Gen**, 88 (3): 344-346.

Goodpaster, B.H. and Wolf, D. (2004) Skeletal muscle lipid accumulation in obesity, insulin resistance, and type 2 diabetes. **Paediatr Diabetes**, 5 (4): 219-126.

Goubareva, I., Gkaliagkousi, E., Shah, A. et al. (2007) Age decreases nitric oxide synthesis and responsiveness in human platelets and increases formation is monocyte-platelet aggregates. **Cardiovasc Res**, 75 (4): 793-802.

Gresele, P., Momi, S. and Falcinelli, E. (2011) Anti-platelet therapy: phosphodiesterase inhibitors. **Br J Clin Pharmacol**, 72 (4): 634-646.

Gueldner, J., Sayes, C., Abel, E. et al. (2016) Emerging Associations of the ALDH2*2 Polymorphism with Disease Susceptibility. **J Drug Metabo Toxicol**, 7 (2): 202-209.

Guo, J.M., Liu, A.J., Zang, P. et al. (2013) ALDH2 protects against stroke by clearing 4-HNE. **Cell Res**, 23 (7): 915-930.

Hall, A.K., Dodd, V., Harris, A. et al. (2014) Heart failure patients' perceptions and use of technology to manage disease symptoms. **Telemed J E Health**, 20 (4): 324-331.

Hayward, C.P., Pai, M., Liu, Y. et al. (2009) Diagnostic utility of light transmission platelet aggregometry: results from a prospective study of individuals referred for bleeding disorder assessments. **J Thromb Haemost**, 7 (4): 678-684.

Hiebert, J.B., Shen, Q., Thimmesch, A. et al. (2016) Impaired myocardial bioenergetics in HFpEF and the role of antioxidants. **Open Cardiovas Med J**, 10: 159-162.

Hobbs, A. J. and Moncada, S. (2003) Antiplatelet properties of a novel, non-NO-based soluble guanylate cyclase activator, BAY 41-2272. **Vascul Pharmacol**, 40 (3): 149-154.

Im, J.H. and Muschel, R.J. (2017) Protocol for murine/mouse platelet isolation and their reintroduction in vivo. **Bio-Protoc**, 7 (4): 1-7.

Jackson, G., Gibbs, C.R., Davies, M.K. et al. (2000) ABC of heart failure: pathophysiology. **BMJ**, 320 (7228): 167-170.

Jackson, S.P., Nesbitt, W.S. and Kulkarni, S. (2003) Signalling events underlying thrombus formation. **J Thrombosis Haemost**, 1 (17): 1602-1612.

Jarvis, G.E., Atkinson, B.T., Snell, D.C. et al. (2002) Distinct roles of GPVI and integrin $\alpha_2\beta_1$ in platelet shape change and aggregation induced by different collagens. **Br J Pharmacol**, 137 (1): 107-117.

Jin, R.C., Voetsch, B. and Loscalzo, J. (2005) Endogenous mechanisms of inhibition of platelet function. **Microcirculation**, 12 (3): 247-258.

Jin, S., Chen, J., Chen, L. et al. (2015) ALDH2(E487K) mutation increases protein turnover and promotes murine hepatocarcinogenesis. **Proc Natl Acad Sci U S A**, 112 (29): 9088-9093.

Johnson, M., Ramey, E. and Ramwell, P.W. (1975) Sex and age differences in human platelet aggregation. **Nature**, 253 (5490): 355-357.

Jones, C.I. (2016) Platelet function and ageing. **Mamm Genome**, 27: 358-366.

Kadan, M., Doğanci, S., Yildirim, V. et al. (2015) In vitro effect of sodium nitrite on platelet aggregation in human platelet rich plasma – preliminary report. **Eur Rev Med Pharmacol Sci**, 19 (20): 3935-3939.

Kamath, S., Blann, A.D., Chin, B.S. et al. (2002) A study of platelet activation in atrial fibrillation and the effects of antithrombotic therapy. **Eur Heart J**, 23 (22): 1788-1795.

Kamath, S., Blann, A.D., Chin, B.S. et al. (2003) Platelet activation, haemorheology and thrombogenesis in acute atrial fibrillation: a comparison with permanent atrial fibrillation. **Heart**, 89 (9): 1093-1095.

Kapil, V., Weitzberg, E., Lundberg, J.O. et al. (2014). Clinical evidence demonstrating the utility of inorganic nitrate in cardiovascular health. **Nitric Oxide**, 38: 45–57.

Kaposzta, Z., Baskerville, P.A., Madge, D. et al. (2001) L-arginine and S-nitrosoglutathione reduce embolization in humans. **Circulation**, 103 (19): 2371-2375.

Kasjanovová, D. and Baláz, V. (1986) Age-related changes in human platelet function in vitro. **Mech Ageing Dev**, 37 (2): 175-182.

Kelm, M., Dahmann, R., Wink, D. et al. (1997) The nitric oxide/superoxide assay: insights into the biological chemistry of the NO/O_2^- interaction. **J Biol Chem**, 272 (15): 9922-9932.

Kevil, C.G. and Patel, R.P. (2010) 'Preserving' vessel function during ischemic disease: new possibilities of inorganic nitrite therapy. **Expert Rev Cardiovasc Ther**, 6 (9): 1175:1179.

Kevil, C.G., Kolluru, G.K., Pattillo, C.B. et al. (2011) Inorganic nitrite therapy: historical perspective and future directions. **Free Radic Biol Med**, 51 (3): 576-593.

Kirchhofer, D. and Nemerson, Y. (1996) Initiation of blood coagulation: the tissue factor/factor VIIa complex. **Curr Opin Biotechnol**, 7(4): 386-391.

Kleinbongard, P., Dejam, A., Lauer, T. et al. (2003) Plasma nitrite reflects constitutive nitric oxide synthase activity in mammals. **Free Radic Biol Med**, 35 (7): 790-796.

Kleinbongard, P., Dejam, A., Lauer, T. et al. (2006) Plasma nitrite concentrations reflect the degree of endothelial dysfunction in humans. **Free Radic Biol Med**, 40 (2): 295-302.

Kramkowski, K., Leszczynska, A., Przyborowski, K. et al. (2016) Role of xanthine oxidoreductase in the anti-thrombotic effects of nitrite in rats in vivo. **Platelets**, 27 (3): 245-253.

Lam, C.S.P., Santema, B.T., Voors, A.A. (2017) Atrial fibrillation in heart failure: a common and deadly combination. **JACC Heart Fail**, 5 (8): 575-577.

Lang, R.M., Bierig, M., Devereux, R.B. et al. (2006) Recommendations for chamber quantification. **Eur J Echocardiogr**, 7 (2): 79-108.

Langford, E.J., Brown, A.S., Wainwright, R.J. et al. (1994) Inhibition of platelet activity by S-nitrosoglutathione during coronary angioplasty. **Lancet**, 344 (8935): 1458-1460.

Laustiola, K.E., Vuorinen, P., Pörsti, I. et al. (1991) Exogenous GTP enhances the effects of sodium nitrite on cyclic GMP accumulation, vascular smooth muscle relaxation and platelet aggregation. **Pharmacol Toxicol**, 68 (1): 60-63.

LeWinter, M.M. and Meyer, M. (2013) Mechanisms of diastolic dysfunction in HFpEF: if it's not one thing it's another. **Circ: Heart Fail**, 6 (6): 1112-1115.

Li, H., Cui, H., Kundu, T.K. et al. (2008) Nitric oxide production from nitrite occurs primarily in tissues not in the blood: critical role of xanthine oxidase and aldehyde dehydrogenase. **J Biol Chem**, 283 (26): 17855-17863.

Li, Y., Zhang, D., Jin, W. et al. (2006) Mitochondrial aldehyde dehydrogenase-2 (ALDH2) Glu504Lys polymorphism contributes to the variation in efficacy of sublingual nitroglycerin. **J Clin Invest**, 116 (2): 506-511.

Li, Z., Delaney, M.K., O'Brien, K.A. et al. (2010) Signalling during platelet adhesion and activation. **Atheroscler Thromb Vasc Biol**, 30 (12): 2341-2349.

Li, Z., Xi, X., Gu. M. et al. (2003) A stimulatory role for cGMP-dependent protein kinase in platelet activation. **Cell**, 112 (1): 77-86.

Li, Z., Zhang, G., Feil, R. et al. (2006) Sequential activation of p38 and ERK pathways by cGMP-dependent protein kinase leading to activation of the platelet integrin alphaIIb beta3. **Blood**, 107 (3): 965-972.

Linssen, G.C., Rienstra, M., Jaarsma, T. et al. (2011) Clinical and prognostic effects of atrial fibrillation in heart failure patients with reduced and preserved left ventricular ejection fraction. **Eur J Heart Fail**, 13 (10): 1111-1120.

Litvinov, R.I., Farrell, D.H., Weisel, J.W. et al. (2016) The platelet integrin αIIbβ3 differentially interacts with fibrin versus fibrinogen. **J Biol Chem**, 291 (15): 7858-7867.

Lohmann, S.M., Vaandrager, A.B., Smolenski, A. et al. (1997) Distinct and specific functions of cGMP-dependent protein kinases. **Trends Biochem Sci**, 22 (8): 307-312.

Loot, A.E., Schreiber, J.G., Fisslthaler, B. et al. (2009) Angiotensin II impairs endothelial function via tyrosine phosphorylation of the endothelial nitric oxide synthase. **J Exp Med**, 206 (13): 2889-2896.

López Farré, A. and Casado, S. (2001) Heart failure, redox alterations, and endothelial dysfunction. **Hypertension**, 38 (6): 1400-1405.

Loudon, B.L., Noordali, H., Gallop, N.D. et al. (2016) Present and future pharmacotherapeutic agents in heart failure: an evolving paradigm. **Br J Pharmacol**, 173: 1911-1924.

Lundberg, J.O., Gladwin, M.T., Ahluwalia, A. et al. (2009). Nitrate and nitrite in biology, nutrition and therapeutics. **Nat Chem Biol**, 5 (12): 865–869.

Lundberg, J.O., Weitzberg, E., Gladwin, M.T. (2008) The nitrate-nitrite oxide pathway in physiology and therapeutics. **Nat Rev Drug Discov**, 7 (2): 156-167.

MacAllister, R.J. (2000) Arginine and nitrate tolerance. **Br J Pharmacol**, 130 (2): 209-210.

Mackenzie, I.S., Maki-Petaja, K.M., McEniery, C.M. et al. (2005) Aldehyde dehydrogenase 2 plays a role in the bioactivation of nitroglycerin in humans. **Atheroscler Thromb Vasc Biol**, 25 (9): 1891-1895.

Mackman, N. (2009) The role of tissue factor and factor VIIa in hemostasis. **Anaesth Analg**, 108 (5): 1447-1452.

Mahaut-Smith, M.P., Jones, S. and Evans, R.J. (2011) The P2X1 receptor and platelet function. **Purinergic Sigal**, 7 (3): 341-356.

Marjanovic, J.A., Li, Z., Stojanovic, A. et al. (2005) Stimulatory roles of nitic-oxide synthase 3 and guanylyl cyclase in platelet activation. **J Biol Chem**, 280 (45): 37430-37438.

Marti, C.N., Gheorghiade, M., Kalogeropoulos, A.P. et al. (2012) Endothelial dysfunction, arterial stiffness, and heart failure. **J Am Coll Cardiol**, 60 (16): 1455-1469.
Mayer, B. and Beretta, M. (2008) The enigma of nitroglycerin bioactivation and nitrate tolerance: new, views and troubles. **Br J Pharmacol**, 155 (2): 170-184.

Mazzucato, M., Cozzi, M.R., Battiston, M. et al. (2009) Distinct spatio-temporal Ca^{2+} signalling elicited by integrin α2β1 and glycoprotein VI under flow. **Blood**, 114 (13): 2793-2801.

Mazzucato, M., Marco, L.D., Masotti, A. et al. (1998) Characterization of the initial alpha-thrombin interaction with glycoprotein Ib alpha in relation to platelet activation. **J Biol Chem**, 273 (4): 1880-1887.

McKnight, G.M., Smith, L.M., Drummond, R. S. et al. (1997). Chemical synthesis of nitric oxide in the stomach from dietary nitrate in humans. **Gut**, 40 (2): 211–214.

McMurray, J.J., Adamopoulos, S., Anker, S.D. et al. (2012) ESC guidelines for the diagnosis and treatment of acute and chronic heart failure 2012: The Task Force for the Diagnosis and Treatment of Acute and Chronic Heart Failure 2012 of the European Society of Cardiology. Developed in collaboration with the Heart Failure Association (HFA) of the ESC. **Eur Heart J**, 33 (14): 1787-1847.

Mehlem, A., Hagberg, C.E., Muhl, L. et al. (2013) Imaging of neutral lipids by oil red O for analyzing the metabolic status in health and disease. **Nat Protoc**, 8 (6): 1149-1154.

Mellinger, J.L., Pencina, K.M. and Massaro, J.M. et al. (2015) Hepatic steatosis and cardiovascular disease outcomes: an analysis of the Framingham Heart Study. **J Hepatol**, 63 (2): 470-476.

Michelson, A.D. (2010) Antiplatelet therapies for the treatment of cardiovascular disease. **Nat Rev Drug Discov**, 9 (2): 154-169.

Modesti, P.A., Fortini, A., Abbate, R. et al. (1985) Age related changes of platelet prostacyclin receptors in humans. **Eur J Clin Invest**, 15 (4): 204-208.

Mollace, V., Muscoli, C., Dagostino, C. et al. (2014) The effect of peroxynitrite decomposition catalyst MnTBAP on aldehyde dehydrogenase-2 nitration by organic nitrates: role in nitrate tolerance. **Pharmacol Res**, 89: 29-35.

Moncada, S., Palmer, R.M. and Higgs, E.A. (1991) Nitic oxide: physiology, pathophysiology, and pharmacology. **Pharmacol Rev**, 43 (2): 109-142.

Morrell, C.N., Matsushita, K., Chiles, K. et al. (2005) Regulation of platelet granule exocytosis by S-nitrosylation. **Proc Natl Acad Sci U S A**, 102 (10): 3782-3787.

Mueller, C.F., Laude, K., McNally, J.S. et al. (2005) Redox mechanisms in blood vessels. **Atheroscler Thromb Vasc Biol**, 25 (2): 274-278.

Naseem, K.M. and Riba, R. (2008) Unresolved roles of platelet nitric oxide synthase**. J Thrombosis Haemost**, 6 (1): 10-19.
Noordali, H., Loudon, B.L., Frenneaux, M.P. et al. (2017) Cardiac metabolism – a promising therapeutic target for heart failure. **Pharmacol Ther**, 182: 95-114.

O'Donnell, C.J., Larson, M.G., Feng, D. et al. (2001) Genetic and environmental contributions to platelet aggregation: the Framingham heart study. **Circulation**, 103 (25): 3051-3056.

Offermanns, S. (2006) Activation of platelet function through G protein-coupled receptors. **Circ Res**, 99 (12): 1293-1304.

Oktay, A.A. and Shah, S.J. (2015) Diagnosis and management of heart failure with preserved ejection fraction: 10 key lessons. **Current Cardiol Revs**, 11 (1): 42-52.

Olas, B. and Wachowicz, B. (2007) Role of reactive nitrogen species in blood platelet functions. **Platelets**, 18 (8): 555-565.

Omar, S.A., Fok, H., Tilgner, K.D. et al. (2015) Paradoxical normoxia-dependent selective actions of inorganic nitrite in human muscular conduit arteries and related selective actions on central blood pressures. **Circulation**, 131 (4): 381-389.

Oniki, K., Morita, K., Watanabe, T., et al. (2016) The longitudinal effect of the aldehyde dehydrogenase 2*2 allele on the risk for non-alcoholic fatty liver disease. **Nutri Diabetes**, 6 (5): 210-214.

Ormerod, J.O., Arif, S., Mukadam, M. et al. (2015) Short-term intravenous sodium nitrite infusion improves cardiac and pulmonary hemodynamics in heart failure patients. **Circ Heart Fail**, 8 (3): 565-571.

Ormerod, J.O., Evans, J.D., Contractor, H. et al. (2017) Human second window pre-conditioning and post-conditioning by nitrite is influence by a common polymorphism in mitochondrial aldehyde dehydrogenase. **JACC Basic Transl Sci**, 2 (1): 13-21.

Oyama, T., Isse, T., Kagawa, N. et al. (2005) Tissue distribution of aldehyde dehydrogenase 2 and effects of the ALDH2 gene-disruption on the expression of enzymes involved in alcohol metabolism. **Front Biosci**, 10: 951-960.

Palmer. R.M., Ashton, D.S. and Moncada, S. (1988) Vascular endothelial cells synthesize nitric oxide from L-arginine. **Nature**, 333 (6174): 664-666.

Palta, S., Saroa, R. and Palta, A. (2014) Overview of the coagulation system. **Indian J Anaesth**, 58 (5): 515-523.

Parakaw, T., Suknuntha, K., Vivithanaporn, P. et al. (2017) Platelet inhibition and increased phosphorylated vasodilator-stimulated phosphoprotein following sodium nitrite inhalation. **Nitric Oxide**, 66: 1-7.

Park, J.W., Piknova, B., Huang, P.L. et al. (2013) Effect of blood nitrite and nitrate levels on murine platelet function. **PLoS One**, 8 (2): 1-7.
Pearce, A.C., Senis, Y.A., Billadeau, D.D. et al. (2004) Vav1 and Vav3 have critical but redundant roles in mediating platelet activation by collagen. **J Biol Chem**, 279 (50): 53955-53962.

Perlman, D.H., Bauer, S.M., Ashrafian, H. et al. (2009) Mechanistic insights into nitrite-induced cardioprotection using an integrated metabolomic/proteomic approach. **Circ Res**, 104 (6): 796-804.

Pigazzi, A., Heydrick, S., Folli, F. et al. (1999) Nitric oxide inhibits thrombin receptor-activating peptide-induced phosphoinositide 3-kinase activity in human platelets. **J Biol Chem**, 274: 14368-14375.

Procter, N.E., Ball, J., Liu, S. et al. (2015) Impaired platelet nitric oxide response in patients with new onset atrial fibrillation. **Int J Cardiol**, 179: 160-165.

Procter, N.E.K., Hurst, N.L., Nooney, V.B. et al. (2016) New developments in platelet nucleotide signalling: therapeutic implications. **Cardiovasc Drugs Ther**, 30 (5): 505-513.

Qin, L., Liu, X., Sun, Q. et al. (2012). Sialin (SLC17A5) functions as a nitrate transporter in the plasma membrane. **Proc Natl Acad Sci U S A**, 109 (33): 13434-13439.

Radomski, M.W., Palmer, R.M. and Moncada, S. (1990) An L-arginine/nitric oxide pathway present in human platelets regulates aggregation. **Proc Natl Acad Sci U S A**, 87 (13): 5193-5197.

Rajendran, S. and Chirkov, Y.Y. (2008) Platelet hyperaggregability: impaired responsiveness to nitric oxide ('platelet NO resistance') as a therapeutic target. **Cardiovasc Drugs Ther**, 22 (3): 193-203.

Ramsay, B., Radomski, M., De Belder, A. et al. (1995) Systemic effects of S-nitroso-glutathione in the human following intravenous infusion. **Br J Pharmacol**, 40 (1): 101-112.

Randriamboavonjy, V. and Fleming, I. (2005) Endothelial nitric oxide synthase (eNOS) in platelets: how is it regulated and what is it doing there? **Pharmacol Rep**, 57: 59-65.

Rao, G.H.R., Krishnamurthi, S., Raij, L. et al. (1990) Influence of nitric oxide on agonist-mediated calcium mobilization in platelets. **Biochem Med Metab Biol**, 43 (3): 271-275.

Rassaf, T., Kleinbongard, P., Preik, M. et al. (2002) Plasma nitrosothiols contribute to the systemic vasodilator effects of intravenously applied NO: experimental and clinical study on the fate of NO in human blood. **Circ Res**, 91 (6): 470-477.

Rivera, J., Lozano, M.L., Navarro-Núñez, L. et al. (2009) Platelet receptors and signalling in dynamics of thrombus formation. **Haematologica**, 94 (5): 700-711.
Roede, J.R. and Jones, D.P. (2010) Reactive species and mitochondrial dysfunction: mechanistic significance of 4-hydroxynonenal. **Environ Mol Mutagen**, 51 (5): 380-390.

Roger, S., Badier-Commander, C., Paysant, J. et al. (2010) The anti-aggregating effect of BAY 41-2272, a stimulator of guanylyl cyclase, requires the presence of nitric oxide. **Br J Pharmacol**, 161 (5): 1044-1058.

Roger, V.L. (2013) Epidemiology of heart failure. **Circ Res**, 113 (6): 646-659.

Ruggeri, Z.M. (2009) Platelet adhesion under flow. **Microcirculation**, 16 (1): 58-83.

Salas, E., Langford, E.J., Marrinan, M.T. et al. (1998) S-nitrosoglutathione inhibits platelet activation and deposition in coronary artery saphenous vein grafts in vitro and in vivo. **Heart**, 80 (2): 146-150.

Salvemini, D., De Nucci, G., Gryglewski, R.J. et al. (1989) Human neutrophils and mononuclear cells inhibit platelet aggregation by releasing a nitric oxide-like factor. **Proc Natl Acad Sci U S A**, 86 (16): 6328-6332.

Sambrano, G.R., Huang, W., Faruqi, T. et al. (2000) Cathepsin G activates protease-activated recptor-4 in human platelets. **J Bio Chem**, 275: 6819-6823.

Sangkuhl, K., Shuldiner, A.R., Klein, T.E. et al. (2011) Platelet aggregation pathway. **Pharmacogenet Genomics**, 21 (8): 516-521.

Sartipy, U., Dahlström, U., Fu, M. et al. (2017) Atrial fibrillation in heart failure with preserved, mid-range, and reduced ejection fraction. **JACC Heart Fail**, 5 (8): 565-574.

Savage, B., Almus-Jacobs, F. and Ruggeri, Z.M. (1998) Specific synergy of multiple substrate-receptor interactions in platelet thrombus formation under flow. **Cell**, 94 (5): 657-666.

Scatena, R., Bottoni, P., Martorana, G.E. at al. (2005) Nitric oxide donor drugs: an update on pathophysiology and therapeutic potential. **Expert Opin Investig Drugs**, 14 (7): 835-846.

Schneider, S.W., Nuschele, S., Wixforth, A. et al. (2007) Shear-induced unfolding triggers adhesion of von Willebrand factor fibers. **Proc Natl Acad Sci U S A**, 104 (19): 7899-7903.

Schwarz, U.R., Walter, U. and Eigenthaler, M. (2001) Taming platelets with cyclic nucleotides. **Biochem Pharmacol**, 62 (9): 1153-1161.

Seals, D.R., Jablonski, K.J. and Donato, A.J. (2011) Ageing and vascular function in humans. **Clin Sci (Lond)**, 120 (9): 357-375.

Segal, J.B. and Moliterno, A.R. (2006) Platelet counts differ by sex, ethnicity, and age in the United States. **Ann Epidemiol**, 16 (2): 123-130.

Selemidis, S., Dusting, G.J., Peshavariya, H. et al. (2007) Nitric oxide supresses NADPH oxidase-dependent production by S-nitrosylation in human endothelial cells. **Cardiovasc Res**, 75 (2): 349-358.

Senis, Y.A., Tomlinson, M.G., Ellison, S. et al. (2009) The tyrosine phosphatase CD148 is an essential positive regulator of platelet activation and thrombosis. **Blood**, 113: 4942-4954.

Shantsila, E., Haynes, R., Calvert, M. et al. (2016) IMproved exercise tolerance in patients with PReserved Ejection fraction by Spironolactone on myocardial fibrosiS in Atrial Fibrillation rationale and design of the IMPRESS-AF randomised controlled trial. **BMJ Open**, 6 (10): e012241.

Shantsila, E., Wrigley, B.J., Blann, A. et al. (2012) A contemporary view on endothelial function in heart failure. **Eur J Heart Fail**, 14 (8): 873-881.

Shin, E.K., Park, H., Noh, J.Y. et al. (2017) Platelet shape changes and cytoskeletal dynamics as novel therapeutic targets for anti-thrombotic drugs. **Biomol Ther**, 25 (2): 223-230.

Simon, L.M., Edelstein, L.C., Nagalla, S. et al. (2014) Human platelet microRNA-mRNA networks associated with age and gender revealed by integrated plateletomics. **Blood**, 123 (16): 37-45.

Smith, C.J., Sun, D., Hoegler, C. et al. (1996) Reduced gene expression of vascular endothelial NO synthase and cyclooxygenase-1 in heart failure. **Circ Res**, 78 (1): 58–64.

Soskić, S.S., Dobutović, B.D., Sudar, E.M. et al. (2011) Regulation of inducible nitric oxide synthase (iNOS) and its potential role in insulin resistance, diabetes and heart failure. **The Open Cardiovasc Med J**, 5: 153-163.

Srihirun, S., Piknova, B., Sibmooh, N. et al. (2018) Phosphorylated vasodilator-stimulated phosphoprotein (P-VASPSer239) in platelets is increased by nitrite and partially deoxygenated erythrocytes. **PLoS One**, 13 (3): 1-12.

Srihirun, S., Sriwantana, T., Unchern, S. et al. (2012) Platelet inhibition by nitrite is dependent on erythrocytes and deoxygenation. **PLoS One**, 7 (1): 1-9.

Stalker, T.J., Newman, D.K., Ma, P. et al. (2012) Platelet signalling. **Handb Exp Pharmacol**, 210: 59-85.

Stamboul, K., Lorin, J., Lorgis, L. et al. (2015) Atrial fibrillation is associated with a marker of endothelial function and oxidative stress in patients with acute myocardial infarction. **PLoS One**, 10 (7): 1-12.

Stamler, J.S., Jaraki, O., Osborne, J. et al. (1992) Nitric oxide circulates in mammalian plasma primarily as an S-nitroso adduct of serum albumin. **Proc Natl Acad Sci U S A**, 89 (16): 7674-7677.

Stojanovic, A., Marjanovic, J.A., Brovkovych, V.M. et al. (2006) A phosphoinositide 3-kinase-AKT-nitric oxide-cGMP signalling pathway in stimulating platelet secretion and aggregation. **J Biol Chem**, 281: 16333-16339.

Sverdlov, A.L., Ngo, D.T., Chan, W.P. et al. (2014) Ageing of the nitic oxide system: are we as old as our NO? **J Am Heart Assoc**, 3 (4): 1-12.

Taddei, S., Virdis, A., Ghiadoni, L. et al. (2001) Age-related reduction of NO availability and oxidative stress in humans. **Hypertension**, 38 (2): 274-279.

Torregrossa, A.C., Aranke, M. and Bryan, N.S. (2011) Nitric oxide and geriatrics: implications in diagnostics and treatment of elderly. **J Geriatr Cardiol**, 8 (4): 230-242.

Trepakova, E.S., Cohen, R.A. and Bolotina, V.M. (1999) Nitric oxide inhibits capacitative cation influx in human platelets by promoting sarcoplasmic/endoplasmic reticulum Ca^{2+}-ATPase-dependent refilling of Ca^{2+} stores. **Circ Res**, 84 (2): 201-209.

Uchida, K. and Stadtman, E.R. (1992) Modification of histidine residues in proteins by reaction with 4-hydroxynonenal. **Proc Natl Acad Sci U S A**, 89 (10): 4544-4548.

van der Loo, B., Labugger, R., Skepper, J.N. et al. (2000) Enhanced peroxynitrite formation is associated with vascular aging. **J Exp Med**, 192 (12): 1731-1744.

van Heerebeek, L. and Paulus, W.J. (2016) Understanding heart failure with preserved ejection fraction: where are we today? **Neth Heart J**, 24 (4): 227-236.

van Riet, E.E., Hoes, A.W., Wagenaar, K.P. et al. (2016) Epidemiology of heart failure: the prevalence of heart failure and ventricular dysfunction in older adults over time. A systematic review. **Eur J Heart Fail**, 18 (3): 242-252.

Velmurugan, S., Kapil, V., Ghosh, S.M. et al. (2013) Anti-platelet effects of dietary nitrate in healthy volunteers: involvement of cGMP and influence of sex. **Free Radic Biol Med**, 65: 1521-1532.

Vitturi, D.A. and Patel, R.P. (2011) Current perspectives and challenges in understanding the role of nitrite as an integral player in nitric oxide biology and therapy. **Free Radic Biol Med**, 51 (4): 805-812.

Walker, C.P. and Royston, D. (2002) Thrombin generation and its inhibition: a review of the scientific basis and mechanism of action of anticoagulant therapies. **Br J Anaesth**, 88 (6): 848-863.

Walsh, G.M., Leane, D., Moran, N. et al. (2007) S-Nitrosylation of platelet αIIbβ3 as revealed by raman spectroscopy. **Biochemistry**, 46 (21): 6429-6436.

Wang, G.R., Zhu, Y., Halushka, P.V. et al. (1998) Mechanism of platelet inhibition by nitric oxide: *in vivo* phosphorylation of thromboxane receptor by cyclic GMP-dependent protein kinase. **Proc Natl Acad Sci U S A**, 95: 4888-4893.

Wang, L., Frizzell, S.A., Zhao, X. et al. (2012) Normoxic cyclic GMP-independent oxidative signalling by nitrite enhances airway epithelial cell proliferation and wound healing. **Nitric Oxide**, 15 (26): 203-210.

Watson, S.P., Auger, J.M., McCarty, O.J. et al. (2005) GPVI and integrin alpha11b beta3 signalling in platelets. **J Thrombosis Haemost**, 3 (8): 1752-1762.

Wentworth, J.K.T., Pula, G., Poole, A.W. (2006) Vasodilator-stimulated phosphoprotein (VASP) is phosphorylated on Ser^{157} by protein kinase C-dependent and –independent mechanisms in thrombin-stimulated human platelets. **Biochem J**, 15 (393): 555-564.

Willoughby, S., Holmes, A. and Loscalzo, J. (2002) Platelets and cardiovascular disease. **Eur J Cardiovasc Nurs**, 1 (4): 273-288.

Wohner, N., Kovács, A., Machovich, R. et al. (2012) Modulation of the von Willebrand factor-dependent platelet adhesion through alternative proteolytic pathways. **Thromb Res**, 129 (4): 41-46.

Woulfe, D., Yang, J., Prevost, N. et al. (2004) Signalling receptors on platelets and megakaryocytes. **Methods Mol Biol**, 273: 3-32.

Xu, T., Liu, S., Ma, T. et al. (2017) Aldehyde dehydrogenase 2 protects against oxidative stress associated with pulmonary arterial hypertension. **Redox Biol**, 11: 286-296.

Yamamoto, E., Hirata, Y., Tokitsu, T. et al. (2015) The pivotal role of eNOS uncoupling in vascular dysfunction in patients with heart failure with preserved ejection fraction. **Int J Cardiol**, 190: 335-337.

Yokoyama, K., Zhang, X.P., Medved, L. et al. (1999) Specific binding of αvβ3 to the fibrinogen γ and α_E chain C-terminal domains. **Biochemistry**, 38 (18): 5872-5877.

Yoshida, A., Huang, I.Y. and Ikawa, M. (1984) Molecular abnormality of an inactive aldehyde dehydrogenase variant commonly found in Orientals. **Proc Natl Acad Sci U S A,** 81 (1): 258-261.

Zamani, P., Rawat, D., Shiva-Kumar, P. et al. (2015) Effect of inorganic nitrate on exercise capacity in heart failure with preserved ejection fraction. **Circulation**. 131: 371-380.

Zarbock, A., Polanowska-Grabowska, R.K. and Ley, K. (2007) Platelet-neutrophil-interactions: linking hemostasis and inflammation. **Blood Rev**, 21: 99-111.

Zhang, Q., Zheng, J., Qiu, J. et al. (2017) ALDH2 restores exhaustive exercise-induced mitochondrial dysfunction in skeletal muscle. **Biochem Biophys Res Commun**, 485 (4): 753-760.

Zhou, J. and Weiner, H. (2000) Basis for half-of-the-site reactivity and the dominance of the K487 oriental subunit over the E487 subunit in heterotetrameric human liver mitochondrial aldehyde dehydrogenase. **Biochemistry,** 39 (39): 12019-12024.